Expanding the capabilities of lateral flow assays using computationally designed affinity proteins

Caitlin E. Anderson

A dissertation

submitted in partial fulfillment of the

requirements for the degree of

Doctor of Philosophy

University of Washington

2019

Reading Committee:

Paul Yager, Chair

Daniel Ratner

Lara Gamble

Program Authorized to Offer Degree:

Bioengineering

University of Washington

Abstract

Expanding the capabilities of lateral flow assays using computationally designed affinity proteins

Caitlin E. Anderson

Chair of the Supervisory Committee:
Prof. Paul Yager
Bioengineering

Point-of-care diagnostics have enabled clinical testing in areas previously considered challenging, specifically for underserved populations and in low resource settings. Lateral flow tests, such as the ubiquitous pregnancy test, have proven relatively successful in their implementation due to their low cost and ease of use; however their application has been limited to a select group of targets and types of assays. There is a need for novel molecular recognition elements that address some of the key limitations of antibody use in lateral flow assays. The following dissertation describes the development of lateral flow assays using novel molecular recognition elements, computationally designed proteins. We describe the first lateral flow assays using computationally designed binders, targeting the head and stem region of the influenza glycoprotein, hemagglutinin (HA). The best performing of these assays, using

a head region specific HA binder, was integrated into a two-dimensional paper network that integrated enzymatic amplification. Not only did this device sensitively detect native influenza virus from a spiked patient sample, the computationally designed binders proved highly thermostable when integrated into a paper network. Lastly, we used our knowledge of lateral flow assays to use modular design to develop an Ebola glycoprotein (GP) assay using an Ebola specific computationally designed binder. While we began by investigating the use of a nitrocellulose binding protein to anchor our Ebola binder, we found that the use of a streptavidin test line with biotinylated binder led to the best performance for detection of Ebola GP. All together, this work introduces computationally designed affinity proteins as an antibody alternative for lateral flow assay development. Future work developing modular protein assembly for lateral flow assays will enable more rapid development of this novel low cost diagnostic platform for a wider range of applications than previously possible.

TABLE OF CONTENTS

LIST OF FIGURES

LIST OF TABLES

ACKNOWLEDGEMENTS

There's an old Swahili proverb, "umoja ni nguvu", that roughly translates to "unity is strength". This rings true to my experience in graduate school, as this would not have been possible without the help and support of so many incredible people.

Firstly, I would like to thank my PhD advisor Professor Paul Yager, whose teaching and guidance throughout graduate school have helped me learn and grow into the scientist I am today. His ability to seek out solutions to important problems in this ever-changing scientific landscape is one that I will continually admire. I will forever be grateful that he pushed me to learn to stand up and argue my point of view. I would like to thank my supervisory committee, Professors Daniel Ratner, David Baker, Lara Gamble, Paul Drain, for all their support and guidance throughout the course of my PhD. I would also like to thank members of my qualifying exam committee, Professor Wendy Thomas and Dr. Janet Englund, whose thoughtful questions helped me form better questions in my own research.

I have had the opportunity to collaborate with many people during the PhD, and I am grateful to have had the chance to learn from and work with so many people at GE, PATH, Seattle Children's Hospital and from the Baker and Bloom labs from the University of Washington. I would like to give a special thank you Dr. Eva Maria Strauch for the many years of collaboration testing and designing proteins for the detection of influenza. I would also like to thank Lauren Carter, Dr. David La and Dr. Lance Stewart for all their hard work and help with the development of the Ebola assays. Undergraduate students Rosemichelle Marzan, Alexis Fleming, and Debbie Chen all deserve special shout outs for their contributions to this work, specifically with 2DPN development, flu device development and microfluidic flow chamber, and the microfluidic flow chamber respectively.

I would like to thank all members, past and present, of the Yager lab. Words alone cannot express how grateful I am to have joined such a supportive laboratory environment. Dr. Carly Holstein, who was a senior graduate student in the Yager lab when I first started, deserves a very special thank you for her guidance and mentorship during the entirety of my PhD. This project would not have been possible without her, and I will forever be grateful that I was able to learn from her and continue her incredible work. I would also like to thank Dr. Samantha Byrnes, Dr.

Joshua Buser, and Dr. Joshua Bishop, for I would have been lost without their guidance and support, and our afternoon tea/coffee trips, during the last four years. In addition, I am grateful to those lab members who directly contributed to this work: Dr. Paula Ladd, Peter Kauffman, Tinny Liang, Dr. Shichu Huang, Kamal Shah, Sujatha Ramachandran, Dr. Xiaohong Zhang, Dr. Koji Abe, and the amazing Chelsea Musick.

This work was supported by the National Institute of Allergy and Infectious Diseases of the National Institutes of Health under award number R01AI096184 and the Defense Threat Reduction Agency of the United States Department of Defense under award number HDTRA1-16-C-0029. The content in this document is solely the responsibility of the author and does not represent the official views of the National Institutes of Health or the United States Department of Defense.

Lastly, I would like to thank my incredible support system. To my family and friends, your encouragement through this process has enabled me to stick with it in the hardest of moments and kept me laughing through it all. I'm especially grateful for my mom and dad, for I would not be who I am today without their unwavering support in all my endeavors (which included, but was not limited, to sitting through hundreds of gymnastics meets). And to Ayo, chair of my "no" committee, for being the most amazing partner and helping support me across the finish line.

DEDICATION

For my grandfather, Ronald F. Challman

Chapter 1. INTRODUCTION

1.1 SIGNIFICANCE OF PROBLEM

Point of care diagnostics have the potential to improve accessibility to medical testing by bringing the capabilities of medical laboratory directly to the patient. One class of diagnostic, the lateral flow assay (LFA), is of particular interest due to its lost cost, ease of use, and limited need for electricity or additional machinery [1], [2]. LFAs have been developed for applications ranging from detection of pregnancy, infectious disease, and environmental pathogens [3]. Traditionally, LFAs use antibodies on the test line and in the conjugate pad to enable capture and labeling of the analyte of interest. However, the use of antibodies in LFAs limit their potential application to diagnostic applications for three primary reasons; (1) they are labor intensive and expensive to manufacture, (2) they require an immunogenic and nontoxic antigen and (3) they are lacking in thermostability. While there has been a surge in the number of alternative molecular recognition elements, such as aptamers, antibody variable fragments and nanobodies, their application to LFAs has remained relatively limited. To our knowledge, there is not a commercially available lateral flow assay that uses an alternative molecular recognition element to date.

1.2 PROPOSED SOLUTION

Our group has worked to address the aforementioned problems by replacing the antibodies with computationally designed proteins in LFAs. In collaboration with the Baker lab from the University of Washington, we aim to increase the capabilities of LFAs through the use of these unique proteins. Designed for optimal kinetics, these computationally designed proteins are both significantly less expensive and more thermostable than antibodies. In addition, we have significantly more control over specific properties of these proteins. These properties include, but are not limited to, isoelectric point, number, type and location of conjugation sites, and oligomerization to closely mimic biological binding sites. We believe that computationally designed proteins are ideal molecular recognition elements for integration into an LFA due to their low manufacturing cost, high thermostability, and customizability.

In order to demonstrate the utility of computationally designed proteins, this work follows the first application of these proteins to the influenza glycoprotein, hemagglutinin. With the demonstration of these proteins for the detection of both recombinant and native hemagglutinin, we then moved to integrate them into prototype device for the detection of flu from nasal swab samples. With a novel fluidic system, these proteins were shown to be stable on device and enable detection from spiked clinical samples. With these successes, we wanted to take a step backwards and develop a method to more readily integrate new computationally designed proteins into lateral flow assays without the need for significant assay development and optimization. Using these methods, we were able to develop a new set of LFAs for the detection of a viral glycoprotein for the Ebola virus. We believe the lessons learned from this work inform the development of LFAs for computationally designed proteins and beyond, with the ultimate goal of enabling more rapid response in viral disease outbreaks.

1.3 SUMMARY OF DISSERTATION

This dissertation focuses on the integration of this new class of affinity reagents, computationally designed affinity proteins, into lateral flow assays. This work is divided into three specific aims, listed on the next page. Ultimately, this dissertation aims to demonstrate the use of computationally designed affinity proteins to expand the capabilities of lateral flow assays and to improve the lateral flow assay development process.

Aim 1. Assays for the detection of the influenza virus using computationally designed proteins
In this aim we describe the development of assays for the detection of the influenza hemagglutinin protein using computationally designed affinity proteins. Of the assays developed, two are of particular note; (1) the most sensitive colorimetric LFA for hemagglutinin and (2) detection of the native hemagglutinin from the intact influenza virus. This is the first demonstration of the use of these proteins in the context of a lateral flow assay.

Aim 2. An integrated 2DPN for sensitive detection of the influenza hemagglutinin
The second aim in this document describes the development of a prototype device for the automation of the hemagglutinin assay. This assay uses an enzymatic amplification assay that requires the sequential delivery of multiple fluidic steps; therefore, the development of a paper network that led to optimal assay performance was of utmost importance. The prototype device used a novel paper network for the successful detection of virus from spiked nasal swab samples.

Aim 3. Modular design of assay stacks using computationally designed proteins
The final aim of this work builds upon our experience developing assays using computationally designed affinity proteins through the development of modular assay components. The modular assay components described in this work include nitrocellulose-binding proteins, a conjugation system that had not previously been demonstrated in nitrocellulose using SpyCatcher and SpyTag, and the application of these two components to build an assay for the detection of the Ebola glycoprotein.

Chapter 2. BACKGROUND

Parts of this section were modified from a chapter from Methods in Enzymology written together with Kamal Shah and Dr. Paul Yager [4].

2.1 POINT OF CARE DIAGNOSTICS

2.1.1 *Need for diagnosis at the point of care*

Of the 30 leading causes of death worldwide between 2005 and 2015, eight are directly related to an infectious disease pathogen, **Figure 2.1** [5]. While the overall global burden of disease due to infectious diseases has decreased in the last 10 years, there remains a huge need for technology for the diagnoses and treatment of these diseases. The recent Ebola and Zika epidemics have highlighted how large scale, rapid testing is important for public health and patient outcomes. These epidemics also served to identify some of the gaps that exist in current diagnostic testing methods [6]. Chronic and pandemic infectious diseases suffer from similar gaps, where the existing diagnostic infrastructure is inadequate or ineffective in influencing clinical outcomes. The influenza virus, for example, is responsible for between 9 and 35 million infections in the United States annually, however the existing rapid diagnostic tests continue to perform poorly in the clinical setting [7], [8].

There is a specific need for low cost diagnostics able to diagnose disease at the point of care (POC), for both under-served populations in the United States and low resource settings around the world [9]. POC diagnostics are often marketed for use in the developing world, with the additional challenges of needing to be extremely low cost, require no additional machinery, and the ability to be implemented in areas where there is limited public health infrastructure and challenging transportation and storage conditions [10]. The WHO has specified that a diagnostic for the developing world fit the ASSURED criteria, which suggest that it is affordable, sensitive, specific, user friendly, rapid and robust, equipment free, and deliverable to the end user [11]. These criteria are not exclusive to developing world settings, as they pertain to many applications for the United States and Europe. Accurate diagnosis is a critical step in both prevention and treatment of disease, as diagnosis at the POC has the potential to streamline healthcare and improve clinical outcomes [12]. POC testing enables immediate results in non-

laboratory settings, which can translate to the development of healthcare delivery approaches that much more patient specific [9].

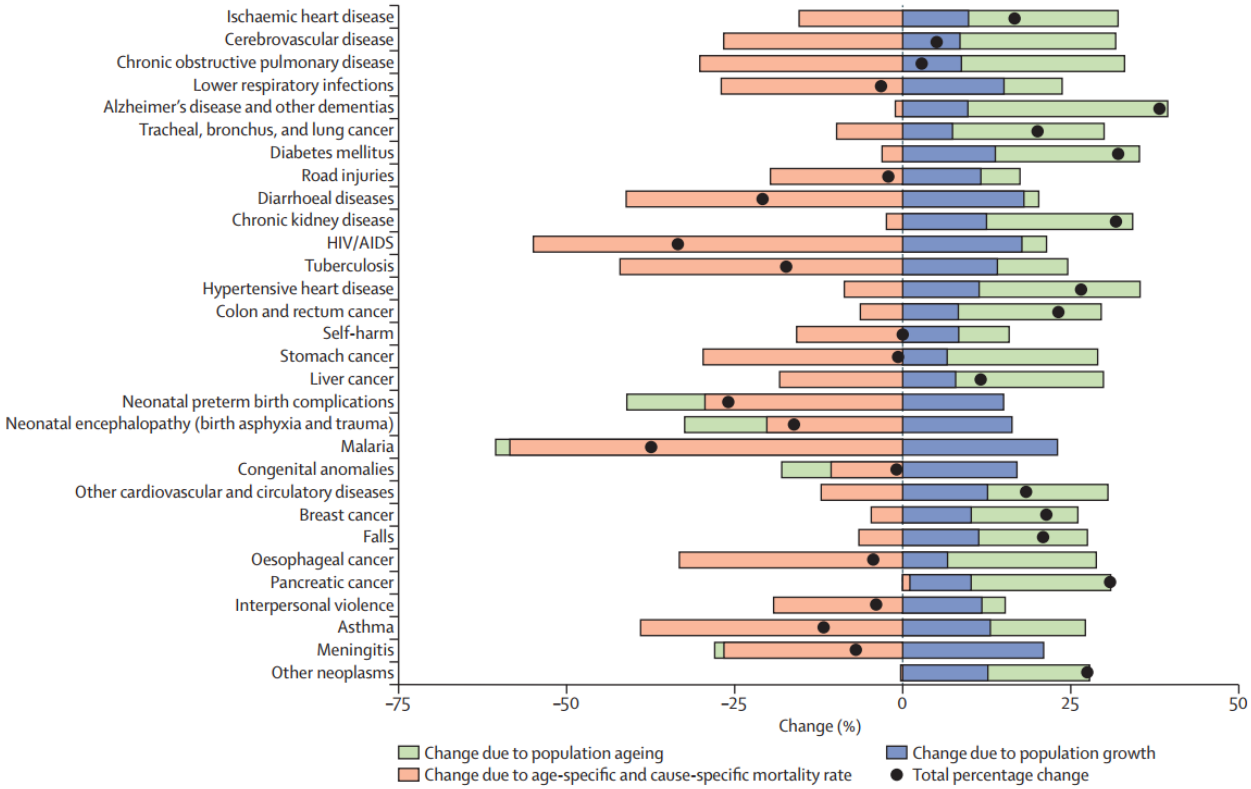

Figure 2.1. 30 leading causes of death worldwide between 2005 and 2015.
Includes changes due to population ageing, growth, age and cause-specific mortality. Source: [5].

The improvement in patient outcomes promised by POC testing is limited by the ability of a new diagnostic device or laboratory technique to be implemented. For this reason, context is an important factor to consider throughout the device development process. While various classifications have been developed to identify different use cases, one interesting classification decouples budget and infrastructure as a way to categorize four distinct use cases [6]. As shown in **Figure 2.2**, the four use cases would require very different design considerations. For example, Use Case 1 requires both health infrastructure and moderate budget, and therefore would not require specific design considerations that limit the use of electricity and trained personnel. Use Case 4, on the other hand, requires use in the field under a limited budget, as would be required in many home testing and low resources settings. In this case, a successful

device would likely be low cost, easy to use by an untrained user, and is more likely to be equipment free.

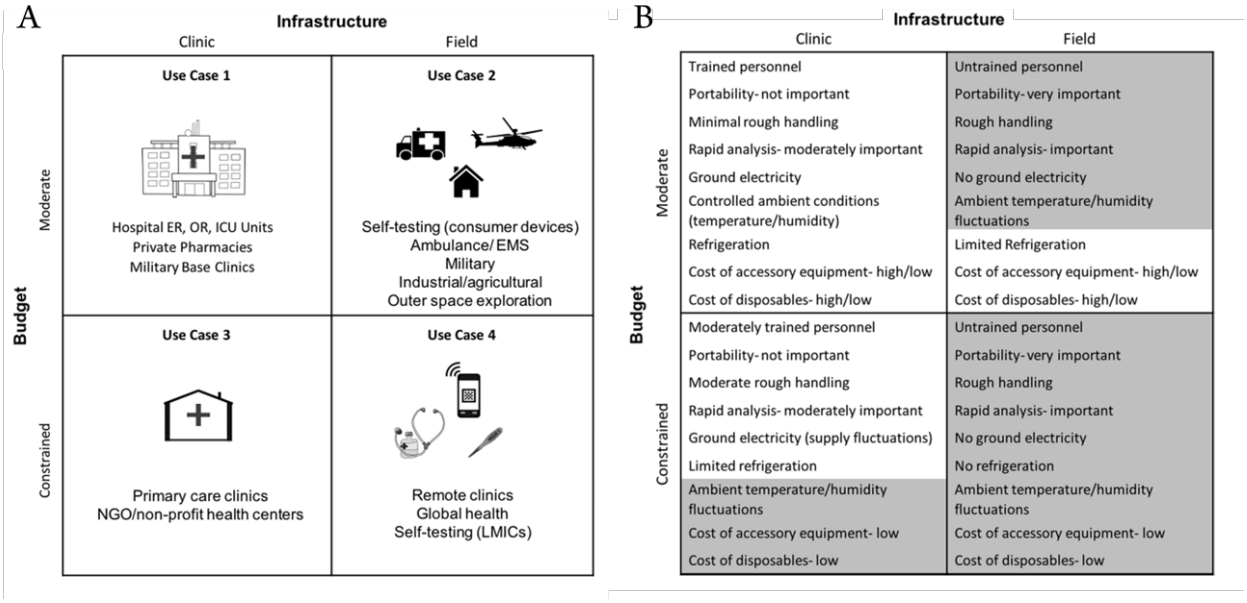

Figure 2.2. Graphical representation of use cases for diagnostics at the point of care. Use cases are broken down based on infrastructure and budget constraints (A). More detailed descriptions of the specifics of these use cases is also shown (B). Source: [6]

2.1.2 *Current point of care diagnostics*

The market for POC diagnostic testing was estimated to be $16 billion (USD) in 2016, and is anticipated to grow to $36 billion by 2021 [13]. As the market continues to grow, there has been a push for diagnostics that enable the prevention of disease, early disease detection, and management of chronic conditions [9]. The POC testing market was pioneered by the pregnancy test and the glucometer, both of which are used in the home by the end user for their respective purposes. However, the need for more diverse assays has led to a focus on microfluidic approaches, which are ideal due to their low volumes, ease of integration, and ability to create fully automated systems [14].

The most readily available commercial microfluidic approaches involve instrumented systems, where the microfluidic portion of the device is maintained with a chip or card, which is placed into a larger instrument that handles the fluidic handling and detection. The Cepheid GeneXpert is an example of a POC system that has been successfully implemented in a number of diagnostic settings. The GeneXpert is a sample in, result out system that uses a combination of

macro and microfluidics for nucleic acid detection [15]. Originally built to target *Mycobacterium tuberculosis*, this system has since been expanded to diagnose other infectious pathogens including enterovirus, methicillin-resistant *Staphylococcus aureus* (MRSA), *Clostridium difficile*, influenza virus, and chlamydia [16]–[19]. The GeneXpert machine itself costs approximately $17,000 (USD), not including hidden delivery and installation costs, with a cost per cartridge of approximately $17 depending on the presence of governmental and non-governmental subsidies [20]. The Quanterix developed Simoa analyzer is an example of a microfluidic system that is used for ultrasensitive protein detection, with a range of assays for clinical and research applications [21]. While this platform is the most sensitive protein assay on the market, the expense and overall instrument footprint limit accessibility for many potential applications. The Alere triage and Abbot iSTAT are two POC systems on the market that were designed to enable protein detection at the POC on a much smaller size scale, both of which have assays for a range of non-communicable diseases such as heart failure and endocrinology [22]–[24]. These instrumented systems are not without their drawbacks, as there is the additional need for temperature control and moderately trained personnel to complete the sample preparation required to run these laboratory tests [6]. Additionally, the cost and reliance on electricity make these systems inappropriate for certain use cases.

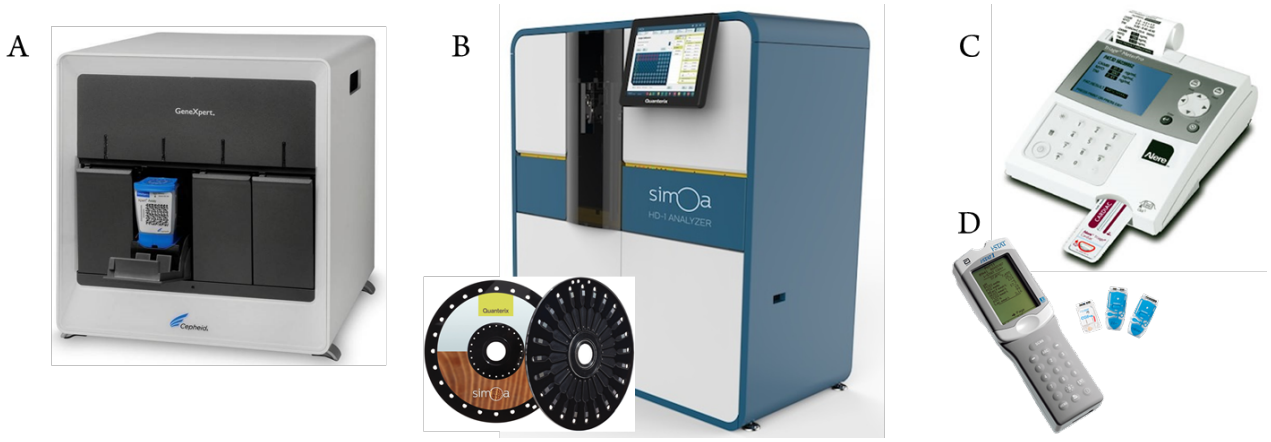

Figure 2.3. Examples of commercially available instrumented systems.
Most of these systems use cartridges for the detection of pathogens or other clinical biomarkers, and include the Cepheid GeneXpert (A), Quanterix Simoa (B), Alere Triage (C), and Abbott iSTAT (D). Sources: (http://www.microbeonline.com, http://www.quanterix.com, http://www.ultralabealtd.co.ke/triage-product.php#, and http://www.pointofcare.abbott)

Lateral flow assays (LFAs) are an example of an inexpensive diagnostic technology that has been highly successful in its implementation in a variety of point of care settings. This success can be attributed to their low cost, portability, and ease of use [2]. The pregnancy test is an example of an LFA that is commonly used and commercially available, with other applications ranging from diagnosing disease in humans to environmental heavy metal testing [3]. In the US, lateral flow assays are often used for clinical diagnosis, most commonly pregnancy, influenza, and streptococcus, while they are used primarily to diagnose infectious diseases such as human immunodeficiency virus (HIV) and malaria in low resource settings [10]. However, one of the major limitations of lateral flow assays is the complexity of assay that can be integrated into the simple, one-dimensional architecture.

2.2 PAPER MICROFLUIDIC APPROACHES TO POC TESTING

Various microfluidic approaches have been used to integrate complex assay steps into a simple, easy to use package. However, many of these approaches require additional machinery and expensive manufacturing techniques. Paper microfluidics, alternatively, build on the success of lateral flow immunoassays to enable the development of more complex diagnostic systems that can be easily implemented at the point of care. Paper is considered to be an ideal substrate to be used for the development of POC diagnostic devices due to its low cost, ability to move fluid passively through wicking, and demonstrated compatibility with a variety of analytical chemistry techniques [25].

2.2.1 *Paper-based microfluidics*

LFAs are one of the simplest paper-based devices, consisting of strips of nitrocellulose that wick fluid based on capillary flow without the need for pumps or additional machinery [26]. A sample pad is usually present at the "input" end, which is often a glass fiber pad onto which a sample is added. The sample then elutes into a conjugate pad, which is typically also a glass fiber material, in which reagents for the assay are stored in dry form and are rehydrated by application of a sample to the sample pad, **Figure 2.4**. A wicking or collection pad, often made of cellulose, is typically present at the opposite end to draw fluids through the rest of the device. A typical lateral flow assay has a test line and a control line orthogonal to the flow direction, both of which are zones in which capture agents have been deposited on the membrane. Presence of the target

analyte and adequate fluid delivery, along with rehydration of assay chemistry, is indicated by a change in color at the test and control lines, respectively. Pregnancy tests, which detect human chorionic gonadotropin, are examples of lateral flow assays commonly used for protein detection at the point of care [27], [28].

Key benefits derived from the porous nature of the membranes used in paper-based diagnostics, as compared to traditional microfluidic devices, include improved analytical performance, reduced cost, and electricity-free usage. This contrasts with traditional microfluidic devices that often require electronic pumps and costly fabrication. Paper-based diagnostics eliminate the need for complex machinery, pumps, and other electrical equipment by manipulating fluids with capillary forces through the pores of the paper membrane [25]. In addition, the porous nature of paper provides a large surface area over which protein adsorption and capture can take place [29]. Since the surface area-to-volume ratio (typically 50–200 times greater than that of the bulk material) is inversely related to the pore size of the paper substrate, assay performance may be optimized by simply tuning the physical properties of the paper substrate [25], [29], [30].

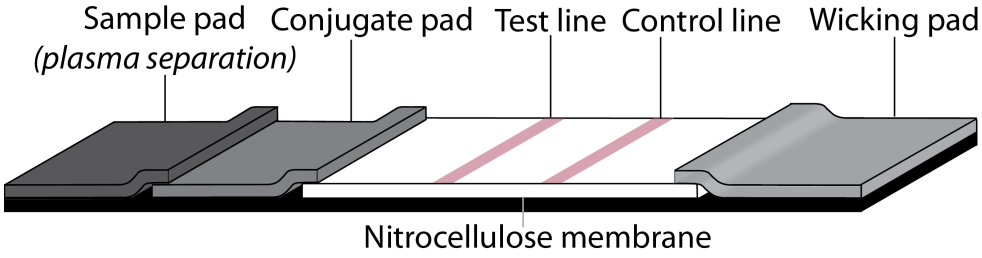

Figure 2.4. Drawing of a traditional lateral flow assay (LFA).
Includes the sample pad, conjugate pad where reagents are stored, nitrocellulose test strip with assay and control lines, and the wicking pad, typically made of cellulose.

Despite the commercial success of the urine-based pregnancy test, many other applications require more complex assays with additional reagent steps. Platforms such as the two-dimensional paper network (2DPN) format or microfluidic paper-based analytical device (μPAD) format enable the design of these more complex assays through selective or sequential delivery of reagents or fluids [25], [31], [32]. First published in 2010, the μPAD relies on patterning of a porous material like Whatman 1 with hydrophobic barriers, though other

fabrication techniques including photolithography, plasma etching, and laser cutting have been used. The μPAD traditionally consists of a sample application site, with legs that branch off to run different tests simultaneously, **Figure 2.5**. This technology has been used for a variety of applications, ranging from protein based clinical diagnoses to foodborne pathogens and nucleic acid detection [33], [34].

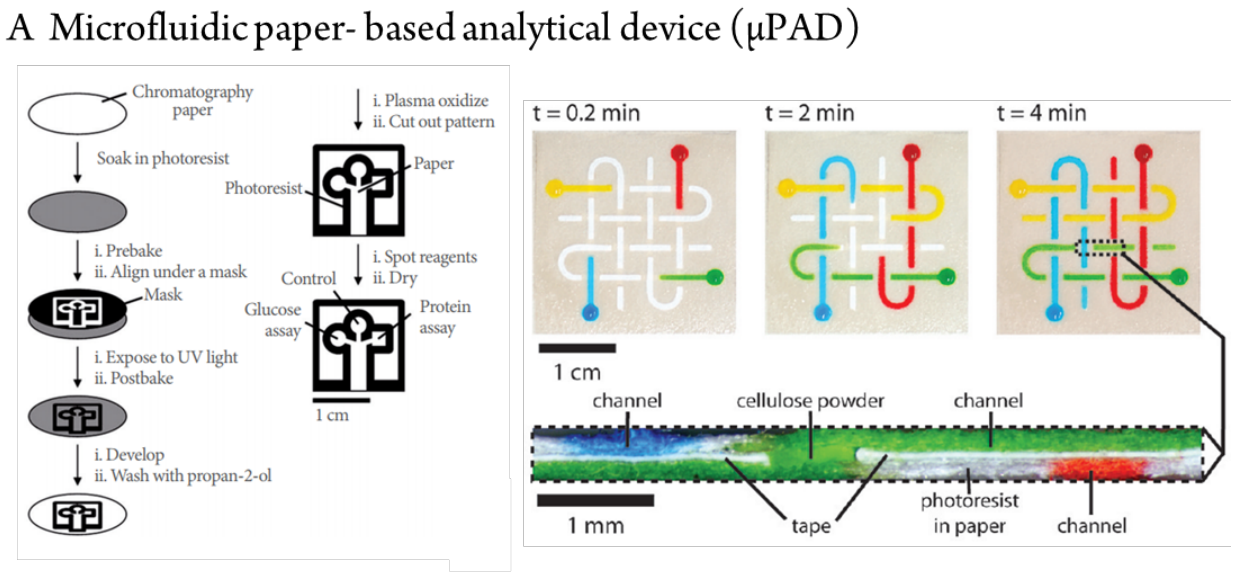

Figure 2.5. Paper microfluidic approaches for the integration of more complex assays. While a number of strategies have been developed, the most widespread approaches are the μPAD, which uses three-dimensional flow to carry out multi-step flow-through assays (A) and the 2DPN, which enables the sequential delivery of reagents using lateral flow (B). Sources: [25], [39].

The 2DPN provides an alternative approach to the integration of more complex assays into the paper microfluidic format. By using geometric variations, this format enables the development of paper microfluidics devices that integrate multi-step assays without increasing

the number of user steps from the LFA [35]. The traditional 2DPN uses subsequent legs to deliver reagents in a particular order across a test region **Figure 2.5**. The addition of bridges and valves has enabled the integration of timing components, controlling not only the order but also the exact time of delivery [36]. Variations of the 2DPN have been used for the development of assays for the detection of malaria and influenza proteins, and nucleic acids from streptococcus from samples including nasal swabs, blood and urine [37], [38].

2.2.2 *Paper Microfluidics - Materials and manufacturing*

There are a handful of materials that are commonly used for the development of paper microfluidics that have varying physical and chemical properties. Shown in **Figure** 2.**6**, these materials include, but are not limited to nitrocellulose, glass fiber, and cellulose. Nitrocellulose is a material most commonly used in lateral flow assays, as well as other molecular biology applications, due to the ability to easily adsorb proteins and create uniform and easily visualized test lines. Nitrocellulose is a polymer derived from cellulose, which is manufactured by either substituting the hydroxyl groups on each sugar unit with nitrate groups through treatment with nitric acid or by a process known as phase inversion [40], [41]. Phase inversion is the method used to manufacture most commercially available nitrocellulose membranes. In this method, porosity and pore size of the material can be controlled easily by adjusting the amount of non-solvent used, as well as other variables such as the temperature, evaporation speed, and humidity [40].

Glass fiber, which can be manufactured with or without binders to keep the material together, is often used to store reagents, as the larger pores can be easily blocked, filled with protein solutions, and lyophilized [42]. Due to the larger pore size, glass fiber materials also have the tendency to wick fluid more rapidly, helping to speed up reagent delivery. Cellulose is the material most commonly used as a wick, to pull fluid from all other membrane types, as the pores in cellulose are much smaller and therefore have a much higher capillary pressure. While these are the most commonly used materials, a range of other materials with other properties have been tested in paper microfluidic systems, such as polyethersulfone and Fusion 5 [43], [44]. Various combinations of the materials presented above can be used to create paper microfluidic systems to deliver assay reagents to a test line.

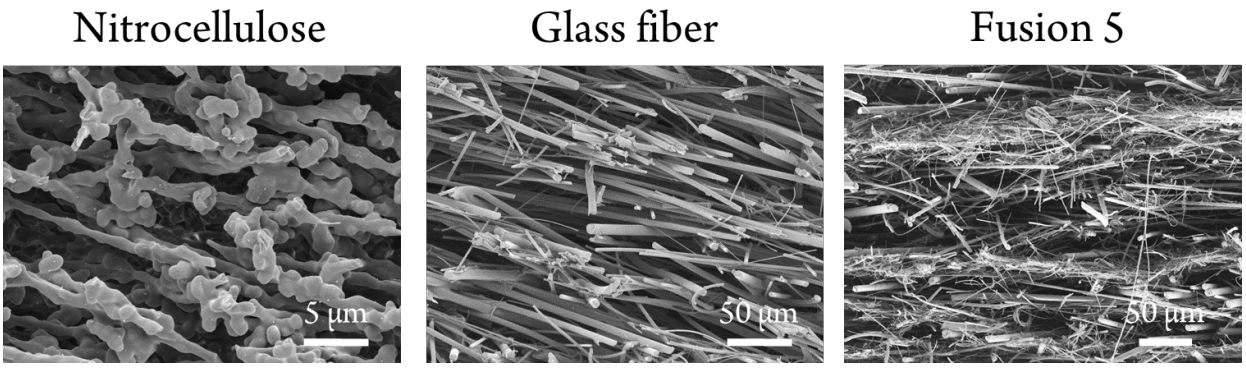

Figure 2.6. Scanning electron microscopy (SEM) images of LFA materials.
The membranes commonly used in lateral flow assay development include nitrocellulose (left), glass fiber (middle) and fusion 5 (right). Scale bars are shown on each individual image. Images taken by Dr. Joshua Buser (nitrocellulose and glass fiber) and Dr. Nerea Alayo (fusion 5).

Manufacturing of 2DPN and µPAD devices have been demonstrated using a variety of techniques, and can be divided into the following categories: patterning, reagent deposition, and flow control [25], [45]–[48]. Various manufacturing processes are used to fabricate the devices and control the movement of fluid through the device, which include photolithography, plotting, inject etching, plasma etching, laser cutting, and wax printing [25]. Reagent deposition into porous materials is typically done using patterning, inkjet printing, or striping techniques. Control of fluidic flow through these materials has been demonstrated using a combination of valves, wax deposition, and layering of materials with varying capillary pressures. These strategies can be combined with 3D printing, casting, or molding for the fabrication of device housing. While traditional lateral flow assays use visual readout for colorimetric change at the test line, the introduction of more quantitative assays and fluorescent detection techniques has lead to the development of quantitative readers and cell phones with filter sets.

2.2.3 *Flow in porous networks*

There have been a few models developed to described flow in porous networks, each of which has its benefits and drawbacks. Specific to lateral flow, the equations that are the most applicable include Lucas-Washburn equation, Darcy's law, and the Richards equation. Beginning with the Lucas-Washburn equation, is an equation designed to describe flow through porous matrices that assumes the material acts like a bundle of capillary tubes [49]. This equation

primarily applies to the "wet out", which is the time where a membrane is encountering liquid for the first time. Described in **Equation 2.1**, the Lucas-Washburn equation predicts that flow velocity decreases with time, which is consistent with experimental observations [50].

$$l(t) = 2\sqrt{\frac{k_s \gamma cos\theta}{\varphi \mu r_m}}\sqrt{t} \tag{2.1}$$

Where k_s is the permeability of the material, θ is the contact angle of the liquid with the material, γ is surface tension, μ is the viscosity of the fluid, t is time, and r_m is the mean pore radius. The assumptions made using the Lucas-Washburn equation are that flow is occurring (1) in a single pore radius (2) as one dimensional flow (3) in a single material (4) with a fully saturating fluid front and (5) no evaporation. However, Lucas-Washburn is unable to predict flow in systems that have multiple materials, partial saturation, or have 2 or 3-dimensional flow. Therefore, the prediction of flow using this equation is not applicable to systems like the μPAD and 2DPN. Alternatively, Darcy's law is commonly used to model flow in porous matrices, and is capable of modeling flow in two dimensions [51]. Darcy's law is described in **Equation 2.2** below.

$$Q = \frac{-\kappa A(p_b - p_a)}{\mu L} \tag{2.2}$$

Where κ is the permeability of the material, A is the cross-sectional area, P is the pressure, μ is the viscosity of the fluid and L is the length being measured. Darcy's law can be used for modeling "quasi" steady state flow, however there are a number of assumptions that are made with Darcy's lab that make it difficult to apply to model flow in porous matrices. The two assumptions that do not hold true are (1) that we have a fully saturating fluid front, and (2) that there is no evaporation. For these reasons, the Richard's equation is believed more appropriate for modeling flow in porous matrices [52]. The Richards equation incorporates partial saturation, as shown in **Equation 2.3**.

$$\frac{d\theta}{dt} = \frac{d}{dz}[K(\theta)\frac{dH(\theta)}{dz}] \tag{2.3}$$

Where θ is the volumetric water content, H is the hydraulic pressure head, z is distance and t is time. Work in our lab has demonstrated that the Richards model can be used for the modeling of fluid flow in these more complex systems with multiple materials [53]. In addition to modeling, understanding of the way partial saturation influences flow in porous matrices has enabled for the development of novel 2DPN device geometries. By using materials with different pore sizes, it is possible to control fluid flow within these devices. First demonstrated for the purification and concentration of DNA from urine, this fluidic tool opens the door for the integration of more complex geometries and laboratory assays [53], [54].

2.3 Molecular Recognition Elements

The analytical sensitivity of a lateral flow assay is first and foremost limited by the affinity of the binding elements for the target analyte [55]. As mentioned in the previous section, the sensitivity and specificity of protein–ligand binding is driven by the binding kinetics of the interaction. A sandwich assay requires a minimum of two specific binding events: capture of the analyte onto a solid surface by an immobilized ligand and detection of the analyte with a label conjugated to a second ligand. Capture and detection of an analyte can be through an antibody, a designed affinity protein, or an aptamer, among others. While traditional lateral flow assays utilize antibodies as the capture and detection elements of a sandwich immunoassay, antibodies cannot be applied to all diagnostic targets. In porous media, there are additional considerations during assay design regarding the strength of immobilization and ability to flow through a porous network for capture and detection. In this section, we will present mechanisms for sensitive, specific analyte binding, including recent work demonstrating the use of designed proteins and nucleic acids as binding elements for protein detection.

2.3.1 *Antibodies*

Antibodies are the most commonly used binding element for lateral flow immunoassays, building from their use in immunoblotting. As the workhorse of the adaptive immune system, antibodies are developed by a host to bind specifically to an antigen and direct the downstream immune response [56]. Antibodies can be raised in live animals, bacterial or eukaryotic cells, after which they are commonly purified by affinity chromatography [57]. Polyclonal antibodies are generated by the total antibody response for a given analyte, while monoclonal antibodies are

specific to one epitope of interest. Monoclonal and polyclonal antibodies can have different diagnostic applications due to their differences in specificity and production; therefore, their use depends on the assay and the analyte of interest. In both cases, each binding arm (F_{ab}) of an antibody serves as an epitope for binding, while the F_c region of the antibody has biological effector functions that can also be utilized. Integration of antibodies into lateral flow assays is facilitated by the fact that most antibodies adsorb robustly to nitrocellulose, such as in Western blotting applications [58], [59].

However, antibodies are limited in their diagnostic applications by a variety of factors. The most prominent of these factors is that production of antibodies is typically both labor intensive and expensive [57]. Challenges include a lack of stability under extreme pH and temperature, batch-to-batch variability, limited control over functional sites, and the inability to target nonimmunogenic or toxic analytes [60]–[62]. A number of these limitations have been addressed through the production of antibody fragments that contain just the single chain or multivalent fragments [63]. These antibody fragments can be grown in bacteria, and therefore are much less expensive to manufacture and have greater specificity control. However, this only applies to targets for which antibodies can be produced in the first place, and not all antibodies can be broken down into smaller pieces and remain stable. Nanobodies, which are recombinant, antigen-specific, single-domain variable fragments produced in camelids, provide an alternative approach due to their size and stability, however their use as molecular recognition elements in lateral flow assays has been somewhat limited [64].

2.3.2 *Aptamers*

One class of binding molecules that has been utilized in place of antibodies is aptamers. Aptamers are oligonucleotides (DNA or RNA) that can fold into well-defined secondary, tertiary, and quaternary structures [65]. They are easily amplified by polymerase chain reaction (PCR), which can be done in a variety of conditions that are not restricted physiologically [65], [66]. Manufacturing of aptamers that bind to a particular target is accomplished through a process known as systematic evolution of ligands by exponential enrichment (SELEX). SELEX screens large combinatorial libraries of oligonucleotides; they are then further refined using iterations of in vitro selection and amplification [67], [68]. Higher affinity can be selected

through additional rounds of enrichment. This process is similar to the production of proteins through the evolutionary design process.

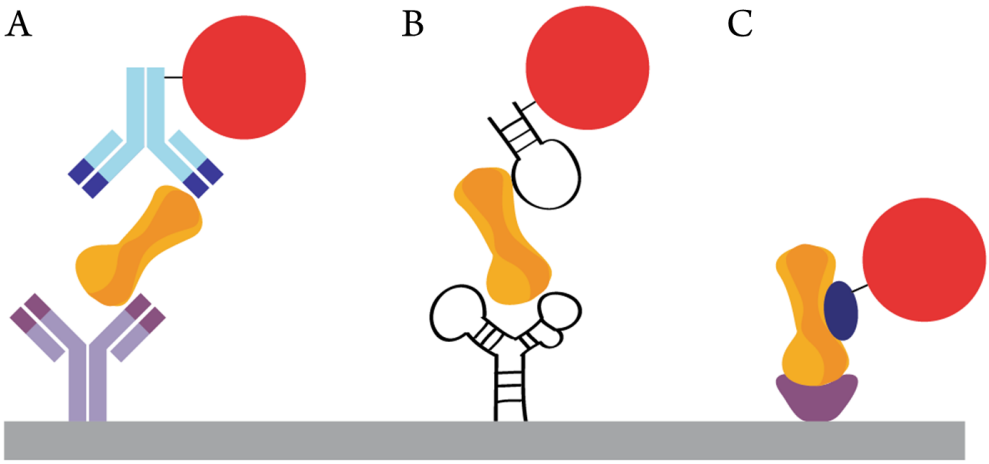

Figure 2.7. Drawing of assay stacks using different molecular recognition elements. In this case, for the capture and detection of recombinant hemagglutinin (HA). In all three cases, the capture and detection elements were raised or designed to target different epitopes of the HA protein. (A) Antibody detection of recombinant hemagglutinin (B) Aptamer capture and detection (C) Affinity protein detection. Note that the molecular components are not to scale.

Aptamers retain many of the benefits of designed affinity proteins, which include ease of production, low cost, and improved stability. They can be produced to bind any target, even ones that are non-immunogenic or toxic. Because aptamers are nucleic acids, they have the ability to return to their tertiary structure after being unfolded by heat or pH [69]. This property is beneficial in the context of point-of-care diagnostics that need to have a long shelf life under variable temperature and humidity. Aptamers, like affinity proteins, can be designed with a single reactive group for site-specific conjugation to facilitate assay development [65]. To this day, aptamers have not been successfully demonstrated for as wide a range of targets as antibodies. This is in part because polynucleotides do not possess the full range of chemical moieties as are presented by amino acid side chains.

2.3.3 *Designed affinity proteins*

Affinity proteins are a class of proteins that have been utilized for the development of assays for the detection of target analytes. These proteins are expressed recombinantly in bacterial cells, enabling production that is both much simpler and lower cost than for monoclonal antibodies. In the case of lateral flow assay development, antibodies cost, on average, $0.01USD per test, whereas recombinant affinity proteins cost approximately $0.0006USD per test. One approach to develop proteins that bind to a target of interest is computational (*de novo*) design, in which the tertiary structure of a protein is predicted based on primary amino acid sequence [70]. This design concept, also known as rational molecular design, utilizes molecular approximations that generally require further affinity maturation that enables improvement in binding affinity. Another mechanism for the development of binding proteins is phage display, which is instead based on evolutionary molecular design [71], [72]. Phage display typically utilizes a randomized library that is made through any of a variety of mutation techniques to create protein variants that bind to the target of interest and is expressed on the exterior of the phage; tight binders are identified by a simple filtration, and the binding protein(s) are then amplified from the nucleic acid encoding it in the phage itself. Affinity maturation is also used with phage display to develop proteins with successively higher affinities.

One of the advantages of affinity proteins is that they can be designed to bind a specific epitope on a target protein, providing more control in the development of a sandwich assay. As these proteins are expressed in bacteria, they can be produced rapidly and inexpensively. Designed proteins can also be expressed with additional functionalities, such as a functional group for conjugation to a fluorescent label or a paper-binding protein [73]. Despite these benefits, proteins generated using *de novo* design require the existence of a high-resolution structure for the analyte of interest. As these crystal structures do not account for movement, and may represent a minority structure present in solution, predictions of proteins that will bind to a specific epitope can be incorrect. Additionally, there are often some conformations of an analyte for which protein prediction is additionally difficult. One example of this is the hemagglutinin (HA) protein on the influenza virus. In the California/09 strain of H1N1, there is a mutation in the sialic acid binding pocket, which makes it difficult to design a protein that can effectively bind in that pocket. While evolutionary design more closely replicates the mutations that take place in antibody production in vivo, it is limited in the degree of mutation that can be made to a

single protein without significantly altering the overall structure, function, and stability of the protein [74]. In the case of both rational and evolutionary design, the developed proteins can be evolved to have specific desired properties, such as stability under specific or varying pH or temperature conditions [75], [76].

2.4 CRITICAL FUNCTIONS OF MOLECULAR RECOGNITION ELEMENTS FOR LFAS

There are two functions required of a molecular recognition element to enable successful integration into a lateral flow assay; that it can be immobilized in the porous matrix, and then subsequently bind the analyte of interest. Antibodies, which are traditionally used in LFAs, are fairly straightforward to immobilize and capable of analyte binding after immobilization. With the introduction of new molecular recognition elements, it is crucial that they can be effectively immobilized in a manner than they can subsequently bind the target analyte. The following sections will describe immobilization and analyte capture in more detail within the context of lateral flow assay design and development.

2.4.1 *Immobilization onto porous matrices*

A critical requirement for the capture molecule in a lateral flow assay is that it is effectively immobilized onto the porous membrane. Classification of immobilization techniques can be binned into three larger categories; physical methods such as those that rely on electrostatic interactions or size, biological or biochemical methods that rely on a binding event to prepare the surface, and chemical methods such as covalent attachment and crosslinking, **Figure 2.8** [77]. Immobilization strategies can be compared based on their difficulty of the technique, overall capacity of the membrane for the protein of interest, stability of the immobilized protein over time, availability of the protein to bind a target analyte, and cost.

Physical methods for immobilization rely primarily on physical forces to stick a capture entity to the surface. Direct adsorption is the easiest and most commonly used physical method for immobilization in a porous matrix [58]. It has been proposed that protein adsorption to nitrocellulose is influenced primarily by electrostatic interactions, hydrogen bonding, and the hydrophobic effect [78]. Advantages of this technique are that it is fairly easy and can be stable over long periods of time, while limiting the need for specialized machinery, chemical modifications, or washing steps. Major limitations of using adsorption for immobilization is that

it is not orientation specific and does not work for all capture molecules. An alternative physical method for immobilization is entanglement, which relies on the size of the pores within a membrane to physically confine a larger entity. Entanglement has been used to create test lines in Fusion 5 by trapping beads within the porous material that can be functionalized with a range of capture molecules [44]. While entanglement is fairly easy to implement and inexpensive, this technique is a weak and non-permanent interaction with the potential for strong washing to remove the trapped entity and thereby reduce the number of biomolecules available for binding in the test zone.

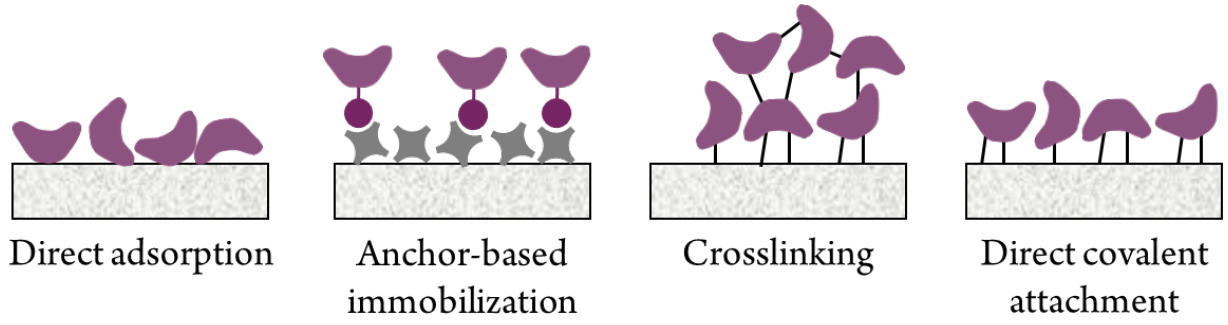

Figure 2.8. Drawing of different strategies for protein immobilization in nitrocellulose. This is specifically focused on methods that have been demonstrated in the literature. While there are many effective strategies, direct adsorption is commonly used, along with anchor-based immobilization, chemical crosslinking, and direct covalent attachment. Note that the molecular components are not to scale.

Biological and biochemical methods for immobilization require binding of the capture molecule to the physical support, which is nitrocellulose in most lateral flow assays. Also known as anchor based immobilization, this technique addresses the challenges faced by traditional adsorption by separating the capture molecule from the portion that adsorbs to nitrocellulose. One example of this technique for immobilization in the LFA context involves the use of streptavidin adsorbed at the test line, with a biotinylated capture molecule that flows across the test line and binds to the streptavidin immobilized there [58]. This method has proved optimal for other capture systems because it is strong, specific, reversible, and can be orientation specific for the capture molecule [77].

Chemical methods for immobilization require chemical modification of either the support material or capture molecule. Direct covalent attachment is a method commonly used for site directed immobilization in an irreversible, highly reproducible fashion. This has the potential to generate the most optimal binding surfaces for an analyte of interest, however these techniques are not without their drawbacks. The majority of chemical methods demonstrated for immobilization of biomolecules to porous materials are labor intensive, require harsh solvents, or other hazardous materials. Additionally, the treatment that is used to perform the covalent coupling can lead to the modification or alteration of the structure or bioactivity of the capture molecule being immobilized [77]. While a number of techniques for the modification of cellulose to enable covalent coupling of a biomolecule have proved successful, the few attempts to create modified nitrocellulose membranes performed poorly due to their lack of stability long term [58]. Chemical crosslinking of a biomolecule can reduce the influence of microenvironment changes due to the various surface treatment techniques, and is therefore most commonly used for the immobilization of enzymes, which are particularly sensitive to such changes [79]. However, crosslinking faces many of the same challenges of other chemical methods, specifically the need for added complexity to generate a surface immobilized with the biomolecule of interest.

2.4.2 *Binding Kinetics in Porous Networks*

The second critical requirement of a molecular recognition element is the ability to bind to an analyte of interest under lateral flow. The affinity of these two elements for one another are particularly important, as they influence the overall analytical sensitivity of a lateral flow assay [55]. Such affinity, and the corresponding binding kinetics, is dictated by the summation of the interactions between a protein and the ligand to which it binds. These binding interactions consist of a number of molecular forces, including charge–charge interactions, hydrogen bonds, hydrophobic interactions, and van der Waals forces. Note that these forces are influenced by the fact that the binding element is immobilized on a matrix that has its own contribution to the forces felt by the ligand.

In this section, we will consider the role of binding kinetics in assay sensitivity, with special consideration of the influence of reagent delivery. The underlying kinetics of a binding reaction can provide insight about the interaction between an analyte and a ligand. Interpretation

of a binding event can be directed by an understanding of the underlying kinetics of a reaction between an analyte and a ligand. A simple binding reaction involves an analyte (A) and a ligand (L), which reversibly forms a bound complex (AL). As shown in **Equation 2.4**, the conversion between association and disassociation is determined by the dissociation constant, K_D. Three factors that should be taken into consideration are (1) the concentrations of protein and ligand that are present, (2) the concentration of complex that is formed, and (3) how quickly the complex breaks apart [80]. These three factors enable quantitative interpretation of a binding event within a Michaelis–Menten kinetics framework [81].

$$A + L \overset{K_D}{\Leftrightarrow} AL \tag{2.4}$$

The dissociation constant (K_D) of a reaction is defined as the rate at which the binding reverses (k_{off}) divided by the rate at which the complex associates (k_{on}). With these rate constants, concentration does play a role in the amount of complex that is formed since the observed net rate of formation (or dissociation), $k_{obs} = k_{on}[analyte] - k_{off}$. As the local concentration of a protein or analyte is increased, the probability of a collision between the two molecules, and subsequent binding event, also increases. When considering binding at a test line, the local concentration in the microenvironment of test line influences the observed on rate for this interaction. Therefore, the transport of a protein to the test line through either convection or diffusion influences the rate at which a binding event can take place.

While traditional methods to measure reaction kinetics are able to provide an estimate for the kinetics of a binding interaction, the rate constants determined by kinetic measurement systems might not necessarily translate directly into those relevant in paper microfluidic systems. This is primarily due to two properties of lateral flow assays: (1) the constant movement of fluid by capillary action and (2) porous nature of the membrane. There are additional effects from the matrix itself, effects that can be seen whether or not a surface has been passivated by a blocking protein such as bovine serum albumin (BSA). Porosity is a measure of the empty space in a material and serves as a key parameter in the design of the lateral flow assays [82]. The larger the void space, or mean pore size, the smaller the surface area-to-volume ratio is for a given segment of membrane. When a ligand is immobilized onto the exposed surface area of a test region, larger amounts of protein can be deposited on membranes with smaller pore sizes.

However, as pore size decreases, overall assay speed can suffer as the flow rate is reduced. While this may increase the probability of a collision event as the distance to diffuse to the surface decreases, the primary tradeoff is an increase in time from sample to result.

Experimentally determined rate constants provide insight into the affinity between a protein and a ligand that can translate to improved performance of an assay integrated into a paper microfluidic system. Specifically, empirically determined association and dissociation rate constants may shed light on the kinetics of assay binding for varying reagent delivery formats in porous media [83]. Reagent delivery can be either sequential, in which each reagent is delivered independently across the test line, or premixed, in which the analyte and detection stack are mixed before they are delivered to the test region. The Fu group has demonstrated a 4- to 10-fold improvement in the limit of detection for the malaria antigen PfHRP2 using the sequential delivery format [83]. In contrast, recent work has also shown an improved limit of detection for the influenza nucleoprotein using the premixed delivery format [84]. While the underlying mechanisms are not yet fully understood, the difference in performance of these two assays is likely due to differences in antigen binding; this could include multivalency of the antigen, kinetics of binding of the antibodies, or the size of the bound analyte–ligand complex. The overall assay performance is therefore influenced not just by the affinity of the binding elements, but also by the manner in which they are delivered across the test region.

2.5 GAPS IN THE LITERATURE

We identified two key gaps in the literature related to the use of computationally designed proteins in paper-based diagnostics that will be addressed in this dissertation.

(1) While computationally designed affinity proteins have been demonstrated to be effective as therapeutics, and initial validation of these proteins has been demonstrated in paper diagnostics, the clinical application of these proteins for diagnostic applications has not been thoroughly investigated. Their use for infectious disease diagnostics could provide a less expensive and more customizable alternative to antibodies as a reagent for the development of point of care diagnostics for protein detection.

(2) Although there has been significant work in the development of paper architectures and protocols for the long-term storage of proteins for various microfluidic applications, including paper based systems, these systems have not previously been applied to this new class of affinity proteins. Designed to be both inexpensive and highly thermostable, these proteins are ideal for the implementation into lateral flow assays for use at the point of care.

The work presented herein will explore this space, including the development, application, and optimization of computationally designed affinity proteins for their application to the detection of disease at the point of care.

Chapter 3. ASSAYS FOR THE DETECTION OF THE INFLUENZA VIRUS USING COMPUTATIONALLY DESIGNED PROTEINS

3.1 BACKGROUND

Influenza, commonly known as the flu, infects 5-20% of Americans each year, accounting for 15 to 60 million infections annually [7]. These infections lead to over 200,000 hospitalizations and an average of 23,000 deaths in the U.S. alone each year, making the flu deadlier than HIV and cervical cancer combined [7], [85], [86]. While the flu is especially problematic for young children, pregnant women, the elderly, and people with other health conditions, the flu can also be a severe respiratory disease for otherwise-healthy adults. This is especially true for specific flu strains [87]. During the 2013-2014 flu season, adults 18-64 years old accounted for the majority of flu-related hospitalizations and deaths [88].

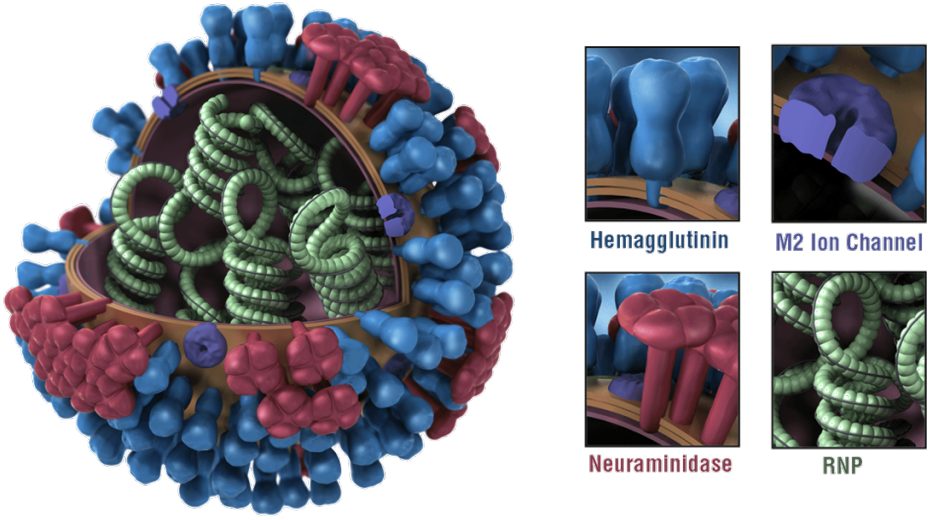

Figure 3.1. Drawing of the influenza virus and important proteins.
Images of the virus (left) and the four proteins critical for virulence; hemagglutinin, neuraminidase, M2 ion channel, and ribonucleoprotein (RNP). Source: (cdc.gov).

In addition to being a significant health problem, the flu is also an enormous financial burden. A study on the economic burden of flu found that influenza costs the U.S. economy $87B each year, including direct medical costs, loss of productivity, and loss of economic value due to early [89]. Despite these grim numbers, the flu is treatable. Antiviral medications such as

Tamiflu®, also known as oseltamivir, are available for treatment of most influenza strains and have been shown to reduce the severity of symptoms, shorten the duration of illness, and decrease the risk complications—but only when prescribed within the first 48 hours of symptoms [7], [90]. Timely and accurate diagnosis of influenza is therefore the first line of defense against the virus and key for successful disease management.

Influenza is a single stranded RNA virus that is known to infect humans as well as a range of other animals, including pigs and birds. The virus has eight RNA segments that code for a total of 11 viral proteins for some strains of the virus [87]. Key proteins of the virus are the surface proteins hemagglutinin and neuraminidase, responsible for receptor binding and virion release respectively, the nucleoprotein, which forms the ribonucleoprotein structure with the viral RNA, and the M2 membrane protein which serves as an ion channel, **Figure 3.1**. While there are three strains of influenza known to infect humans, influenza A, B, and C, influenza A is known to cause the most severe clinical symptoms among the three. Influenza A can be further divided into subtypes, which are described by the specific hemagglutinin (HA) and neuraminidase (NA) on the surface of that subtype. There are currently 18 known subtypes of HA, and 11 subtypes of NA, which can lead to many different combinations of the two proteins [88]. Of the 198 possible combinations, only three strains of Flu A have lead to human pandemics, H1N1, H2N2, and H3N2 [91]. There are two influenza A subtypes currently circulating among the human population, H1N1 and H3N2, though the distribution of infectious varies annually, **Figure 3.2**. In addition, there are some subtypes that occasionally lead to illness in humans who have close contact with animal reservoirs, such as the highly pathogenic influenza virus H5N1.

As an RNA virus, influenza is constantly evolving to evade the human immune system, through processes known as antigenic drift and antigenic shift [92]. Antigenic drift is the process by which small mutations occur over time, even during the course of one influenza infection, that eventually result in viruses that are antigenically different from the original [93]. The mutations we see occur between flu seasons are examples of antigenic drift. Antigenic shift, on the other hand, typically occurs when a new subtype jumps from an animal reservoir into humans, with antigens that are so different from the human version of that subtype that most humans do not have immunity to the new virus [94]. One example of antigenic shift is the H1N1 pandemic that occurred in 2009, which lead to an estimated 60 million cases in the United States alone [95].

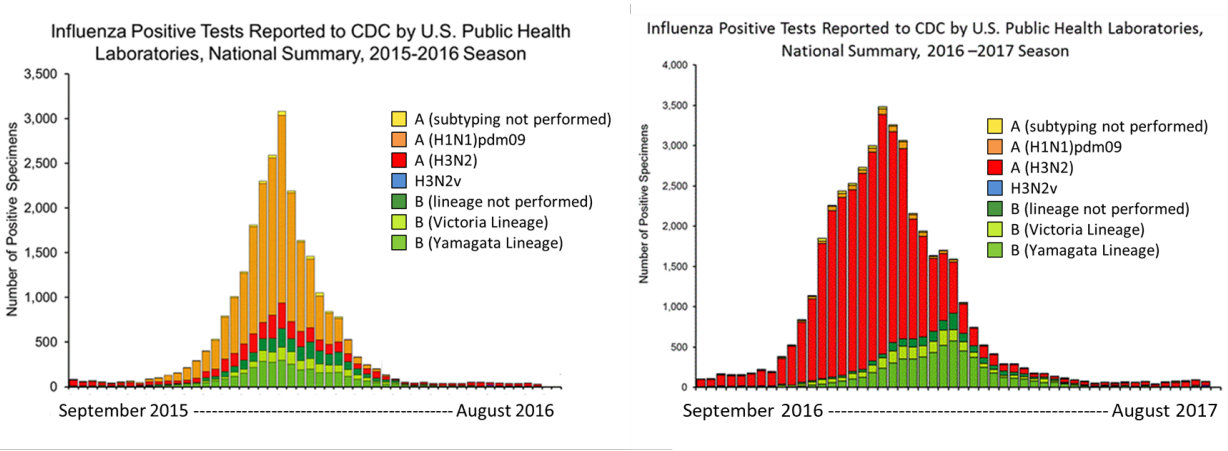

Figure 3.2. Number of influenza positive tests reported to the CDC since 2015. There was an obvious shift between the two flu seasons with regards to the strain distribution, as visible by the colored bars. In these graph, non-subtyped flu A is shown in yellow, H1N1 from the 2009 pandemic strain in orange, H3N2 in red, and a variant of H3N2 in blue. All flu B strains are shown in shades of green. Source: www.cdc.gov/flu/weekly/index.htm.

Given the importance of influenza diagnosis, several lateral flow-based rapid diagnostic tests (RDTs) have been developed for point-of-care detection of influenza. It has been demonstrated that the correct use of an RDT for influenza can significantly reduce the cost of treatment, time of hospitalization, and minimizing the incorrect use of antibiotics versus antivirals [96]. Commercially available RDTs are based upon detection of the internal nucleoprotein, which require lysis of the influenza virus and can potentially add complexity to the integrated assay [8]. Alternatively, detection of intact virus is an attractive option for simple point-of-care tests, in which sample pre-processing must be minimized or eliminated. Not only does this strategy minimize the sample prep required, the presence of approximately 500 HA molecules on the surface of the intact virus enables multiple detection events for every virus captured, as seen in **Figure 3.1** [97].

Hemagglutinin (HA) is a valuable diagnostic target for influenza, as it is both an antigen targeted by the human immune system and is used to identify the subtype of the infecting flu virus (e.g., H1 vs. H3). While HA undergoes a high degree of antigenic drift, driven, in part, by pressure to evade the host immune system, highly conserved areas exist that are crucial for viral function and replication [98]. For example, the receptor binding site of the head region undergoes limited variation, as it is required for attachment of the virus to the host cell through

sialic acid moieties [87], [99]. The stem region of the HA protein, which is involved in conformational changes critical to endosomal escape, has also been demonstrated to be highly conserved [100]. Careful epitope selection is therefore essential for design of a diagnostic assay to target HA.

Antibodies are traditionally used for protein capture and detection in lateral flow assays due to their affinity, specificity, and ability to adsorb strongly to nitrocellulose [46], [101], [102]. However, their utility is limited by the large batch-to-batch variability and high production and purification costs associated with current commercial antibodies, as described in Chapter 2. Similarly, aptamers have been demonstrated for the detection of HA, however the process for selection (systematic evolution of ligands by exponential enrichment; SELEX) requires significant resources and often fails to yield molecules with suitable binding affinities [82], [103]–[105]. Our approach for sandwich (immuno)assay development for influenza involves the use of computationally designed (*de novo*) affinity reagents. *De novo* design of recombinant affinity proteins enables the development of binding proteins to target highly specific epitopes on the hemagglutinin protein.

Computationally designed recombinant affinity proteins have been designed by our collaborators to bind the stem and head regions of HA (**Figure 3.3**). These two epitopes each play a unique role in influenza infection; the head region serves to bind sialic acid on human lung epithelial cells, while the stem region acts as a hinge to enable membrane fusion with the human epithelial cell. Design of affinity proteins to the highly-conserved stem region was guided by the discovery of neutralizing antibodies to HA, the binding of which block the pH induced refolding of HA [75]. The "stem region binder" used in this work was a designed scaffold that underwent affinity maturation, containing a group of helices, one of which packs tightly into the hydrophobic grove on HA. Alternatively, our "head region binder" targets the readily accessible sialic acid receptor-binding site that enables attachment of the virus to human epithelial cells. The head region binder was designed to be a trimer with the same C3 symmetry and spacing of the HA trimer, thereby maximizing the avidity of binding through association with all three epitopes [106]. Influenza virions are densely covered with HA trimers, which provide many sites for attachment of either head or stem region binders.

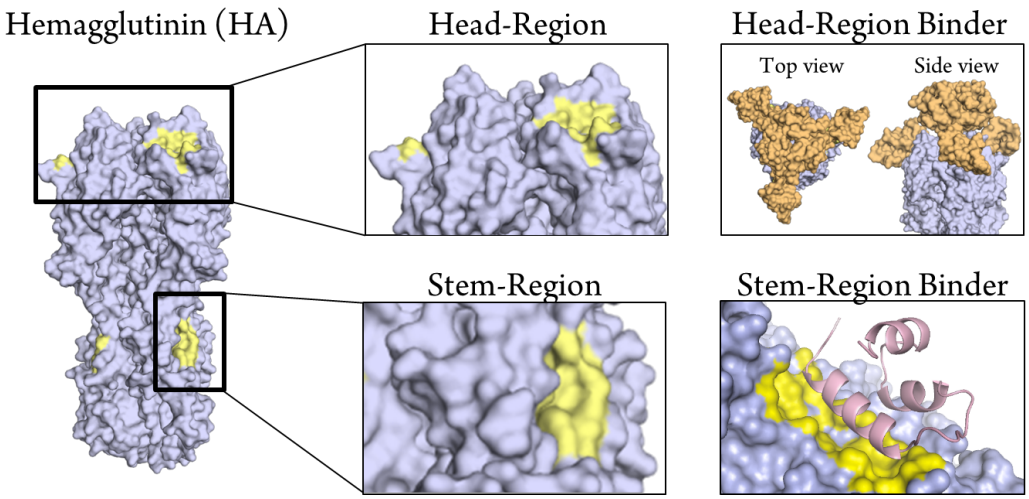

Figure 3.3. Illustrations of the influenza virus and targeted sites for binder development. The hemagglutinin protein is shown in purple. Images at the left and center show the two classes of conserved sites (in yellow) to which the synthetic binders were designed to target. The images on the right show HA bound to the computationally designed head region binder (orange, top) and stem region binder (pink, bottom). Detailed information about the binder proteins can be found in the following references [70], [106].

This aim describes the development of a set of paper-based assays for detection of the influenza surface protein hemagglutinin (HA) using a combination of de novo proteins and antibodies. The overarching goal of this aim is the demonstration of an assay that enables detection of native hemagglutinin with clinically relevant sensitivity. This work is divided into the following sections:

- Development of an assay for the detection of HA using combined stem and head region binders.
- Development of an assay for the detection of native HA from intact influenza using an all head region binder based assay.

3.2 Materials and Methods

Membrane Preparation. Nitrocellulose membranes (GE FF80HP, GE Healthcare, Piscataway, NJ) were cut into test strips using a CO_2 laser cutter (Universal Laser Systems, Scottsdale, AZ). Each test strip was 3 mm wide by 24 mm long, and sets of 4 strips were cut

together and connected by a 6 mm tall section at the top of the device in order to promote batch processing using a microplate. The distance between strips was 6 mm, designed to allow each set of strips to fit into the wells of a 96-well plate. Capture proteins were deposited onto the membrane strips to form test lines using a piezoelectric printer (sciFLEXARRAYER S3, Scienion AG, Berlin, Germany). Head region binder (Trimer 11) was prepared at 0.7 mg/mL (10 μM), capture antibody (Influenza Reagent Resource (IRR) #FR-504, mouse monoclonal anti-influenza hemagglutinin antibody) was used at its stock concentration of 0.5 mg/mL (3 μM), and nitrocellulose binding streptavidin (AbCam #ab51404) was prepared at 1 mg/mL. All protein solutions were prepared in phosphate-buffered saline (PBS, pH 7.4, Sigma-Aldrich, St. Louis, MO). To avoid clogging the printer with particulate matter from the samples, the protein solutions were filtered through a centrifugal filter device with 0.2-μm nylon membrane (VWR, Radnor, PA) at 6000×g for 5 minutes prior to spotting. Test lines consisted of 12 spots spaced 250 μm apart, with 30 droplets per spot, and two passes were printed for each test line in order to saturate the membrane region. Each droplet was 450-500 pL, resulting in test lines comprising ~300 nL of protein solution in total.

Head and stem region binder manufacturing. The additions and mutations of all computationally designed proteins was done using Rosetta software suite (www.rosettacommons.org). The head region binder, variant Tri-HSB.2, was cloned into the pET29b expression vector between the NdeI and XhoI restrictions sites with an additional C-terminal cysteine residue (as described in Strauch et al). The protein was expressed in BL21* (Invitrogen) cells using autoinduction and media supplemented with TB(Difco)33. The protein was purified using standard Ni-NTA purification and PBS-based buffers. Elution was achieved using 250 mM imidazole supplemented with 2 mM DTT to avoid oxidation of the cysteines. The stem region binder, variant HB36.5, was cloned, expressed into E. coli, and purified using metal affinity chromatography using Ni-NTA resin to recognize C-terminal His tags. Biotinylated versions of the protein was created by the addition of a C-terminal AVI tag at the genetic level, and biotinylation occurred after purification using the biotin protein ligase BirA [70]. This resulted in a stem binder with a single biotin on each binder. Proteins were stored in PBS with a pH 7.4 at -80°C and thawed before use.

Gold nanoparticle conjugation. For conjugation, the head region binder underwent buffer exchange into PBS using a desalting column (P10-GE) and was then incubated with

maleimide-activated gold nanoparticles (Innova Biosciences) for 6 h at 25°C and for another 8 h at 4°C before the conjugate was purified by centrifugation at 9,000×g for 10 minutes to remove unconjugated binder. The antibodies used for detection in the all antibody assay were conjugated using the same conjugation kit. They were incubated with the maleimide-activated gold nanoparticles for 15 minutes at 25°C before purification by centrifugation at 9,000×g for 10 minutes to remove unconjugated antibody. All gold conjugates were stored at 4°C until use.

Horseradish peroxidase conjugation. For conjugation, the head region binder underwent buffer exchange into PBS using a desalting column (P10-GE) and was then incubated with maleimide-activated horseradish peroxidase commercial conjugation kit (ThermoFisher, Waltham, MA, USA) for 6 h at 25°C and for another 8 h at 4°C. Each head region binder was estimated to be conjugated to between 0 and 3 HRP molecules each, and stored at 4°C until use.

Hemagglutinin Detection Assays. Each assay was performed using a dipstick lateral flow format with a 96-well plate pre-loaded with the given assay reagents into which the nitrocellulose membrane is manually placed for each step. The novel "assay stack" demonstrated herein used the head region binder for capture and monoclonal antibody for detection. Recombinant HA, virus, and anti-influenza antibodies were acquired from the International Reagent Resource (previously Influenza Reagent Resource), WHO Collaborating Center for Surveillance, Epidemiology and Control of Influenza, Centers for Disease Control and Prevention, Atlanta, GA, USA. Phosphate-buffered saline (PBS) + 0.1% v/v Tween-20 (Fisher BioReagents #BP337, Thermo Fisher Scientific, Waltham, MA) (PBST) was used as the wash buffer in all cases. All non-wash reagents were diluted in a running buffer of PBST + 1% w/v bovine serum albumin (BSA, Sigma-Aldrich #A7030) (PBST+BSA). Both the recombinant HA antigen (IRR #FR-67) and cultured influenza virus (IRR #FR-331) were from the A/Solomon Islands/03/2006 (H1N1) strain of influenza. Detection antibody (IRR #FR-502) was developed for this strain of HA as well, and it was used at 100 nM. gold-conjugated secondary antibody ("Au-2°," Au-goat-anti-mouse IgG, Arista Biologicals, Inc., Allentown, PA) was purchased commercially. For the all-antibody assay, detection antibody was conjugated directly to gold label as described in the previous section. The assays were all run by the sequential delivery of each reagent, unless otherwise stated, with PBST wash steps in between using a 96 well plate to deliver the 20 µl used in each step. Recombinant HA was tested at concentrations of 78 nM, 15 nM, 3 nM, 625 pM, 125 pM, 25 pM, and 5 pM. Influenza virus was tested at 1.25×10^8, 2.5 x

10^7, 1.25 x 10^7, 2.5 x 10^6, 1.25 x 10^6, 2.5 x 10^5, and 1.25 x 10^5 chicken embryo infectious dose ($CEID_{50}$/mL), with four replicates per concentration. Buffer-only (PBST+BSA) negative controls were also tested. After each assay was complete, all devices were taped to a standard piece of printer paper and imaged at 48-bit HDR color, 600 dpi, $\gamma = 1$ using a desktop scanner (Perfection V700 Photo Scanner, Epson, Long Beach, CA).

Signal Quantification. All signal intensities from test lines were quantified using a custom script in MATLAB (MathWorks, Natick, MA). Using this program, a region of interest (ROI) was drawn around the test line of interest, and the average pixel intensity inside this test ROI, I_{test}, was determined. After background subtracting the average pixel intensity, I_{bkgd}, the resulting value was then normalized on a scale from 0 to 1 to generate the normalized pixel intensity of the spot, I_{norm}, using **Equation 3.5**.

$$I_{norm} = \frac{I_{test} - I_{bkgd}}{0 - I_{bkgd}} \tag{3.5}$$

For the assay data herein, all colorimetric signals were generated using either gold nanoparticles or precipitated DAB. Because gold nanoparticles are red, the green channel of the RGB image was used for analysis. For DAB, which is yellow/brown, the blue channel of the RGB images was used for analysis. Overall, the normalized pixel intensities represented a range from no signal (0) to maximum (fully saturated green channel) signal. For significance testing between two sets of data, Welch's t-test was used (also known as Student's t-test with unequal variances). Unless otherwise specified, a significance threshold of $\alpha = 0.05$ was applied. Where given, statistical limits of detection (LODs) were calculated based on the signal level corresponding to a 5% chance of false-positive signal and 5% chance of false-negative signal, mapped to the associated HA concentration using a four-parameter logistic curve [107], [108]. The 95% confidence interval (CI) for each estimate was also determined as previously described [58].

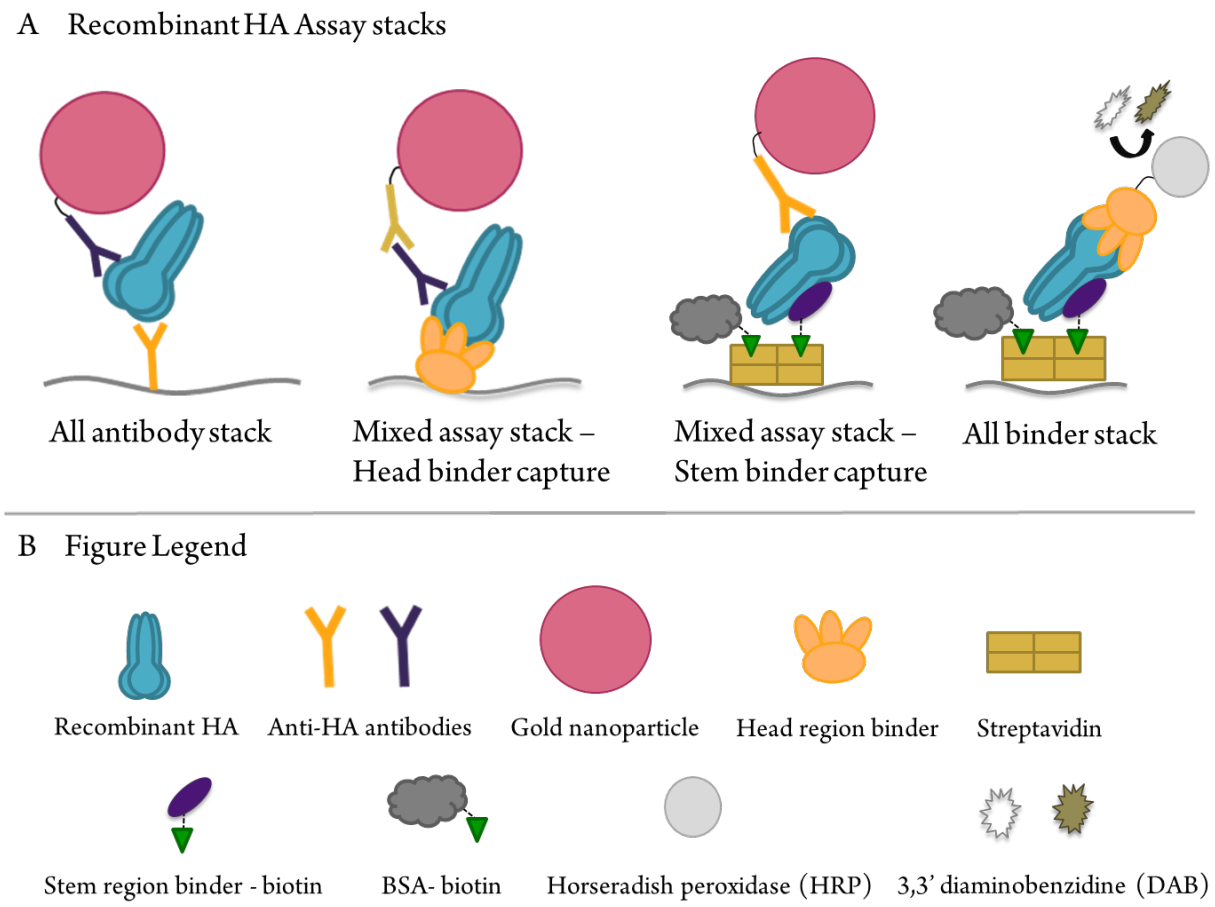

Figure 3.4. Assays for the detection of recombinant hemagglutinin (HA).
(A) Schematic representation of these assays. From left to right: antibody capture and detection with gold nanoparticle readout, head region binder capture with antibody detection and gold nanoparticle readout, stem region binder and streptavidin capture with antibody detection and gold nanoparticle readout, and stem region binder and streptavidin capture with head region binder detection using horseradish peroxidase (HRP). (B) Figure legend. Note that the molecular components are not to scale.

3.3 Results and Discussion

3.3.1 *Hemagglutinin detection using combined head and stem region binders*

We developed a series of assays to detect recombinant hemagglutinin using a combination of the head and stem region binders. Similar to antibody based immunoassay

development, the assays were designed to target two different epitopes on the same antigen. Because the stem region binder could not be effectively immobilized directly to nitrocellulose, modified streptavidin was used to capture biotinylated version of the binder instead. The four assays described in Section 3.3.1 are show in **Figure 3.4,** beginning with antibody capture and detection, head or stem region binder capture with antibody detection, and finally with stem binder capture and head binder detection.

The assays described in this section were developed and compared using the recombinant HA from the A/Solomon Islands/3/2006 (H1N1) strain of influenza A. The dose-response curves for the detection of recombinant HA using head region binder capture are shown in Figure 3.5. The head region binder (67 kDa) can be effectively immobilized by direct adsorption to nitrocellulose, and serve as the base of the assay stack. Dilution series of recombinant HA antigen yielded a statistical LOD for this assay of 451 pM HA, as compared to 7.6 nM for the full immunoassay. Despite the significant improvement in LOD, neither of these assays enables detection of hemagglutinin within the clinical range, which is estimated to be between 300 fM and 3 nM.

An alternative strategy for the detection of recombinant HA is to use the stem region binder for capture. Because this assay uses streptavidin modified specifically to adsorb to nitrocellulose, we overcome the previously demonstrated challenges in immobilization [58], [109]. The dose-response curve for the detection of recombinant HA using the stem region binder for capture is shown in **Figure 3.5**. Dilution series of recombinant HA antigen yielded the LOD for this assay to be 14 pM (95% CI [8, 25]), which is a significant improvement over the previously demonstrated assays. In an attempt to further lower the LOD, we replaced the gold detection with HRP by directly conjugating the HRP enzyme to a head region binder. From this all binder stack, we found comparable results to the gold-based assay. While enzymatic amplification often leads to an improvement in sensitivity, the gold nanoparticles (InnovaCoat) used in these experiments have a proprietary surface coating that we have found leads to approximately 10x improvement in LOD as compared to competitors (Arista).

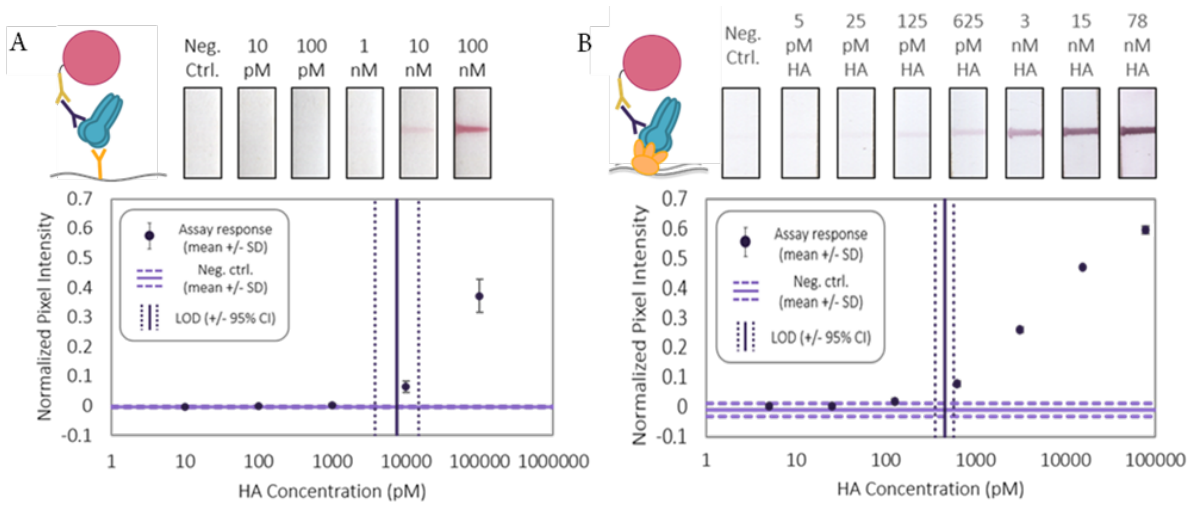

Figure 3.5. Recombinant flu HA assays.

Both assays, using either antibody or novel head region binder, use gold conjugated antibodies for detection. Representative test lines and the full assay response curves are provided. Each condition was tested with n=4 replicates. (A) Antibody capture assay run with recombinant HA. (B) Head region binder capture assay run with recombinant HA.

Detection strategies that utilize both the head and stem region binders will enable greater coverage over the circulating forms of the virus. However, one major drawback of this assay is that it has not been successfully demonstrated to capture and detect native hemagglutinin. The inability of the stem region binder assay to detect actual influenza virus limits the clinical relevance of the assay. Initial attempts to capture whole influenza virus proved challenging, presumably due to steric hindrance preventing access of the stem region epitope of the viral hemagglutinin when the stem binder was immobilized onto paper. This motivated the need to solubilize and detect the native HA protein from the influenza virus.

Preliminary testing with a range of surfactants, including Triton X-100 and octyl glucoside (OG) lead to complete loss in assay signal. Future work towards development of a solubilization technique would enable the use of a combination of the stem and head region binder assays to more sensitively detect native hemagglutinin. To start, a screen of surfactants with varying properties for their ability to solubilize HA without interfering with assay performance, beginning with the non-ionic detergent Triton X-114, the non-ionic and non-denaturing detergent octylphenoxy poly(ethyleneoxy)ethanol (IGEPAL), and the zwitterionic detergent 3-((3-cholamidopropyl) dimethylammonio)-1-propanesulfonate (CHAPS). These

detergents have been found to effectively solubilize membrane glycoprotein for non-immunoassay applications, including mass spectrometry, gel electrophoresis and immunoblotting [110]–[112]. However, our application requires that not only is the membrane glycoprotein solubilized effectively, but also maintains its ability to bind in the same manner as before. A potential solution was developed by researchers from Emory who found the combination of Triton X-100 and saponin lead to effective solubilization at 4°C to remove the effects of proteases, however this method might prove challenging to integrate into an LFA [113].

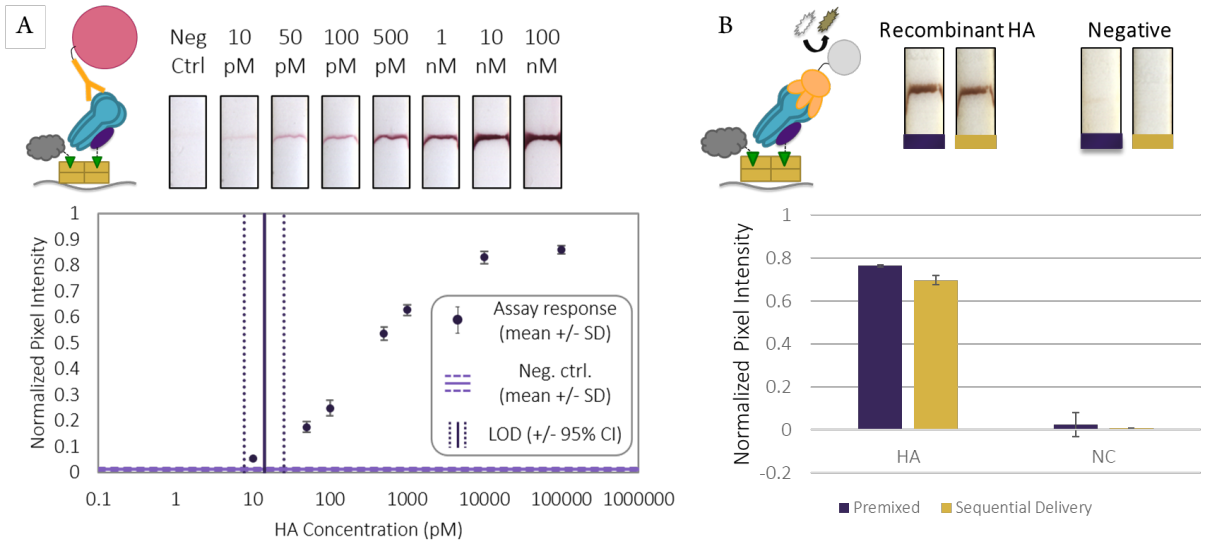

Figure 3.6. Recombinant flu HA assays using stem binder capture.
These assays use antibody (A) or head region binder (B) detection. Representative test lines and full assay response curve is provided for each, however limit of detection analysis has not yet been completed for (B). All binder stack was tested at 10 nM of HA. Each condition was tested with n=3 replicates.

3.3.2 *Assays for the detection of native hemagglutinin*

Many assays for HA described in the literature demonstrate successful detection of the recombinant form of HA [114]–[116]. While the recombinant version of HA serves as a good model for assay development, it is not an exact replica of the native form of HA. Specifically, recombinant HA is traditionally expressed in either mammalian or insect larvae cells, meaning the recombinant protein's structure, conformation, and microenvironment may differ from the native form [117]–[119]. Because of these potential differences, the success of the assays

described in the previous section might not translate to the native form of the protein. Therefore, we sought to develop an assay strategy that enabled detection of the native hemagglutinin from influenza virus. This section describes a new approach for the detection of hemagglutinin, of which there are an average of 500 per virus, targeting the head region of HA for both capture and detection of the protein.

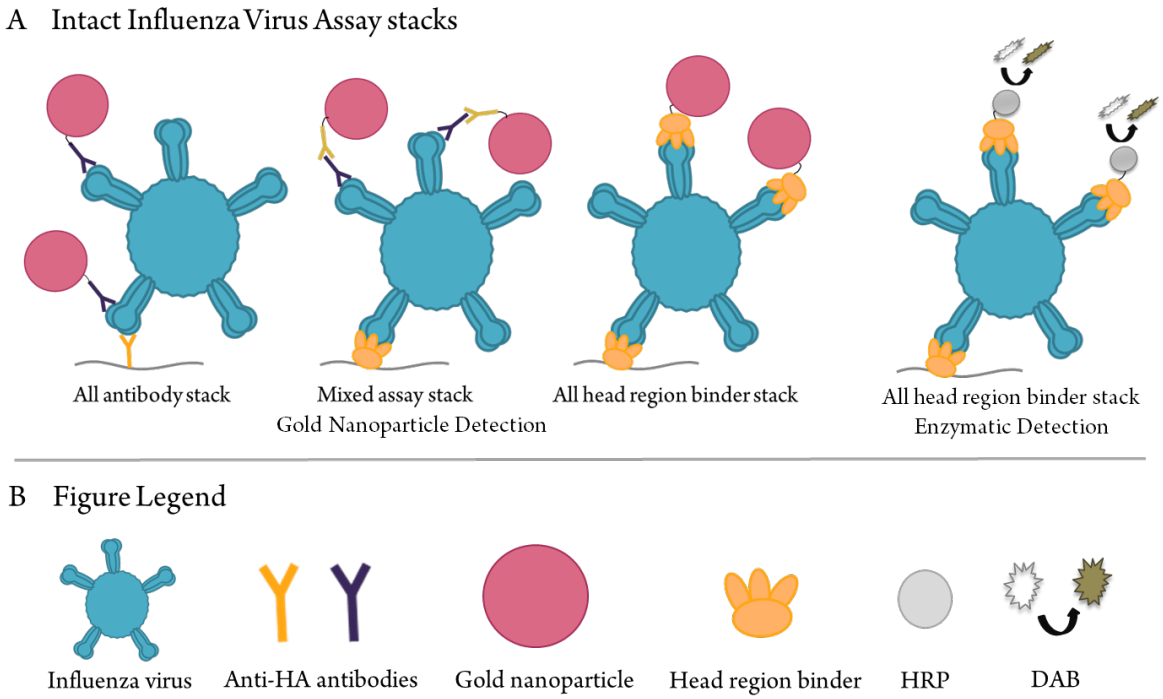

Figure 3.7. Illustrations of the novel HA assay stacks for intact influenza virus. (A) From left to right, assay stacks for recombinant HA detection including all antibody detection, head region binder capture with antibody detection, head region binder capture and detection with gold nanoparticle readout, and all head region binder assay stack with enzymatic detection. Enzymatic amplification was accomplished using horseradish peroxidase (HRP) and 3,3' diaminobenzidine. (B) Figure legend describing each molecular component. Note that the molecular components are not to scale.

The assays depicted in **Figure 3.8** were compared with respect to detection of live influenza virus of the A/Solomon Islands/3/2006 (H1N1) strain. The dose-response curves for the whole virus assays are shown in **Figure 3.9.** Note that, while the virus signal intensities were low in some cases, we were limited to these test concentrations due to the concentration of the virus stock solution (2.5 x 10^8 $CEID_{50}$/mL) and the need to dilute in running buffer by at least

50% to enable flow. Unfortunately, there is no direct relationship between molar concentration of HA and the infectious dose of either cultured virus or virus from a clinical sample. Dr. Carly Holstein used values based on values published in the literature to suggest that the assays using *de novo* binders had LODs that were within the clinically relevant range of HA concentration during influenza infection [58].

To quantify the benefit of using the head region binder as a capture agent as compared to the typical IgG antibody, a traditional, all antibody-based lateral flow test was evaluated using a dilution series of the same recombinant HA and whole virus as above, **Figure 3.8**. The standard error of the LOD estimate for virus was extremely high, owing to the noisy and low signal in this regime, resulting in an unproductive 95% CI of [-2, infinity]. This large confidence interval was largely due to the absence of an observable signal in this concentration range. As we were limited by the stock concentration of the virus, this rendered us unable to generate an effective LOD estimate. However, these results clearly indicated that the antibody assay was less sensitive than the novel assay with recombinant head region binder, which produced both signal and a reliable LOD estimate for this concentration range.

In an attempt to further demonstrate the capabilities of the recombinant head region affinity proteins, they were used as both capture and detection agents. In this assay, the recombinant capture and detection agents bind the same epitope on the HA protein, so the signal at the test line is dependent on the presence of at least two available HA proteins. Therefore, recombinant HA, which contains only one head region binder binding site, was not capable of simultaneous capture and detection. However, using the head region binder as both capture and detection agents, we were able to observe detection of intact influenza virus, **Figure 3.8C**. The LOD for the assay using solely *de novo* binders was found to be 1.34×10^7 $CEID_{50}$/mL (95% CI [7.25×10^6, 1.90×10^7]), which was substantially better than the LOD for the all-antibody assay, 2.5×10^8 $CEID_{50}$/mL (95% CI [-2, infinity]). The LOD of the all-de novo binder assay was 2-fold better than the LOD of the assay with binder capture and antibody detection, 3.54×10^7 $CEID_{50}$/mL, **Figure 3.8**. The introduction of enzymatic amplification enabled further improvement of the assay, with an LOD of 1.35×10^7 $CEID_{50}$/mL. With regards to reproducibility, the conjugation of HRP to the head region binder was much more consistent from batch to batch, leading to an overall improvement in assay performance over time.

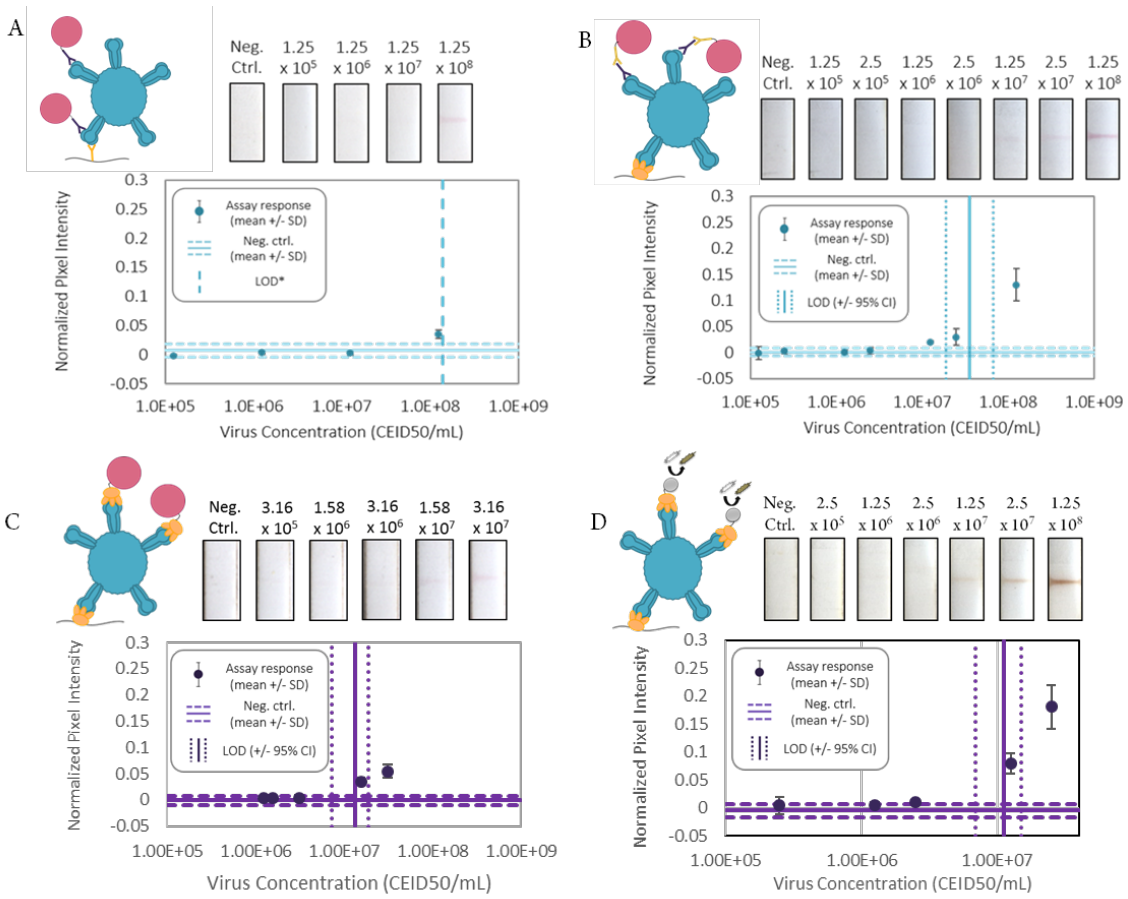

Figure 3.8. Results of the flu HA assay using novel head region.

(A) Antibody capture and detection of intact influenza virus. (B) Head region binder capture and antibody detection of intact influenza virus. (C) Head region binder capture and detection of intact influenza virus. (D) Head region binder capture and detection of intact influenza virus with horseradish peroxidase (HRP) for enzymatic signal amplification. As the antibodies are replaced with the head region binders, a reduction in the lower limit of detection can be seen, with the lowest LOD shown in panels C and D. Representative test lines and the full assay response curves are provided. Each condition was tested with n=3 replicates.

Detection of intact virus is an attractive option for simple point-of-care tests, in which sample pre-processing must be minimized or eliminated. When lysis agents were added to the virus sample, signal from the assay described in **Figure 3.8D** was eliminated altogether, **Figure 3.9**. High concentrations of Triton X-100, which have been proven to effectively lyse the influenza virus and free the viral nucleoprotein, lead to a complete loss in signal in the all head region binder assay. This supported our hypothesis that these assays detected—and depended

on—the capture and retention of whole influenza virions. This approach enables detection of the virus without additional processing steps, whereas most approaches to influenza diagnosis rely on sample preparation steps for the isolation of the molecular target of interest [120]. In addition, the presence of approximately 500 HA molecules on the surface of the intact virus enables signal amplification through the binding of multiple detection binders for each [97].

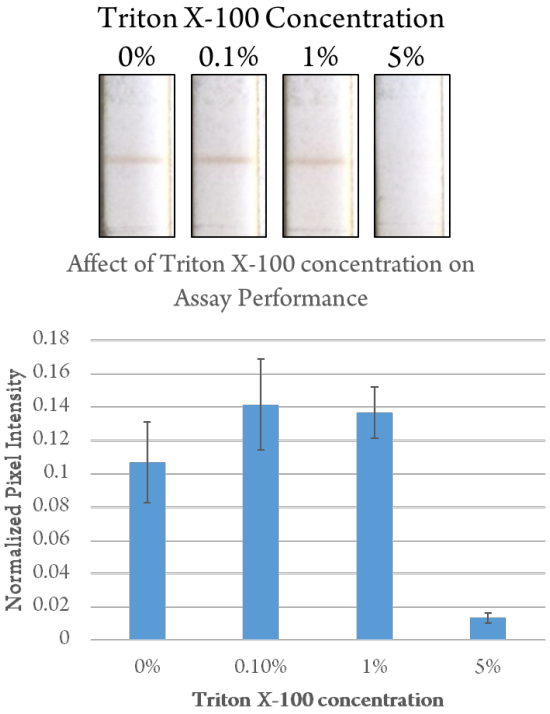

Figure 3.9. Reduction of assay performance at high detergent concentrations.
Intact virus assay run with a range of Triton X-100 concentrations, with a loss in assay performance at 5% Triton X-100. Representative test strips (top) and normalized pixel intensity across the test line (bottom) are shown. All conditions were run with an n=4.

The assay results for all eight assays described in this Chapter are summarized in **Table 3.1**, combined with comparisons to the estimated clinically relevant ranges of virus and HA, calculated in the Supplemental Methods from [121]. The data in **Figure 3.10** indicates that the head region binder assays had LODs that were estimated to be within the clinically relevant range for both HA and virus targets, albeit in the higher end of that range. The traditional antibody assay, however, fell outside of the clinically relevant range for recombinant HA and was at the very high end of the range for virus. Therefore, the traditional antibody assay would be unlikely to be clinically useful, while the head-region-binder based assays would be useful for

detecting mid to high concentrations during infection. While there are no commercially available rapid diagnostics currently available to detect HA, existing nucleoprotein tests can be used as a benchmark for analytical sensitivity. The lower limit of detection of the available diagnostics for nucleoprotein has been found to vary between approximately 10^6 and 10^7 $CEID_{50}$/mL depending the diagnostic test and the strain being detected [114]. The lower limits of detection for the HA assays demonstrated herein are within this range, suggesting that the analytical sensitivity of the all binder HA assay is comparable to the commercially available rapid tests for influenza nucleoprotein.

The head region binder used in the assays presented here was designed using the crystal structure of the H1N1 Solomon Islands 2006 strain of the influenza virus. Strains of both H1N1 and H3N2 circulate seasonally and have been responsible for four major influenza pandemics [120]. The mutagenic nature of the head region prevents anti-HA antibodies against one strain from protecting individuals from a different strain of the virus. As a consequence, high affinity to one strain could also increase strain-specificity; one binder may have reduced affinity to HA of another strain. Targeted binding enables greater specificity and differentiation between the circulating strains of the virus. For complete clinical coverage, careful design of binders to other strains of the virus for use in a multiplexed device will be necessary. A screen of the most recent strains of influenza A and B circulating in the human population identified that the head region binder is capable of binding two of these strains, the Solomon Islands 2006 strain of H1N1 to which it was designed, and the Switzerland 2013 strain of H3N2, **Figure 3.10**. Despite the fact that these two strains of the virus are different subtypes, the conformation of the sialic acid binding pocket are similar enough that the designed binder is capable of binding with similar affinity to both. Limit of detection analysis of the H3N2 strain lead to statistically similar results to the H1N1 strain, with LODs of 1.11×10^7 $CEID_{50}$/mL and 1.35×10^7 $CEID_{50}$/mL respectively.

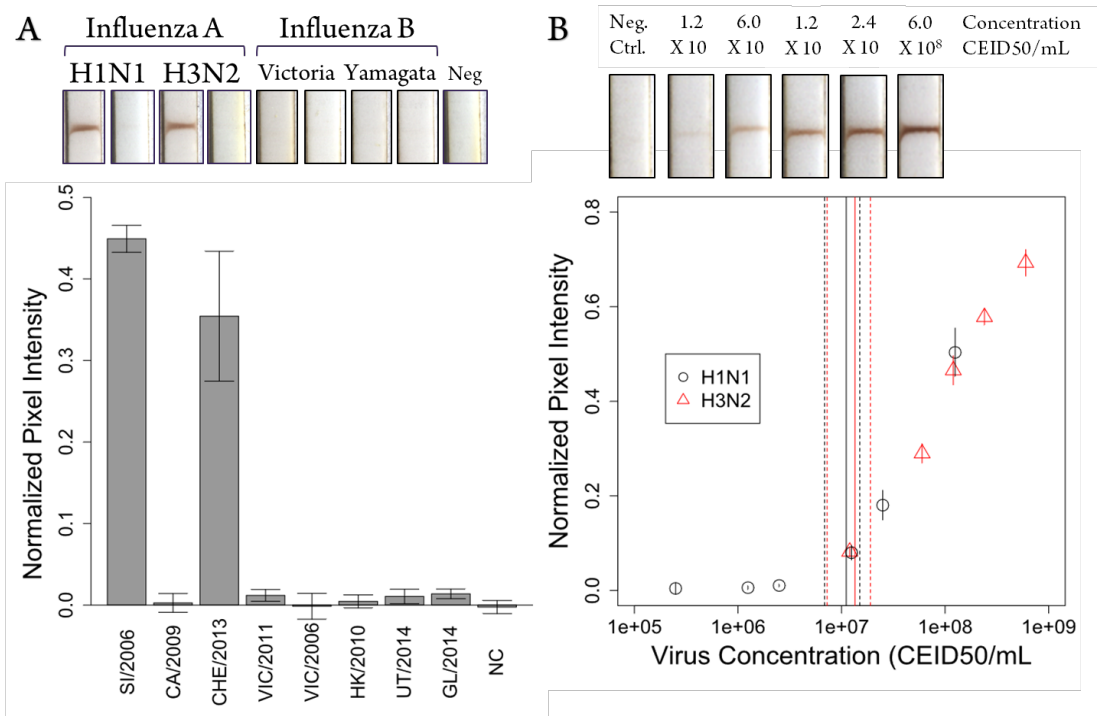

Figure 3.10. Specificity and sensitivity of the head region binder assay. Horseradish peroxidase was used to visualize influenza bound at the test line, shown in brown. (A) Screening of clinically relevant influenza A and influenza B strains including representative test lines (top) and normalized pixel intensity (bottom). (B) Limit of detection analysis for H1N1 and H3N2 strains. The limits of detection were found to be 1.35 x 10^7 $CEID_{50}$/mL (95% CI: [7.26 x 10^6,1.90 x 10^7]) and 1.11 x 10^7 $CEID_{50}$/mL (95% CI: [6.85 x 10^6, 1.50 x 10^7]) respectively. The solid lines indicate the calculated LOD, while the dashed lines indicate the 95% confidence interval. Each condition was tested with n=4 replicates.

Based on these results, both recombinant head region binder-based assays yield superior analytical sensitivity to the lateral flow immunoassay developed using commercially available monoclonal antibodies for capture and detection of HA. Even though the LOD is not improved as compared to the commercially available nucleoprotein based rapid diagnostics, these affinity proteins offer the potential to better inform patient management by offering differentiation between subtypes of influenza at a fraction of a cost to antibodies. We have therefore demonstrated that the use of a computationally designed, recombinant affinity protein not only offers greater design control at a lower cost than antibodies, but that such targeted de novo proteins can be used to improve the performance of paper-based assays.

Table 3.1. Summary of influenza assay results.

The LOD with 95% CI for each assay is listed and compared to the clinically relevant range of influenza. Influenza virus infectivity is reported using two different units, tissue culture infectious dose 50% endpoint (TCID50/mL) or chicken embryo infectious dose 50% endpoint (CEID50/mL) depending on which cell line is used to determine the infectious titer. The clinically relevant range of virus in TCID50/mL of nasopharyngeal wash is known from the literature [87]. It is important to note that these concentrations will differ from different sampling techniques. The ranges in terms of HA [M] and virus [CEID50/mL] were estimated by Dr. Carly Holstein, described in the supplemental methods of the following paper [121].

Clinical Range for H1N1 Influenza Infection			
	Low	Medium	High
Virus [$TCID_{50}$/mL]	1×10^3	1×10^5	1×10^7
Virus [$CEID_{50}$/mL]	1.5×10^4	1.5×10^6	1.5×10^8
HA [M]	300 fM	30 pM	3 nM
Recombinant HA Assay LODs			
	Lower 95% CI	LOD	Upper 95% CI
All antibody stack	3.8 nM	7.6 nM	14.8 nM
Head binder capture, antibody detection	358 pM	451 pM	569 pM
Stem binder capture, antibody detection	8 pM	14 pM	25 pM
Influenza Virus Assay LODs			
	Lower 95% CI	LOD	Upper 95% CI
All antibody stack ($CEID_{50}$/mL)	NA	$>1.25 \times 10^8$	NA
Head binder capture and antibody detection ($CEID_{50}$/mL)	1.88×10^7	3.54×10^7	6.66×10^7
All head binder stack, gold detection ($CEID_{50}$/mL)	7.25×10^6	1.34×10^7	1.90×10^7
All head binder stack, HRP detection ($CEID_{50}$/mL)	7.26×10^6	1.35×10^7	1.90×10^7

While enzymatic amplification lead to a slight improvement in the sensitivity of the intact influenza virus assay, the calculated limits of detection are still at the middle to high end of the clinical range of the strains, **Figure 3.11**. Therefore, an alternative approach is will be needed to further improve the sensitivity of our influenza assay. Other approaches, such as silver enhancement or fluorescence readout, have been demonstrated for the reduction in the assay LOD, however the resulting sensitivity is only improved by an order of magnitude or two [122]. The Gao lab at the University of Washington has explored the use of polydopamine with HRP,

which has been demonstrated to improve the sensitivity of immunoassays down to 10 pg/mL for the HIV biomarker p24 [123]. While this improvement is quite significant, p24 exists in the serum of infected individuals at much lower concentrations, suggesting that this sensitivity improvement is insufficient for some protein targets [124]. The most dramatic improvements in sensitivity have been demonstrated by coupling nucleic acid amplification with protein binding, with limits of detection down to 3 CFU/mL for *Staphylococcus aureus* [125]. Coupling an immunoassay with polymerase chain reaction (PCR) is an approach used to increase the sensitivity of enzyme linked immunosorbent assays (ELISAs). While immuno-PCR has had some success, the increased complexity and overall assay time makes it difficult to implement in some settings [126]. Further work integrating developing and integrating these more complex, and more sensitive, amplification methods into simple to use diagnostics will have huge impact for protein detection at the point of care.

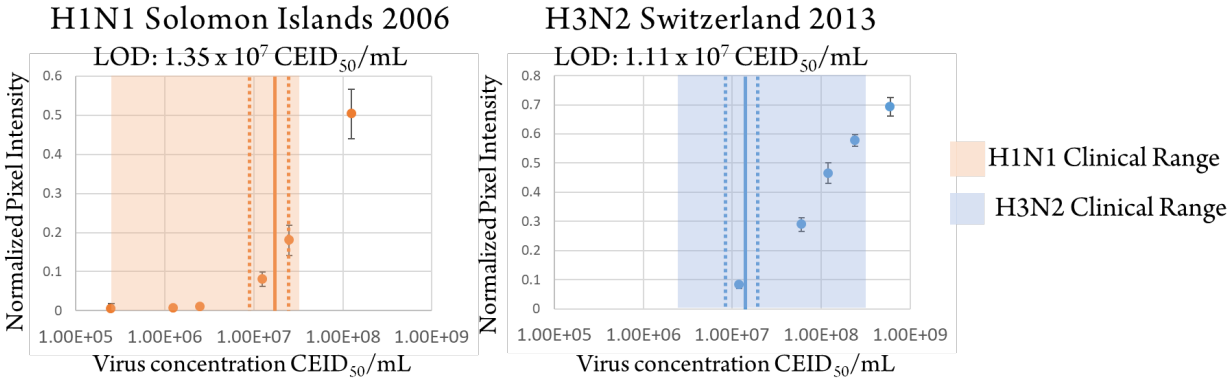

Figure 3.11. Limit of detection analysis overlaid over the influenza virus clinical range.
The results of the intact influenza virus assay are shown for both H1N1 (orange) and H3N2 (blue). All conditions were run with an n=4.

3.4 Conclusions and Future Work

Using a combination of novel HA head region-binding affinity proteins and antibodies, we have demonstrated the detection of intact influenza virus using a collection of paper-based assays. The first of these assays uses a combination of stem and head region binders to the hemagglutinin protein, demonstrating significantly improved sensitivity over the antibody-based alternative. However, detection of native hemagglutinin using this assay stack has proved challenging. Therefore, an alternative approach using the head region binder for both capture and

detection enabled the detection of native hemagglutinin on the influenza virus, without the need for additional lysis or preparation steps. To our knowledge, this represents the first report of whole influenza virus detection on paper. The use of computationally designed, recombinantly expressed affinity proteins also provides exquisite customizability, leveraged here for binding epitope specificity and avidity, matching the trimeric nature of the HA protein.

We believe this to be a general approach that can be applied for rapid, simple detection of a range of viruses at the point of care. Targeting the surface-expressed HA protein also offers the possibility for additional diagnostic information that is not possible when the internal nucleoprotein is targeted, as is the case for currently available commercial influenza RDTs [8]. In particular, the HA subtype could be determined by the use of subtype-specific HA binders, which represents an important area of future work. The ability to determine the HA subtype with a simple point-of-care test would provide valuable information for epidemiological surveillance and the clinical management of disease treatment and prognosis. Especially, for example, as the HA subtype (H1 vs. H3) distinguishes the two currently circulating subtypes of influenza A virus (H1N1 and H3N2) [127].

The subtype of the virus can have clinical implications as well. While there is treatment for the flu, such as oseltamivir and zanamivir, some subtypes of flu A have developed resistance to these drugs, thereby necessitating the need for an inexpensive test for subtype differentiation [128]. However, given that the highly conserved receptor binding site of the HA head region is surrounded by regions with high mutation rates [87], [99], future challenges will include maintaining binding for evolving strains of HA. As there are only two influenza A virus subtypes currently circulating in the general human population, it would be possible to combine the existing assays to enable strain exclusion and inclusion for diagnostic determination. In addition to achieving a more sensitive and information-rich influenza detection assay, the use of the recombinant affinity proteins opens the door for companion therapeutics, because these influenza binders have shown the potential for therapeutic use [103], [105]. In such a companion system, the influenza binder-based diagnostic test would not only diagnose the flu, but it would also indicate which flu binder should be given for treatment, based on which binder is able to recognize the specific strain at hand most sensitively.

Overall, this work demonstrates the power of recombinant affinity proteins for influenza detection, with the potential to apply to a number of diagnostic applications. Future directions

include improving the sensitivity of the assay below the clinical range, incorporation of the demonstrated assay into an automated device, and validation of these assays with clinical samples. This work is a significant step toward the development of a high-sensitivity, low-cost influenza test for improved diagnosis and disease management at the point of care.

3.5 ORAL AND WRITTEN PUBLICATIONS

Holstein, C.A.; Chevalier, A.; Bennett, S.; **Anderson, C.E.**; et al. Analytical and Bioanalytical Chemistry. "Immobilizing Affinity Proteins to Nitrocellulose: A Toolbox for Paper-Based Assay Developers." 2016, 408(5):1335-1346.

Anderson, C.E.*; Holstein, C.A.*; et al. Analytical Chemistry. Analytical Chemistry. "Development of a Paper-Based Assay for Whole Influenza Virus Detection using a Computationally Designed Hemagglutinin Head Region Binder." 2017. DOI: 10.1021/acs.analchem.7b00769.

Strauch, E.M.; Bernard, S.M.; La, D.; Bohn, A.J.; Lee, P.S.; **Anderson, C.E.**; et al. Nature Biotechnology. "Computational design of trimeric influenza neutralizing proteins targeting the hemagglutinin receptor binding site." 2017. DOI: 10.1038/nbt.3907.

* denotes equal contribution

In addition, this work has been presented in the following conferences.

Anderson, C.E.; Strauch, E.M.; Marzan, R.; et al. "Detection of intact influenza virus from clinical samples using computationally designed affinity proteins." Oral presentation; October 6, 2016. Biomedical Engineering Society Annual Meeting.

Yager, P.; **Anderson, C.E**.; Lafleur, L. "Development of paper-based point-of-care diagnostics." Oral presentation; December 10, 2015. BioEngage Technical Symposium, University of Washington, Department of Bioengineering, Seattle, WA.

Chapter 4. AN INTEGRATED 2DPN FOR SENSITIVE DETECTION OF THE INFLUENZA HEMAGGLUTININ

4.1 BACKGROUND

The implementation of lateral flow assays at the point of care has been highly successful due to their cost and ease of use. However, these tests generally lack the ability to perform additional chemistry and multi-step assays that are often required for more complex laboratory assays [40]. The conventional enzyme-linked immunosorbent assay (ELISA), for example, requires the manual delivery of each reagent to enable protein detection. While ELISAs are sensitive protein assays, the need for refrigeration, electricity, and trained personnel complicate their implementation at the point of care [6]. The traditional LFA involves one assay step, where the sample rehydrates the conjugate pad and travels downstream to the test line, where a capture antibody is immobilized, **Figure 2.4**. This works well for sandwich assays that use colorimetric detection, such as by gold nanoparticles, but proves challenging when attempting to integrate assays that use signal amplification chemistries. There has been an emphasis on strategies that allow more complex fluidic manipulation within the context of paper-based diagnostic systems.

Various approaches to introduce more complex fluidic manipulation have been demonstrated. The Whitesides group spearheaded the use of paper for diagnostics through the layering of paper and tape to create three-dimensional paper microfluidic devices that deliver different reagents required for the assay at each individual layer [25]. The Filipe group has described the use of dry pullulan films for the sequential delivery of reagents in a lateral flow or flow through format [129]. Alternatively, the Ying group has used the stacked flow immunoassay to significantly reduce non-specific signal due to substances present in a patient sample. Using separate paths for sample and conjugate pad with a flow regulator in between, the stacked flow immunoassay enables control the order of reagent delivery across the test region [130]. Our lab has developed a platform to address these limitations using a two-dimensional paper network (2DPN). The 2DPN allows the sequential delivery of reagents across a test line in a fully automated manner [35]. The 2DPN platform has been demonstrated for the integration of assays using enzymatic amplification for more sensitive detection of an analyte, including gold

enhancement and horseradish peroxidase (HRP) for signal amplification of an immunoassay [37], [131], [132].

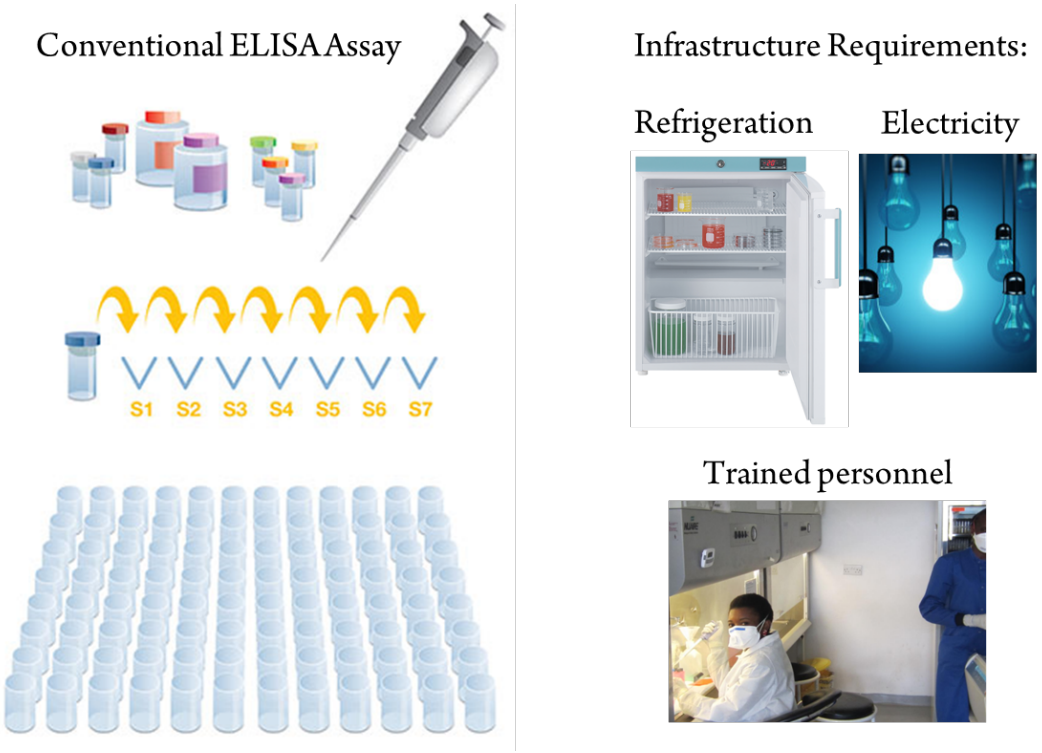

Figure 4.1. Requirements of traditional clinical laboratory tests.
Schematic describing the conventional enzyme linked immunosorbent assay (ELISA) (left), and the infrastructure required to implement these assays (right). These requirements include refrigeration to keep reagents viable, electricity for the refrigeration and detection, and trained personnel to run the immunoassay. Images adapted from thermofisher.com (left), globalspec.com (upper right), and Jean Gratz (bottom right).

2DPN geometries are often limited in their ability to control the rate and direction of flow for delivery of multiple fluidic steps. Our previously-demonstrated 2DPN architecture for enzymatic amplification required that the last assay step flow through a long section of porous material [37], [132]. This has led to reduced performance in integrated devices; specifically, long assay run times and decreases in sensitivity due to reagent loss to the porous material, and increased background outside of the capture lines due to nonspecific adsorption of enzyme-labelled conjugates upstream of the capture line.

Recent advances in the understanding of fluid flow in paper microfluidics have shown that understanding the effects of partial saturation are critical to predicting fluid flow in LFAs, and particularly in complex multicomponent 2DPNs [53], [135]. Controlled partial saturation effects enable the assay developer to sequence fluid delivery using specific material choices. This understanding allows for the design of devices that can control flow rates of subsequent assay steps independently and provide better spatial control of reagent transport. This understanding of membrane wetting and fluid flow has enabled the implementation of more complex fluidic handling into integrated paper microfluidics. Other applications using partial saturation include the automation of DNA extraction from a urine sample and concentration from large sample volumes and an automated dilution series for downstream immunoassay detection [53].

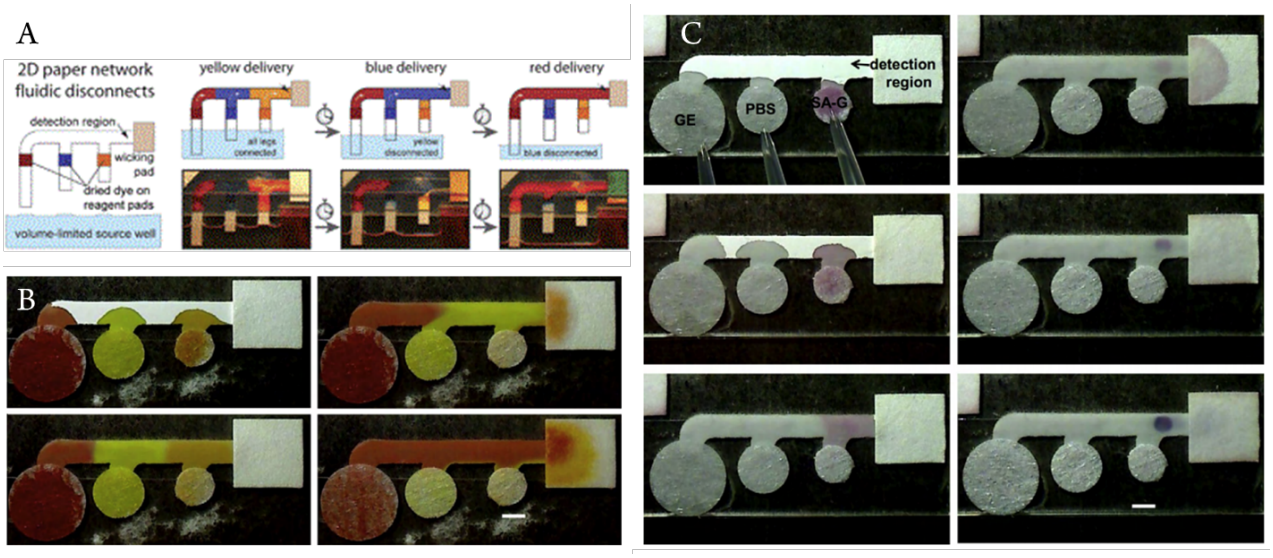

Figure 4.2. Images of the traditional two-dimensional paper network (2DPN).
The 2DPN is used for the sequential delivery of multiple assay steps across a test line, demonstrated using dye (A,B) and signal amplification assay using gold enhancement to increase signal from gold nanoparticles bound at the test region (C). Sources: [133], [134].

This chapter describes work towards a prototype device that integrates the assay described in Chapter 3 using computationally designed head region binders for capture and detection of intact influenza virus, **Figure 4.3**. This assay utilizes enzymatic amplification for the visualization of binding at the test line, in the form of horseradish peroxidase (HRP). The original binder-based hemagglutinin assay relied on gold nanoparticles for signal development;

however, poor sensitivity of the assay necessitated the need for enzymatic signal amplification [121]. The modified 2DPN platform presented here harnesses partial saturation to create two distinct, independently controllable fluidic paths, enabling more precise control over assay timing, reagent concentrations, and fluid flow rates. This modified platform also enables reagent delivery while minimizing interaction between the enzyme and its colorimetric substrate before reaching the test line. This novel device architecture is demonstrated for the sensitive detection of influenza hemagglutinin from nasal swab samples.

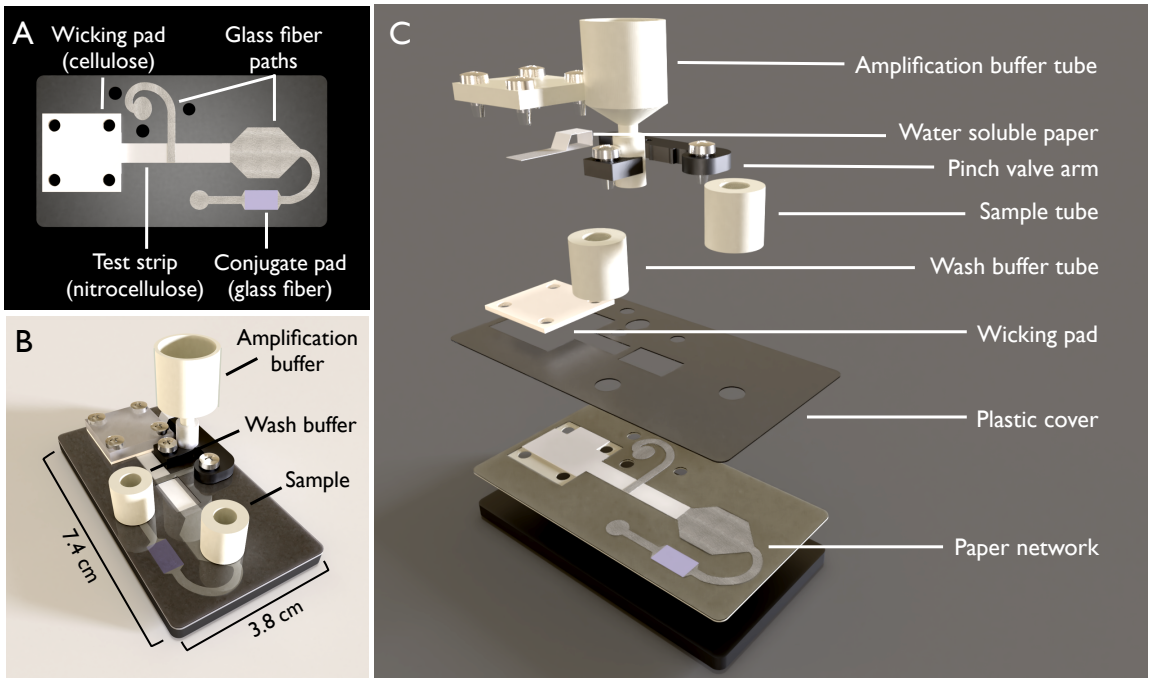

Figure 4.3. Hemagglutinin device schematic.
(A) The two-dimensional paper network (2DPN) used in this device. This network contains a nitrocellulose test strip, glass fiber paths for the delivery of sample, conjugate, wash and amplification buffers, and a cellulose wicking pad. (B) The fully assembled device. (C) The expanded view of the device, containing the two-dimensional paper network (2DPN) and automatic release mechanism for the amplification tube. The automatic release mechanism consists of a pinch valve that is held closed until the water-soluble paper wets and releases the "arm". Once the arm is released, the amplification buffer is delivered to the paper network.

As described in the previous chapter, influenza is a viral respiratory tract infection responsible for 15-60 million infections in the United States annually, causing more than

200,000 flu related hospitalizations [7]. While there are three strains of the influenza virus that circulate in the human population, influenza A is responsible for both the seasonal and pandemic flu. Influenza A can be further characterized based on two surface proteins that are constantly undergoing antigenic drift, hemagglutinin and neuraminidase [86], [87], [136]. The hemagglutinin protein is the rapidly mutating glycoprotein responsible for receptor binding and membrane fusion to the α(2,6) sialic acid of human epithelial cells [137]. This surface protein is of particular interest as a diagnostic target due to its role in virulence and immunological relevance, as it constantly evolving to escape the host immune system. While hemagglutinin protein classification provides both diagnostic and epidemiological information, there is no existing method for screening and detection of circulating viral strains at the point of care. We have previously published the development of an assay using computationally designed affinity proteins to bind HA, termed "binders" [121]. These "designer" protein binders bind specific epitopes on the hemagglutinin surface protein with higher affinity than traditionally used antibodies [70], [75]. These binders have higher stabilities and lower production costs than antibodies, enabling devices to be more robust and affordable. We have developed an assay using these binders for the detection of intact influenza virus and HRP amplification, which we want to integrate into a prototype device and validate with patient samples.

This chapter details the integration of an assay for the detection of the influenza virus surface protein hemagglutinin (HA) into a modified 2DPN. The overarching goal of this aim is to demonstrate the use of a novel 2DPN geometry for the integration of an enzymatic amplification technique while optimizing overall assay performance. This work is divided into the three following sections:

- Development of a 2DPN to effectively integrate enzymatic amplification
- Demonstration of long term stability of the protein binders on device
- Integration of the influenza assay into the novel 2DPN geometry to demonstrate detection of intact virus from a spiked patient sample

4.2 Materials and Methods

Recombinant hemagglutinin binder preparation. Two computationally designed proteins were used for this work, both iterations of the head region binder (Trimer 11 and Trimer 11.2) [106]. The recombinant influenza HA binders were cloned, expressed in *Escherichia coli*,

and purified using metal affinity chromatography using Ni-NTA resin that recognizes a C-terminal His tag [70]. Thiolated versions of these binders were made by mutating a select amino acid to cysteine to introduce a single thiol moiety for site-specific immobilization to a thiol-reactive surface. This allowed for the direct conjugation of HRP to the head region binder, with a range of 0 to 3 horseradish peroxidase (HRP) molecules conjugated to each binder using a commercial conjugation kit (ThermoFisher, Waltham, MA, USA). All additions and mutations were made to the recombinant hemagglutinin binders through the Rosetta software suite (www.rosettacommons.org), which allowed minimal impact on the binding functionality of these proteins.

Dipstick assay for hemagglutinin detection. A dipstick assay was used for high throughput assay development and optimization. Test strips for the dipstick assay were made by cutting nitrocellulose membranes (GE FF80 HP, GE Healthcare, Piscataway, NJ, USA) into 3 mm wide by 24 mm tall strips using a CO_2 laser cutter (VLS3.60, Universal Laser Systems, Scottsdale, AZ, USA). Sets of four test legs were cut together and connected by a 6mm section at the top of the device, enabling rapid batch assembly and processing. Protein solutions were filtered through a centrifugal filter with a 0.2 μm nylon membrane (VWR, Radnor, PA, USA) at 8000g for 5 minutes before spotting. Head region binder was prepared at 0.62 mg/mL and anti-HRP antibody (ThermoFisher) was prepared at 0.5 mg/mL. A piezoelectric printer (sciFLEXARRAYER S3, Scienion AG, Berlin, Germany) was used to deposit capture proteins onto the nitrocellulose membranes. Each line was made by the deposition of 12 spots of the reagent, each of which were separated by 250 μm, at 30 drops per spot and 450-500 pL per drop. Each test line received approximately 300 nL of total protein solution. The spotted membranes were stored overnight in the desiccator and were tested within 7 days. Influenza A virus of the following strains was obtained from the International Reagent Resource (IRR), Solomon Islands 2006 H1N1 (FR331), Switzerland 2013 H3N2 (FR1416), Victoria 2011 H3N2 (1027). Influenza B virus for the Yamagata (FR1373, FR1370) and Victoria (FR20, FR663) strains were also obtained from the IRR.

The prepared nitrocellulose membranes described above were assembled into holding cards with cellulose wicking pads to maintain consistent contact across the entire width of the device. These comb-shaped devices were prepared the same day as the assay was run. Each assay was performed using a 96-well plate, which had been preloaded with the reagents required

for each step. Assay reagents were delivered sequentially by moving each test leg from one well to the next when all 20 μL of each step was depleted from the well. Each step for the head region binder assay consisted of the following reagents delivered in order (1) Sample containing influenza virus or negative control (2) Wash (3) Head region binder directly conjugated to an HRP molecule diluted to 100 nM (4) Wash (5) Amplification buffer with 0.0125% H_2O_2 from sodium percarbonate and 144 mg/mL of 3,3'-diaminobenzidine (DAB) as the substrate for HRP. Phosphate-buffered saline (PBS) + 0.1% v/v Tween -20 (Fisher BioReagents #BP337, Thermo Fisher Scientific, Waltham, MA) (PBST) was used as the wash buffer in all cases. All non-wash reagents were diluted in a running buffer of PBST +1% w/v bovine serum albumin (BSA, Sigma-Aldrich #A7030). The total assay before the optimization of wash steps took approximately 58±5 minutes.

Two-dimensional paper network construction and testing. Prototype device "cards" were comprised of layered plastic with a single-side adhesive (T-5501-10/1, Melinex, Fralock, Valencia, CA, USA) used as backing and spacer layers. Glass fiber membrane (8964, Ahlstrom-Munksjö, Stockholm, Sweden) was used for the glass fiber and conjugate pad regions of the network shown in Figure 1. 5mm nitrocellulose strips were used for the assay region, and cellulose (CFSP223, Merck Millipore, Billerica, MA, USA) for the wicking pad. Nitrocellulose membranes were prepared similarly to the dipstick assay described above. Because the nitrocellulose strips were 2mm wider on the integrated device, 20 spots of reagent were deposited across the width of the strip instead of 12.

Glass fiber conjugate pads were prepared using a method previously published by our group [42]. Pads were pre-blocked by soaking in a 10 mM phosphate buffered saline (PBS) solution with 1% BSA and 0.01% Tween 20 for 30 minutes. Once blocked, pads were stored in a desiccator at 25°C to dry overnight. A master mix was made containing 300nM Trimer 11.2-HRP, 0.1% BSA, 4% trehalose 0.005M $FeSO_4$ and 0.01M EDTA. 20 μL of the master mix was added to each pre-blocked conjugate pad (5 mm by 12 mm), and flash frozen in liquid nitrogen. The frozen pads were then placed onto a lyophilizer at room temperature 24 hours before being stored with desiccant until use.

Devices were run by the manual application of the wet assay components onto the assembled device. Volumes of 70 μL, 100 μL, and 80 μL were applied for the sample, rehydration/wash buffer, and amplification buffer respectively. For the assays described here,

colorimetric signal was generated by the precipitation of oxidized DAB. Device runs were considered complete after all glass fiber on device no longer visibly contained liquid.

qRT-PCR. Quantitative reverse transcription polymerase chain reaction (qRT-PCR) was used to determine the concentration of the different influenza virus stocks used in this chapter. UltraSense One-Step Quantitative RT-PCR assay mix (Life Technologies, Carlsbad, CA) was used with primer and probe sequences published previously [138], [139]. 20μL reactions were run on CFX96 Touch (BioRad) using the following protocol: 50°C for 15 min, 95°C for 2 min, followed by 40 cycles of 95°C for 15 s and 60°C for 55 s. Concentrations were determined using a standard curve developed from influenza A RNA of known copy number.

Clinical nasal swab specimens. Clinical nasal swab specimens were acquired from Seattle Children's Hospital between January and March 2016 from pediatric patients with suspected influenza infection after signed parental informed consent. Each nylon flocked mid-nasal swab was collected in the hospital or emergency department and placed into 750 μL of PBS, 0.05% Tween-20 and 0.01% sodium azide. The diluted nasal swab sample was used for RT-PCR and immunoassay detection of influenza. In order to determine the minimum dilution of nasal swab required for this device, diluted nasal swab samples were concentrated using a protein concentrator with a molecular weight cut-off of 5kDa (VivaSpin). Seattle Children's Hospital Institutional Review Board approved the sample collection and analysis of specimens. Written consent was obtained from a parent or legal guardian, as approved by the Seattle Children's Institutional Review Board, with paper copies given to both a parent and maintained under secure storage by the research team.

Fully integrated system for hemagglutinin detection. The base of the automated device (**Figure 4.3**) was built from 1/4 inch black acrylic (8505K754, McMaster-Carr, Santa Fe Springs, CA, USA) cut using a CO_2 laser into a 3.8cm by 7.4cm rectangle. An automatic, saturation-dependent fluid transfer element (the "valve") was designed to deliver the amplification buffer after the first three assay steps were complete. To do so, water-soluble paper (Water Soluble Paper, Edmund Scientific, Tonawanda, NY, USA) was placed above the cellulose wicking pad between the wicking pad and the clear acrylic cover. This paper holds closed a pinched ~10 mm length section of silicone tubing (STHT-C-093-2; Saint-Gobain, Valley Forge, PA, USA) that prevents the flow of amplification buffer out of the cut off syringe and onto the secondary membrane. As the water-soluble paper dissolves, the pinch is released,

thereby allowing fluid to flow into the glass fiber pad below. The amplification buffer then flows through the overlap junction and into the nitrocellulose test strip, **Figure 4.8**.

The device assembly is split into two main components – preparation of the 2DPN and integration of the 2DPN into fluidic delivery system. Assembly of the 2DPN is described on page 64. The 2DPN is integrated into the full device, which incorporates the pinch valve, water-soluble paper, and lever arm to enable automated delivery of the amplification buffer. The 2DPN is placed onto a thick acrylic platform and screwed into the platform. The pinch valve stopper is screwed through the 2DPN and the acrylic backing and a nut is used on the backside to ensure that the stopper does not rotate during use. The lever arm is attached to the acrylic platform *via* a peg at the fulcrum. A piece of water-soluble paper is wrapped around the end of the lever arm and placed overtop the cellulose wicking pad. The pinch valve is then inserted between the lever arm and the pinch valve stopper. The lever arm is held tight while a clear acrylic piece is screwed into the platform such that it clamps down onto the spy paper and the wicking pad. Finally, small ports are added to the sample and buffer inlet ports and secured with adhesive.

Signal quantification and analysis. For the assays described here, colorimetric signal is generated by the precipitation of DAB. All membranes are scanned at 48-bit HDR color, 600 dpi, gamma=1 using a desktop scanner (Perfection V700 Photo Scanner, Epson, Long Beach, CA) while the membranes were still wet. The blue channel of the RGB scanned image was used for quantification. All reported signal intensities were quantified using a previously-published custom script in MATLAB (MathWorks, Natick, MA, USA) [108]. This script computes the average pixel intensity in a region of interest manually drawn around the test line. This value is then normalized based on computed average pixel intensity of a region directly downstream from the test line, resulting in a series of values between 0 and 1 which represent the minimum and the maximum respectively.

All significance testing utilized Welch's t-test, which is also known as a Student's t-test with unequal variances, and a significance threshold of $\alpha=0.05$. The limits of detection (LODs) were calculating using the signal intensity quantified as described above, looking specifically at the 5% chance of false-positive signal and false-negative signals. This was then mapped to the associated HA concentration using a four-parameter logistic curve, with the data presented

alongside a 95% confidence interval for each estimate. All statistical comparisons were performed using the open-source statistical package R (64 bit, version 3.3.2) [140].

4.3 Results and Discussion

4.3.1 *Development of a 2DPN geometry to integrate enzymatic amplification*

In the last chapter, we described the development of a series of assays for the detection of the hemagglutinin protein from the influenza virus. Of the assays developed, the assay using head region binder for both capture and detection was demonstrated for its ability to bind native hemagglutinin from influenza virus of both the H1N1 Solomon Islands 2006 and H3N2 Switzerland 2013 strains. The most sensitive assay relied on horseradish peroxidase (HRP) and 3,3' diaminobenzidine (DAB) for the amplification of a binding event at the test line. Variations of this multi-step assay have previously been integrated into the 2DPN format; therefore we sought to use that expertise for the development of a prototype device for the detection of hemagglutinin. The first step towards a prototype device required that we determine the order and number of steps required for optimal assay performance. This assay requires the sequential delivery of the sample and HRP-binder conjugate as the capture and detection binders target the same epitope on the influenza hemagglutinin. During assay development, we included two wash steps, one after the delivery of sample, and one after delivery of the HRP conjugate. If possible, we wanted to reduce the total number of steps that needed to be integrated into the integrated 2DPN. In testing the two wash steps separately, we found that the second wash, between the delivery of the HRP conjugate and the amplification buffer, containing both DAB and hydrogen peroxide, lead to equivalent performance of the assay (**Figure 4.4**).

The first attempt for integrating this assay used the traditional 2DPN format using a folding card containing each of the four required assay steps, **Figure 4.5**. The volumes used in this assay were selected based on previous work developing a 2DPN for the influenza nucleoprotein [37]. Initial validation using dye demonstrated the successful delivery of all four steps across a test region (**Figure 4.5B**), and identified the optimal membrane choices for each step. We found that fusion 5 was the best membrane to pull reagents from the glass fiber source pads into the nitrocellulose test region, which was used for all tests shown below. Fusion 5 allowed for effective separation of each step, while limiting the overall assay time to under an

hour. Once the assay chemistry was integrated into the 2DPN, we discovered challenges getting the positive test line to appear in the presence of influenza virus, **Figure 4.5C,D**. The primary source of these challenges was the loss of reagents to the device before the test line, which can be seen on both the positive and negative controls. This reagent loss is due to the contact of HRP and DAB before the test line, over a significant distance of Fusion 5. In addition to reagent loss, we also found that fluid did not flow evenly across the width of the test region, which was due to the shape of the corners in the 2DPN. This problem could be solved by creating rounded corners or through the introduction of a flow regulator [130], [141]. However, we decided to take a different approach to the integration of enzymatic amplification in a way that increased overall assay performance by delivering the amplification buffer orthogonally.

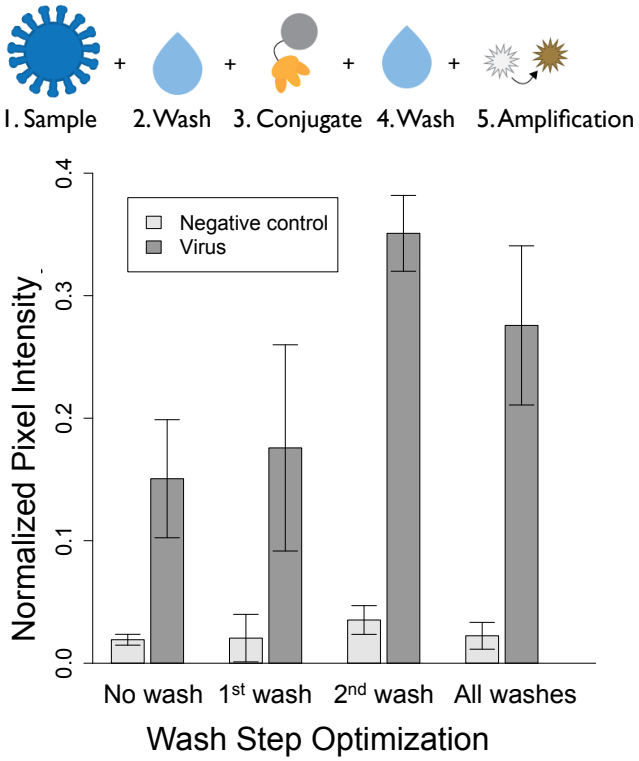

Figure 4.4. Optimization of wash steps.

(A) Schematic depicting the assay to be integrated, using head region binders for capture and detection of the influenza virus (B) Wash step optimization, with normalized pixel intensity and representative test strips with all four conditions, no wash, with the first wash step (after sample), second wash step (after conjugate) and both washes. Molecular components are not drawn to scale.

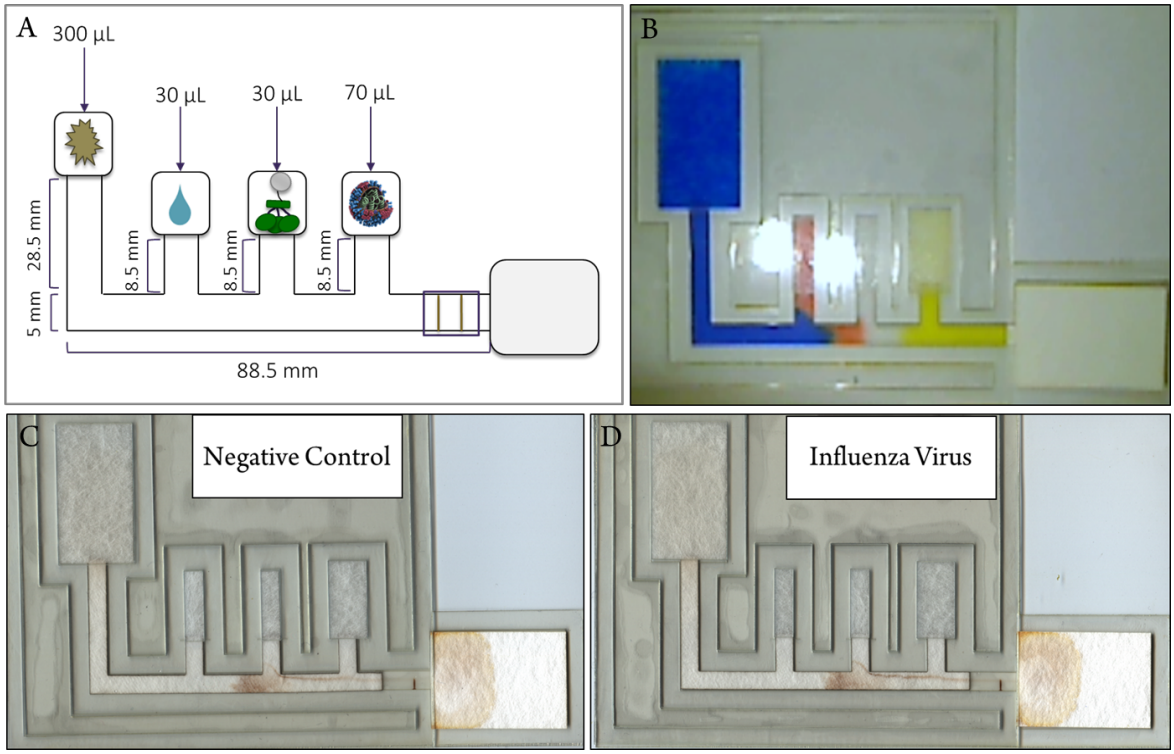

Figure 4.5. Traditional 2DPN developed for the integration of the HRP assay. Includes a drawing of the assay schematic (A), fluidic validation using dye (B), and integration of the enzymatic amplification assay demonstrated with a negative control and influenza virus (C,D).

Recent advances in the understanding of fluid flow in paper microfluidics have shown that understanding partial saturation effects are critical to describing fluid flow in paper microfluidics [53]. Controlled partial saturation effects enable the assay developer to sequence fluid delivery using material choices, and allow for the design of devices which can control flow rates of subsequent assay steps independently. This understanding of membrane wetting and fluid flow has enabled the integration of more complex fluidic handling into paper microfluidic approaches. Other applications of this phenomenon include automated DNA extraction and concentration from large sample volumes and an automated dilution series for downstream immunoassay detection [53]. While the traditional 2DPN has been used for enzymatic amplification within porous matrices, the traditional 2DPN architecture required the amplification chemistry, the last assay step, to flow through a long section of paper.

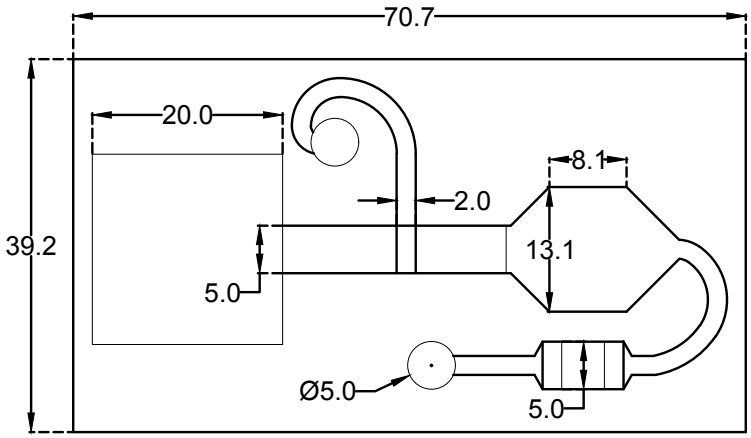

Figure 4.6. Drawing of 2DPN device.

Dimensions are shown in mm. The 2DPN components consist of glass fiber, nitrocellulose, and cellulose as shown in **Figure 4.7**.

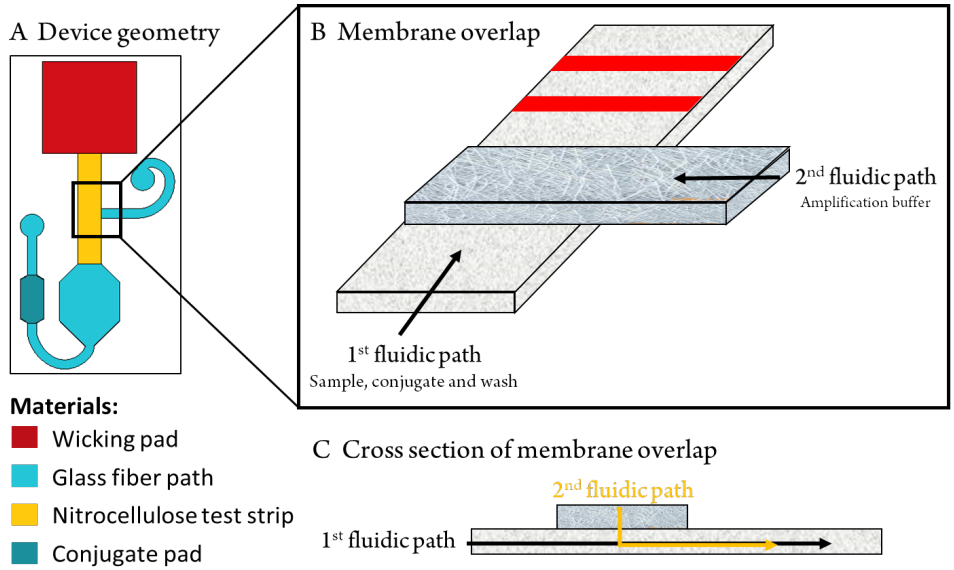

Figure 4.7. 2DPN for orthogonal delivery of amplification buffer.

(A) The device consists of a cellulose wicking pad, primary and secondary glass fiber fluidic paths, a glass fiber conjugate pad, and a nitrocellulose test strip. The membrane overlap between the first and second fluidic paths enables delivery of each set of fluids orthogonally (B), where the second fluidic path is only activated when the automatic release mechanism delivers the amplification buffer to the glass fiber strip (C).

Prototype devices have been designed to automate the steps for enzymatic amplification in a controlled manner. Enzymatic amplification has been used to improve sensitivity in lateral flow assays, however the additional steps required for the assay increase the overall complexity of the end device. Previous devices to automate the delivery of enzymatic amplification have relied on delivery of each subsequent step over the region of the step before. While these devices have been demonstrated in the literature [53], there is some degree of reagent loss along the device before the test line. In addition, the fluid resistance increases with the length of the membrane through which that flow must pass. By forcing the last reagent to flow through the entire downstream paper network, the time to assay completion increases, while limiting the ability to individually tune assay steps. We thereby aimed to deliver amplification buffer across the test line orthogonally after the sample, conjugate, and wash steps were complete.

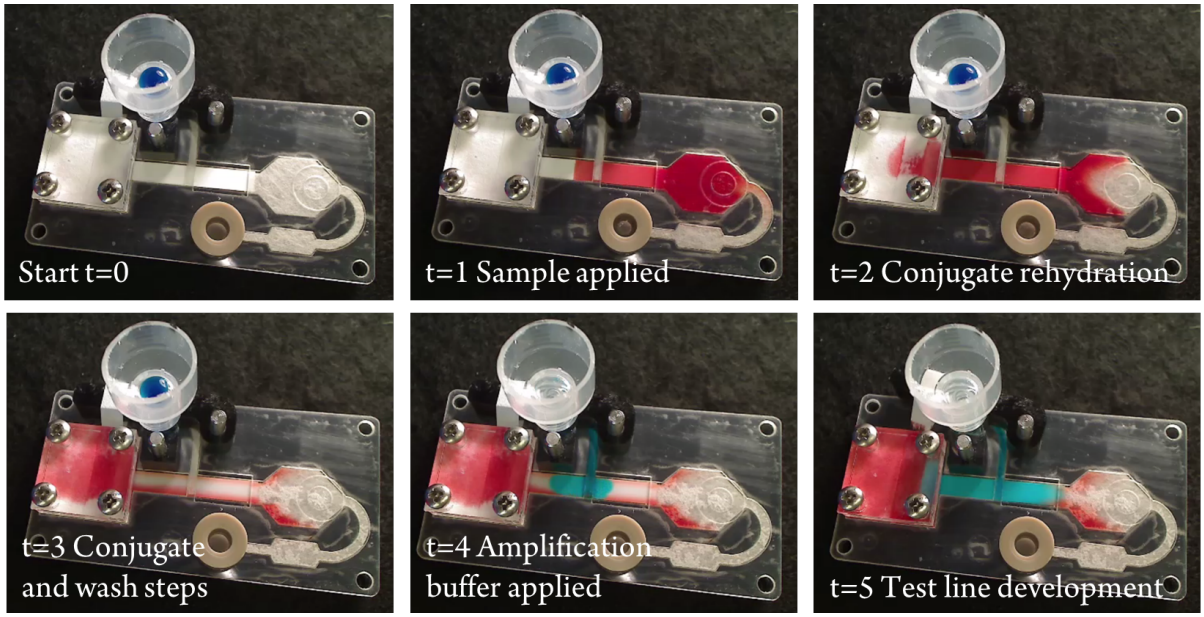

Figure 4.8. Automated delivery of assay on device with food coloring.
(t=0) device before the beginning of the assay (t=1) sample applied to the sample pad (t=2) conjugate rehydration by wash buffer (t=3) conjugate and wash buffer delivered across the test lines (t=4) amplification buffer applied after the water-soluble membrane releases the pinch valve (t=5) the test line develops as the amplification buffer is applied to the tests line.

Orthogonal delivery was accomplished using an overlapping section of glass fiber membrane, which has larger pores and lower suction pressure than the nitrocellulose assay membrane. This allows exploitation of partial saturation to create two distinct, independently

controllable fluidic paths, **Figure 4.7**. This fluid phenomenon has been previously demonstrated for use in processing large fluid samples, like urine [54]. The device is activated by the addition of the sample, wash buffer, and amplification buffer to their respective ports by the user. The solution addition steps, specifically wash and amplification buffers, can be simply automated in a commercial product [142]. The first three solutions are delivered sequentially in the traditional manner: the sample, rehydrated conjugate solution, and wash buffer respectively. When a sufficient volume of fluid has moved into the wicking pad, water-soluble paper in contact with the wicking pad dissolves and releases the arm pinching the tubing preventing amplification buffer flow. This releases the amplification buffer into the glass fiber, which subsequently flows through the detection strip. Images of this process using food coloring are shown in **Figure 4.8**.

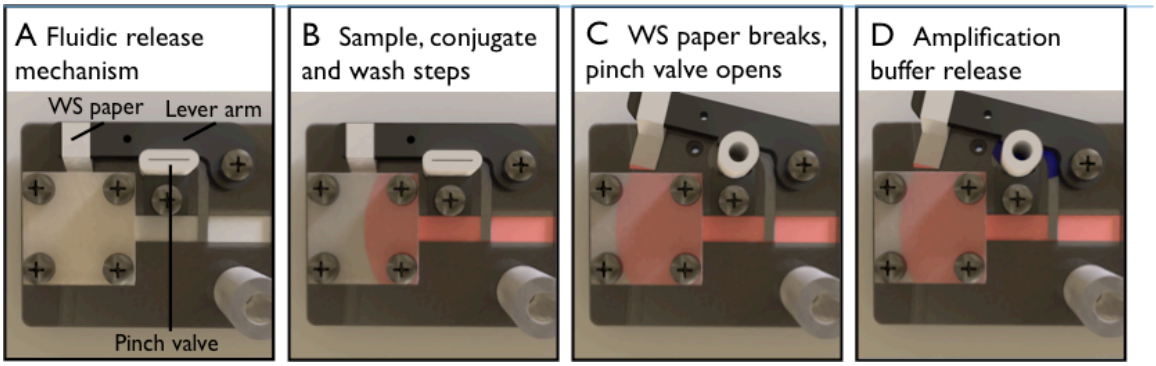

Figure 4.9. Schematic describing fluidic release on device.
Amplification buffer delivery using the novel paper network geometry involving two dissimilar porous materials and pinch valve. The membrane overlap between the first and second fluidic paths enables delivery of each set of fluids orthogonally. The device uses water-soluble (WS) paper surrounding a lever arm that holds a pinch valve close (A). The first three steps; sample, conjugate, and wash steps, are delivered across the primary fluidic path (B). As the wicking pad wets, the water-soluble paper that is placed in contact with it wets until the force of the lever arm overcomes the strength of the paper. This leads to the release of the lever arm and opening the pinch valve (C). Open, the amplification buffer is delivered *via* the secondary fluidic path and onto the nitrocellulose test membrane (D).

This device uses a paper-based fluid delivery system to automatically deliver the amplification buffer to the test line at the right time, after the sample, conjugate, and wash buffer steps are all complete. Once the cellulose wicking pad wets a defined amount, water soluble

paper in contact with the wicking pad as shown in **Figure 4.9** dissolves enough to lose tensile integrity, ripping due to the force applied by the pinch valve arm holding the silicone tubing closed. The pinch valve arm can then rotate, enabling the amplification buffer to pass through the silicone tubing and be delivered to the test line through 2nd glass fiber fluidic path. The location, width, and length of the water-soluble paper can be adjusted to tune the release of the amplification buffer. Optimization of these parameters are shown in **Table 4.2**. For the final dimensions of the prototype device, release of the amplification buffer occurred at 29.4± 3.6 minutes.

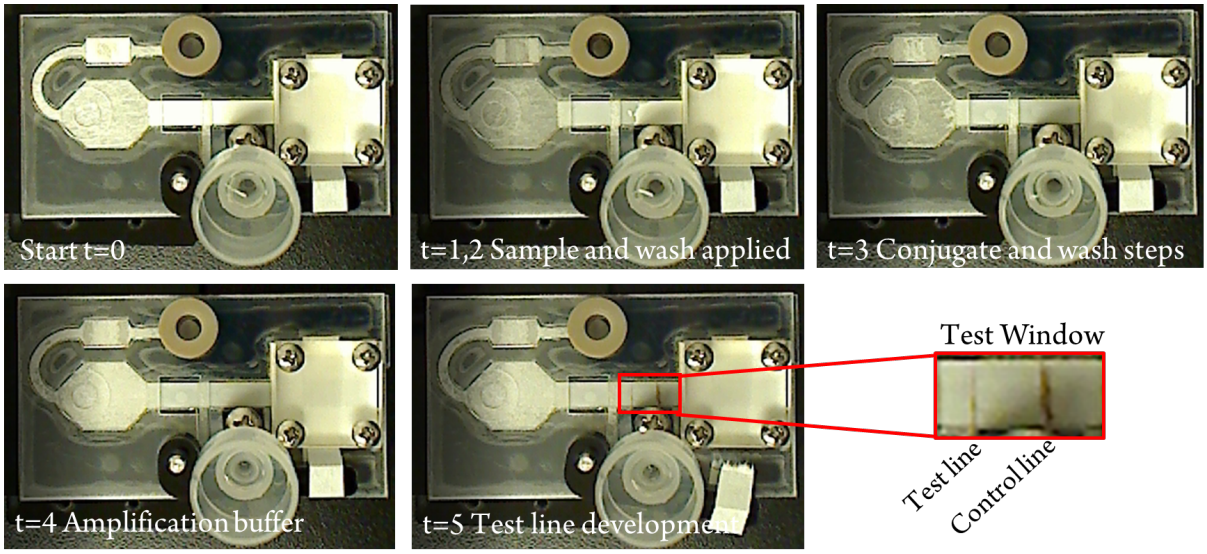

Figure 4.10. Integration of enzymatic amplification into the designed prototype device. Images showing the automated delivery of each of the assay steps across the test region, as shown with food coloring the represent each step. (t=0) device before the beginning of the assay (t=1,2) sample applied to the sample pad and conjugate rehydration by wash buffer (t=3) conjugate and wash buffer delivered across the test lines, as the glass fiber pads can be seen to drain of fluid (t=4) amplification buffer applied after the water soluble membrane releases the pinch valve (t=5) the test line develops as the amplification buffer is applied to the tests line, shown in the bottom right.

After demonstrating the delivery of each assay step in a sequential manner using the prototype device, we tested the HRP assay by pipetting each required step into their respective locations and allowing the assay to run. Initial tests using this geometry were highly successful, shown in **Figure 4.10**. The test line and control line, which consisted of an anti-HRP antibody,

both appeared visibly across the entire width of the nitrocellulose test strip. The initial geometry was selected based on the ability to sequentially deliver reagents in the correct order without leaking of the amplification buffer, which occurs when the nitrocellulose test strip is short. We also tested longer lengths of nitrocellulose, anticipating that a longer test strip will slow down flow enough to increase the sensitivity of the assay. However, we found that there was no statistically significant difference in the performance of the two lengths of nitrocellulose tested, **Figure 4.11**. This suggests that the shorter nitrocellulose length is preferred, because it leads to equivalent performance of the assay within a shorter time. There was one device that had flow issues, leading to a significant increase in the average time and overall standard deviation, however this was due to errors in assembly that could be easily addressed.

Table 4.2. Optimization of pinch valve for amplification buffer release.
By varying the width of water-soluble (WS) paper release, the timing of delivery of amplification buffer varies between 21 and 40 minutes.

Spy WS paper width	8 mm	9mm	10mm
Rep 1	23	29	48
Rep 2	23	28	47
Rep 3	17	24	39
Rep 4	24	31	33
Rep 5	18	35	37
Average	21	29.4	40.8
Std Dev	2.898275349	3.611094017	5.810335619
Percent deviation	13.8%	12.3%	14.2%

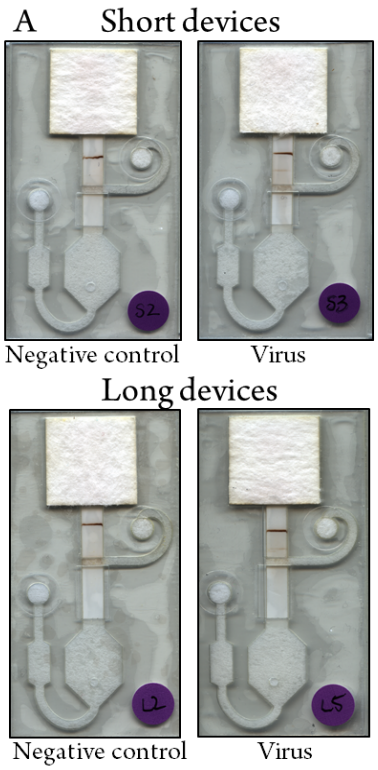

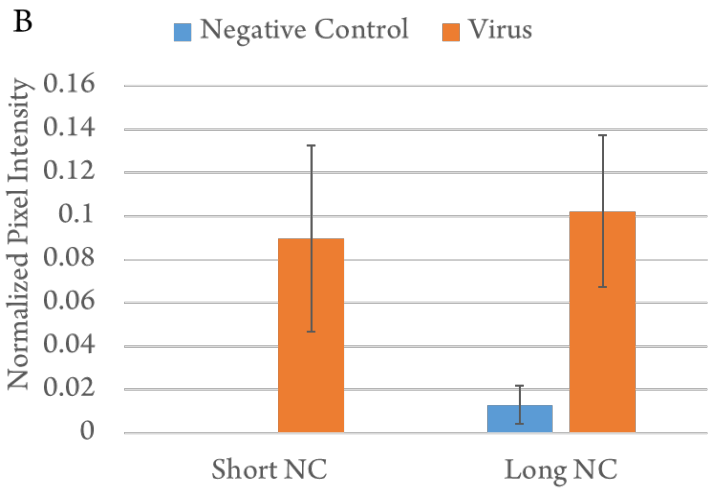

C

TOTAL TIME (MINUTES)	LONG DEVICES	SHORT DEVICES
REP 1	52	49
REP 2	52	49
REP 3	51	57
REP 4	50	45
REP 5	50	45
AVERAGE DEVICE RUN TIME	51 +/- 1	49 +/- 4.9

Figure 4.11. Effect of nitrocellulose length on assay performance.
(A) Scanned images of representative tests for each length, both long and short nitrocellulose length for positive (virus) and negative controls, (B) Normalized pixel intensity for the short and long devices with negative control and virus, and (C) the total time required for the short and long devices.

In 4.3.1, we have demonstrated a new geometry that uses the orthogonal delivery of amplification buffer to increase performance of an assay using enzymatic amplification. This new geometry, taking advantage of the capillary pressure in different materials, limits the distance over which the two reactive elements of this assay (HRP and DAB) to the test window. As we limit this distance, we saw an improvement in the overall performance of the assay. The following sections in this chapter will build upon this success, demonstrating the long-term stability of proteins when stored on device (**4.3.2**), and characterizing the total assay sensitivity on device and successful detection of virus from patient samples (**4.3.3**).

4.3.2 *Long term stability of protein binders*

Traditional laboratory tests are difficult to run at the point of care due to their need for refrigeration and trained personnel to run the assay successfully. One of the major advantages of lateral flow assays are their ability to be implemented at the point of care, whether at a doctor's office or out in the field, with the automated delivery of each reagent that has been dried on the device itself. Depending on the assay, any number of the following components need to be stored on the device: biomolecules, such as antibodies, proteins, enzymes, and nucleic acids, buffers, and labeling agents such as gold nanoparticles and fluorophores. Each of these components has their unique challenges. For example, RNA can be hydrolyzed when stored improperly, whereas proteins have the tendency to denature or unfold when exposed to extreme temperature or pH. Long-term stability is a critical property for any lateral flow assay, as it ensures that the assay works properly after transportation and storage at ambient conditions. For the development for a 2DPN for the detection of influenza virus, the long-term stability of the biomolecules used for capture and detection is extremely important. This section will explore the storage of two biomolecules necessary for the success of the influenza assay; the capture binder that is spotted at the test line and the detection binder stored in the conjugate pad. In the case of the capture binder, it is critical that the protein stays put and retains function. For the detection binder, on the other hand, it is important that the reagent can be rehydrated and flow downstream, while retaining function of both the binder and the enzyme it is conjugated to.

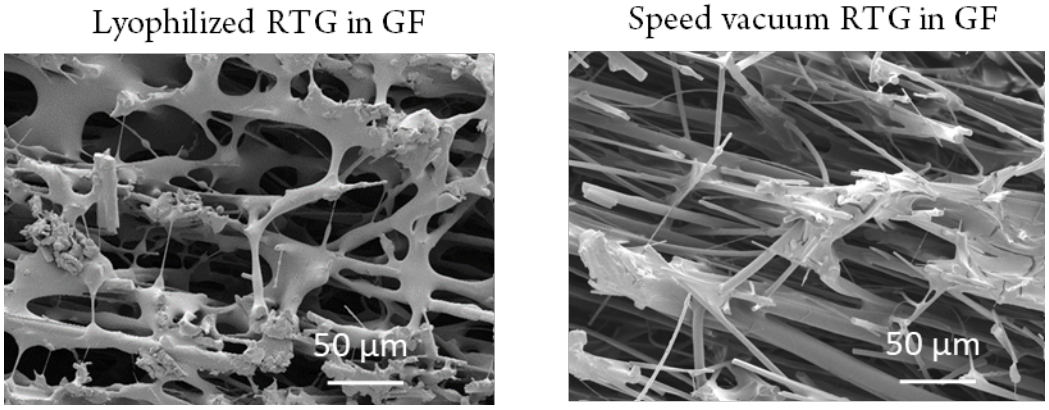

Figure 4.12. SEM images of glass fiber dried with RTG stabilizer mixture.
These membranes were prepared using either lyophilization (left) or speed vacuum (right). Images taken by Dr. Joshua Buser.

Specific methods for dry reagent storage in porous matrices include air drying, oven drying, vacuum drying, and lyophilization. Not only do these methods vary in their complexity, they also lead to differences in the structure of the reagents once fully dry, **Figure 4.12**. Lyophilization is one of the more commonly used methods for long term storage of protein solutions, often used for the conjugate pad, consisting of separate freezing and drying steps [46]. Stabilizers are often required in conjunction with these methods because the stresses involved in freezing and drying can lead to specific stresses that influence the stability of a protein [143]. Sugars and sugar alcohols are commonly used to stabilize proteins, such as sucrose, dextrose, and trehalose. There are a few schools of thought when it comes to protein stabilization. Specifically, it is believed that protein stabilization works due to vitrification, where a glassy cocoon physically protects a protein from abiotic stress, preferential exclusion, where reduction in the protein radius is accomplished by isolating water molecules away from the proteins, and water replacement, where hydrogen bond formation with the protein replaces water molecules with a sugar stabilizer [144]–[146].

In this section, we aimed to study the effect of different sugar stabilizers on the overall stability of the capture binder when spotted onto nitrocellulose. The four stabilizers tested were dextrose, sucrose, trehalose, and the proprietary Ready-To-Go (RTG) manufactured by GE. While RTG is proprietary, searches into the patent literature suggest that the sugar used in the mixture is melizitose. Trehalose, one of the most commonly used sugar stabilizers for biopreservation, is typically used for a number of applications due to its high glass transition temperature. **Table 4.2** highlights some of the important properties of these sugar stabilizers, including the category, chemical formula, and glass transition temperature.

For the test line, we have previously demonstrated a high degree of success using air drying to immobilize the protein binder onto a nitrocellulose membrane. Because these proteins are highly thermostable, the addition of heat during oven drying would not influence the structure of the protein as it dries. However, had not yet explored the role that sugars play in the stability of the binder over time. With our collaborators at GE and PATH, we carried out a long-term stability study of the capture binder when stored in the presence of trehalose, dextrose, sucrose, and a proprietary GE product known as Ready To Go (RTG). Protein binder was striped at GE in the presence or absence of a sugar additive before being stored at either 30 or 40°C in a

controlled humidity room for up to 4 months. Simultaneously, our collaborators at PATH were completing a study with antibodies used as capture for the influenza nucleoprotein.

Table 4.3. Sugars used in the capture stability study.
The table depicts the category of sugar, chemical formula, glass transition temperature, and structure of each sugar. While we do not know the specific sugar(s) used in the RTG system, we have included a trisaccharide for comparison. Sources: [147], [148].

	Dextrose	Sucrose	Trehalose	Melezitose
Category	Monosaccharide	Disaccharide	Disaccharide	Trisaccharide
Chemical Formula	$C_6H_{12}O_6$	$C_{12}H_{22}O_{11}$	$C_{12}H_{22}O_{11}$	$C_{18}H_{32}O_{16}$
Tg (°C)	36	60	107	160
Structure	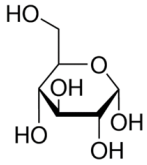	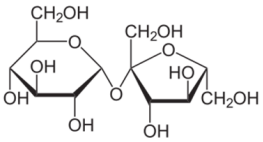	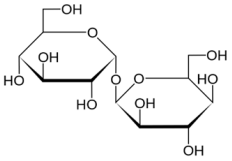	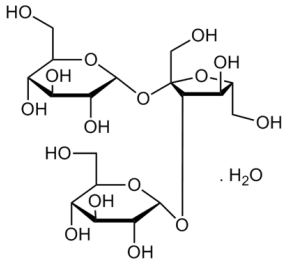

The initial time point, Day 0, was intended to set a baseline from which to compare all future testing of these membranes. It provided additional information about the effect of specific additives on the ability of head region binder to function as capture. We cannot state definitively whether the additives affected the long-term adsorption of the head region binder to the test line, though this can be easily tested by using a protein stain on membranes that have not been tested. One of the biggest differences between the membranes lined at GE and those prepared here at UW is the thickness of the line width. With the GE membranes, we see more of a coffee ring effect, with binding primarily at the edges of the test line. For the membranes we spotted at UW, we instead see consistent binding take place cross the entire thickness of the line. Though their lining methods were optimized for ideal visualization of an antibody-based test line, it appears that this is not the ideal method for this particular assay. At Day 0, the performance of three conditions, no additive, trehalose, and sucrose, led to equivalent results for both the virus and negative control cases, **Figure 4.13**. Alternatively, the presence of dextrose or RTG led to a complete loss in signal in the positive controls for both sets of strips. This suggested that these

two sugars blocked the adsorption of the capture binder or binding of the analyte to the capture binder at the test line.

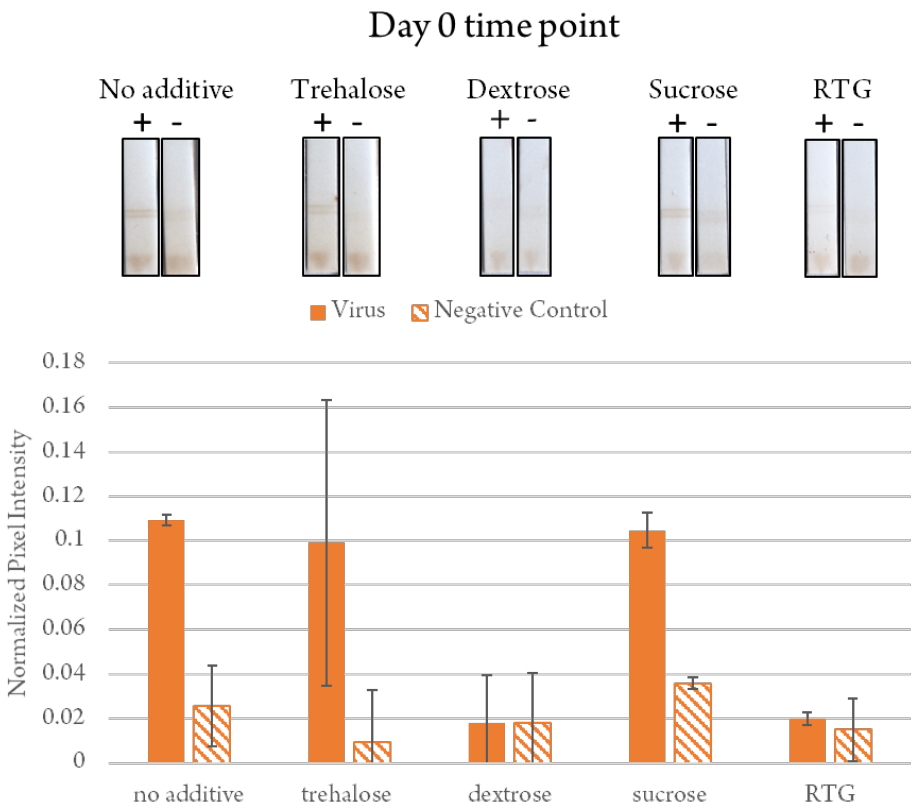

Figure 4.13. Day 0 of the capture storage stability study.

All conditions were run with an influenza virus concentration of 6.25 x 10^7 $CEID_{50}$/mL. Includes scanned images and normalized pixel intensity. Demonstrates the influence of trehalose, dextrose, sucrose, and RTG on assay performance at the start of the study. All conditions were run with an n=3, and images were scanned at 600 dpi.

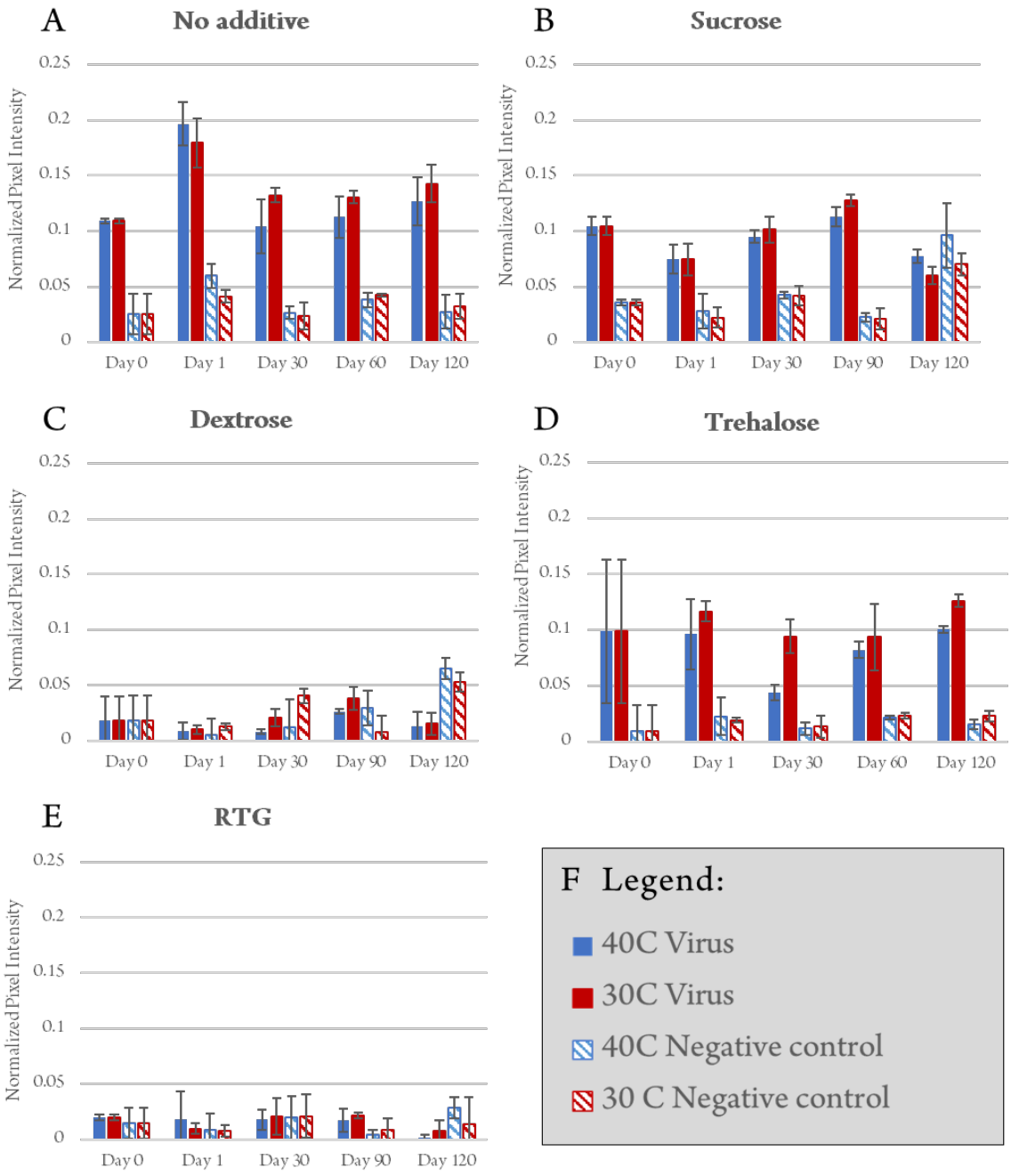

Figure 4.14. Storage stability study of head region binder by additive.

The five storage conditions include (a) no additive (b) sucrose (c) dextrose (d) trehalose (e) Ready-to-go (RTG). All conditions were run with an influenza virus concentration of 6.25 x 10^7 $CEID_{50}$/mL. The figure legend shows the two conditions tested, with both positive (virus) and negative controls. Depicted on each graph are the normalized pixel intensities calculated from scanned images of the test strips at 600 dpi. All conditions were tested with an n=3.

Over the course of the stability study, we found that the 'no additive' case lead to the best performance. This is demonstrated by the consistency in signal, maintaining the degree of signal and low background in the negative control at each time point and at both storage temperatures. Trehalose was the best performing sugar additive over the course of the time study, showing similar results as compared to the no additive case. Over time, the dextrose, sucrose, and RTG membranes all began to see a higher degree of non-specific signal on the negative control. This data suggests that the no additive case, which involved spotting membranes with the head region binder without the presence of an additive, is the most promising due to superior performance while simultaneously minimizing the manufacturing complexity. The head region binder is designed to be highly thermostable, with stability demonstrated up to 80°C in aqueous form, which is advantageous for the integration and design of point of care assays using these binders. The results from all time points organized by additive are shown in **Figure 4.14**. According to the standardized scorecard created by HIV researchers to better evaluate point of care diagnostic tests, this would rate our assay in the top category as stability is maintained when stored at 40°C for a minimum of three months [149].

Once we had demonstrated the stability of the head region binder as capture, the next step was to develop a storage protocol for the conjugate used in this assay. We are using an HRP conjugated directly to the head region binder via maleimide chemistry, therefore we need a storage solution that maintains the integrity of the entire conjugate, which includes the enzymatic activity of HRP. Building from previous work using an antibody-HRP conjugate, we started with a preservation protocol that used 0.1% BSA, 0.01M EDTA, 0.01M $FeSO_4$, and 10% trehalose that is combined with the conjugate and lyophilized in a glass fiber pad [42]. Each of these additives plays a separate role in the stability mixture. For example, BSA serves as a sacrificial protein for the blocking of the glass fiber membrane, and any other membrane connected to the pad. The first required test was to determine the concentration at which the conjugate should be stored in the glass fiber conjugate pad. Testing a range of concentrations of head region binder conjugate with the starting concentration of the other additives, we found that the 300-1000 nM concentration range lead to comparable results, **Figure 4.15**. However, none of these concentrations performed as well as the fresh head region binder, likely due to flow issues and the loss of protein to the fluidic path.

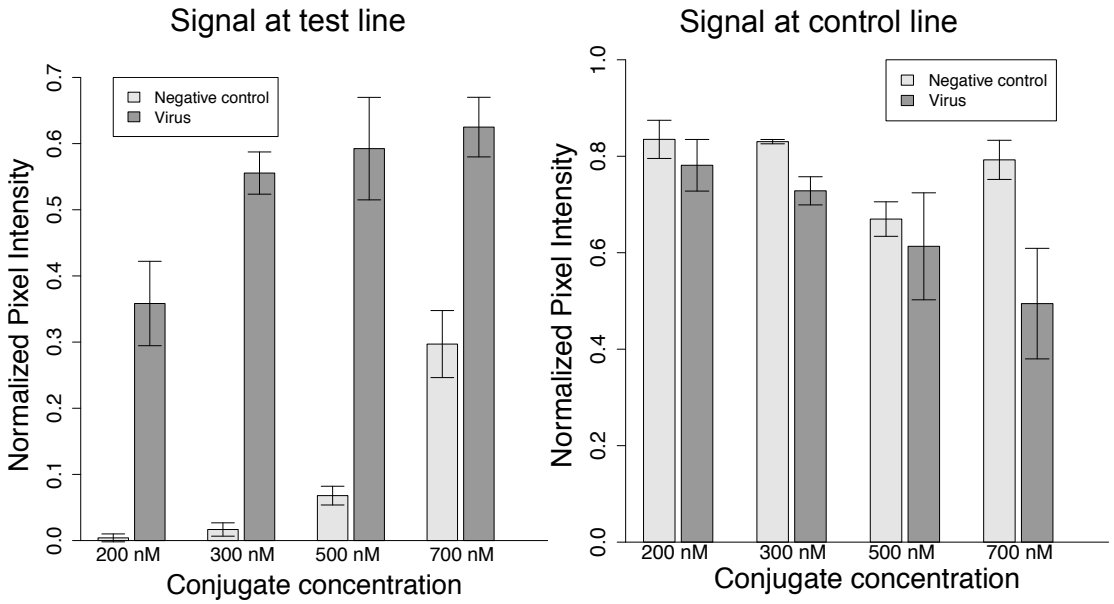

Figure 4.15. Concentration optimization of head region binder-HRP conjugate. Optimizing primarily with the test line in mind (left), we found the optimal concentration of conjugate to be around 300 nM based on the difference in signal between the negative and the positive. At the control line (right), we found that higher concentrations of conjugate led to lower signal in the presence of virus. The normalized pixel intensity was calculated for both the test line and control line. All conditions were tested with an n=4.

For the concentrations of BSA, EDTA, and $FeSO_4$, previous optimization found the optimal range of Fe-EDTA to be between 0.005 and 0.2 M [42]. Even though the glass fiber membranes were pre-blocked with BSA, the addition of BSA in the dry storage mix as well helped reduce the loss of conjugate to the membrane. We chose to use the same concentrations for iron, EDTA, and BSA as was previously optimized in the antibody based HRP system. One important note regarding EDTA and $FeSO_4$ is their stoichiometry in the conjugate pad mixture. EDTA serves to chelate iron sulfate, and the lack of EDTA leads to false positives at the test line, as seen in **Figure 4.16**. We found that it only appears at the test line, and not throughout the membrane itself, suggesting that the iron is interacting with the head region binder adsorbed on the test line, causing it to pile up at that location. Therefore, when DAB is added into the system the iron can oxidize the DAB into its precipitated form.

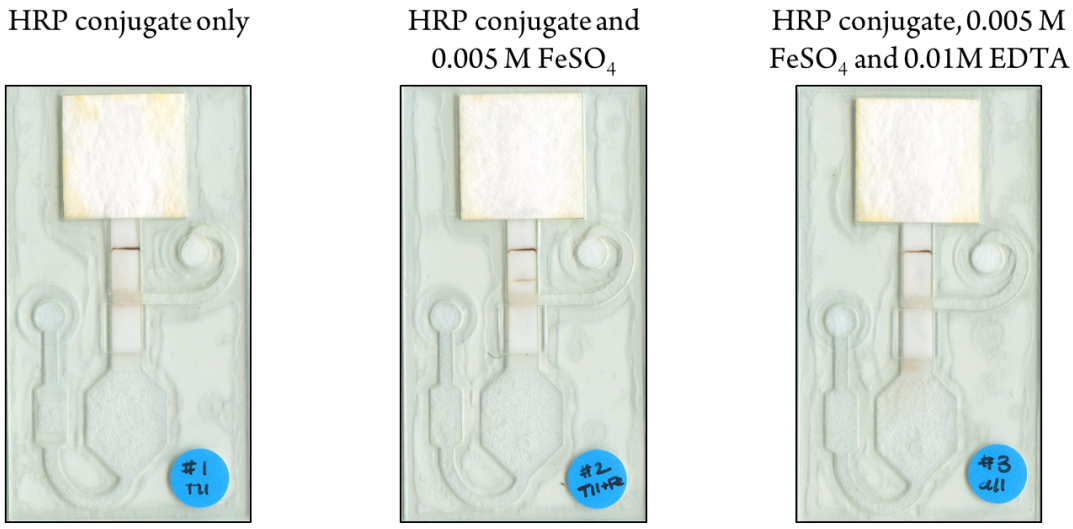

Figure 4.16. Troubleshooting false positives during dry storage optimization. Scanned devices used to troubleshoot the false positives by looking at each reagent involved in the dry storage mix. Tested solutions included (A) just the head region binder-HRP conjugate (B) head region binder HRP conjugate with 0.005M $FeSO_4$ (C) head region binder HRP conjugate with 0.005M FeSO4 and 0.01M EDTA.

The final optimization step for the conjugate pad dry storage mixture required a closer look at the concentration of trehalose. Previously published work used a 4% trehalose in the dry storage mix, however optimization of the concentration of trehalose for long term storage remained necessary. Because trehalose has been demonstrated to stabilize proteins, suppress auto-oxidation of DAB, and facilitate rehydration, we wanted to test a larger range of trehalose concentrations to determine the optimal concentration for this assay [42], [150], [151]. Over time, tests with and without trehalose have demonstrated the need for trehalose at a minimum of 4%(w/v). However, when membranes are lyophilized and tested after storage at room temperature for a day, we found that the concentration of trehalose in the dry storage mix does not lead to a significant difference in the performance of the assay, in the positive or negative control, **Figure 4.17**. This is consistent with our understanding of dry storage, that trehalose helps to stabilize the HRP enzyme when stored at high temperatures for long periods of time.

The capture stability study done on the head region binder suggests that the protein itself is reasonably stable, even when stored at high temperatures. Therefore, the goal for the conjugate storage mix is to maintain the overall HRP activity. The first is that head region binder, which

has been designed to be highly thermostable, might not need that additional stability of the sugar during the dry storage process. The capture stability study done on the capture head region binder when adsorbed onto nitrocellulose suggested that this might be the case, as the presence of trehalose does not enhance the assay performance. Because the lowest tested concentration of trehalose was sufficient for assay performance, the conjugate pads used in the final device will be made with 4%(w/v) of the stabilizing sugar.

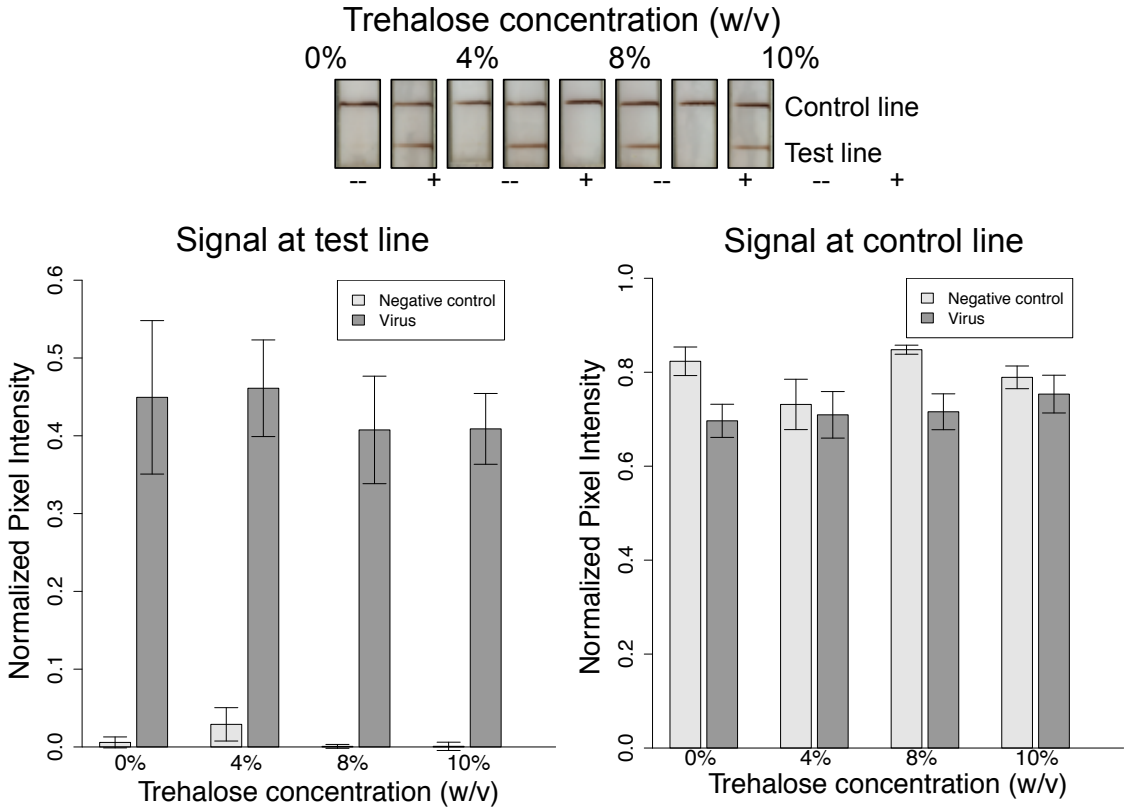

Figure 4.17. Trehalose optimization on device.
Optimization of the concentration of trehalose included in the dry storage mixture prior to lyophilization. Scanned images (at 600 dpi) and normalized pixel intensity of the test and control line on these devices were run to test the effect of trehalose concentration in the dry storage mix. Four concentrations of trehalose were tested, 0, 4, 8, and 10% with both virus and PBST with an n=3 for each concentration.

In this section, we have described the development of dry storage protocols for the capture and detection binders used in the influenza assay. For the capture binder, we found that the protein is stable enough to be spotted and stored in nitrocellulose without the need for sugar

additives. The detection binder required further optimization because of the need for effective rehydration and to stabilize the HRP enzyme. We found a dry storage mix that included specific concentrations of $FeSO_4$, EDTA, BSA, and trehalose lead to the best performance of the assay, which could then be integrated into our final device.

4.3.3 *An integrated device for the detection of the influenza hemagglutinin*

With the fluidics and the dry storage protocols developed, the next step was to integrate each of these pieces into a final device. The four-step assay for the detection of the influenza hemagglutinin was integrated to the device shown in **Figure 4.1**, with dry reagents stored in the conjugate pad and at the test and control lines. As demonstrated in 4.3.1, the orthogonal delivery of the amplification buffer led to an increase in the overall signal intensity as compared to more traditional 2DPN designs. A limit of detection analysis, comparing the performance of the device to the traditional dipstick format, found an improvement in the performance of this enzymatic amplification assay on device, **Figure 4.18**. The limit of detection for the device was calculated to be 4.45×10^2 $TCID_{50}$/mL (95% CI: [2.29×10^2,6.26×10^2]) on device, as compared 1.15×10^3 $TCID_{50}$/mL (95% CI: [7.56×10^2, 2.18×10^3]) for the dipstick format.

While the total assay time required for the dipstick averaged 54 +/- 3 minutes, the device delivers larger volumes across the test line in 41 +/- 4 minutes. Therefore, the device decreases the total time to result for this complex assay while maintaining assay performance. One major difference between the dipstick and the device assay is the volume of sample. The volume used on device, 70 µL, was the amount required to cover the nasal swab; alternatively, the standard 20 µL was used for sample delivery in the dipstick format. Directly comparing the same volume between the two assay formats, we found comparable results in significantly less time, requiring 94 minutes to run the dipstick format with 70 µL of sample. When corrected for volume, the LOD on device was statistically similar as compared to the dipstick format, with a steeper slope of the concentration curve, **Figure 4.19**. Not only does this enable processing of larger volumes of nasal swab sample with comparable limit of detection, the steeper slope of the concentration curve translates to improved analytical sensitivity, as defined by the International Union of Pure and Applied Chemistry (IUPAC) [152].

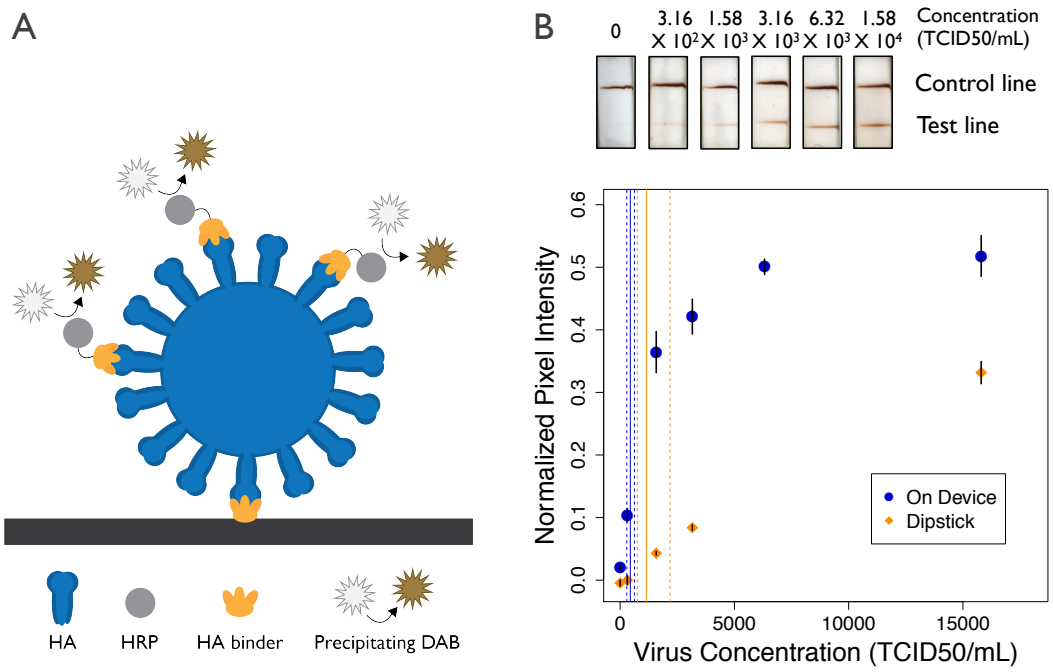

Figure 4.18. Limit of detection analysis on device.
Includes direct comparison between the device (black) and dipstick (blue) formats. (A) Schematic of the assay stack, molecular components are not drawn to scale. (B) Representative scans of device test strips and normalized pixel intensity for the assay run on device and in the dipstick format. The limits of detection were found to be 4.45 x 10^2 $TCID_{50}$/mL (95% CI: [2.29 x 10^2,6.26 x 10^2]) and 1.15 x 10^3 $TCID_{50}$/mL (95% CI: [7.56 x 10^2, 2.18 x 10^3]) in the on device and dipstick formats respectively. The solid lines indicate the calculated LOD, while the dashed lines indicate the 95% confidence interval. Data points are mean ± standard deviation, n=6.

The quantification of influenza virus in a sample or stock solution has traditionally been characterized using infectious units, protein amount or activity, or RNA content. In this work we report influenza virus infectivity using two different units: tissue culture infectious dose 50% endpoint ($TCID_{50}$/mL) or chicken embryo infectious dose 50% endpoint ($CEID_{50}$/mL). However, the magnitude of these infectivity units is dependent on the cell line the viruses were grown in and the cell line used to determine infectious titer. Clinical influenza virus loads in nasopharyngeal washes have been reported to peak at 10^3 to 10^7 $TCID_{50}$/mL [153]. By RNA copy number, the virus load in nasopharyngeal washes have been found to range between 10^5 and 10^7 copies/mL for H1N1 and 10^6 to 10^8 copies/mL for H3N2 [154]. The correlation of

different units used to characterize the influenza virus will vary depending on the virus strain and the cell line used for growing the virus.

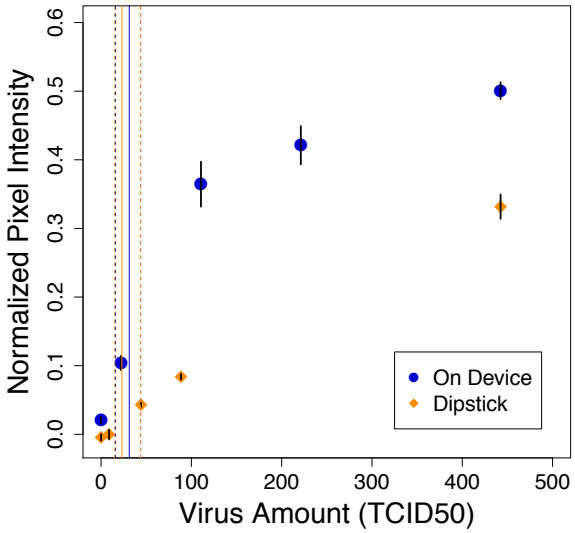

Figure 4.19. Limit of detection by TCID50.
Determination of the limit of detection for the device (blue) and dipstick (orange) assays for virus amount ($TCID_{50}$) instead of concentration, as shown in Figure 4.18. Normalized pixel intensity for the assays run on device and in the dipstick format. The limits of detection were found to be 31.22 $TCID_{50}$ (95% CI: [16.03, 43.82]) and 23 $TCID_{50}$/mL (95% CI: [15.12, 43.6]) in the on device and dipstick formats respectively. The solid lines indicate the calculated LOD, while the dashed lines indicate the 95% confidence interval. Data points are mean ± standard error, n=6.

As discussed in 2.3.2, the assays for H1N1 and H3N2 were found to yield statistical LODs of 1.35 x 10^7 $CEID_{50}$/mL and 1.11 x 10^7 $CEID_{50}$/mL respectively, with 95% confidence intervals of [7.26 x 10^6,1.90 x 10^7] and [6.85 x 10^6, 1.50 x 10^7], **Figure 3.11**. These results are consistent with the gold nanoparticle based assay for detection of H1N1, with a sensitivity improvement that can be attributed to enzymatic amplification. Due to the need to source a larger quantity of influenza virus, the assay for H1N1 was tested with a new stock of virus grown in Madin-Darby Kidney cells (MDCK) and was found to have a statistical LOD of 1.15 x 10^3 $TCID_{50}$/mL, with a 95% confidence interval of [7.56 x 10^2, 2.18 x 10^3]. The variation in LOD between virus stocks suggested the need for further characterization of the virus samples. To do

so, RNA copy number was determined for each virus stock using qRT-PCR, and the LODs by copy number were found to be statistically similar, **Figure 4.20**. With the LOD of 1.15 x 10^3 $TCID_{50}$/mL, this assay is capable of detecting the lowest clinical range during peak infection.

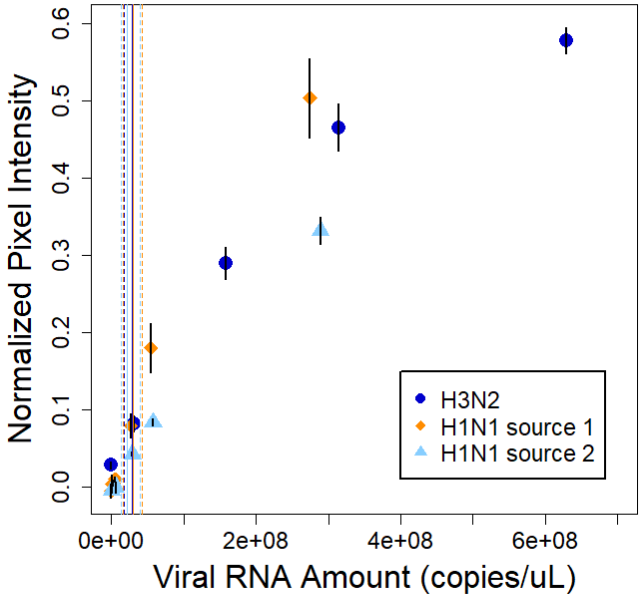

Figure 4.20. Limit of detection by RNA amount.
Viral RNA amount was determined using qRT-PCR for each source of virus. The limits of detection for these three virus strains were found to be statistically similar, as depicted by the LOD (line) and 95% CI (dotted line). The LODs are 2.91 x 10^7 copies/µL [1.80 x 10^7, 3.94 x 10^7], 2.96 x 10^7 copies/uL [1.59 x 10^7, 4.17 x 10^7], and 2.10 x 10^7 copies/µL [1.38 x 10^7, 3.98 x 10^7] for the H3N2, H1N1 source 1, and H1N1 source 2 respectively. The H3N2 and H1N1 source 1 virus stocks were obtained from the Influenza Reagent Resource. H1N1 source 2 was grown in the Bloom lab at the University of Washington.

Nasal swabs are most commonly used for the detection of influenza virus from a patient presenting with influenza-like illness [155]. Because true sensitivity of a diagnostic requires that known concentrations of target analyte are tested in the context of a clinical sample, it is crucial to validate the head region binder assay in a complex sample matrix. Nasal swab samples contain a wide variety of proteins and other components that might interfere with the hemagglutinin assay, including albumin, antibodies and mucins [156]. Initial testing with nasal swab samples was completed with influenza negative patient samples received from Seattle Children's hospital during the 2015-2016 flu season. This testing demonstrated two primary modes of failure for the

assay; poor flow of the viscous sample within the porous network and non-target binding on the test line. To address both modes of failure, we explored dilution with a sample buffer containing surfactant (Tween 20) and 1% BSA to reduce the effect of the nasal swab sample by improving flow and reducing non-target binding respectively.

Using a serial dilution of patient sample, we found that high concentrations of the influenza-negative patient sample lead to assay failure. This was primarily due to a combination of problems with solute and solvent transport to the test line. Due to the viscosity of the nasal swab sample at high concentrations, the analyte and conjugate both were becoming trapped where they first met the nitrocellulose membrane. However, a 10-fold dilution was sufficient to regain assay performance, **Figure 4.21**. This is the equivalent of placing the nasal swab into a tube with 700 µL of buffer.

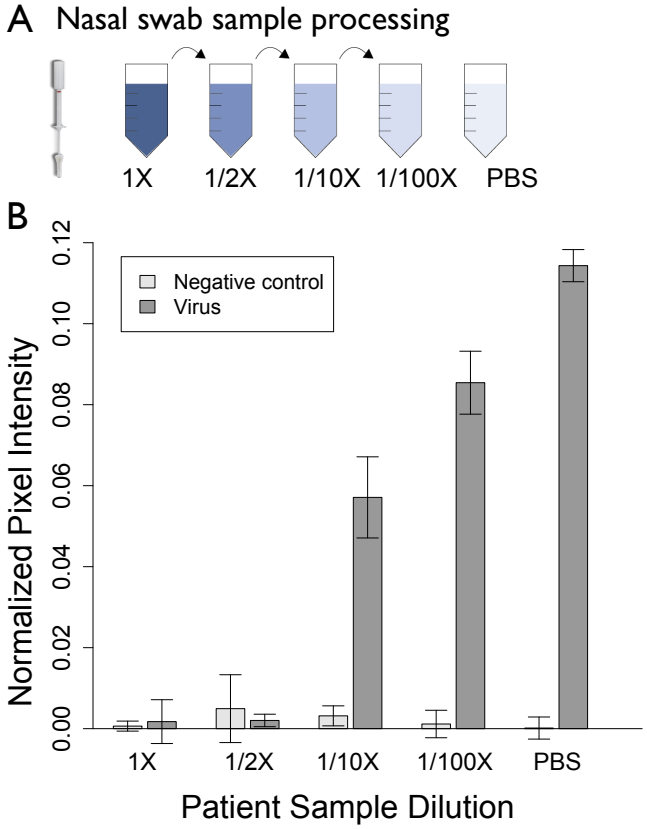

Figure 4.21. Testing the HA assay with spiked patient samples.
Flu HA assay tested with virus spiked into nasal swabs that tested negative for influenza. Graphical representation of the patient sample dilution (A) and normalized pixel intensity of the test strips tested with decreasing concentrations of patient sample (B). Data points are mean ± standard deviation, n=4.

Dilution of nasal swab samples showed signal restoration after a 10-fold dilution of influenza negative nasal swabs spiked with influenza virus. 1X represents a swab diluted into 70 µL of PBS, the volume required to cover the entire swab. As the patient sample is diluted, signal begins to be restored at the 1/10X dilution, which translates to 700 µL of PBS. This is significantly less dilution than the current standard, which involves dilution in approximately 3 mL of universal transport medium (UTM) or other buffer [157]. A ten-fold dilution of the nasal swab is significantly less than the dilution currently required for commercially available tests for the detection of the influenza nucleoprotein [114]. However, the dilution of sample does lead to a reduction in the concentration of analyte delivered to the test line. Future work will involve the investigation of preparation techniques to treat nasal swabs samples that limit overall sensitivity losses.

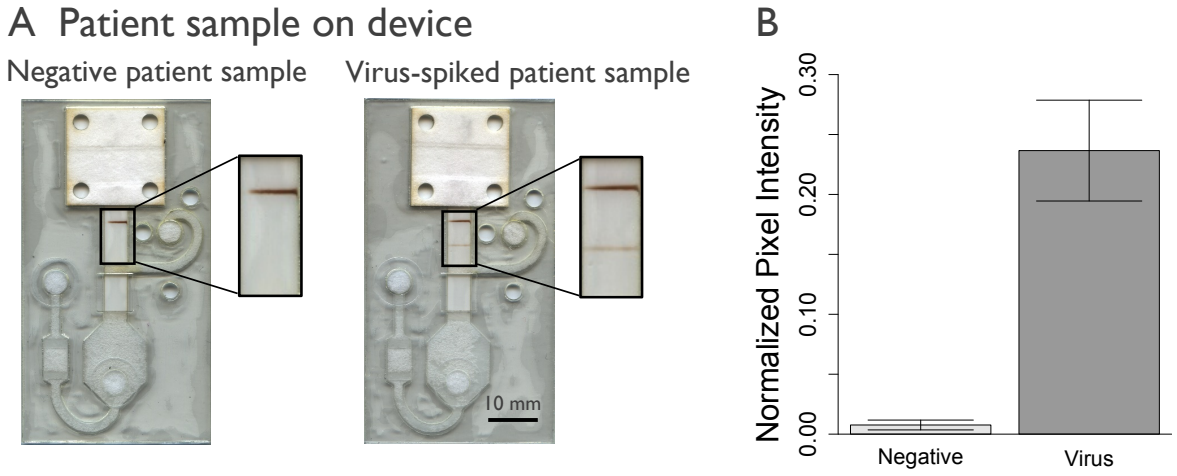

Figure 4.22. Spiked patient samples tested on device.
The device was tested with influenza virus spiked into nasal swabs samples that tested negative for influenza, at 6.32 x 10^3 $TCID_{50}$/mL for 70 µL of sample. Representative scans of the devices run (A) and normalized pixel intensity of these scans (B) are shown. Negative patient samples were run with n=3, and spiked patient sample was run with n=4.

Negative nasal swab samples spiked with the 2006 Solomon Islands strain of influenza A virus were run on the automated prototype device using the 10-fold dilution factor determined in **Figure 4.21**. The automated delivery of these reagents led to successful detection of influenza virus spiked into a human nasal sample, **Figure 4.22**. This prototype device fully automates the delivery of a multi-step enzymatic assay, demonstrating sensitive detection of influenza virus

within an average of 45 minutes. Not only does assay performance increase on device, we demonstrate that minimal sample preparation is necessary for detection from a complex sample. We have herein demonstrated the successful integration of an automated paper microfluidic device to detect influenza virus in a nasal swab sample.

Specific detection of hemagglutinin is useful for epidemiological tracking, to inform clinical treatment, and as a companion diagnostic. However, there is currently no commercially available test to detect this viral glycoprotein. We believe the hemagglutinin protein is an ideal target for influenza detection. As the hemagglutinin protein undergoes a high degree of antigenic drift due to pressure to evade the host immune system, targeting this protein enables characterization of these viral mutations in a way other protein assay, specifically the nucleoprotein, are otherwise unable. Not only does this viral glycoprotein provide information about the virus, detection of the hemagglutinin protein has the potential to simplify the design of a point of care device. By targeting the readily available viral surface protein in our device, we limit the need to integrate complex sample preparation steps, such as solubilization and purification, into the microfluidic system.

4.4 CONCLUSIONS AND FUTURE WORK

This aim describes the development of a novel 2DPN device architecture to integrate the all binder-based influenza assay. This architecture relies on recent advances in the understanding of flow in porous materials to introduce a secondary fluidic path using a material with different pore sizes and capillary pressure. Sub-aim **4.3.1** describes the development of a 2DPN that integrates enzymatic amplification in a manner that improves assay performance over the gold standard, dipstick method. Long-term stability protocols for the protein binders were also demonstrated, for both the capture and detection binders in sub-aim **4.3.2**. Lastly, the full assay was integrated into the novel 2DPN geometry to demonstrate the detection of intact influenza virus from a spiked patient sample in **4.3.3**. We believe this to be the first demonstration of an integrated prototype device for the detection of hemagglutinin from intact influenza virus.

The thermostability of these binders makes them ideal for point of care applications. By retaining their function without the need for complex storage protocols, they introduce the possibility for simplified manufacturing and storage. Antibody stability is typically enhanced with the use of additives, however there remains a small class of antibodies that undergo surface

induced denaturation upon adsorption to a surface [158]. Aptamers, an alternative affinity reagent to binders and antibodies, have long been touted for their stability over long periods of time at various temperatures. While our binders are incapable of unfolding and refolding in the same manner as aptamers, their performance under high temperatures suggest that they maintain their structure sufficiently even under more extreme conditions. The implications of such stability are huge, as it opens the door for more stable molecular reagents that can be incorporated into point of care diagnostics.

Lateral flow assays are often restricted in their ability to integrate more complex chemistries within their simple one-dimensional architecture. While the traditional 2DPN addresses some of these concerns, there are limitations related to control over timing and interaction of reagents before reaching the test region. The device architecture demonstrated here reduces the potential for unwanted interaction between the three reactive species, HRP, H_2O_2 and DAB, upstream of the test region. In addition, the device takes into account the different timing constraints for each step, allowing sufficient time for analyte and conjugate binding while then delivering the amplification buffer orthogonally with more control over reagent concentrations and flow rates. By taking into consideration the needs for each step of this complex assay, the integrated device outperforms the conventional dipstick assay without requiring user input or timing. This work demonstrates the possibility for fully integrated, sensitive enzymatic assays that can be used for detection at the point of care.

The proof of concept, microfluidic device described in this chapter proved successful for the detection of influenza virus from spiked nasal swab samples. Future work with this device will focus on adapting the design for longer-term storage stability studies and testing with suspected influenza positive nasal swab samples. In addition, new iterations of this paper-based microfluidic device can be adapted to other multistep analytical assays that are currently limited in their use at the point of care. By enabling the integration of these more complex assays into automated, paper-based device, we believe it will open the door to more sensitive and specific diagnostics that can be easily implemented at the point of care.

4.5 WRITTEN AND ORAL PUBLICATIONS

Anderson, C.E., Buser, J.R., Flemming, A.M., Strauch, E.M., Ladd, P.D., Englund, J., Baker, D., Yager, P. Lab on a Chip. "An integrated device for the rapid and sensitive detection of the influenza hemagglutinin." Manuscript submitted.

Portions of this section have been presented at the following conferences.
Lutz, B.; **Anderson, C.E**.; Buser, J.R.; Byrnes, S.A; et al. "Paper Microfluidics: Integration Challenges & Solutions for Point-Of-Need Testing." Workshop; October 2016 MicroTAS, Dublin, Ireland.

Anderson, C.E.; Buser, J.R.; Strauch, E.M.; et al. "A two-dimensional paper network for automated detection of the Influenza virus employing computationally-designed affinity proteins." Poster presentation; The 20th International Conference on Miniaturized Systems for Chemistry and Life Sciences (MicroTAS 2016), Dublin, Ireland.

Chapter 5. MODULAR DESIGN OF ASSAY STACKS USING COMPUTATIONALLY DESIGNED PROTEINS

5.1 BACKGROUND

In Chapter 3, we described the development of the first lateral flow assays using computationally designed proteins. Through this process, we learned many lessons along the way regarding assay development with these novel proteins. One of the hardest lessons we learned was the importance of effective immobilization for each designed protein. Computationally designed proteins, unlike antibodies, do not always adsorb to nitrocellulose easily. As our collaborators developed smaller, more robust *de novo* proteins, the need for a universal immobilization system became more critical as they were less likely to adsorb to nitrocellulose. The application of cellulose binding domain (CBD) proteins has long been demonstrated in the literature as an immobilization mechanism for immunoassay development [157]–[161]. Despite its ubiquity as a lateral flow assay membrane, the development and use of nitrocellulose binding proteins is much more rare. Our group has previously identified nitrocellulose binding proteins, and carried out preliminary work integrating these proteins into lateral flow assays [162]. After screening a handful of globular proteins for adsorption for nitrocellulose, the strongest adsorber (D1) was fused to the hemagglutinin stem region binder and used in a lateral flow assay. Using this approach, the immobilization of computationally designed proteins that did not naturally adsorb to nitrocellulose became possible.

While the fusion proteins demonstrated some success for the detection of hemagglutinin, we sought to develop an approach that enabled the modular assembly of our proteins. Modular assembly, also described as “plug and play”, would enable us to attach our different assay components together after expression. For our specific application, this would allow us to independently express and validate our nitrocellulose binder and antigen binding binder. Modular assembly limits the possibility for differences in expression or folding that can occur when two proteins are combined and expressed together as a fusion protein. In addition, modular assembly allows for simplified assay development as the antigen-binding component can be easily switched out and applied to a different target or to a mutated version of the antigen in

question. While this can be accomplished using streptavidin and biotin for either the capture or detection antibody, we hoped to identify a solution that could be used for both simultaneously.

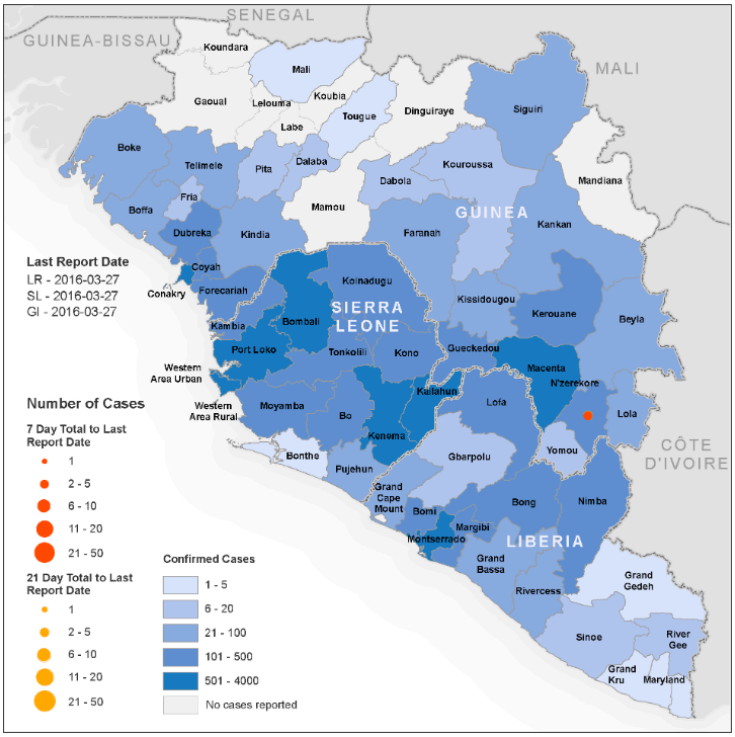

Figure 5.1. Map of total cases for the 2014-2016 Ebola virus outbreak.
New cases are indicated by red or orange dots in the respective geographical locations. Source: World Health Organization [165].

In this sub-aim, we will describe the application of this approach to the Ebola virus, the filovirus responsible for 28 outbreaks since 1976 [163]. The current outbreak in the Democratic Republic of Congo has led to 591 confirmed cases and 357 deaths as of the 26th of December, 2018 [164]. The largest Ebola outbreak ever recorded, which spanned from 2014-2016 in West Africa, led to more than 28,600 suspected deaths and over 11,300 deaths over the course of two years [165]. The countries primarily affected by this outbreak included Guinea, Sierra Leone, and Liberia, **Figure 5.1**. While Ebola outbreaks have been occurring since the 1970s, there is believed to be an increased probability in recent years for Ebola outbreak due to changes in the way that the Ebola virus interacts with humans. Specifically, changes in the size of urban and rural populations and how connected these populations are is believed to have increased the probability of another Ebola outbreak [166], [167]. Considering the number of lives lost, along

with the estimated $2.2 billion lost in GDP for 2015 alone, the overall impact of an Ebola outbreak is quite large.

Ebola virus outbreaks are particularly scary because of the speed and severity of symptoms that occur. Symptoms of infection with Ebola virus can include fever, fatigue, headache, aching muscles or joints, vomiting, diarrhea, abdominal pain, unexplained hemorrhage and weakness [168]. Infection with this virus is deadly, often leading to multiple organ failure and septic shock between 6-9 days after the symptoms first appear [169]. The virus is transmitted through contact with bodily fluids, including blood, urine, saliva, sweat, feces, breast milk, and semen [170]. While the most contagious during infection, the most recent outbreak produced data demonstrating that the virus can remain dormant in semen, breast milk, ocular fluid, and spinal column fluid up to months after a person has recovered from Ebola Virus Disease (EVD) [171]–[175]. The epidemiological risk factors for EVD range from exposure to bodily fluids to being in close contact with an infected patient briefly, however any contact with a symptomatic person carries some risk [168]. While humans are the primary reservoir for Ebola virus, fruit bats and nonhuman primates also serve as an animal reservoir [170]. The percent mortality rate for Ebola virus varies based on species, ranging anywhere from 25-90% [169]. The high mortality rate, combined with the ease of transmission, makes it particularly challenging to halt transmission of the virus.

There are five known species of Ebola virus, Zaire, Sudan, Cote d'Ivoire, Reston, and Bundibugyo, however only three (Zaire, Sudan, and Bundibugyo) have led to outbreaks in human populations [169]. As a filovirus, Ebola virus also carries some similarities to Marburg virus, which has caused outbreaks as recently as the 2014 outbreak in Uganda [176]. The genome for Ebola virus contains information to encode seven genes; the nucleoprotein (NP), glycoprotein (GP), matrix protein (VP35), nucleocapsid proteins (VP40, VP30, and VP24) and Polymerase (L), **Figure 5.2** [169], [177]. VP40 and 24 are responsible for protein assembly, viral budding, and to block the immune response, while VP 30 is responsible for RNA transcription [178]. Our work is focused on the development of lateral flow assays for the readily accessible viral surface glycoprotein (GP). Not only is this protein easily accessed at high quantity on the viral membrane surface, but it also plays a primary role in virulence, making it a particularly attractive target for lateral flow assay development.

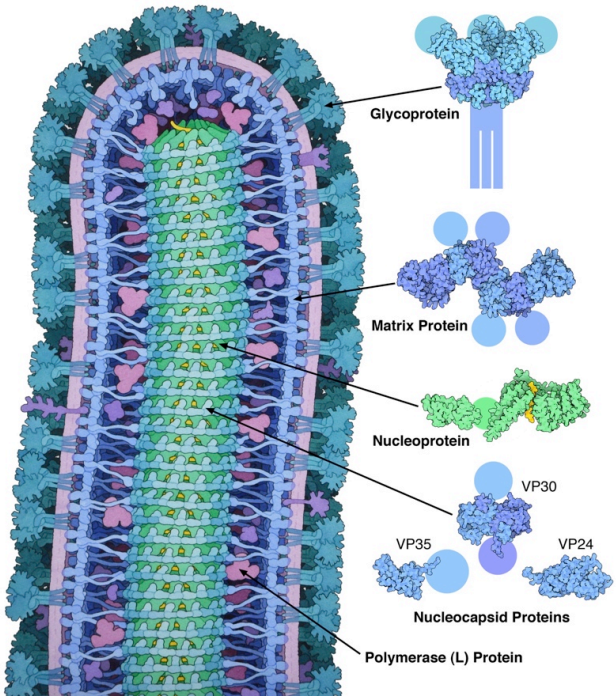

Figure 5.2. Drawing of Ebola virus structure.
The seven proteins encoded in viral RNA are shown to the right, with a detailed drawing of how they assemble on the left. Image is not to scale. Source: David Goodsell [177].

The viral glycoprotein (GP) is composed of two components, GP1 and GP2, which assemble to form the trimeric GP1/2, **Figure 5.3**. GP1 and GP2 play different roles in infection; GP1's primary role is in cell-surface attachment, while GP2's primary role is in fusion of the viral and host cell membranes [179]. Together, the GP1/2 protein plays a crucial role in the infection process by impacting the cell attachment and fusion process. The majority of therapeutic and vaccine approaches for Ebola virus have focused on targeting or mimicking this particular protein, due to its role in virulence and accessibility on the viral surface. Similar to our work with the influenza virus described in Chapters 3 and 4, we believe this protein is an optimal target for the development of a lateral flow test. In addition to the trimeric viral glycoprotein (GP) that exists on the surface of the viral membrane, the Ebola virus also secrets a version of the glycoprotein (sGP). sGP is a dimeric form of the GP protein that has been found in high quantities in the blood of infected Ebola patients [180], [181], and is believed to act as a decoy protein during infection due to the quantity of antibodies in sera that preferentially recognize sGP over GP [182], [183].

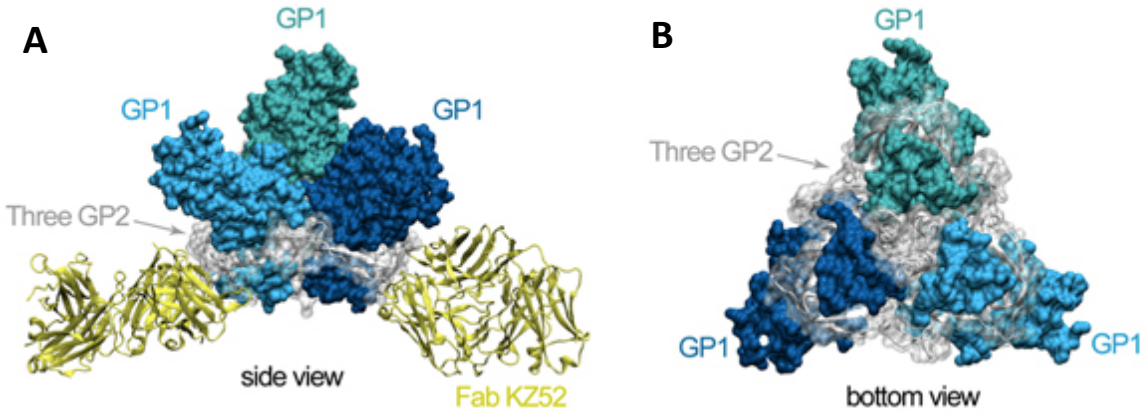

Figure 5.3. Crystal structure of Ebola GP1/2.
Side (A) and bottom (B) views of the GP1/2 protein. Three GP1 subunits are identified by three shades of blue, while the three GP2 subunits are identified in grey. KZ52, a neutralizing antibody found to bind the GP1/2 protein, is shown in yellow. Source: [184].

Our collaborators in the Baker lab have developed a protein that binds specifically to the GP1/2 protein on the Ebola virus surface, **Figure 5.4**. This protein, named "ZX", targets the base region of the GP protein. This is a similar location to neutralizing antibodies identified for the Ebola virus, including KZ52, and the c2G4 and c4G7 antibodies in the neutralizing antibody cocktail for Ebola virus, ZMapp [185]. While originally developed as a therapeutic binder to behave in a broadly neutralizing manner, this protein contains a number of characteristics ideal for use in lateral flow. ZX is a 27kDa protein that is both highly thermostable, with stability up to 95°C, and high affinity, with a K_D of 50nM [186]. In addition, the protein is grown in yeast, making it both easy and inexpensive to manufacture. Similarly to the stem region binder discussed in Chapter 3, this protein has the potential to lead to highly sensitive lateral flow assays.

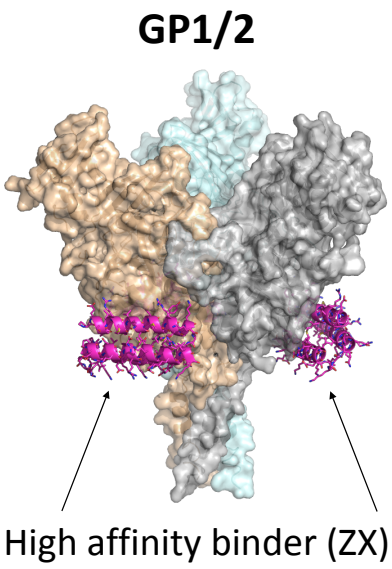

Figure 5.4. High affinity binder for Ebola GP1/2.
The ZX protein (magenta) was designed to target the base region of the GP protein. As a trimeric protein, there are three available epitopes for binding (blue, grey and orange), and either neutralization or capture, of ZX to GP1/2.

A point of care test for Ebola virus would help minimize spread of the virus, particularly in the event of another outbreak. Clinically, filovirus infection, and Ebola virus infection specifically, is difficult to differentiate from other febrile illnesses [187]. Historically, clinical management of EVD patients has been quite variable, though often included fluid monitoring and IV fluids [187], but also included anti-malarial drugs and antibiotics due to the similarity in symptoms. Specific therapeutic and vaccine efforts have made progress, however there remains the need for a sensitive, specific diagnostic for Ebola virus [185], [188], [189]. In the 2014-2016 outbreak in West Africa, the WHO and its partners showed that vaccination of contacts of an infected person was highly effective [190]. This process, known as ring vaccination, is the only effective vaccination strategy with effectiveness data found for Ebola virus to date [191]. An inexpensive, easy to use diagnostic to rapidly identify infected people and quickly provide treatment and vaccination for their contacts could help minimize the overall spread of the virus.

Diagnosis of infection with Ebola virus has historically been through the isolation and growth of the virus, but in recent years the primary target for detection has been viral RNA [192]. There are at least 10 RT-PCR assays that have been approved by either the WHO or the

FDA for detection of Ebola virus from patient samples. However, PCR requires laboratory infrastructure, electricity, and highly trained laboratory technicians. Despite attempts to increase overall laboratory capacity and throughput, the largest number of tests run per day on the GeneXpert real time PCR system was approximately 64 with two laboratory personnel [193]. While this might be sufficient for some contexts, this requires significant infrastructure that might be difficult to develop in the event of an outbreak. While their use has been somewhat limited, antigen specific ELISAs and LFAs have been developed for protein targets including NP, VP40, and GP [192]. Three LFAs for Ebola antigen detection have been commercialized; the OraSure Ebola test, ReEBOV Antigen Rapid Test, and the SD Q Line Ebola Zaire Ag, **Table 5.4**. The OraSure Ebola Rapid test, with its high sensitivity and specificity, suggests that LFAs are capable of detecting the vast majority of Ebola cases. Ebola RDTs, however, could still benefit from the low cost and high thermostability that are enabled by the integration of computationally designed proteins.

This chapter will describe work towards the development of a lateral flow assay for the development of the Ebola GP using the novel ZX protein. In an attempt develop a method for modular assembly of the assay stack, Sections 5.3.1 and 5.3.2 describe the identification of nitrocellulose binders that can be used to immobilize the ZX protein. Section 5.3.3 describes progress towards a full assay stack for the detection of the GP1/2 protein. The work described in this chapter, while it is the first use of an Ebola specific computationally designed binder in a diagnostic platform, also introduces methods to allow for more rapid, modular assembly of lateral flow assays.

Table 5.4. Summary table for Ebola RDTs.
Sensitivity and specificity testing was done by the WHO as a part of their emergency use assessment [194]–[196].

Ebola RDT	Manufacturer	Antigen target	Sensitivity	Specificity
Q Line Ebola Zaire Ag	SD Biosensor Inc	NP, GP, and VP40	84.9%	99.7%
OraSure Ebola Rapid Test	OraQuick	VP40	94.12%	100%
ReEBOV Antigen Rapid Test	Corgenix	VP40	91.8%	84.5%

5.2 MATERIALS AND METHODS

Lateral flow challenge. The lateral flow challenge is a method developed by Dr. Carly Holstein and Dr. Gina Fridley to analyze the strength and speed at which a protein adsorbs in order to more accurately compare a range of computationally designed materials with different properties, as shown in **Figure 5.5**. Devices are then assembled in holding cards with cellulose wicking pads the day of testing. Half of the membranes are challenged with 1 mL of PBST, which is the buffer used in all wash steps of our assay, while the other half are left dry until staining. All membranes are then stained with Ponceau S stain in 10% methanol for 10 minutes, followed by two wash steps in DI water for 2 minutes each. These membranes are then immediately transferred to a piece of white printer paper and scanned at 600 dpi.

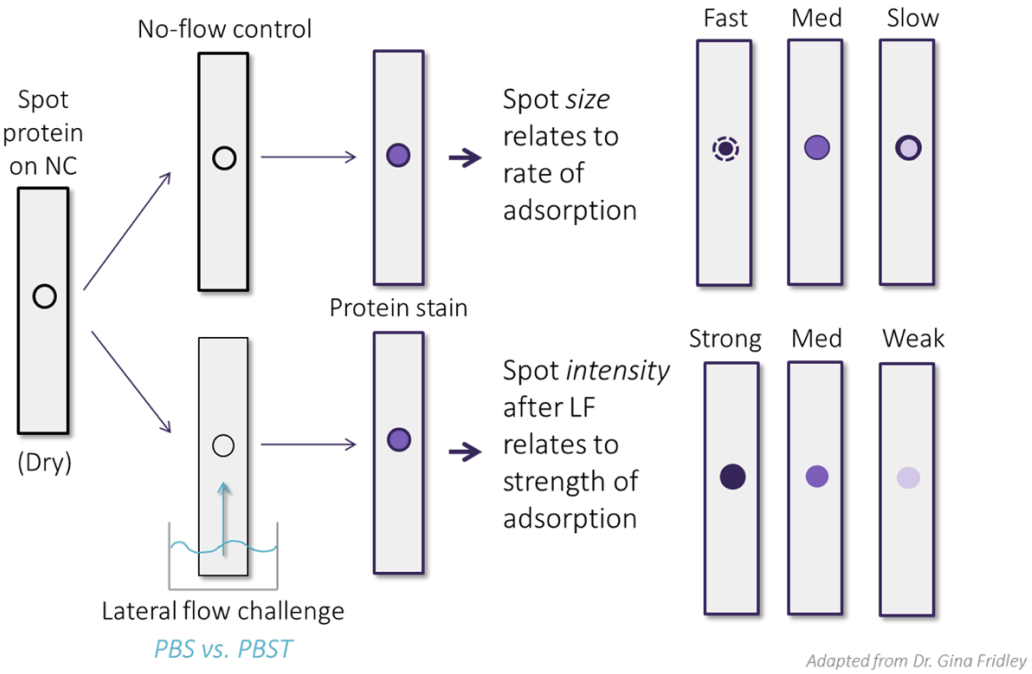

Figure 5.5. Schematic drawing of the lateral flow challenge.
This includes the flow challenge and general interpretation of the protein stain. Figure adapted from Dr. Gina Fridley and Dr. Carly Holstein.

We utilized the full protein spot analysis method as a rigorous and holistic testing mechanism for the analysis of protein adsorption on nitrocellulose. This method utilizes nitrocellulose strips cut to 0.8 cm in width and 5 cm in height that have protein spots deposited on them at a very precise volume of 1000 droplets at 450-500 pL per droplet in a controlled

chamber at ~50% relative humidity and ~68°F ambient temperature. A control spot of the same volume was deposited using red food coloring diluted using a 1:10 ratio in distilled water. This control spot was assumed to maintain minimal interaction with the membrane and therefore served as a visual display for the full area that was wetted by the applied volume, which will be referred to as the full wet out area. The membranes were stored overnight in a desiccator to enable full adsorption to the membrane before all further testing. These membranes were then spotted with the modified nitrocellulose binding protein, named 2lk8_superpos, with three replicates for this and all other test cases. The concentration of the protein was found to be 0.24 mg/mL for 2kl8_superpos by nanodrop the day of testing. Two additional controls were used in this experiment, the original D1 protein before modification and a monoclonal antibody to aid in the estimation of adsorption speed, which were tested at 1 mg/mL and 0.2 mg/mL respectively. Half of the membranes were challenged with 5 mL of PBST, which is the buffer used in all wash steps of our assay, while the other half were left dry until staining. All membranes were then stained with Ponceau S stain in 10% methanol for 10 minutes, followed by a wash step in DI water for 2 minutes. These membranes were then immediately transferred to a piece of paper and scanned at 600 dpi.

Computationally designed proteins. The majority of proteins in this chapter were manufactured by the Institute for Protein Design (IPD), unless otherwise stated. Recombinant glycoprotein (sGP and GP1/2) was manufactured by the Molecular Design and Therpeutics lab (MDT) at the Fred Hutchinson Cancer Research Center. The Ebola specific computationally designed binder (ZX) was expressed in *E. coli* and purified by immobilized metal affinity chromatography using an Ni-NTA column and size exclusion chromatography. Synthetic gene constructs of ZX with N-terminal fusion to SpyCatcher were expressed and purified using the same method. Proteins screened for nitrocellulose adsorption are described in more detail in **Table 5.6**, were also expressed in *E.coli* and purified using an Ni-NTA column. The nanobody-like proteins generated by the Gu lab were expressed in the periplasm of *E.coli* as His tagged proteins. These proteins were partially purified using osmotic shock, followed by immobilized metal affinity chromatography with Ni-NTA biosensors. All proteins were stored at 4°C until use.

Protein conjugation. Proteins containing SpyCatcher and SpyTag were conjugated by combining a molar excess (2X) of SpyTag containing protein with the SpyCatcher protein and

allowed to incubate at room temperature overnight**.** Excess SpyTag in the reaction was removed using a 7kDa molecular weight cutoff ZebaSpin desalting column (ThermoFisher Scientific, Waltham, MA, USA). In one experiment, the conjugation was completed under lateral flow by running the same molar concentration of SpyTag-Au across the IPD14028 test line. SpyTag was conjugated to 40 nm gold nanoparticles using the InnovaCoat Gold Maleimide Conjugation Kit (Expedeon, United Kingdom). 5ug of SpyTag-cysteine was combined with the Maleimide Reaction Buffer and Diluent and mixed with the lyophilized gold material. The reaction was allowed to incubate at 25°C for 30 minutes, after which the reaction quencher was added. The final conjugate was then spun at 9,000g for 6 minutes to complete a buffer exchange and remove unconjugated SpyTag. Horseradish peroxidase conjugation of the D1 protein used the maleimide-activated horseradish peroxidase commercial conjugation kit (ThermoFisher, Waltham, MA, USA). D1 protein underwent buffer exchange into PBS using a desalting column (P10-GE) and was incubated with the maleimide-activated HRP for 6 hrs at 25°C and for another 8 hrs at 4°C, and stored at 4°C until use.

Ebola Assay - Membrane Preparation. Capture proteins were immobilized to nitrocellulose membrane strips (CN95, Sartorius, AG) using a piezoelectric printer (sciFLEXARRAYER S3, Scienion, AG), depositing 12 spots at 30 drops per spot and 450-500 pL per drop. Protein solutions were filtered through a centrifugal filter (0.2 μm nylon membrane, VWR) before spotting. Nitrocellulose binding streptavidin (GWB-43A5FD, GenWay Biotech) or anti-Ebola antibody were spotted on nitrocellulose at 1mg/mL. Anti-Ebola antibodies tested were c13c6, KZ52, and C6D8 (IBT Bioservices, Rockville, MD, USA). Each test line received approximately 300 nL of solution. The spotted membrane strips were assembled into a comb device for ease of use, with 20 μL of each solution pre-loaded into a 96 well plate.

Ebola Glycoprotein Detection Assays. For membranes spotted with anti-GP1/2 antibody, each strip was moved from one well to another to apply the following solutions in order: (1) 250 nM of biotinylated ZX mixed with known concentration of GP1/2, (2) PBST wash with 1% BSA (w/v), (3) 1.25 OD streptavidin gold nanoparticle, (4) PBST wash with 1% BSA. For the inverted set up, membranes spotted with nitrocellulose binding streptavidin were moved from one well to another to apply the following solutions: (1) 250 nM of biotinylated ZX mixed with known concentration of GP1/2, (2) PBST wash with 1mg/mL biotinylated BSA to block unbound biotin binding sites, (3) 100 nM anti-GP1/2 antibody (c13c6), (4) PBST wash with 1%

BSA (w/v), (5) 1.25 OD of gold conjugated anti-mouse Ab, (6) PBST wash with 1% BSA (w/v). Once all reagents were delivered across the test region, the membranes were scanned at 600 dpi (Perfection V700 Photo Scanner, Epson, Long Beach, CA) while the membranes were still wet. The green channel of the RGB scanned image was used for quantification.

Signal Quantification. All reported signal intensities were quantified using a previously published custom script in MATLAB (MathWorks, Natick, MA, USA) [56]. For the limit of detection analysis, a concentration range from 0.08 to 200µg/mL of GP1/2 protein was tested. A four parameter curve fit was generated using the signal intensities calculated, and the limit of detection was calculated using a method that looks specifically at the 5% chance of false-positive signal and the 5% chance of false-negative signal [108]. This method generates the limit of detection alongside a 95% confidence interval.

5.3 Results and Discussion

5.3.1 *Computationally designed nitrocellulose binders*

Immobilization of antibodies to nitrocellulose is most often through direct adsorption of the antibody. As novel molecular recognition elements are developed, the mechanism by which the protein or aptamer is immobilized is something that needs to be carefully considered. Similarly to how universally antibodies can be immobilized to nitrocellulose through adsorption, we sought to develop a universal immobilization for the computationally designed proteins that we work with. Previous work by Dr. Carly Holstein had tested a number of hypotheses as to the mechanism behind adsorption to nitrocellulose. Adsorption appeared to be primarily influenced by the pH of the solution in which the protein was spotted, and the isoelectric point (pI) of the protein itself [56]. Initial screening of five different globular proteins and a helical bundle identified two different candidates for a universal nitrocellulose binder, the Design 1 and 3-helix proteins [56].

While the 3-helix protein did not express well as a fusion protein due to issues with protein folding, the Design 1 (D1) protein was expressed as a fusion to the influenza stem region binder and tested in a lateral flow assay for hemagglutinin, **Figure 5.6**. Holstein demonstrated that the length of the linker between the stem region and paper binders did not significantly impact the overall assay performance, while the purification process appeared to play a

significant role [56]. While all three fusion proteins worked well for the detection of hemagglutinin under lateral flow, the performance of these assays never quite reached the sensitivity of the streptavidin capture. In order to improve assay performance, we sought to modify our nitrocellulose binding proteins to improve adsorption to nitrocellulose.

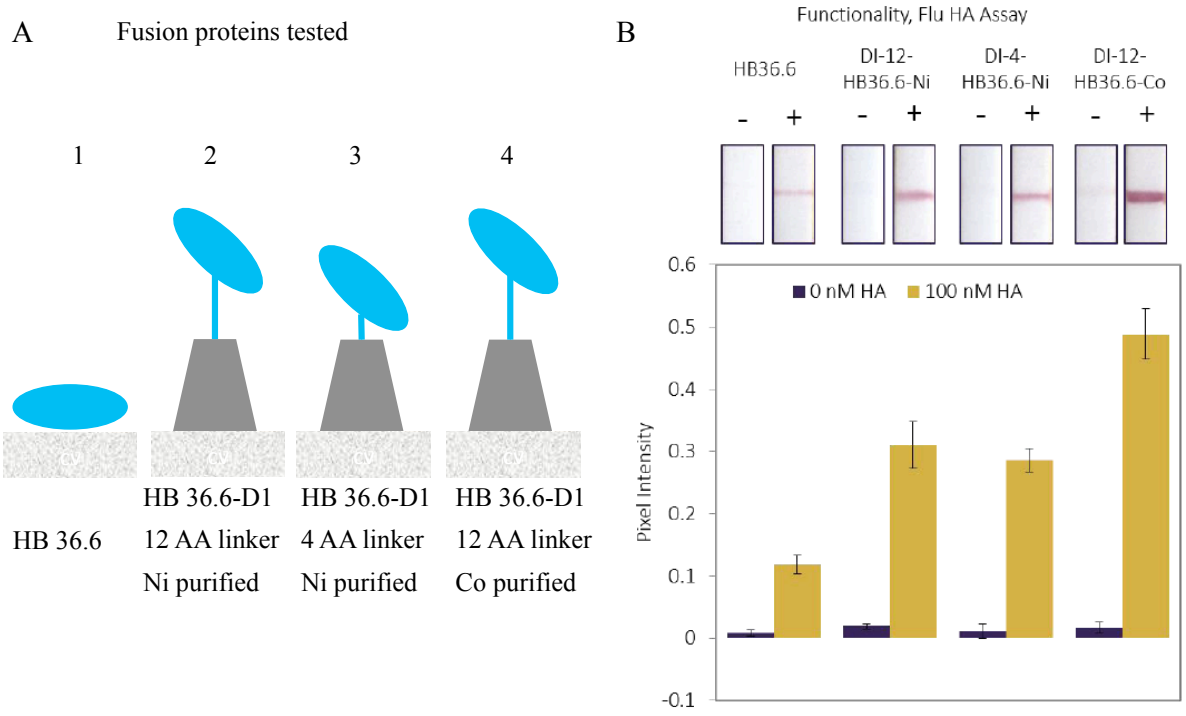

Figure 5.6. Fusion proteins for the detection of HA.
Three fusion proteins were tested, with two different linker lengths and purification protocols, (A). The linker length did not appear to impact the overall performance in the flu assay (B), however the purification process significantly impacted the overall assay performance. Data from the thesis of Dr. Carly Holstein [56].

Adsorption is a process governed by entropy. When a protein adsorbs to a surface, there is entropy gained from the release of water molecules ordered at the surface, as well as from structural rearrangements that happen inside the protein [197]–[199]. As mentioned above, the pI and the pH both influence the adsorption behavior of a protein to a surface. If a protein is spotted at or near the pI, the protein exhibits a net neutral charge, allowing higher packing densities on a surface because of a reduction in electrostatic protein-protein interactions [200]. Similarly, electrostatics play a role in the interaction between the protein being spotted and the surface.

When the protein and surface have opposite charges, the movement of the protein to the surface is accelerated thereby leading to an increased rate of adsorption [200]. With this understanding, we wanted to take advantage of the fact that nitrocellulose is naturally negatively charged. Building from the success of the D1 protein, we introduced positively charged residues into the protein in a manner that did not affect the overall structure (2kl8_superpos). As a control, we added positively charged residues to a similar protein, though one that had not previously been tested using the lateral flow challenge (2mq8_superpos). A description of each protein, including the original 2kl8 and 2mq8 can be found in **Table 5.5**.

Table 5.5. Positively charged nitrocellulose binding proteins.

Protein Name	Size (kDa)	pI	Size (AA)	+ residues	- residues
2kl8 (D1)	10.19	6.29	86	15	11
2kl8-superpos (NCB1)	10.91	10.20	89	14	2
2mq8-superpos (NCB2)	12.77	11.18	111	17	8

The size of a protein spot with respect to the full wet out area represents the relative speed at which adsorption to the membrane occurs. A quickly adsorbing protein will have a spot that is significantly smaller than the full wet out area as demonstrated by the red food coloring. This is because the protein adsorbs to the membrane at a faster rate than the rate at which the protein solution wicks through the membrane. In addition to the speed of adsorption, the relative robustness of adsorption of the protein was tested using a lateral flow challenge. The degree of protein stain compared before and after challenge enabled the relative robustness of protein adsorption to be observed, as a strong adsorber will not be stripped from the membrane under those wash conditions. We found that the positively charged D1 protein is able to bind much more rapidly and robustly than the original D1 protein, **Figure 5.7**. This supports our hypothesis that the isoelectric point is one of the main contributing factors in protein adsorption to nitrocellulose. The small diameter for the 2kl8_superpos is indicative of a very rapid adsorption to nitrocellulose, as shown in **Figure 5.5**. Additionally, the exposure to 5mL of PBST does not

strip away the protein from the place it was spotted. This suggests that the protein also adsorbs robustly to the membrane. This protein was patented under US patent number US1527650 [201].

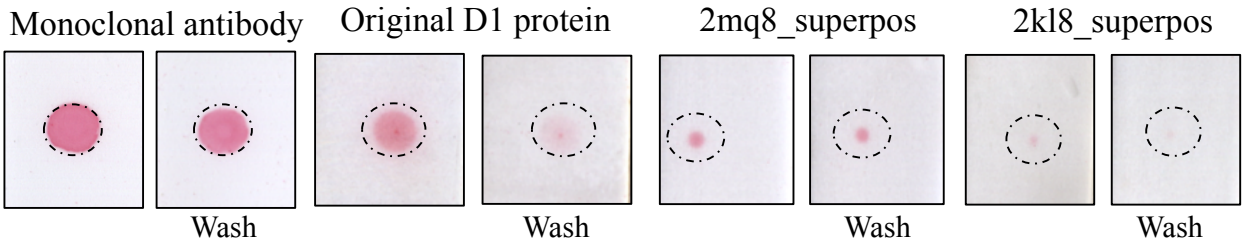

Figure 5.7. Lateral flow challenge of positively charged nitrocellulose binders. Red food coloring was used to demonstrate the total wet out area, the monoclonal antibody served as an adsorption speed indicator, and the original D1 protein served as a direct comparison for the newly modified paper binder. All images on the left hand side were stained as is, and the images on the right were challenged with 5mL of PBST before staining. The dotted line depicts the wet out area as determined by the red food coloring.

There are two major challenges with using fusion proteins in an LFA. First of all, fusion proteins are generally more challenging to express than individual binding components due to their increased complexity. Specific challenges include failure to express entirely, or successful expression with subsequent folding issues. The connection between the two proteins fused together is not as stable as the proteins are individually, leading to a significant loss in overall stability. Additionally, the presence of another protein in the fusion can have an effect on protein folding. The second major challenge with this approach is that is requires that the entire fusion be made individually for each use case. For example, you could not use the same protein as both the capture and detection entities. As an example, we tried flowing our paper binder across a nitrocellulose test strip and found that it adsorbs to nitrocellulose under flow, **Figure 5.8**.

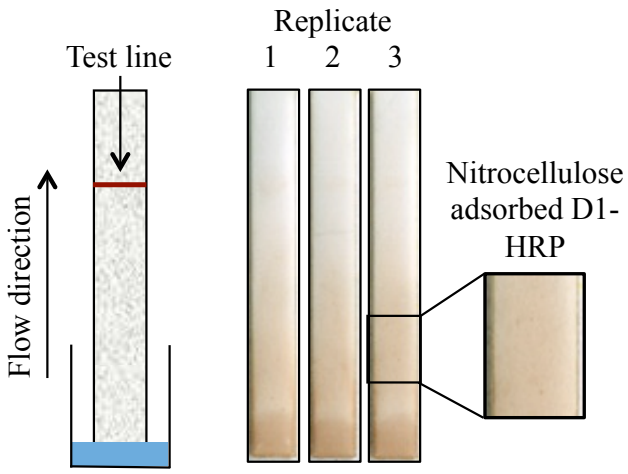

Figure 5.8. Adsorption of paper binder under lateral flow.
Nitrocellulose binder (D1) labeled with HRP was flowed across a nitrocellulose test line containing influenza head region binder (details about this protein can be found in Chapter 3). Schematic (left) and three technical replicates (right) show adsorption of nitrocellulose binder to nitrocellulose under lateral flow.

5.3.2 *Modular assay stack assembly using spy catcher and spy tag*

The challenges described in 5.3.1 encouraged us to look for alternative ideas that would enable us to more modularly build assay stacks using computationally designed proteins. While biotin and streptavidin are commonly used to build assay stacks in lateral flow and other applications, we hoped to use a protein pair that formed a covalent attachment between the two proteins. A covalent attachment would allow for conjugation of the protein components for both capture and detection, which we would not be able to do with biotin and streptavidin. SpyCatcher and SpyTag are engineered proteins modified from the *Streptococcus pyogenes* CnaB2 protein that spontaneously form an intramolecular isopeptide bond [202]. By splitting CnaB2 into two individual peptide components, named SpyCatcher and SpyTag, they can be expressed on separate binding proteins. When the binding proteins are mixed in solution, they form an isopeptide bond and can be used in the same manner as the fusion proteins described in 5.3.1, **Figure 5.9**. The reaction between SpyCatcher and SpyTag is both rapid and robust, with 40% of product produced within the first minute and occurring under a variety of different conditions (changes in pH, buffer composition, etc) [202].

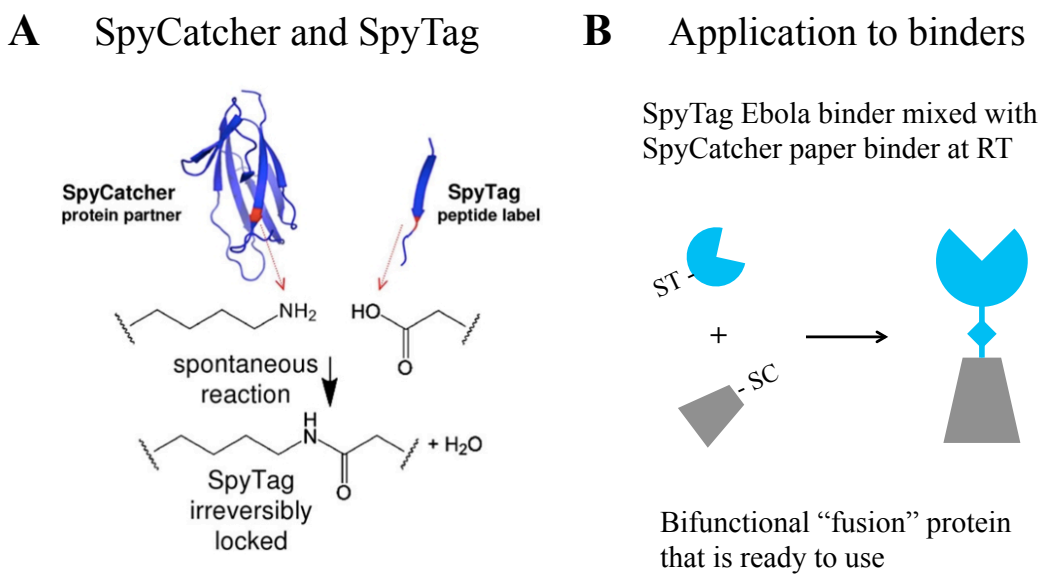

Figure 5.9. Schematic describing use of SpyCatcher and SpyTag.
The irreversible isopeptide bond that forms between SpyCatcher and SpyTag occurs spontaneously (A), and can be used in a plug and play manner to generate "fusion" proteins, (B). Source: [202]

While the majority of applications of this conjugation system are centered around drug delivery and vaccine development [203]–[205], there have been publications describing applications ranging from industrial biocatalysis to diagnostic applications [206]–[208]. Specifically for diagnostics, a recent manuscript by Park et al described the use of SpyCatcher and SpyTag to create fusions between their peptide of interest and single stranded DNA (ssDNA) with sensitivities as low as 5 nM in complex sample matrices [207]. In each of these examples, this conjugation approach facilitates more rapid design and development because the various components can be combined in a "plug and play" manner.

The original paper binding proteins were not designed with either the SpyCatcher or SpyTag component. In order to utilize the benefits of this modular assembly system, we needed to attach one, or both, peptides to our paper binder. However, we found that when we attached SpyCatcher, a 15 kDA protein, to our paper binding proteins, they no longer adsorbed strongly to all three nitrocellulose membranes tested, **Figure 5.10**. Based on our previous understanding of electrostatics, we believe change in theoretical pI, as determined from the amino acid sequence by ExPASy, from 10.9 to 8.91 for the SpyCatcher fusion protein affects the rate and strength of

adsorption. SpyTag containing nitrocellulose binders, on the other hand, did not express well. Because SpyTag is a smaller peptide, with just 13 amino acids, it can insert itself into other areas of a protein and dramatically impact protein folding.

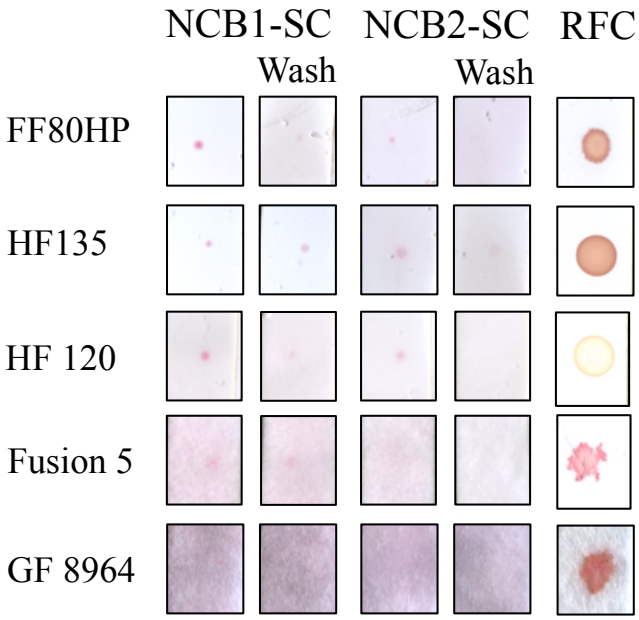

Figure 5.10. Effect of SpyCatcher on nitrocellulose adsorption.
Proteins were hand spotted onto nitrocellulose (FF80HP, HF135 or HF120), Fusion 5, or glass fiber (GF8964) and tested for adsorption using the lateral flow challenge. NCB1-SC and NCB2-SC refers to SpyCatcher containing versions of 2mq8-superpos and 2kl8-superpos respectively. Red food coloring (RFC) was used to measure the total wet out area.

These results brought us back to the drawing board. Not only did we need a protein that would stick to nitrocellulose, but we also wanted a way to easily attach this protein to our high affinity protein binders. Our collaborators in the Baker lab had expressed and purified SpyCatcher and SpyTag containing cage components that self assembled and in order to express specific proteins of interest on the surface. Starting from this large library of SpyCatcher containing proteins, we screened for their adsorption to nitrocellulose, Fusion 5, and GF 8964, **Figure 5.11** and **5.12**. Through these screens, we were able to identify one protein in particular that adsorbed well to our porous materials, named IPD 14028.

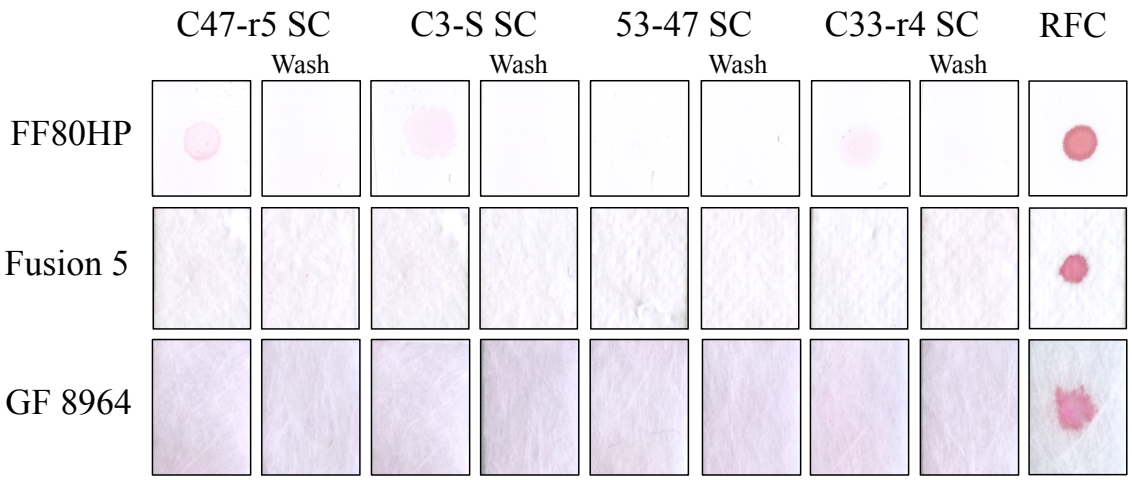

Figure 5.11. LFC for spy catcher containing proteins, part 1.

Proteins were hand spotted onto nitrocellulose (FF80HP), Fusion 5, or glass fiber (GF8964) and tested for adsorption using the lateral flow challenge. C47-r5 SC, C3-SC, 53-47 SC, and C33-r4 SC all are cage components developed by the Institute for Protein Design at the University of Washington. Red food coloring (RFC) was used to measure the total wet out area.

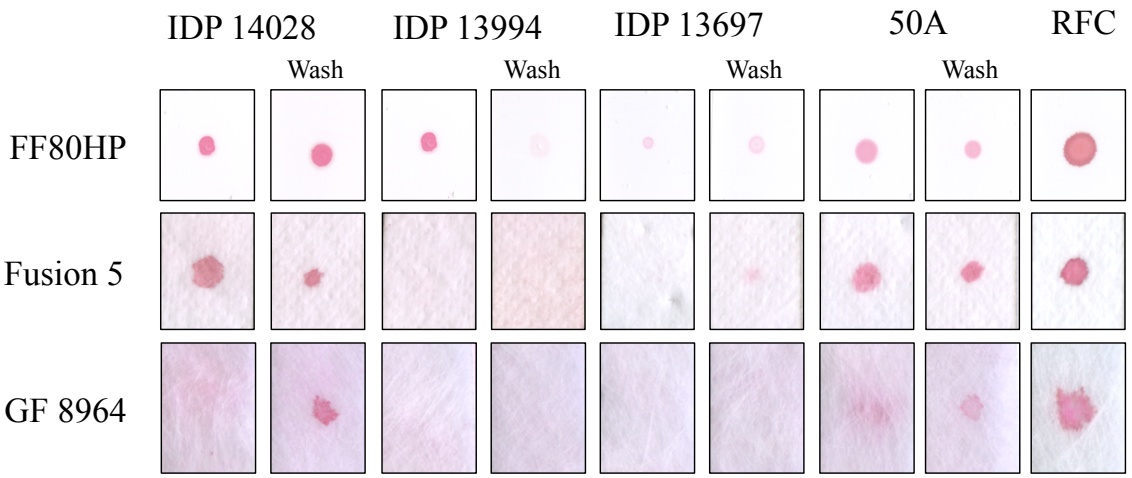

Figure 5.12. LFC for spy catcher containing proteins, part 2.

Proteins were hand spotted onto nitrocellulose (FF80HP), Fusion 5, or glass fiber (GF8964) and tested for adsorption using the lateral flow challenge. IPD 14028, 13394, and 13697 all are cage components developed by the Institute for Protein Design at the University of Washington. 50A is an individual component of IPD 14028. Red food coloring (RFC) was used to measure the total wet out area.

IPD 14028 is a fusion protein containing three different components; a monomeric streptavidin, SpyCatcher, and a cage component named "50A", **Figure 5.13**. Interestingly, the theoretical pI of this protein is 5.30, which suggests that adsorption of this protein does not follow the same convention as our previously demonstrated nitrocellulose binding proteins. Testing of the cage component within IPD 14028 (50A) suggested that 50A plays a large role in the adsorption of this protein to nitrocellulose, **Figure 5.12**. Additional testing of SpyCatcher-50A found that without the presence of monomeric streptavidin, the fusion protein did not adsorb as robustly to nitrocellulose as IPD 14028.

With a SpyCatcher containing nitrocellulose-binding protein, we then sought to generate fusion proteins containing our nitrocellulose protein and a peptide of interest. For initial testing, we attached a preliminary version of the Ebola binding protein for GP1/2, IPD 14676. We also attached two recombinant GP1/2 proteins, MDT 386 and 337, both of which were expressed with the SpyTag peptide. Recombinant proteins MDT 386 and 337 are Ebola Mayinga strain GP1/2 and ManoRiver sGP proteins respectively. We found that on its own, IPD 14676 does not adsorb well to any of the nitrocellulose membranes we tested (HF120, HF135 or FF80HP), **Figure 5.14**. Once attached to our paper binder, IPD 14028, we saw rapid and robust adsorption to nitrocellulose. We saw similar performance for paper binder attached to recombinant GP/12 proteins, 386 and 337. These results were promising, and suggested that we could use IPD 14028 for immobilization of any designed protein as long as it contained the SpyTag peptide sequence.

IPD 14028

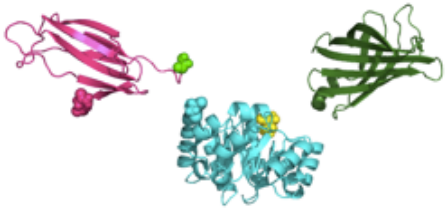

Figure 5.13. Molecular structure of IPD 14028.
IPD 14028 is a fusion protein containing three primary components, monomeric streptavidin (magenta), 50A (blue) and SpyCatcher (green). 14028 has a molecular weight of 51.87 kDa and a theoretical isoelectric point of 5.30.

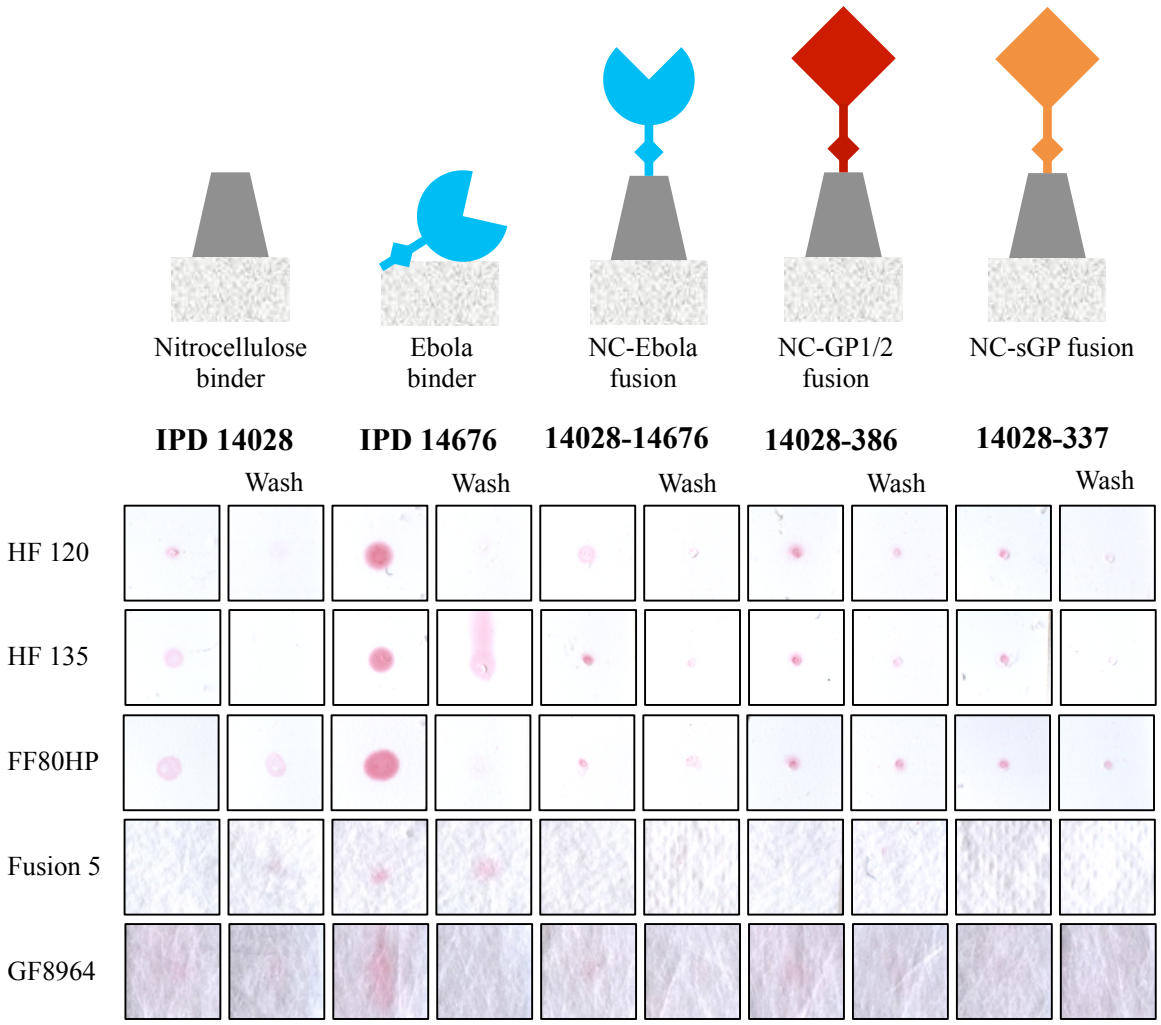

Figure 5.14. LFC for paper-binder containing conjugates.
Graphical depiction of each protein is shown above. Proteins were hand spotted onto nitrocellulose (HF120, HF135, or FF80HP), Fusion 5, or glass fiber (GF8964) and tested for adsorption using the lateral flow challenge with PBST. IPD proteins were developed by the Institute for Protein Design at the University of Washington, and MDT 386 and 337 were developed from the MDT lab at the Fred Hutchinson Research Center.

In an attempt to improve the adsorption of our fusion protein to nitrocellulose, we introduced a heated incubation step for the nitrocellulose membranes after spotting. For most antibodies, the addition of a heated incubation step can help facilitate adsorption [209]. We found, however, that the adsorption of the fusion protein does not improve with the introduction of a heated incubation step, **Figure 5.15**. Alternatively, the adsorption of an Ebola GP1/2

specific antibody (KZ52) demonstrates slight improvement after the heated incubation step when spotted on HF120. There is no significant difference between KZ52 spotted on FF80HP.

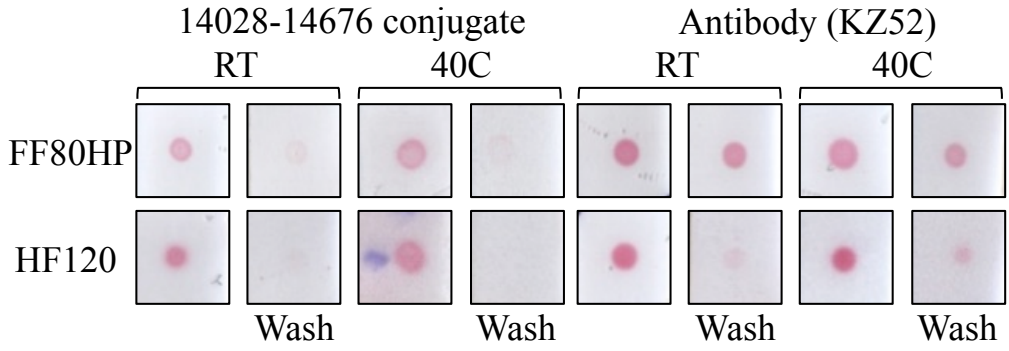

Figure 5.15. Effect of heat incubation on adsorption of NCB conjugates.
Proteins were hand spotted onto nitrocellulose (FF80HP or HF120) and tested for adsorption using the lateral flow challenge with PBST. Half of the membranes were placed in an oven at 40°C for 1hr after spotting, after which all membranes were placed in a desiccator to dry overnight.

With data supporting that fusion proteins containing IPD 14028 adsorb strongly to nitrocellulose, we sought to use this fusion as the capture entity in a lateral flow assay. With our paper anchor conjugated to the ZX binder, we saw very faint signal at 500 nM of antigen, **Figure 5.16**. Of the three different forms of recombinant GP1/2 tested, it was only the IBT GP1/2 that led to results that were significantly different than the negative control. These results were promising, but suggested that there was significant development needed to improve the overall assay performance. However, while there was room for further optimization with this assay to improve sensitivity, we started to encounter issues with the IPD 14028 protein. This particular protein consists of three different proteins that are fused to one another, and we found that over time this protein started to fall apart. In addition, expression of this protein was “hit or miss”, complicating the manufacturing process. For both of these issues, we believe the problems to be directly associated to the success of this protein as a nitrocellulose binder. The traits that facilitate adsorption, including the readily available hydrophobic domains, to nitrocellulose directly contributed to the instability of the protein and the expression difficulties. We therefore decided to seek another alternative for this project for the short term.

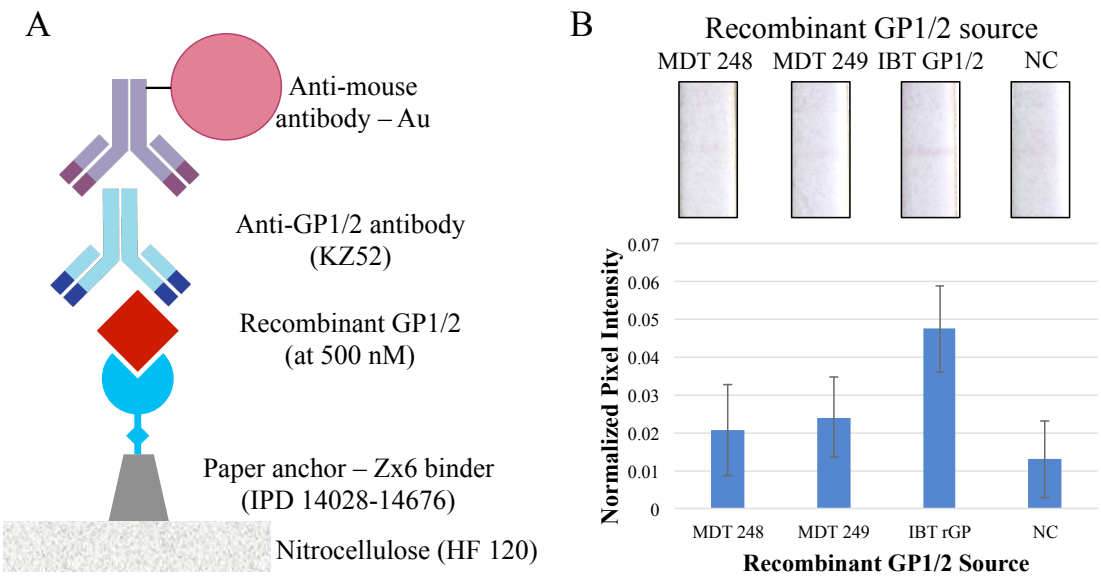

Figure 5.16. Initial lateral flow assay testing with paper binder fusion protein. Paper anchor (IPD 14028) was attached to an early version of the Ebola GP1/2 binder ZX (IPD 14676) using SpyCatcher and SpyTag, with anti-Ebola antibody (KZ52) and secondary gold labeled antibody used to visualized at the test line (A). Three different recombinant GP1/2 proteins (MDT 248, MDT 249, and IBT) were tested at 500 nM with an n=3 for each condition, (B). Nitrocellulose membranes were scanned at 600 dpi.

The fusion proteins shown in **Figures 5.14** and **5.16** were conjugated prior to spotting onto nitrocellulose. The modular assembly approach will be more useful if the conjugation can occur under lateral flow. This would allow us to add the capture and detection components in the conjugate pad. In doing so, we see two added benefits. Firstly, the test strip would remain the same independent of the target of interest thereby simplifying the manufacturing process and enabling more rapid assay development. Secondly, the increased interaction time during flow from the conjugate pad to the test line could potentially increase overall analyte captured. To test the conjugation of SpyCatcher and SpyTag under flow, we spotted IPD 14028 onto nitrocellulose and flowed across SpyTag conjugated to a gold nanoparticle, **Figure 5.17**. As a control, we blocked the available SpyTag by conjugating the gold nanoparticle with a SpyCatcher containing protein. The three proteins tested were the ZX binder, and #7 and #21, nanobody-like proteins developed by the Gu lab at the University of Washington to bind GP. This preliminary data

suggests that the reaction is quick enough to occur under lateral flow, though further characterization is still required.

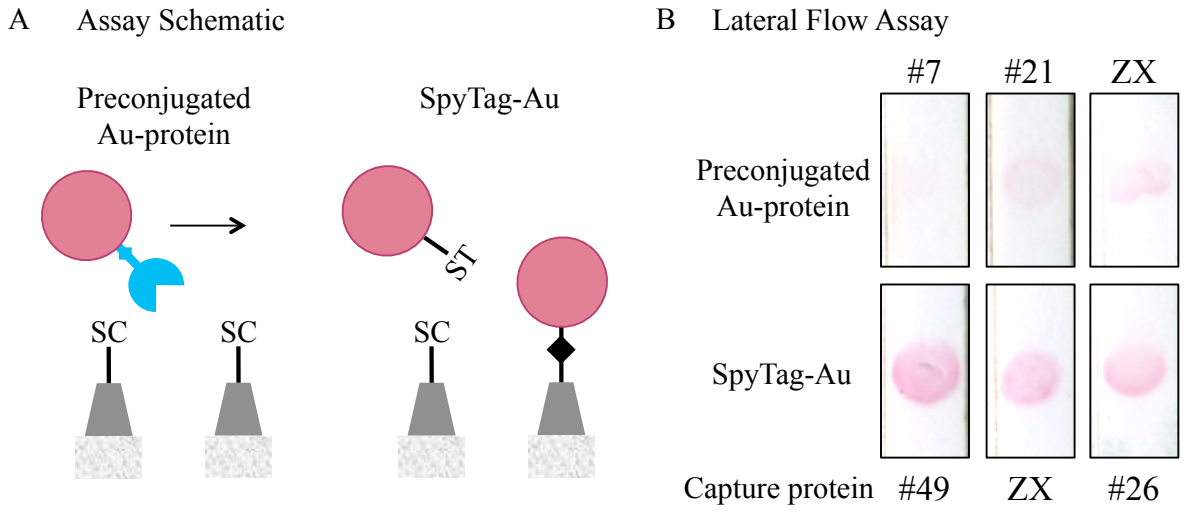

Figure 5.17. Conjugation of SpyCatcher and SpyTag under lateral flow. SpyTag-Au nanoparticles were flowed across a test line continuing SpyCatcher containing proteins (Gu lab protein #49, ZX, and #26 from left to right). As a control, SpyTag-Au nanoparticles were conjugated with SpyCatcher conjugates (Gu lab proteins #7, #21, and ZX) and flowed across the same test lines.

In this sub-aim, we attempted to develop a modular assembly system using SpyCatcher and SpyTag to connect our nitrocellulose-binding component to our antigen binding protein of interest. Towards this end, we identified a nitrocellulose binding protein containing SpyCatcher and demonstrated that it can be covalently attached to a SpyTag containing protein before or after spotting onto nitrocellulose. A summary of computationally designed proteins screened for binding to nitrocellulose is listed in **Table 5.2.** Due to instabilities with the identified protein, we were unable to continue with its use as we developed our final assays for the detection of the Ebola virus.

Table 5.6. Summary table for nitrocellulose binder screening.

Protein ID	Protein Name	Ponceau Result	MW (kDa) monomer	MW (kDA) total	pI	Charge at pH7
13994	DR64_C5_HS_SpyCatcher	Supernatant is weak, pellet (fibers) are strong	39.6	Not bounded	4.92	-15.1
13998	Spy catcher 2mq8	Medium	25.7	25.7	8.91	1.8
14045	Spy catcher 2kl8	Weak	25.7	25.7	8.91	1.8
13697	Spycatcher-I53-50A	Medium	37.2	111.6	5.91	-9.5
13692	SpyCatcher-I301		38	2736	5.97	-6.1
NA	Mica18-spycatcher	Weak	107.9	NA	4.14	-99
NA	Spycatcher-mica18	Weak	107.9	NA	4.14	-99
14028	His-SpyCatcher-I53-50A1-Tev-mSA-Flag	Strong	51.9	155.7	5.07	-16.1
14528	1BH_38	Strong	32.2	96.6	4.95	-14.1
14529	1BH-41	Strong	32.3	96.9	4.94	-14.5
14065	SpyC_ank1C2_G3	Weak	29.5	88.5	5.05	-17.3
14066	SpyC_ank1C2_G3_r5	Medium-weak	36.5	109.5	5.54	-16.7
14067	1na0C3_int2_SpyC	Medium	26.9	80.7	4.46	-16.3
14068	1na0C3_int2_r4_SpyC	Medium-weak	26.9	80.7	4.46	-16.3
14069	NA	Medium-strong	TBD	TBD	TBD	TBD
14070	NA	Medium-strong	TBD	TBD	TBD	TBD
14851	SC-SB13		11.8	35.4	4.11	-7.9
Nitrocellulose adsorbing, non-Spy catcher containing proteins						
NA	3 helix	Strong	29.6	29.6	9.4	TBD
NA	Design 1	Medium strength	10.1	10.1	6.32	TBD
NA	50A	Strong	TBD	TBD	TBD	TBD

While this work made some progress in the development of a modularly assembled assay stack, we decided to move away from nitrocellulose binding proteins for the immobilization of our Ebola binding, ZX binder. This decision was motivated by our desire to exploit the low limit of detection we found using streptavidin for immobilization of a biotinylated protein. However, there remains potential for this approach to be highly valuable for lateral flow assay development. For this potential to be reached, there is a need for a greater understanding of what factors impact adsorption of a computationally designed protein to nitrocellulose. While we

initially hoped the larger screen for nitrocellulose binding proteins described in this sub-aim would help to solidify our understanding of nitrocellulose, we found more exceptions to the rule. Therefore, a larger protein screen, ideally using a system with higher throughput such as phage or yeast display, would allow us to more carefully elucidate protein characteristics that lead to optimal adsorption to nitrocellulose and other porous materials.

5.3.3 *Assays for the detection of Ebola Glycoprotein, GP1/2*

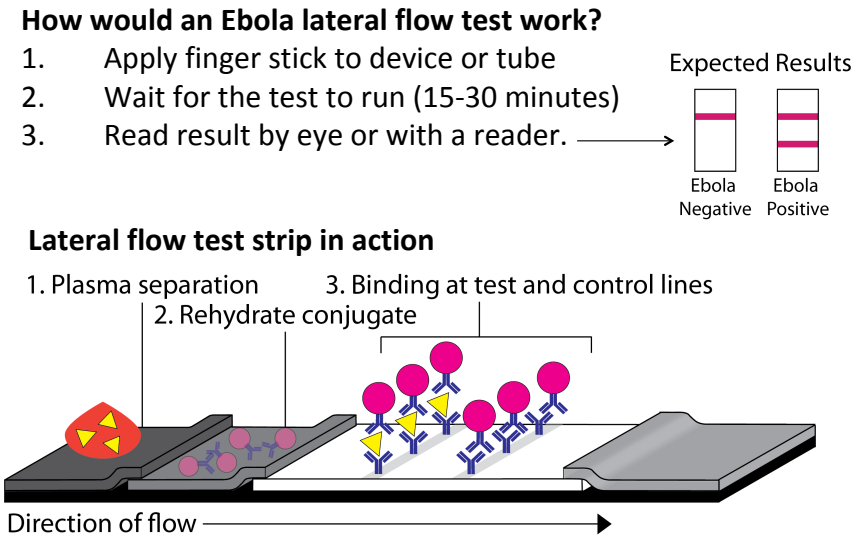

Figure 5.18. Ebola lateral flow assay schematic.
Intended assay use (top) with three steps after the blood sample is applied to the strip; (1) plasma separation, (2) conjugate rehydration, (3) and binding of analyte and antibody gold conjugate at the test and control lines.

We developed a series of assays to detect the Ebola glycoprotein GP1/2 using a combination of antibodies and the computationally designed protein, ZX. The ultimate goal for this work is the integration into an inexpensive, easy to use, non-instrumented lateral flow assay, **Figure 5.18**. Similar to the flu assays described in Chapter 3, the assays for integration into LFAs were designed with binding proteins that target different epitopes on the viral glycoprotein. Similar to the stem region binder for HA, the ZX protein does not naturally adsorb to nitrocellulose. 5.3.1 and 5.3.2 describe attempts to immobilize the computationally designed ZX protein to nitrocellulose using a paper binder. As an alternative immobilization approach, we used the available SpyCatcher on ZX to biotinylate with a SpyTag-biotin for use in either capture

or detection. The assays described in this sub-aim for the detection of GP1/2 are shown in **Figure 5.19**.

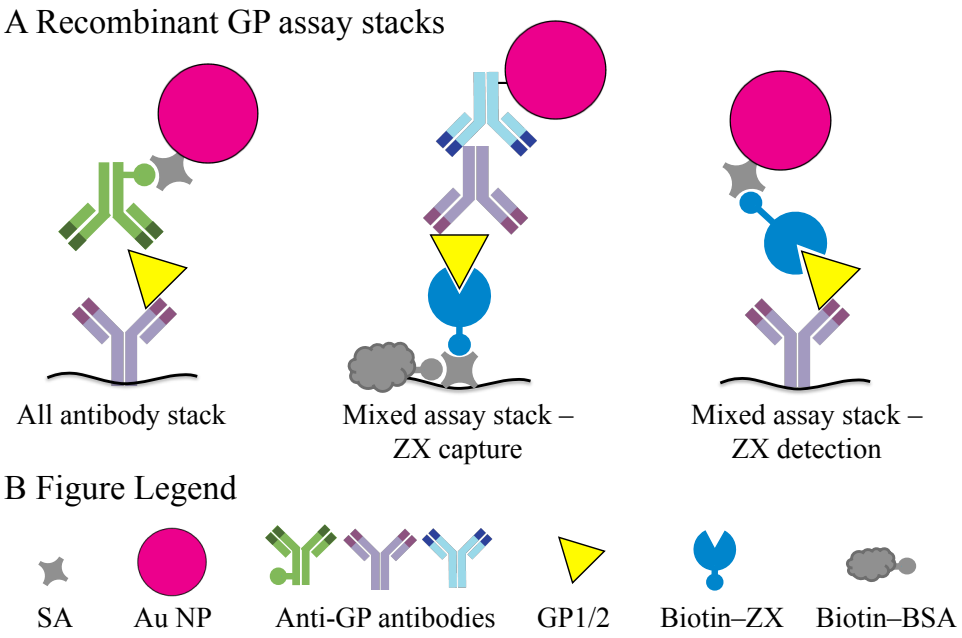

Figure 5.19. Assays for the detection of recombinant GP1/2.
(A) Schematic representation of these assays. From left to right: antibody capture and detection, biotinylated-ZX binder capture and streptavidin capture with antibody detection, and antibody capture with biotinylated-ZX binder detection with streptavidin (SA) gold nanoparticle (Au NP) readout. (B) Figure legend. Note that the molecular components are not to scale.

On the GP1/2 protein, there are two primary regions where protective antibodies have been discovered. Neutralizing antibodies have primarily targeted the base region of the GP protein, while non-neutralizing antibodies target the chalice region of the protein, **Figure 5.20** [185]. Antibodies to the mucin-binding domain have also been identified.

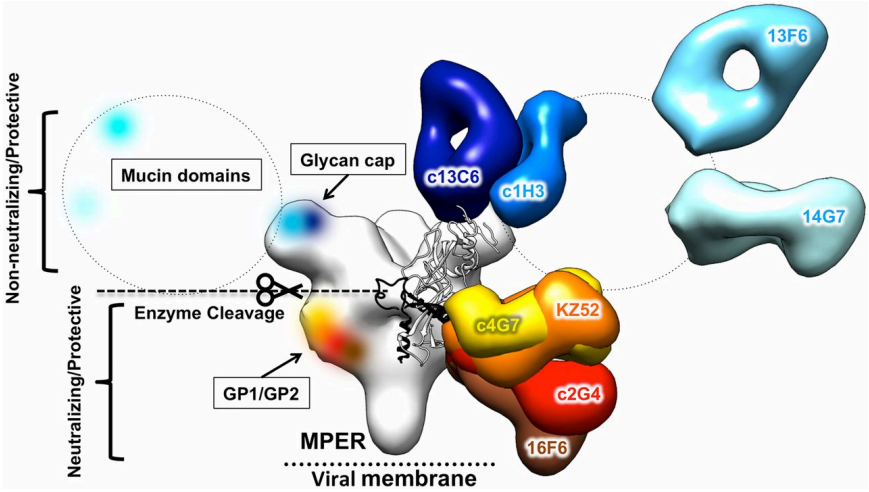

Figure 5.20. Protective antibody epitopes for Ebola GP.
Antibodies in orange, red, and yellow indicate viral neutralizing ability, while antibodies in blue have been found to be protective without neutralizing as they are can be removed before receptor binding [185]. Of these antibodies, our work has included the integration of KZ52, 13F6 and c13C6 antibodies into LFAs. Source: [185].

Our group developed an antibody assay to detect GP1/2 using the KZ52 antibody and a biotinylated mucin binding domain antibody. Testing with recombinant GP1/2 and virus-like particles (VLPs) led to an LOD of 0.261 µg/mL (95% CI [0.15, 3.48]) and 0.18 µg/mL (95% CI [0.0944, 2.965]) respectively, **Figure 5.21**. This testing was done using IBT Bioservices recombinant GP1/2 and VLP, however subsequent testing using the same antibodies and the recombinant GP1/2 manufactured by MDT led to lower signals and poorer performance, **Figure 5.22**. Because we do not have specific information about the recombinant GP produced by IBT, we believe this difference to be primarily due to minor differences in the antigens, and potentially strain, used for development of the antibody and protein binders respectively. All testing with the ZX protein shown in this document were done with MDT 248, the Mayinga strain of GP1/2 expressed without the mucin and transmembrane domains, unless stated otherwise. While other GP sources were tested, we found the ZX binder performed the best with MDT 248 as the antigen of interest.

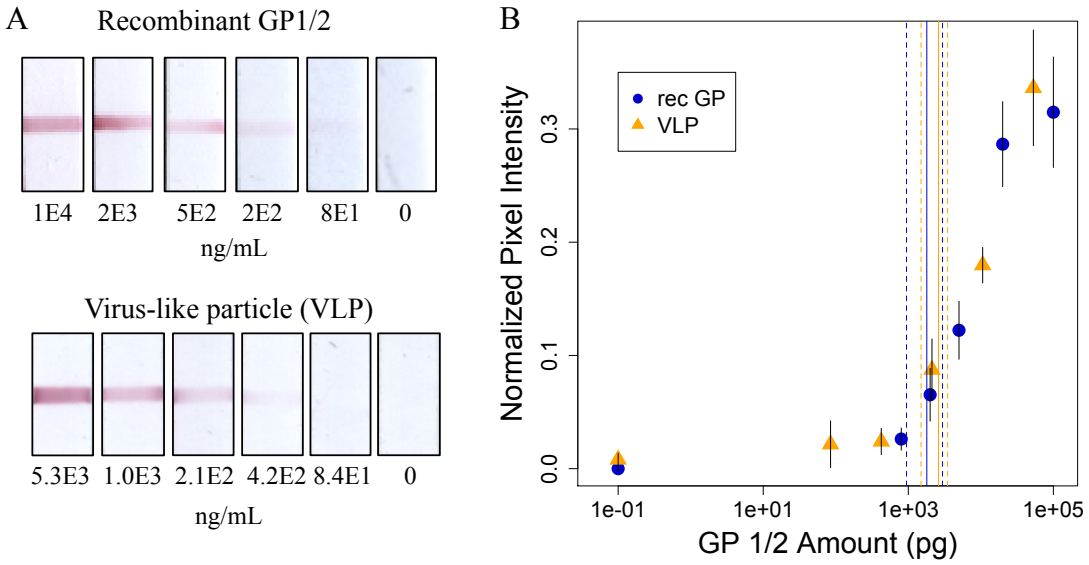

Figure 5.21. Limit of detection using antibodies for capture and detection.
Assay stack uses KZ52 antibody and a biotinylated mucin-binding domain polyclonal antibody with streptavidin gold nanoparticles for detection. Representative test lines (A) and the full assay response curves (B) are provided. Limits of detection for recombinant GP and VLP assays were found to be 0.261 µg/mL (95% CI [0.15, 3.48]) and 0.18 µg/mL (95% CI [0.0944, 2.965]) respectively, with 10 µL of sample tested per test strip. Each condition was tested with n=6 replicates.

The ZX binder was integrated into a lateral flow assay for the detection of the GP1/2 protein. We systematically replaced the capture and detection antibodies to demonstrate that the ZX binder can be used in either position, **Figure 5.23 and Figure 5.24**. The biotinylated form of the ZX protein was used in both orientations of the GP1/2 assay. Because the ZX binder does not naturally adsorb to nitrocellulose, immobilization was enabled through the use of a nitrocellulose binding streptavidin.

While both assays demonstrated detection of the trimeric GP1/2 protein, capture using the ZX binder demonstrated the best performance with a calculated limit of detection of 0.255 µg/mL, with a 95% confidence interval of [0.119, 0.378], **Figure 5.24**. This is equivalent to 4.5 ng of GP1/2 in the 20µL sample volume. The use of the chimeric version of the secondary antibody led to a decrease in overall assay performance. The calculated limit of detection was found to be 3.04 µg/mL with a 95% confidence interval of [1.40, 5.02]. This was expected, as the

chimeric version of the c13c6 antibody had less favorable kinetics over the isolated, neutralizing antibody. With these results, the use of biotinylated ZX with streptavidin to capture GP1/2 under flow led to comparable results to our high performing antibody stack, **Figure 5.21**. As the ZX protein is much less expensive and easier to manufacture than an antibody, replacing our capture antibody with the novel computationally designed protein could lead to a reduction from approximately $3,000/g to $10/g in cost for the final LFA [105].

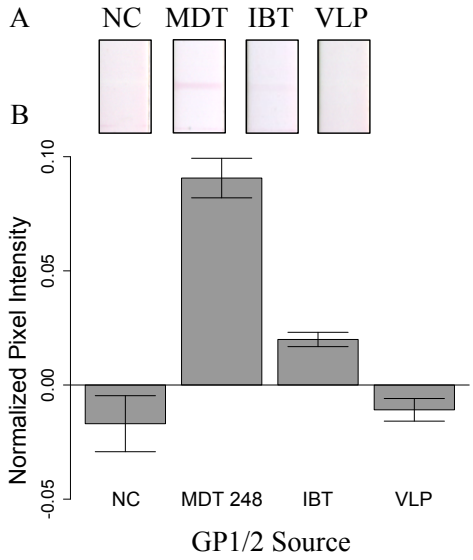

Figure 5.22. Effect of GP1/2 source on LFA signal.
Three GP1/2 sources were tested, MDT 248, IBT GP1/2, and IBT VLP, all at 400 μg/mL of GP1/2. Representative test lines (top) and calculated normalized pixel intensities (bottom) are shown. All conditions were tested with an n=3.

The soluble glycoprotein (sGP), alternatively, is an interesting protein diagnostic target for EVD due to the high concentration of this protein secreted during Ebola virus infection. While we initially intended to develop an assay to detect sGP at the beginning of this project, our collaborators were unable to get a crystal structure of the sGP protein. As an alternative, Liangcai Gu's group at the University of Washington used their novel protein screening method to identify proteins that bind to the sGP protein. The protein library was originally generated as a mutation library of small, variable fragment like, proteins expressed on phage. As our ultimate goal is to create a system that allows us to easily swap out individual components, we switched out the ZX protein with the novel binding proteins developed by the Gu lab. We had some issues

with cross-reactivity between the Gu lab binding proteins and themselves and the binding proteins and our GP1/2 antibodies. Despite these issues, we were able to integrate one of the Gu lab proteins into a lateral flow assay for improved detection of the sGP protein, **Figure 5.25**. Additional work characterizing this improvement is still required.

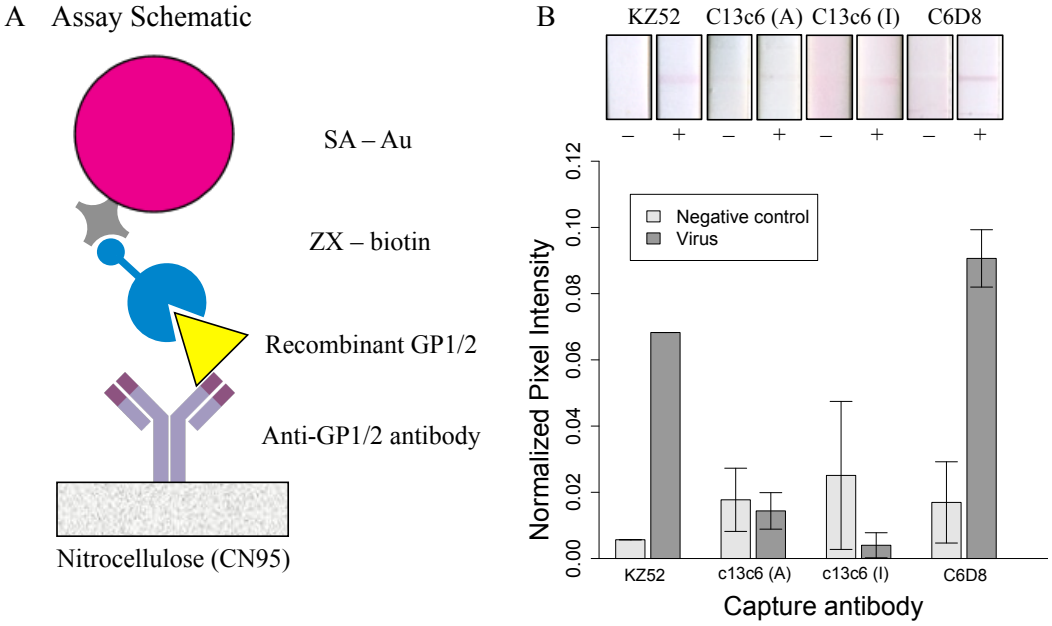

Figure 5.23. Recombinant GP1/2 lateral flow assays with antibody capture.
Assay stack uses anti-GP antibody, either KZ52, C13c6 or C6D8, to capture GP1/2 at the test line. Biotinylated ZX with a 40 nm streptavidin gold nanoparticle was used to visualize the test line (A). For C13c6, SA-Au from two different manufacturers were tested; Innova Biosciences (I) and Arista (A). Recombinant GP1/2 was tested at 200 µg/mL in a 20 µL sample. Representative test lines and the full assay response curves are provided (B). C13c6 and C6D8 were each tested with n=3 replicates, while KZ52 was tested with n=1.

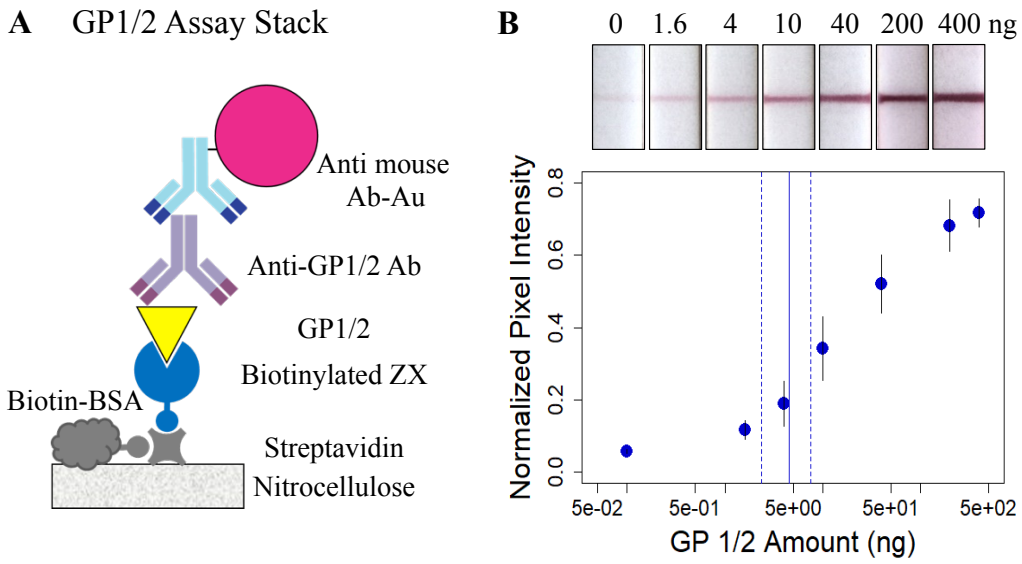

Figure 5.24. Limit of detection using ZX binder for GP1/2 capture.
Assay stack uses biotinylated ZX binder to capture GP1/2 when immobilized on the streptavidin test line. Biotin BSA prevents non-specific adsorption at the test line. Anti-GP1/2 antibody (c13c6) acts as the secondary antibody, with anti-mouse antibody-Au to visualize GP at the test line, (A). Representative test lines and the full assay response curves are provided (B). Each condition was tested with n=3 replicates. Limit of detection was calculated to be 0.255 µg/mL (95% CI [0.119, 0.378]).

For detection of Ebola virus from a suspected individual, we aim to detect the Ebola virus from a blood or plasma sample. However, detection of Ebola virus was not possible as a part of this project because it requires a BSL-4 level facility. Alternatively, we used virus like particles (VLP) that contained recombinant GP, nucleoprotein (NP), and matrix protein (VP40). While these proteins used many of the recombinant proteins expressed by the native Ebola virus, there could be differences in performance as compared to native Ebola virus. While the VLP available through IBT Bioservices binds well to their GP specific antibodies, it did not lead to positive test lines using the ZX binder. This is most likely due to strain specificity, as we found that the MDT 248 the ZX was designed against did not bind well to the IBT recombinant GP protein. To validate that the ZX protein could bind a VLP, we would need more control over the GP strain expressed on the surface.

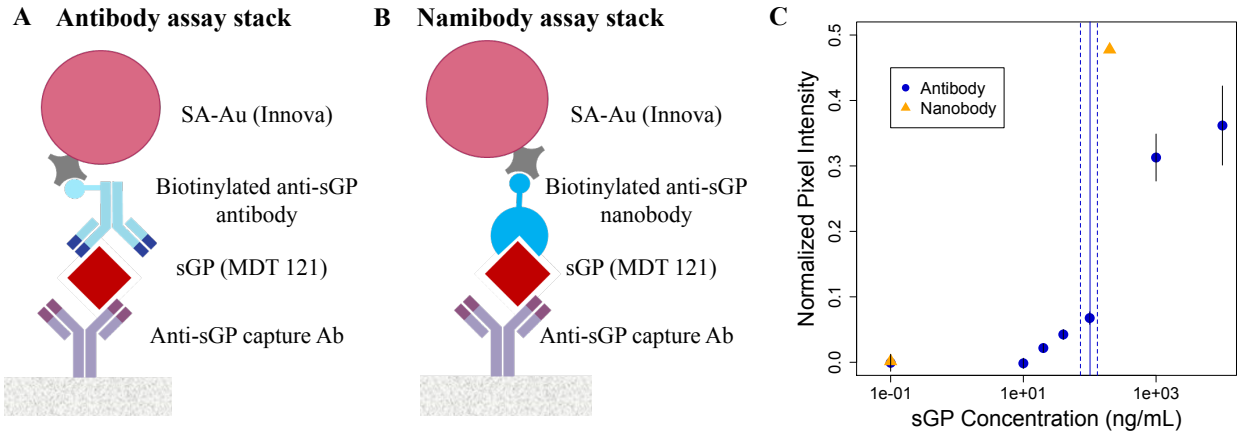

Figure 5.25. Assays for the detection of Ebola sGP.
Assay stack uses an anti-sGP antibody, BDBV, to capture sGP at the test line. Biotinylated protein #49 with a 40 nm streptavidin gold nanoparticle was used to visualize the test line (A). Recombinant sGP was tested at 200 ng/mL in a 20µL sample. Representative test lines and the full assay response curves are provided (B). LOD analysis run using antibody capture and detection is shown in blue (n=6), and the performance of namibody detection is shown in orange (n=2).

Testing of recombinant GP from plasma led to a similarly challenging issue. As a part of this project, our group developed a plasma separator that could separate red blood cells from blood without significantly increasing the overall footprint. However, initial tests with plasma led to a couple problems. Our best performing assay uses a human anti GP antibody, which cannot be used when testing with a human sample. Antibodies in the human sample led to very high false positive signal. We saw a similar issue with the chimeric KZ52 antibody, where the negative control had a large amount of signal generated in the negative control, **Figure 5.26**. We hypothesized that the streptavidin test line, which we had never previously tested with any patient sample, binds to other protein components found in blood. Biotin, which is present in the blood in healthy individuals at concentrations above 400 pg/mL and up to nearly 3000 pg/mL in patients taking biotin supplements, could be one of the primary contributors to false-positive signal [211]. With the addition of a biotin depletion section on the lateral flow test, any contribution of biotin to non-specific binding at the test line can be easily reduced. Future work

is still needed to test this hypothesis and implement any required sample preparation steps into the LFA format.

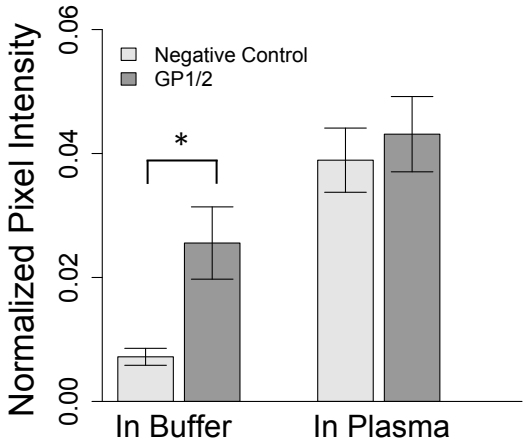

Figure 5.26. Detection of GP1/2 in plasma.
Non-specific signal increases when plasma (50% dilution) is used instead of buffer. GP1/2 (MDT 248) was spiked at 200 ng/mL. Normalized pixel intensity with standard deviation is shown, tested with an n=4. Asterisk signifies $p<0.05$ using a student's t test.

5.4 CONCLUSION

In this chapter, we describe the progress we have made towards a modular assembly system for more rapid lateral flow assay development, with application to an Ebola glycoprotein target as an example. We demonstrated a novel use for nitrocellulose binding proteins when combined with SpyCatcher and SpyTag for modular assay stack assembly. While we encountered some issues with protein stability, we were able to continue to use SpyCatcher and SpyTag as our conjugation system for our final Ebola assay stack. Using the computationally designed binder specific to the Ebola GP1/2 protein, we developed an assay stack to detect the protein with comparable sensitivity to our high affinity antibodies, with LODs of 0.261 µg/mL (95% CI [0.15, 3.48]) and 0.255 µg/mL (95% CI [0.119, 0.378]) for antibody and computationally designed protein respectively. This assay represents the second set of lateral flow assays using computationally designed affinity proteins.

Remaining work with this assay will focus on sample preparation for whole blood and the more realistic VLPs. One of the big questions that remains is the utility of a streptavidin test line for more complex sample types. Prior to this work, we had not tested this particular anchor with

a complex assay type, but the non-specific binding at the test line suggests the need for investigation into the cause of non-specific binding and potential solutions. Similar to the solubilization of influenza hemagglutinin that is required for detection of the native glycoprotein, there is a need for additional sample preparation work to enable detection of the GP1/2 protein from the Ebola VLPs. However, we have limited control over the strain of GP1/2 integrated into the VLP. There is a need for methods of viral glycoprotein solubilization for downstream LFA detection, however the development of these methods is most likely to be successful using our influenza assay due to strain specificity.

As demonstrated with the Ebola sGP, the ultimate goal is to develop an LFA system where we can easily plug in antigen specific binders without requiring significant lateral flow assay optimization development. With the same protein, nitrocellulose binding protein or streptavidin, spotted on the test line, the capture and detection proteins can instead both be integrated into the conjugate pad(s). Test line optimization is much more difficult than conjugate optimization, due to the need for spotting or striping to generate the test line. In addition, test line optimization requires at minimum an overnight incubation to allow for adsorption for the spotted protein. By using either of our test line anchors, the nitrocellulose binding protein or streptavidin, we can produce large quantities of lateral flow test strips at once that can be used to vary capture and/or detection protein concentrations and buffer composition more easily. The modular assay assembly system described here made progress towards this ultimate goal of a set of "plug and play" LFA assays.

5.5 Written and Oral Publications

La, D., et al. "De novo computational design of proteins that broadly neutralize Ebolaviruses." Manuscript in preparation.

Yager, P., **Anderson C.E.,** Baker, D., Lin, Y., Holstein, C.A. 2016 September 23. "Porous Membrane Binding Peptides." United States Patent US1527650.

In addition, this work has been presented at the following conference.

Anderson, C.E., Bishop, J.D., La, D., Baker, D., Yager, P. **"**Lateral flow assay for Ebola virus using computationally designed affinity proteins." Oral and poster presentation; Gordon Research Conference, Bioanalytical Sensors 2018, Rhode Island, USA.

Anderson, C.E., Bishop, J.D., La, D., Baker, D., Yager, P. **"**Lateral flow assay for Ebola virus using computationally designed affinity proteins." Poster presentation; Gordon Research Seminar, Bioanalytical Sensors 2018, Rhode Island, USA.

Chapter 6. CONCLUSION

6.1 Conclusions and Future Directions

The work described in this dissertation was motivated by the need for a broader class of antigen binding elements for use in lateral flow assays. Despite their ubiquity, antibodies are lacking in a few key categories that are important for LFAs; with their high production cost, limited thermostability, and minimal customizability limiting their success when integrated into the LFA format. Novel molecular recognition elements, such as the ones described in this dissertation, open the door for a broader selection of LFAs for a variety of targets. As demonstrated by our assays for the influenza and Ebola viruses described in Chapters 3 and 5, computationally designed affinity proteins can be incorporated into LFAs and outperform the available antibodies for a specific antigen. Not only that, but the increased customizability enabled by this new class of binding proteins opens the door for more precise protein conjugation. With increased thermostability, as described in Chapter 4, customizability, and low cost, these proteins are an extremely attractive option for antigen binding in a low cost, point of care diagnostic.

Despite these positive characteristics, the integration of novel molecular recognition elements like computationally designed proteins into lateral flow assays is not entirely straightforward. In our experience, the integration of computationally designed affinity proteins into LFAs was particularly challenging with regards to immobilization on a test line. Where antibodies adsorb easily to nitrocellulose, the majority of computationally designed proteins that we screened, as described in Chapter 5, do not. These challenges are not unique to computationally designed proteins, as similar issues have been demonstrated for antibody fragments and aptamers [215]–[217]. The development of a universal anchor system has the potential to streamline lateral flow assay development independent of the final target. While Chapter 5 describes progress towards this goal, there remains significant work to be done. Additional screening for nitrocellulose binding proteins, similar to the manner in which novel cellulose binding proteins have been identified [218], would help elucidate specific characteristics of strong nitrocellulose binding proteins. This information, building upon our knowledge of nitrocellulose binders from Chapter 5 and from the dissertation of Dr. Carly

Holstein, would enable the development of assay stacks made entirely of proteins expressed inexpensively in *E. coli*.

As we move from antibody based LFAs to those that use novel computationally designed affinity proteins, there is a need for methods that enable improved assay development. With computationally designed proteins, we have greater control over charge, size, and type and number of conjugation sites than we do with antibodies. The flow chamber system described in Appendix C aimed to help streamline the assay development process by decoupling protein immobilization and analyte capture from the performance of the entire assay stack. Remaining work with this flow chamber system requires investigation into precise sealing methods and preliminary data validating the sensitivity of the downstream protein quantification assays, specifically by microBCA and ELISA. With the development of new methods for lateral flow assay development, there is potential to learn more about protein adsorption to nitrocellulose and analyte capture at a test line than previously possible. One particularly interesting set of questions involves the role that protein immobilization, including directionality and packing density, plays on analyte capture under lateral flow. With antibodies, we have been limited in optimizing these parameters due to their larger size and randomness of immobilization by adsorption. Computationally designed proteins, as well as other novel molecular recognition elements, have optimization potential that might enable them to further outcompete antibodies when used in an LFA.

Beyond the traditional LFA, more complex paper microfluidic networks are required for a vast majority of assays that could benefit diagnosis at the point of care. While the 2DPN and μPAD have made significant strides with regards to automation of multistep assays in an easy to use format, recent understandings in fluid flow in porous matrices have opened the door for improved assay integration. Partial saturation, a concept described in Chapter 4 and Appendix B, has allowed us to layer porous materials such that orthogonal delivery of reagents across a test line can be easily automated. Orthogonal delivery of reagents is particularly interesting for enzymatic assays with reactive species, as demonstrated by the improved assay performance on our hemagglutinin prototype device in Chapter 4. Applications of this phenomenon to sample preparation, purification, and serial dilution open the door to a wider variety of assays that can be integrated into the inexpensive, easy to use LFA format.

A major concern with novel molecular recognition elements is that the promise of these antigen-binding elements might outweigh their practicality. Aptamers, an example of a molecular recognition element that has been developed for a wide range of targets, have not yet been integrated into a commercial LFA despite their initial promise [219], [220]. With challenges that include industry resistance and failure to garner government approval, aptamer use in therapeutics and diagnostics on the market has remained limited. As computationally designed affinity proteins could face similar challenges, there is a need for efforts demonstrating to the research and clinical communities the utility of these novel proteins. The work demonstrated in this dissertation is a first step to show the utility of computationally designed proteins for the development of inexpensive, accurate diagnostics for infectious disease.

In conclusion, this dissertation represents significant progress towards the use of computationally designed affinity proteins in lateral flow assays. The significant achievements of this work include (1) novel assays for the detection of influenza and Ebola viruses using computationally designed proteins, (2) the first prototype device integrating computationally designed proteins, and (3) methods for improved LFA assay development using modular design. All together, this work highlights the potential of this novel class of affinity reagents to increase the capabilities, specifically with regards to performance and range of applications, of the lateral flow assay platform.

6.2 List of contributions

The work described in this dissertation has been published and presented in the following journal articles and conference proceedings, respectively.

6.2.1 *Peer reviewed publications*

- **Anderson, C.E.,** Buser, J.R., Flemming, A.M., Strauch, E.M., Ladd, P.D., Englund, J., Baker, D., Yager, P. *Lab on a Chip*. "An integrated device for the rapid and sensitive detection of the influenza hemagglutinin." 2019, 19, 885-896. DOI: 10.1039/C8LC00691A.
- Buser, J.R.*; Byrnes, S.A.*; **Anderson, C.E.**; et al. *Analytical Methods*. "The P-switch: A pressure-based system for controlling flow and automating assays in paper microfluidics." 2019, 11, 336-345. DOI: 10.1039/C8AY01977K

- **Anderson, C.E**.*; Holstein, C.A.*; et al. *Analytical Chemistry*. "Development of a Paper-Based Assay for Whole Influenza Virus Detection using Computationally Designed Hemagglutinin Head Region Binder." 2017. DOI: 10.1021/acs.analchem.7b00769.

- Strauch, E.M.; Bernard, S.M.; La, D.; Bohn, A.J.; Lee, P.S.; **Anderson, C.E.**; et al. *Nature Biotechnology*. "Computational design of trimeric influenza neutralizing proteins targeting the hemagglutinin receptor binding site." 2017. DOI: 10.1038/nbt.3907.

- Huang, S.; Abe, K.; Bennett, S.; Liang, T.; Ladd, P.; Bishop, J.; **Anderson, C.E.**; et al. *Analytical Chemistry*. "Disposable Swab-to-Result Autonomous Device for Rapid Diagnosis of Influenza." 2017, DOI: 10.1021/acs.analchem.6b04801.

- **Anderson, C.E.***; Shah, K.G.*; Yager, P. *Methods in Enzymology*. "Sensitive protein detection and quantification in paper-based microfluidics for the point of care." In Richard Thompson, Carol A. Fierke, editors: Enzymes as Sensors, Vol 589, MIE, UK: Academic Press, 2017, pp. 383- 411.

- Holstein, C.A.; Chevalier, A.; Bennett, S.; **Anderson, C.E**.; et al. *Analytical and Bioanalytical Chemistry.* "Immobilizing Affinity Proteins to Nitrocellulose: A Toolbox for Paper-Based Assay Developers." 2016, 408(5):1335-1346.

* denotes equal contribution

6.2.2 *Oral and poster presentations*

Oral presentations

- **Anderson, C.E.,** Bishop, J.D., La, D., Baker, D., Yager, P. **"**Lateral flow assay for Ebola virus using computationally designed affinity proteins." Oral presentation; Gordon Research Conference, Bioanalytical Sensors 2018, Rhode Island, USA.

- Lutz, B.; **Anderson, C.E.**; Buser, J.R.; Byrnes, S.A; et al. "Paper Microfluidics: Integration Challenges & Solutions for Point-Of-Need Testing." Workshop; October 2016 MicroTAS, Dublin, Ireland. *(invited workshop)*

- **Anderson, C.E.**; Strauch, E.M.; Marzan, R.; et al. "Detection of intact influenza virus from clinical samples using co mputationally designed affinity proteins." Oral presentation; October 6, 2016. Biomedical Engineering Society Annual Meeting.

- Yager, P.; **Anderson, C.E.;** Lafleur, L. "Development of paper-based point-of-care diagnostics." Oral presentation; December 10, 2015. BioEngage Technical Symposium, University of Washington, Department of Bioengineering, Seattle, WA.

Poster Presentations

- **Anderson, C.E.,** Bishop, J.D., La, D., Baker, D., Yager, P. **"**Lateral flow assay for Ebola virus using computationally designed affinity proteins." Poster presentation; Gordon Research Seminar, Bioanalytical Sensors 2018, Rhode Island, USA.

- **Anderson, C.E.**; Buser, J.R.; Byrnes, S.A.; Yager, P. "An automated dilution series enabled by partial saturation in a porous microfluidic system." Poster presentation; Gordon Research Conference and Seminar, Physics and Chemistry of Microfluidics 2017, Lucca (Barga), Italy.

- **Anderson, C.E.**; Buser, J.R.; Strauch, E.M.; et al. "A two-dimensional paper network for automated detection of the Influenza virus employing computationally-designed affinity proteins." Poster presentation; The 20th International Conference on Miniaturized Systems for Chemistry and Life Sciences (MicroTAS 2016), Dublin, Ireland.

6.2.3 *Patents*

- Yager, Paul; **Anderson, Caitlin**; Baker, David; Lin, Yu-ru; Holstein, Carly, inventors; University of Washington, assignee. Porous membrane-binding peptides. US patent US15272650. September 23, 2016.

APPENDIX A – LIST OF ABBREVIATIONS

Abbreviation	Description
2DPN	Two-dimensional paper network
BCA	Bicinchoninic acid assay
BLI	Biolayer inferometry
BSA	Bovine serum albumin
CBD	Cellulose binding domain
CDC	Centers for Disease Control
CEID	Chicken embryo infectious dose
CHAPS	3-((3-cholamidopropyl) dimethylammonio)-1-propanesulfonate
CT	Cycle threshold
D1	Design 1 protein
DAB	3,3'-diaminobenzidine
DNA	Deoxyribonucleic acid
DTRA	Defense threat reduction agency
ELISA	Enzyme linked immunosorbent assay
FDA	Food and drug administration
GDP	Gross domestic product
GE	General Electric
GF	Glass fiber
GP	Glycoprotein
HA	Hemagglutinin
HIV	Human immunodeficiency virus
HRP	Horseradish peroxidase
IGEPAL	Octylphenoxy poly(ethyleneoxy)ethanol
IgG	Immunoglobulin G
IPD	Institute for Protein Design
IRR	International Reagent Resource (formerly Influenza Reagent Resource)
IUPAC	International Union of Pure and Applied Chemistry
LFA	Lateral flow Assay
LOD	Limit of Detection
MDCK	Madin-Darby Canine Kidney cells
MDT	Molecular Design and Therapeutics lab

microTAS	Microfluidic total analysis systems
MRSA	Methicillin-resistant Staphylococcus aureus
NC	Nitrocellulose
NCB	Nitrocellulose binding protein
NIH	National Institutes of Health
OG	Octyl-β-D-Glucopyranoside
PBS	Phosphate buffered saline
PBST	Phosphate buffered saline with tween 20
PCR	Polymerase chain reaction
pI	Isoelectric point
PMMA	Poly(methyl methacrylate)
POC	Point of care
qRT-PCR	Quantitative reverse transcriptase polymerase chain reaction
RDT	Rapid diagnostic test
RFC	Red food coloring
RNA	Ribonucleic acid
RT-PCR	Reverse transcriptase polymerase chain reaction
RTG	Ready to go
SC	SpyCatcher
SELEX	Systematic evolution of ligands by exponential enrichment
SEM	Scanning electron microscope
SPR	Surface plasmon resonance
ssDNA	Single stranded DNA
ST	SpyTag
TCID	Tissue culture infectious dose
µPAD	Microfluidic paper-based analytical device
UTM	Universal transfer media
UW	University of Washington
WHO	World Health Organization

APPENDIX B – AUTOMATED DILUTION SERIES

Development of an automated dilution series that uses partial saturation for fluidic control

The work described in Appendix B is my contribution to a manuscript in Analytical Methods from our group, full citation below. I have presented this work at the 2017 Gordon Conference on the Physics and Chemistry of Microfluidics in Lucca (Barga), Italy in a poster entitled "An automated dilution series enabled by partial saturation in a porous microfluidic system".

Buser, J.D., Byrnes, S.A., **Anderson, C.E.**, Howell, A.J., Kauffman, P.C., Bishop, J.D., Wheeler, M.H., Kumar, S., Yager, P. "Understanding partial saturation in paper microfluidics enables alternative device architectures." *Analytical Methods*. DOI: 10.1039/C8AY01977K

B.1 INTRODUCTION

The use of porous materials as a platform for bioassays dates back to the 1930s with the development of paper chromatography [221]–[223]. In the mid to late-1970s, the home-based pregnancy test popularized the use of porous materials to bring diagnostics to the point-of-care (POC) [28], [224]. More recently, George Whitesides' group helped lead a renaissance in paper-microfluidic technology when they patterned cellulose paper in two dimensions to simultaneously detect glucose and proteins in urine samples [25]. Paper-microfluidic devices have since evolved to include systems that offer advantages such as the ability to perform complex, multi-step processes [31], [134], the sequential timed delivery of reagents [31], [40], and compatibility with various amplification and detection techniques [225]–[228].

Perhaps the most useful feature of paper-microfluidic systems is passive fluid transport by capillary action. The automation of more complex assay procedures, however, has required new fluidic controls using a variety of valving techniques. For example, materials embedded into a membrane can slow or delay flow. Noh et al. patterned wax at various concentrations to control fluidic timing in porous devices [229], [230]. Lutz et al. embedded sugar barriers into porous materials. Higher concentrations of sugars resulted in longer delays for fluid delivery [150]. Chen et al. developed a fluidic diode using a combination of hydrophobic and hydrophilic coatings to control direction and sequencing of fluid flow [231]. Many of these systems

introduce an additional reagent (wax, sugar, etc.) into the reaction, which may negatively impact sensitive reactions such as nucleic acid amplification [232]–[234].

A number of efforts show progress in implementing valve technologies that do not introduce outside agents into the assay fluids. Both permanent magnets [235] and electromagnetic solenoids [236] have been used to make and break fluidic connections. These elements are outside of the main fluid pathway and do not introduce additional reagents. Toley et al. developed valves that use auxiliary fluidic networks to actuate expanding elements. These expanding valves can turn flow on or off and cause fluid diversion and redirection [237]. More complex switching has also been demonstrated using paper actuators, including both normally-on and normally-off single- and double-throw switches [238]. The Yager, Lutz, and Fu groups have also designed methods for the sequential timed delivery of reagents through two-dimensional paper networks that rely on volume metering [134], [239]–[241].

Recent publications have included reviews of additional valving for paper microfluidics including those detailed above [242]–[245]. Although effective, many of these systems are limited to use with a maximum of a few hundred microliters of input sample. When processing urine or dilute blood, devices may need to manage up to 5–10 mL of sample. In urine, for example, the first ~10 mL often contains the highest concentration of pathogen biomarkers [246]. Due to the dilute nature of urine, at least 1–2 mL is often collected to obtain detectable pathogen at clinically relevant concentrations [247], [248].

In recent years, multiple groups have used isotachophoresis to concentrate pathogen biomarkers from complex samples [249]–[251], but these systems often use small sample volumes and involve multiple pre-processing steps, such as off-device centrifugation and sample dilution [252]. Additionally, isotachophoresis can be sensitive to salt and cell concentrations found in clinical samples [252]. Linnes et al. developed an integrated method for paper-based NA extraction coupled to in-membrane isothermal amplification to detect chlamydia [253]. Although effective, this device required multiple user steps and accepted between 10–100 µL of urine. We previously described an in-membrane sample processing method that concentrated DNA from up to 2 mL of sample, but that system did not include automation to enable development of an integrated device [254].

Alternatively, some samples require dilution prior to processing to reduce high concentrations of interfering species that may inhibit target detection [255] or restrict flow

through porous membranes [254]. Previously-demonstrated paper microfluidic devices effectively dilute samples by submerging a swab in buffer, subsequently delivering the input sample into multiple detection zones causing modest dilution [38], but there are only a few demonstrations of deliberate and automated dilution in paper-based devices. Osborn et al. demonstrated a paper-microfluidic device capable of linear dilutions based on geometry [239] and Songjaroen et al. designed a system that uses a wash step to dilute a sample on-device for blood typing [256]. To date, there have not been any published reports of paper-microfluidic devices that automate multiple, parallel dilutions of a sample.

The complexity of realistic samples—some of which need concentration, and others dilution—required a re-examination of how paper-microfluidic devices process fluids, not least because the current understanding of fluid flow in these devices is based on inadequate flow models: the Washburn equation and Darcy's law. The Washburn equation is limited to one-dimensional flow, while Darcy's law can model multi-dimensional flows. However, we have recently argued that neither of these models are fully representative of complex flow in wetting porous materials because they both assume the existence of a fully saturating wetting front. In reality, a porous membrane supports a partially-saturated wetting front, where the degree of saturation depends on specific physical properties of the membrane along with fluid properties and system geometry. Therefore, we advocate the use of a flow model like the Richards equation, which is widely used in hydrogeology to model partially-saturated flow through soil [52]. Briefly, the Richards equation models the change in saturation of a porous media due to gradients in the pressure head, and can be written as:

$$\frac{\partial \theta}{\partial t} = \frac{\partial}{\partial z}\left[\frac{K(\theta)\partial H(\theta)}{\partial z}\right] \tag{C.6}$$

where θ is the volumetric water content, t is time, K is the hydraulic conductivity, H is the pressure head (m), and z is the position. Both the hydraulic conductivity and pressure are functions of volumetric water content: as the porous media becomes more saturated it generates less suction pressure and becomes a better fluid conductor. The full description of how to use the Richards equation as a basis for flow models for paper-microfluidic systems, and how to perform the requisite physical characterization of the composite porous materials, can be found in the PhD thesis of JR Buser, available from the University of Washington [53].

Using this new insight—that flow in paper-microfluidic devices is dependent on the existence of partially-saturated regions—we have designed a system to automate and control large-volume fluid flow in paper-microfluidic devices to support the integration of more complex sample preparation methods into these devices. We demonstrate this simple-to-use system of multiple porous materials through two examples: (1) automated DNA extraction and concentration from mL-sized samples and, to our knowledge, (2) the first demonstration of automated multiple parallel dilutions in a paper-microfluidic device.

B.2 MATERIALS AND METHODS

B.2.1 *Reagent preparation*

All reagents were prepared with sterile molecular biology grade water (Fisher Scientific, Waltham, MA, USA). The biotinylated probe consisted of the following sequence: 5′–TTTTTTTTTTTTTTTTTTTT–biotinTEG–3′ (T20-biotin). A working solution of T20–biotin probe was prepared at 200 µM in 75 µM TEAB. A working solution of gold nanoparticles was prepared using 40 nm, streptavidin-coated, gold nanoparticles (InnovaCoat Gold; InnovaBiosciences, Cambridge, United Kingdom) diluted to OD 0.0625 in phosphate-buffered saline buffer containing Tween-20 (0.1%, Sigma Aldrich P9416) and 1% (w/v) bovine serum albumin (PBST+BSA).

B.2.2 *Material fabrication and patterning*

All porous and plastic materials were cut to their final shapes using a CO_2 laser (VLS3.60; Universal Laser Systems, Scottsdale, AZ, USA). For DNA purification/concentration, Fusion 5 membranes (GE Healthcare Life Sciences, Niskayuna, NY, USA) were patterned with chitosan and stored in a desiccator; glass fiber (8964; Ahlstrom, Alpharetta, GA, USA) and cellulose (CFSP223000; Millipore, Billerica, MA, USA) membranes were used without modification. Test cards were made with 0.254 mm-thick Melinex backing with adhesive on one side (T-5501-10/1; Fralock, Valencia, CA, USA). For parallel dilution, nitrocellulose membranes (HF135; EMD Millipore, Billerica, MA, USA) were patterned with T20–biotin probe by a piezoelectric printer (sciFLEXARRAYER S3; Scienion AG, Berlin, Germany); 8964 glass fiber, Fusion 5, and CFSP223000 cellulose membranes were used without modification. The T20–biotin probe solution was filtered using a 0.2-µm nylon membrane (VWR, Radnor, PA, USA) at 8000g for 5 minutes prior to spotting. Test lines were created by placement of 20 spots, spaced

250 µm apart, with 30 droplets per spot. The volume of each droplet was 450–500 pL. After spotting them with T20–biotin probe solution, the nitrocellulose membranes were UV treated for 8 minutes with a UV transilluminator (UltraLUM inc, Paramount, CA, USA) at 300–310 nm and stored under desiccation before use.

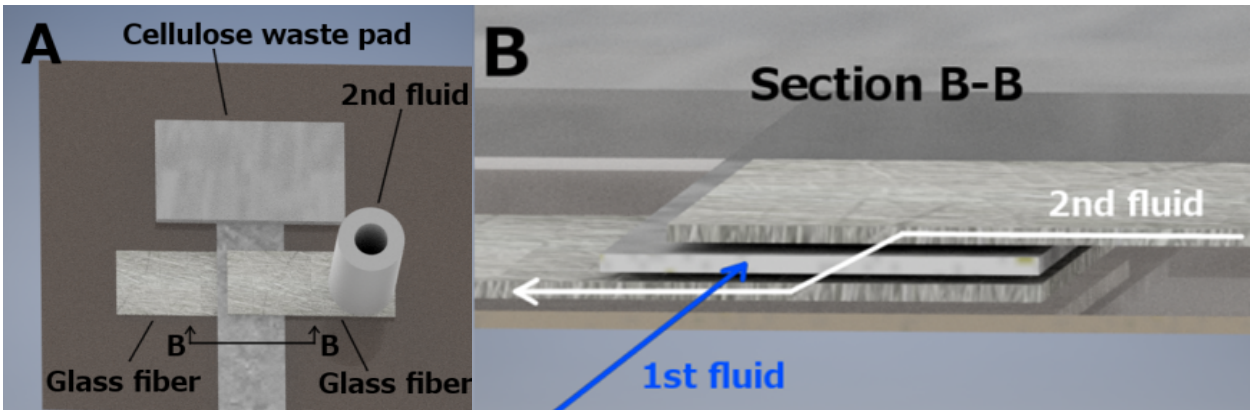

Figure B.1. Schematic of pressure switch (p-switch) overlap.

Capillary driven flow in porous membranes is influenced by the pressure differential between the fluid front and the wetting front. We can automate the delivery of controlled volumes by layering porous membranes with different properties, such as glass fiber and fusion 5.

B.2.3 *Device construction*

Devices were built as shown in **Figure B.1**, with Fusion 5 as the primary membrane and glass fiber as the secondary membrane. Cellulose was used as the waste pad for these devices. Membranes were held in place by the adhesive layer of the Mylar test card. Dilution devices were built as shown in **Figure B.1**, with glass fiber as the source pad, Fusion 5 as the sample pad, nitrocellulose as the test strip, and cellulose as the waste pad. Device tests were run by first introducing 750 µL of gold nanoparticle solution to the upstream end of the sample pad. Upon saturation of the sample pad, the glass fiber source pad was placed into a reservoir containing 3 mL of PBST, which was allowed to flow into the device until the reservoir was empty of fluid. Devices were immediately placed on a scanner (Perfection V700 Photo; Epson America, Inc., Long Beach, CA, USA) and scanned at 600 dpi in 48-bit color. The resulting images were analyzed using ImageJ software (version 1.50g) [257], with which the normalized pixel intensity across the test line was quantified. A calibration curve was generated for test line intensities using known concentrations of gold nanoparticles. Dilutions of the working gold nanoparticle

solution to 0–0.25 OD in PBST+BSA with a final volume of 40 µL were tested to determine the dynamic range for the system.

B.3 RESULTS AND DISCUSSION

B.3.1 *Multiple, parallel dilutions of samples using partial saturation for flow control*

Controlled dilution is a commonly used laboratory technique in chemistry, biochemistry and biology. Diagnostic applications using a dilution series range from measuring binding kinetics to performing sample preparation [258], [259]. For an example of the latter, some samples require dilution to reduce high concentrations of species that inhibit target detection. While plastic-microfluidic devices have been used to generate dilution series, they require additional equipment to pump fluids through the device [258]–[260]. Paper-microfluidic devices automate fluid transport but have not yet been shown to combine automated sample dilution with molecular detection. Such a combination would enable paper-microfluidic devices to scale up small sample volumes and samples that contain high concentrations of assay inhibitors.

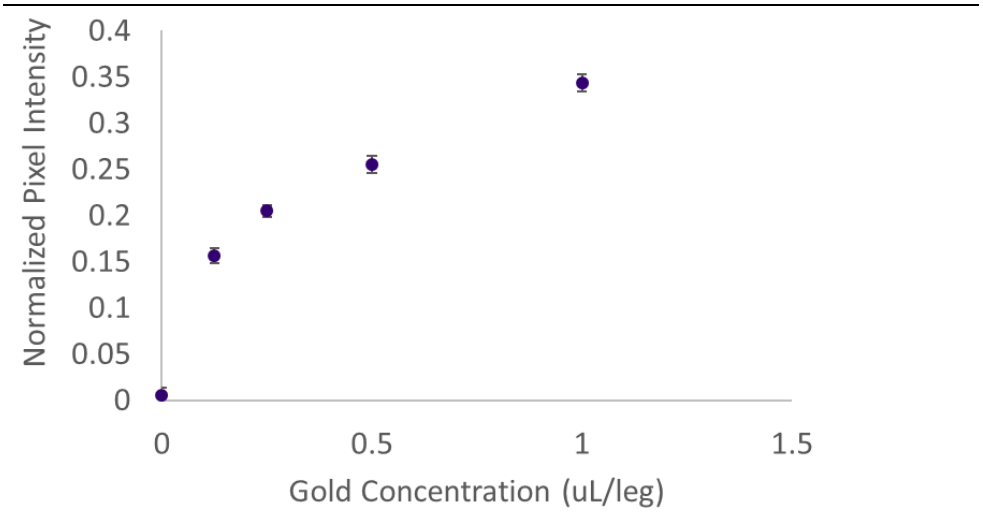

Figure B.2. T20 biotin-streptavidin gold calibration curve.
This calibration curve was used for data analysis for the automated dilution series device.

Therefore, we prototyped a paper-microfluidic device, shown in **Figure B.3**, that uses a series of "partial saturation switches" to automate the creation and delivery of a dilution series

from a sample and to multiple test strips, respectively. To operate the device, the sample was applied to a sample pad, which formed the primary pathway of the switch. The source pad was then placed into buffer, which hydrated the secondary pathway and carried the series of sample dilutions into the test strips.

We found the area of overlap between the primary and secondary pathways to be related to the dilution factor on the sample carried into the secondary pathway. By simple changes in geometry, an arbitrary dilution series can be created with this system that delivers various, specific amounts of a sample, or reagent, across a number of test lines. Both linear and logarithmic series are among those possible to create, depending on the biochemical or biological assay being integrated. This prototype device was designed to create a linear dilution series.

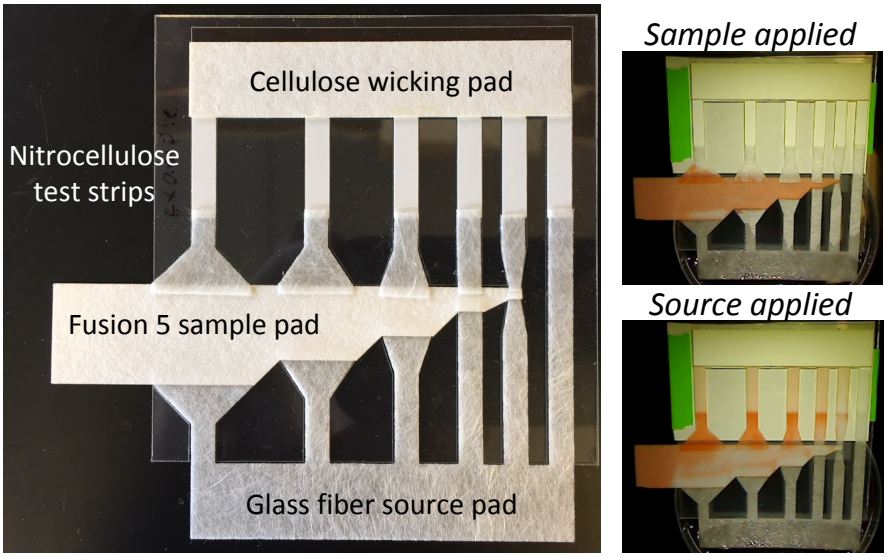

Figure B.3. Paper-microfluidic device for automated dilution.
Device schematic of the automation dilution device, where sample first flows through the Fusion 5 sample pad, followed by applying running buffer to the source pad. Video stills of the dilution device using red dye are shown. Layering of glass fiber, fusion 5, and cellulose enables the delivery of varying volumes of sample across 5 nitrocellulose test lines and one negative control in a two step process, as shown on the right.

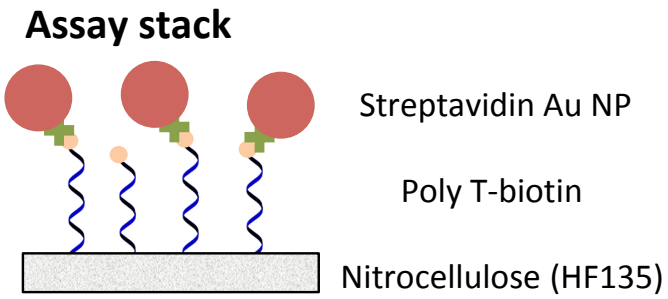

Figure B.4. Graphic describing assay chemistry at the test line.
Poly T-biotin was UV crosslinked to a nitrocellulose membrane, where it would capture streptavidin Au nanoparticles when they flowed across and lead to a red/pink test line.

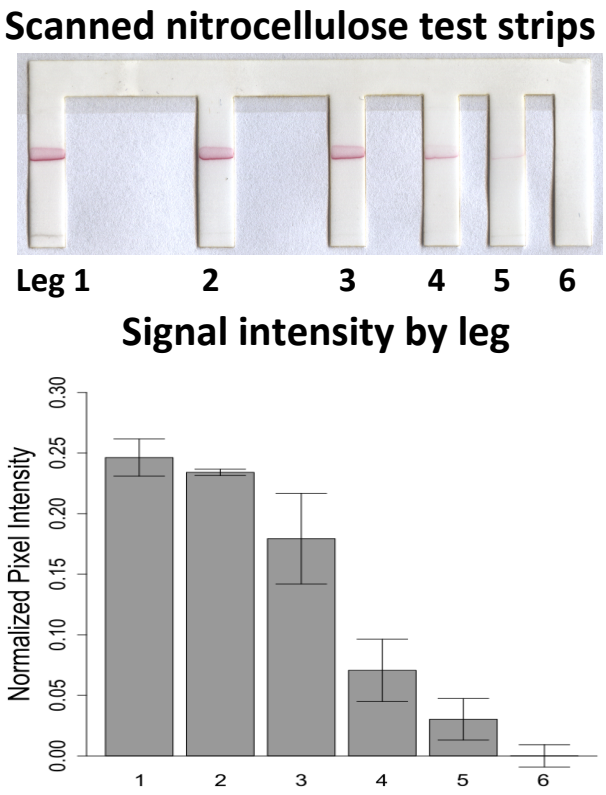

Figure B.5. Automated dilution series results.
Representative test lines and the calculated normalized pixel intensity for each leg of the automated diluter. Averages of N=3 are reported with error bars representing +/- one standard deviation.

The dilution factors were quantified using nitrocellulose test strips, with capture lines comprising UV-cross-linked, biotin–oligonucleotide conjugates. The sample was spiked with

streptavidin–gold nanoparticle conjugates, which were bound by the immobilized biotin–oligo conjugates on the capture line, **Figure B.4**. We generated a calibration curve (**Figure B.2**) by quantifying test strip pixel intensity using known concentrations of gold nanoparticles. Based this data, the dilutions achieve range from 80% of the original concentration down to 10% of the original concentration. The dilution achieved is linearly related to the Fusion 5 sample pad area for each respective leg, **Figure B.6**.

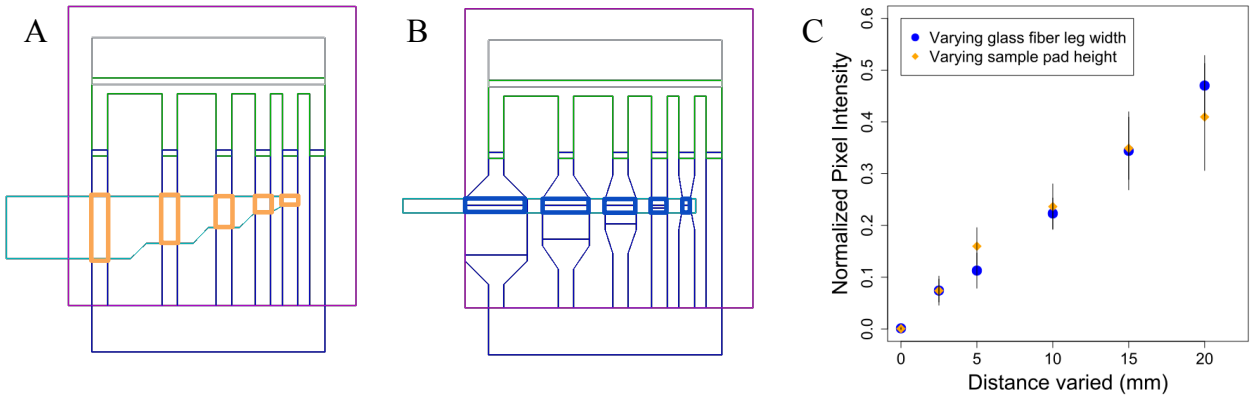

Figure B.6. Dilution optimization on device.
Variation of the height of the sample pad height (A) or glass fiber leg width (B) lead to linear variation in the normalized pixel intensity on device (C). These dimensions can be tuned to generate dilution series specific to the device and assay needs.

B.4 CONCLUSION

This work was the first demonstration of an automated, paper based dilution series. By using partial saturation for fluidic control, dilution of a sample can be completed without the need for additional machinery or user steps. We anticipate that an automated dilution series can be integrated into a variety of devices to support more complex sample preparation techniques and multi-step assays. In particular, the use of an automated dilution series can enable quantitative readout for nucleic acid amplification or conventional lateral flow immunoassay applications, which traditionally limited to non-quantitative or semi-quantitative results.

APPENDIX C – MICROFLUIDIC FLOW CHAMBER

C.1 INTRODUCTION

The first two aims in this dissertation describe the development and integration of assays for the influenza HA using computationally designed affinity proteins – the first demonstration of the use of these proteins within the lateral flow assay context. Through the assay development process, we identified characteristics important to the success of a designed protein when used to capture an analyte of interest. Two properties are particularly notable, the ability to be immobilized to nitrocellulose and the ability to capture the analyte of interest. While the assays shown in aims 1, 2 and 3 were all successfully integrated into lateral flow assays, this was after many previous attempts using various iterations of binders and immobilization techniques [58]. Antibodies are naturally produced with these properties, as demonstrated by their successful integration into lateral flow immunoassays, suggesting that additional design and optimization steps are required for the computationally designed proteins. There is greater potential for assay optimization with designed proteins, as we have greater control over properties including size, shape, and charge, etc. With the introduction of a broader class of affinity reagents, there is a need for a quantitative system to analyze immobilization and analyte capture for more rational design and optimization of lateral flow assays.

Lateral flow assay developers often rely on optimization processes to screen the various assay components for optimal assay performance. These processes are mostly limited to the membranes, biological reagents, and the geometry of the device, however a recent publication describing the development of analytical tools to further improve optimization has provided a framework for improved assay development [2]. There are, however, additional considerations for non-antibody affinity reagents. In the process of designing and testing computationally designed proteins, we have the ability to optimize a greater number of properties than we have ever been able to with antibodies. This opens the door for the development of a more diverse set of lateral flow assays, as these proteins are much more varied and customizable as compared to antibodies. With the introduction of a more diverse set of lateral flow assays, there is the need for the development of laboratory tools that allow for optimization within this larger lateral flow assay development framework.

We were interested in developing universal methods for the integration of computationally designed affinity proteins into lateral flow assays. Because of the nature of antibodies, there has not been a need for these methods previously. This appendix chapter is focused on the development and first attempts at implementation of a new technique for the quantitative measurement of protein immobilization and capture within a porous matrix. The work specifically focuses on the development of a pump-driven microfluidic flow chamber with two applications to porous membranes: measurement of protein immobilization and measurement of analyte capture.

As described in aim 3, the standard method used in our lab for determination of protein immobilization to nitrocellulose involves a protein stain. The stain used in this work, Ponceau S, is a negatively charged stain that attacks positively charged groups in proteins [261]. If proteins are present on nitrocellulose, we see a light red stain form. Because the Ponceau S stain targets positively charged amino acids within the protein, the resulting stain is not quantitative. Instead, we see variability from protein to protein depending on the number and location of the positively charged amino acid groups.

Other methods for the determination of proteins immobilized or captured on nitrocellulose include labeling with either a fluorophore or radiolabel. While fluorophore labeling is more straightforward, the sensitivity of these assays often does not reach the level required when making minor changes to a protein or set of proteins [262]. Radiolabeling has been used to measure forward and reverse rates for binding in an LFA, finding that the forward binding rates differ by at least two orders of magnitude between LFAs and more traditional binding experiments (SPR) [262]. Interestingly, the off rate was found to be nearly identical between the two sets of experiments, suggesting that the protein-protein interactions dominate the release of the captured analyte. This knowledge supports many of our assumptions about binding kinetics under lateral flow, and that the structure of nitrocellulose impacts the interactions between a capture molecule and protein analyte.

An alternative protein staining method, the bicinchoninic acid assay (BCA), is an attractive alternative for protein quantification. The BCA relies on the reduction of Cu2+ to Cu1+ by protein in an alkaline medium and combines it with the detection of Cu1+ using bicinchoninic acid [263]. The first step in this reaction is the chelation of copper with the protein to form a blue colored complex. Peptides that contain three or more amino acid residues form a colored chelate

complex with cupric ions, **Figure C.7**. This is known as a biuret, and can be depicted as NH2-CO-NH-CO-NH2. Biuret reacts with copper to form a light blue tetradentate complex. Only tripeptides and larger polypeptides and proteins produce the light blue to violet complex that can be visualized at 540 nm. One cupric ion forms a colored coordination complex with four to six nearby peptide bonds. The BCA assay is somewhat quantitative [264], where the intensity of the color produced is proportional to the number of peptides bonds that participate in the reaction. This assay is commonly used in clinical labs for the quantitation of total protein in serum. We aim to use it to determine the total amount of adsorbed protein in a porous matrix.

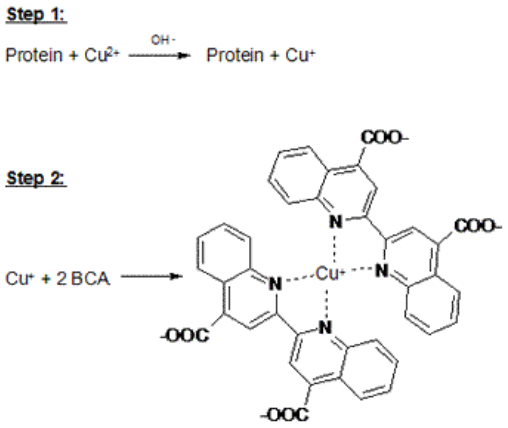

Figure C.7. The mechanism behind the BCA assay.
This schematic depicts the chemistry that leads to a measurable colorimetric change that occurs in the presence of tripeptides or larger. Source: nfsc4500101groupa.weebly.com

Our goal with this work is to develop a system that can quantitatively determine the (1) amount of protein that washes off a nitrocellulose membrane or (2) amount of analyte that binds to a test line. For both protein adsorption and analyte binding, the system needs to enable quantitative detection without altering the behavior of the protein of interest. The system also needs to be higher throughput than the traditional staining technique, which led us to investigate a method that did not require labeling the proteins of interest with a radioisotope or alternative. With the development of a microfluidic flow chamber, our hope was to develop a label free method that would allow us to get quantitative information regarding protein interactions in porous matrices. This chapter of the Appendix will describe the progress made towards this goal, focusing primarily on the fluidics.

C.2 MATERIALS AND METHODS

C.2.1 *Flow chamber*

The flow chamber support fixture is laser cut from polymethyl methacrylate (PMMA), using a silicon gasket to seal the porous membrane between the two PMMA components. Inside the gasket there is space for a membrane that is 10 mm by 5 mm, similar to the size of the lateral flow test strips used in our devices. Plastic tubing on each side of the membrane serve as input and output of the solution of choice. One end of the tubing is connected to a syringe pump, and the other is placed so that fluid can be collected using a 96 well plate, **Figure C.10**. The syringe pump is connected to either a 100 or 500 µL syringe for all experiments described in this chapter.

C.2.2 *Membrane preparation*

Nitrocellulose, glass fiber, and fusion 5 membranes (GE FF80HP, Millipore HF120 and HF135, GE Fusion 5, and Ahlstrom GF 8950) are cut into test strips using a CO2 laser cutter (Universal Laser Systems, Scottsdale, AZ). Each test strip for the flow chamber is 5 mm wide by 10 mm long, to fit inside the silicon gasket. Test membranes for the flow challenge are cut to be 8 mm wide and 20 mm long. Membranes are hand spotted using a pipette with 0.5 µL for each protein, typically at 1 mg/mL unless otherwise stated. After spotting, all membranes are placed in a desiccator at room temperature until use, for a minimum of overnight.

C.2.3 *Lateral flow challenge*

The lateral flow challenge is a method developed by Dr. Carly Holstein and Dr. Gina Fridley to analyze the strength and speed at which a protein adsorbs to more accurately compare a range of computationally designed materials with different properties, **Figure 5.5**. Devices are then assembled in holding cards with cellulose wicking pads the day of testing. Half of the membranes are challenged with 1 mL of PBST, which is the buffer used in all wash steps of our assay, while the other half were left dry until staining. All membranes are then stained with Ponceau S stain in 10% methanol for 10 minutes, followed by two wash steps in DI water for 2 minutes each. These membranes are then immediately transferred to a piece of white printer paper and scanned at 600 dpi.

C.2.4 *Immobilization quantification*

The flow chamber will be used to quantify the amount of protein immobilized on a membrane using the micro BCA assay. Proteins are stored in the porous material using the

method described above. The flow chamber is used to wash PBS (or another buffer) through the porous material being tested at 0.5 µl/second speed into 10, 100 µL aliquots. The choice of aliquot size still needs to be optimized; therefore it is possible this volume will change. Each 100 µL is collected into a well in a 96-well plate that is placed underneath the flow chamber. After collection, these aliquots are used to run a micro BCA assay (ThermoFisher, Waltham, MA).

C.2.5 *Micro BCA*

For the micro BCA, 150 µL of the BCA working reagent is added to each well and the plate is subsequently placed on the shaker for 30 seconds. After shaking, the plate is covered using sealing tape and incubated for 2 hours at 37°C. The plate is then cooled at room temperature, and read at 562 nm on a plate reader. For the data analysis, the average absorbance reading of the black standard replicates are used to background subtract for all samples. A standard curve is prepared to allow for the quantification of protein content.

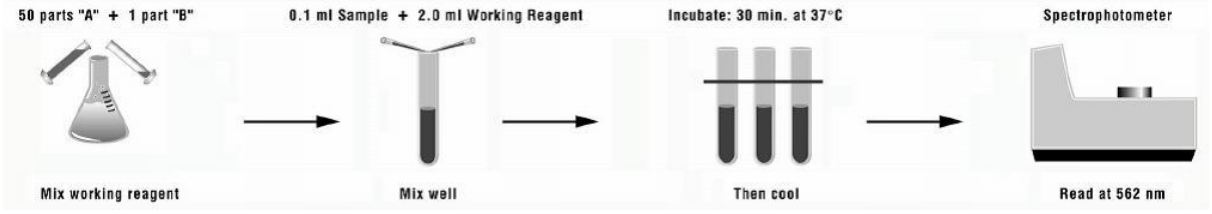

Figure C.8. Schematic of the steps required for a BCA assay.
The assay we ran is a micro BCA in a 96 well plate, making our volumes are much smaller than those indicated in here. Source: (https://www.thermofisher.com/order/catalog/product/23235)

C.2.6 *Flow chamber injection system development*

Analyte depletion was tested using an input syringe to push smaller volumes of analyte through the flow chamber. In the first iteration of the injection system, the glass syringe is connected to a three-way valve, which controls the tubing the sample is pulled from, **Figure C.12**. The sample is loaded into the syringe manually and pumped through the system similarly to the immobilization experiments. In the second iteration of the injection system, using the 6-port injection valve, we used the valve shown in **Figure C.8** connected to the syringe pump and microfluidic chamber using 6 tubes that connect to the pump, flow chamber, antibody, and have a loading coil through which antibody can be loaded before running the experiment.

Testing of the maximum volume allowed by the system was done by pulling dye from a tube while the system was in the load position, meaning the knob was in load and syringe was on

pump in, **Figure C.13**. The volume required to pull before dye appeared in the syringe was measured. Measurement of the unloading profile from the loading tube was measured by running water through all tubes. The tubes were loaded with 220 μL of brilliant blue dye, after which the knob was turned to the unload position and the table tube was placed into a small vial. The dye solution was unloaded into the small vial in 10 μL intervals until the dye first appears in the small tube. The tube was replaced, and the dye was continually pumped out of the system until the fluid coming out of the system was clear, recording the volume again. Determination of the concentration profile output from the 6-port injection valve was done using this same method, however individual aliquots of 20 μL were taken and read on a plate reader at wavelength 600 nm.

The third, and final injection system used in this chapter used air loaded into the syringe itself to reduce diffusion between the sample and the surrounding aqueous solution, as depicted in **Figure C.16**. This was done to prevent loss of dye/analyte to diffusion. In this system, buffer is removed from the syringe and pumped into the tubing connected to the flow chamber by pumping at 0.5 μL/s. 50 μL of air is pumped into the syringe through the valve connected to open tubing (valve 3 in our system) at 5 μL/s. The open tubing is then placed in an Eppendorf tube filled with dye or protein solution, and the remaining volume in the syringe is filled using 5 μL/s. During operation the flow chamber was run at 0.5 μL/s, however it could be run slower with a smaller syringe.

C.3 RESULTS AND DISCUSSION

C.3.1 *Quantitative method to measure protein immobilization*

There are a lot of questions throughout the assay development process that we have been unable to answer using methods traditionally used for paper microfluidics. One of the major capabilities that has been lacking is the ability to extract and measure proteins immobilized on or bound at the test line. This limits our ability to make quantitative assessments during the assay development process. Therefore, we sought to develop a method to look more quantitatively at each individual assay step. Learning from depletion experiments used to study adsorption, I partnered with Dr. Joshua Buser and Dr. Joshua Bishop to develop a microfluidic flow chamber that allows us to measure protein content before and after a solution has been flowed through a

porous material. The flow chamber is driven by syringe pumps, and uses tubing to deliver fluid into a porous material sealed between two pieces of PMMA and a silicon gasket, **Figure C.9**.

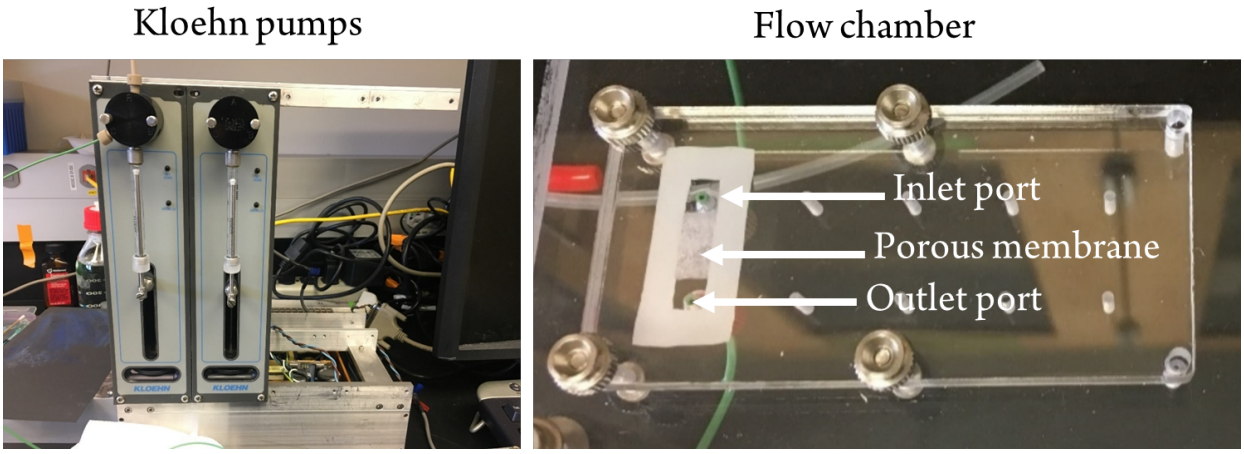

Figure C.9. Images of the flow chamber set up.
Flow is powered by Kloehn syringe pumps (left). The flow chamber itself consists of two layers of PMMA, between which a porous membrane is sandwiched (right). A silicone gasket surrounds the material to prevent damage to and leaking around the membrane. An inlet and outlet port are placed on either side of the membrane, through which fluid can be pumped.

We have developed methods to enable flow in the flow chamber with glass fiber, fusion 5, and nitrocellulose. For glass fiber and fusion 5, we can use the silicone gasket to seal the material between PMMA. Nitrocellulose, however, is much more difficult to seal because of the significant reduction in pore size. An alternative approach for sealing nitrocellulose involved the use of wax sealing, to prevent leaking when pushing fluid using the syringe pump. Additional work involving nitrocellulose sealing are described in the final section of this chapter. While flow through all three materials is possible, we next needed to demonstrate that we could quantitatively measure protein that either washes off or is bound to a test line. The microBCA kit is a version of the BCA assay that has been optimized to measure proteins at concentrations between 0.5 and 200 ug/mL [265], which is optimal for the concentration ranges in which we are working. From these results, we found that the microBCA enables detection of protein within this range, however we found it difficult to detect close to the limit of the assay (around 0.5-1 µg/mL), **Figure C.10**. We do find a good dynamic range at the higher protein amounts, however, which suggest that this method will work well if we assume that the immobilization of proteins in one test line is comparable to the immobilization of ten test lines spotted one after another in

the same membrane. This would allow us to extrapolate the adsorption of one test line based on the summed result of 10. Our classic test lines across 5 mm wide test strips contain approximately 0.6 µg of protein when spotted at 1mg/mL, below the limit that we saw detectable in **Figure C.10**.

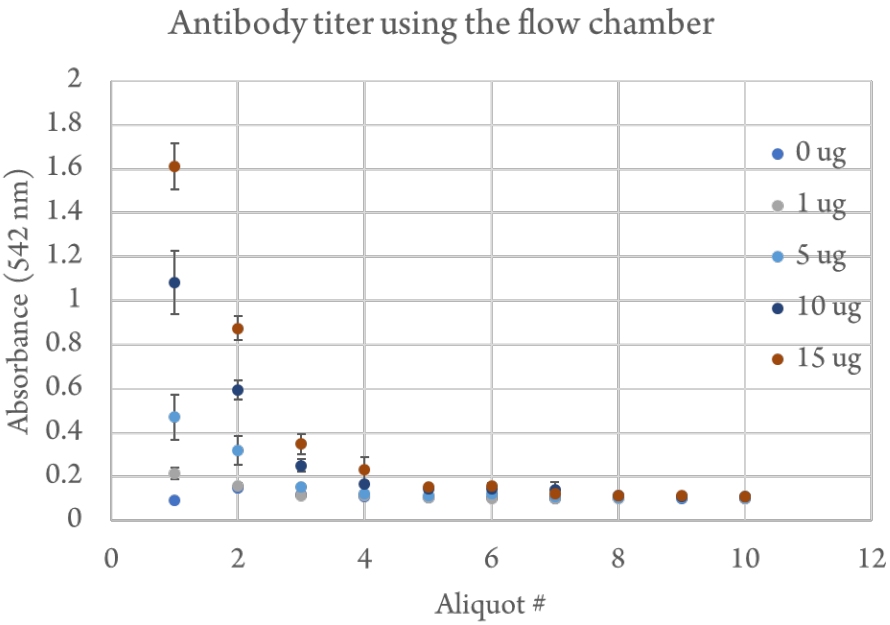

Figure C.10. Antibody titer to explore the sensitivity of the micro BCA assay.
Antibodies were hand spotted at 1mg/mL in glass fiber at a range of volumes (to which they do not adsorb well) overnight before testing on the flow chamber. PBS was used to wash the membranes, and 10, 100 µL aliquots were collected and tested for protein amount. While we were unable to statistically differentiate the difference in signal between 0 and 1 µg of protein, we did see a difference between 5, 10, and 15 µg of protein. All conditions were tested with an n=3, except for the first aliquot of the 0 µg case which only has 2.

Protein immobilization in porous membranes is often measured using non-quantitative protein stains, such as Ponceau S or Coomassie. Our lab traditionally uses a "lateral flow challenge" to determine whether or not a protein adsorbs to a membrane, such as nitrocellulose. The lateral flow challenge involves the use of a Ponceau stain after flow with a LFA buffer to see whether the protein was washed away. We have used this lateral flow challenge to analyze a large range of computationally designed proteins, of a range of sizes, isoelectric points, and overall function. However, it remained quite difficult to down-select to a nitrocellulose binder because of the inability to quantitatively compare these proteins, **Figure C.11A**. A summary of

the majority of proteins screened for use as a protein anchor can be found in **Table 5.6** along with their molecular weight, theoretical isoelectric point, and charge at pH 7.

While these methods are effective in determining whether a protein is immobilized on the membrane, the inability to quantitatively compare proteins limits our understanding of immobilization and adsorption in this system. We aimed to use the flow chamber to be able to more quantitatively analyze protein immobilization in porous membranes, specifically to measure the amount of protein that washes off a membrane after immobilization. A preliminary screen of a range of proteins dried into glass fiber suggests that this tool allows us to replace the qualitative protein stain with the more quantitative flow chamber. As we can see in **Figure C.11B**, the two methods generate data that is in agreement with one another.

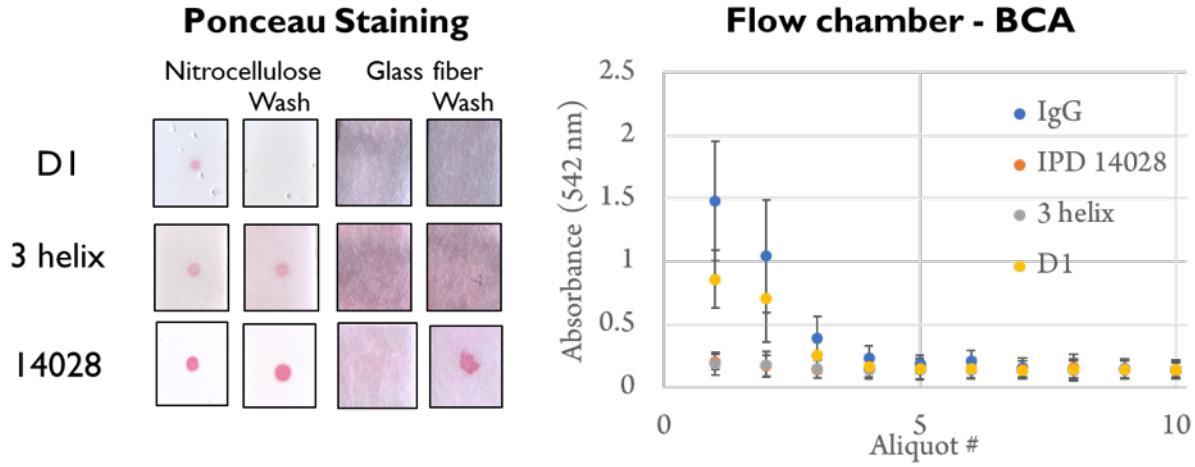

Figure C.11. Comparison of protein adsorption methods.
(A) Example data from the lateral flow challenge. Protein adsorbed to the membrane is visualized using the Ponceau S stain. (B) Proof of concept data from the micro BCA and flow chamber. Four different proteins, IgG, IPD 14028, 3 helix bundle, and Design 1, were stored in glass fiber after hand spotting at 1 mg/mL. IgG and D1 were expected to adsorb to glass fiber less readily than 3-helix and IPD 14028 based on Ponceau S staining. The specific properties of each of these proteins are shown in **Table 5.6**.

The development of a method that enables the quantitative analysis of protein adsorption within the context of lateral flow has the potential to more accurately inform the assay development process. Specifically with regards to the integration of computationally designed affinity proteins, as direct adsorption has not proved to be as universal a method for

immobilization as it has for antibodies [58]. Previous attempts to characterize protein adsorption to nitrocellulose have proved challenging because of our inability to quantitatively compare these proteins. As seen in **Figure C.11**, using the flow chamber we obtained proof of principle data that enabled us to more quantitatively compare the adsorption of different proteins to nitrocellulose.

One major drawback with this method is the throughput. While we found that we can more quantitatively measure the amount of protein that washes off the nitrocellulose membrane using a microBCA assay, the current setup is only feasible when you have a small group of proteins. There is a need for a larger throughput method for screening of protein binding for the larger goal of understanding protein immobilization to nitrocellulose. Yeast and phage display methods have been developed for larger scale screening of protein interactions, including specific applications to cellulose binding proteins for lateral flow assay development [159]. These methods would enable a screen that would help us to elicit the specific interactions that lead to strong adsorption to nitrocellulose. Once we understand this interaction, we can design our protein binders to contain a nitrocellulose binding component within them, and not attached to them as we described in Chapter 5. Similar to the head region binder, which adsorbed well to nitrocellulose without any additional engineering, this would simplify the development of assay stacks within the lateral flow assay context.

C.3.2 *Quantitative method to measure protein capture under flow*

While protein capture is influenced by binding kinetics, the capture of an analyte under lateral flow within a porous material is more complex than classical kinetic tools like surface plasmon resonance (SPR) and biolayer inferometry (BLI). There have been a number of attempts to model assay kinetics and binding within the lateral flow context, specifically with the intention to inform the assay development process [212], [266]–[269]. Much of this work has been done by looking specifically at the signal developed at the test line, without decoupling binding of the analyte by the capture and detection entities. For the design of a computationally designed capture binder, more specific information about how effectively an analyte is captured could be highly valuable. Specifically, knowledge of how much of an analyte is capable of binding at a known concentration of capture protein could inform the protein design and assay development process. Consequently, we have sought to develop a method using the flow

chamber to enable the calculation of the percent of analyte captured when it flows across a test line.

We aimed to develop an injection system to enable the quantification of analyte capture under flow. The goal is to gain a better understanding to enable optimization of the kinetics and delivery of our affinity reagents for lateral flow. This has the potential to improve overall percent analyte captured within the lateral flow context. For the measurement of analyte capture through the flow chamber, we have developed two different methods for the injection of the analyte into the system. This particular task proved more challenging, as we had specific design constraints that needed to be satisfied to enable accurate quantification of protein binding. The first system we developed involved the addition of a valve connecting a glass syringe where reagent can be introduced into the system. Shown in **Figure C.12**, this system has been used to introduce food dye into the flow chamber in volumes less than 200 µL. The analyte is diluted to a known concentration in the syringe, and delivered across the porous material where a capture protein is immobilized. The ultimate goal is to use a 96-well plate to collect the aliquots that flow through the material and run through an analyte specific ELISA.

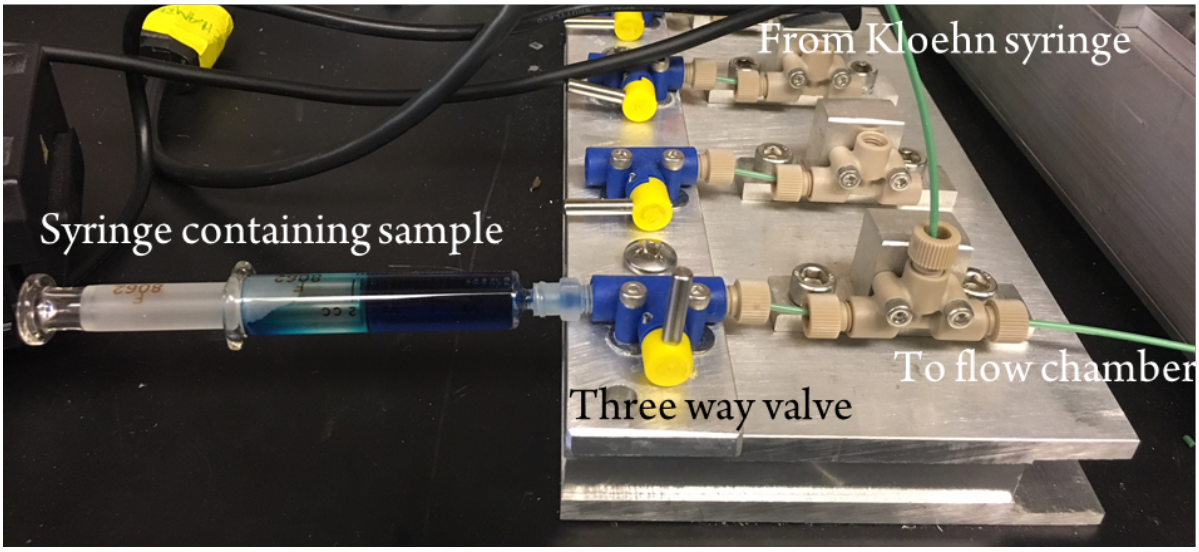

Figure C.12. Image of the three-way valve system for sample injection.
Set up requires a glass syringe, a three-way valve, and tubing to connect to the syringe pump and flow chamber. This enables the injection of smaller amounts of analyte without waste. The three-way valve is used to control which liquid is delivered to the flow chamber.

This first pass at a valving system, while great in theory, involved a much larger volume of analyte than we required. Where we hoped to have little dead volume, due to the cost and amount of protein reagent, the original valving system lead to a dead volume of a couple hundred microliters. This led us to consider alternatives for the injection of an analyte into the flow chamber. Taking inspiration from flow cytometry, we developed an injection system that used a 6-port injection valve that was connected between the syringe pump and flow chamber, **Figure C.13**.

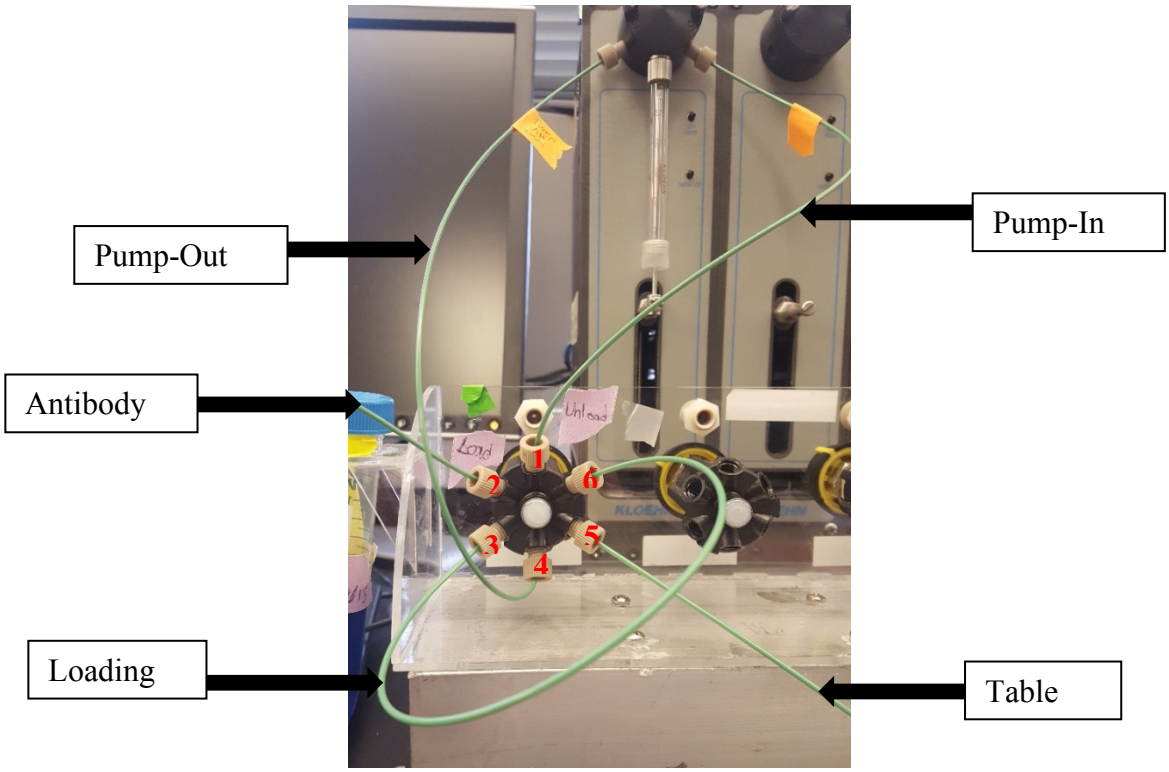

Figure C.13. Image of 6-port injection valve system.

Syringe acts as driving force to move fluid through the system; it can push/pull from the pump in tube, the pump out tube, and a waste tube. Knob on back of valve can be turned to two positions, load and unload. This changes the functionality as shown in **Figure C.14.**

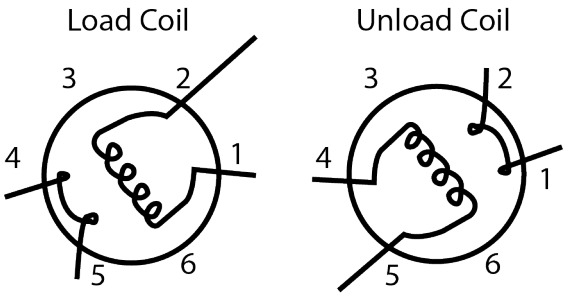

Figure C.14. Schematic of 6-port injection valve.

The coil (between ports 3 and 6, labeled as loading tube in **Figure C.13**) is loaded on the *left* by the antibody and pump-in tubes. Then the configuration can change using the knob on the valve. The coil can then be unloaded (as seen on the *right*) through the table tube and pump-out tube.

Table C.1. Volume of tubes in 6-port injection valve system.

Tube	Volume (uL)
Antibody Tube	73.4
Loading tube	133.2
Pump In Tube	140.9
Port to Port Volume	5.1

The volumes of each of the tubes shown in **Figure C.13** are described in **Table C.1**. This system allowed us to use smaller volumes, with the max volume enabled in the system calculated to be approximately 262 ± 2.36 μL (n=3) using Blue brilliant. Blue brilliant has a molecular weight of 792.85 Da, whereas our primary analyte of interest, hemagglutinin, has a molecular weight of 61.686 kDa. Due to this size difference, diffusion of the dye is likely to be different from our proteins of interest. Using the Stokes-Einstein equation for diffusion, shown in **Equation C.1**, we can estimate the assumed difference in diffusivity for these two species, where D is the diffusion constant, k_b is the Boltzmann constant, η is viscosity, and r is the radius of the diffusion species [270]. Assuming that size correlates to molecular weight, we calculated that the diffusion constant for the brilliant blue due to be approximately 80 times larger than that of the hemagglutinin protein.

$$D = \frac{k_b T}{6\pi\eta r} \tag{C.7}$$

Our next step was to look at the unloading profile of the dye into the microfluidic flow system. We found that even when the entire system was primed, we were seeing dilution of dye into the buffer on either side of it as measured by the plate reader, **Figure C.15**. The integral of the outlet profile was compared to the integral of the positive control (as an analog to the input profile) using MATLAB, and the numbers were found to be 58.85 and 57.46 respectively. This suggests that all dye input into the system is found in the output, with dilution that occurs across a larger volume. While this could be useful for some applications, this is not entirely useful when looking specifically at binding kinetics that are sensitive to analyte concentration.

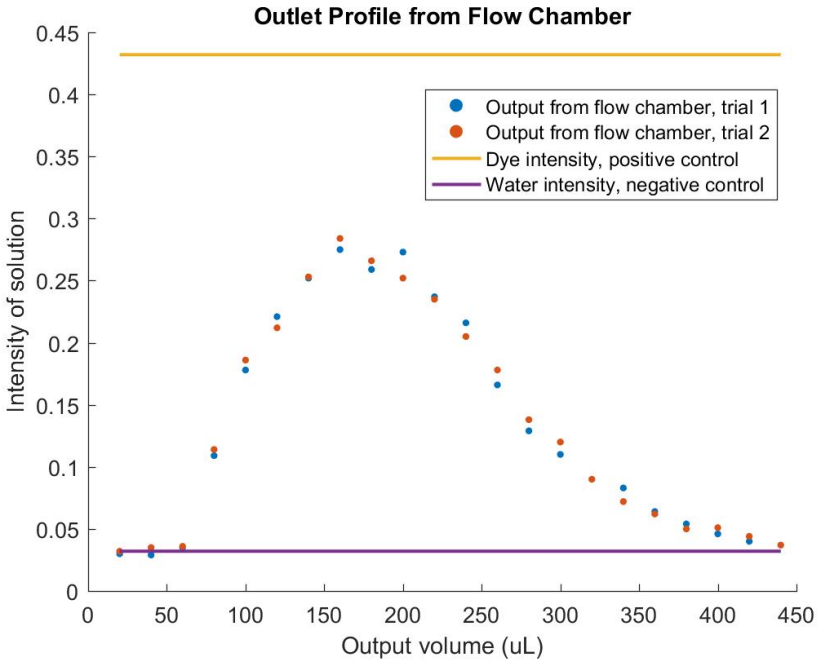

Figure C.15. Outlet concentration profile from the flow chamber, n=2.

Dye added to the microfluidic flow chamber system with the 6-way valve is found to diffuse into the surrounding aqueous solution, generating a concentration profile that follows a 200 µL sample that was measured over approximately 400 µL.

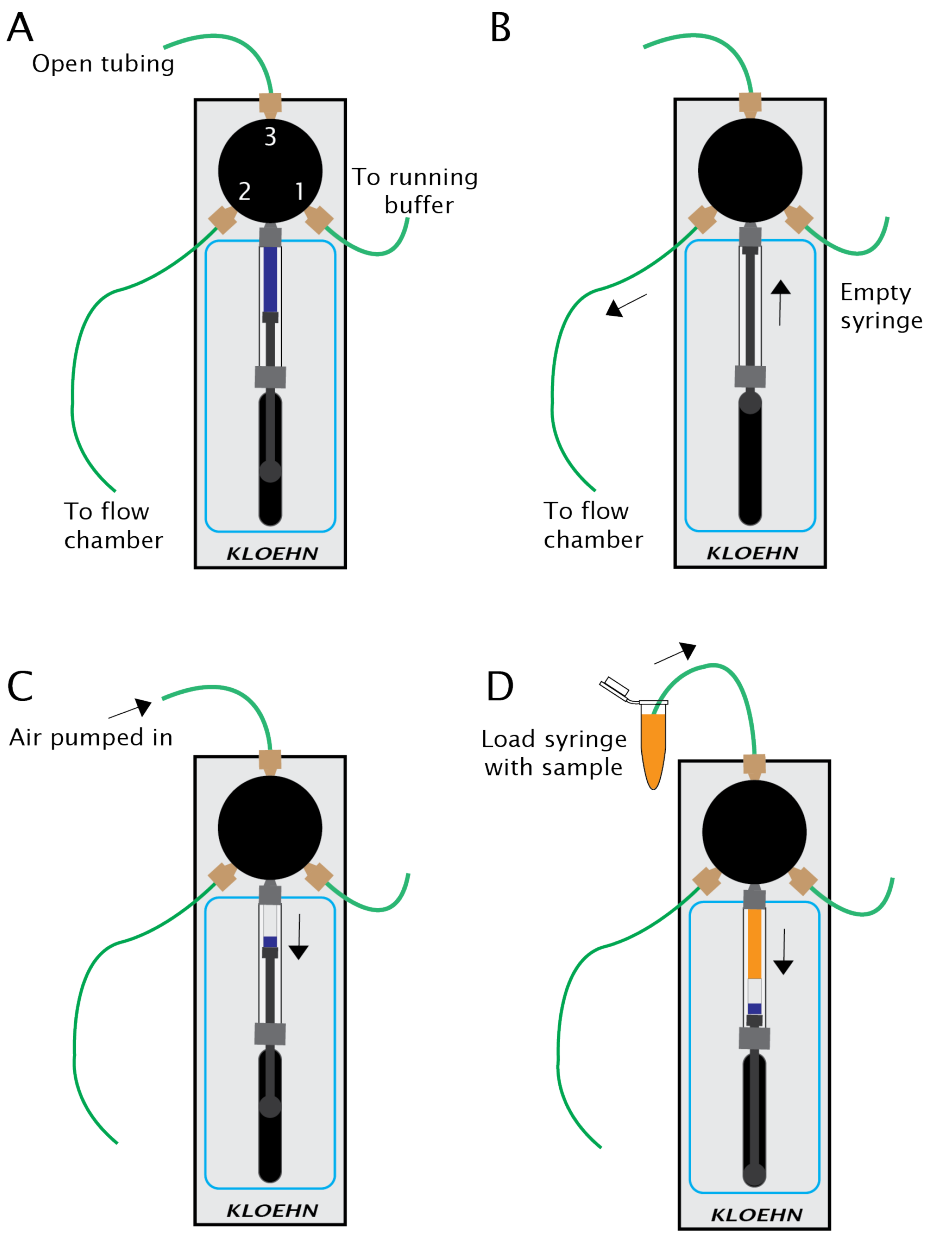

Figure C.16. Schematic describing the air-gap injection system.

The three way valve has tubing that connects to running buffer (valve 1), the flow chamber (valve 2), and contains an open tube through which we can pump in air and our sample of interst (valve 3), (A). The air gap is created by first expelling as much liquid as possible (B), after which air can be pumped in (C). The same valve is kept open, through which sample can be loaded (D). There will always be a small amount of running buffer remaining in the syringe, shown in blue. However, the air gap prevents either liquid from coming into contact with another, which allows us to ensure consistent concentration of the analyte throughout the course of an experiment.

We therefore sought to find another solution that enabled injection of our analyte at low volumes with additional control over concentration. The solution that we developed involved using an air gap that was placed in between the sample and any other fluid added into the system. This was accomplished by adding an additional tube in valve 3 on the syringe pump through which air and sample were to be loaded, **Figure C.16**. First, the system is told to pump 50 µL from valve 3, which pulls from the surrounding air, into the syringe pump itself. This ensures that water or buffer that remains in the pump never comes into contact with the sample. We are next able to place the tubing connected to valve 3 into an Eppendorf containing our sample of interest. Initial testing with dye showed that the air gap was sufficient to prevent movement between the two solutions. Using this method, we are able to load a 100 µL syringe with up to 60 µL of sample, which is sufficient for the experiments planned to measure analyte capture under flow.

C.3.3 *Analyzing flow within microfluidic flow chamber*

With our injection method developed and optimized, we then sought to investigate the consistency of flow through the flow chamber system. The method developed to seal nitrocellulose for the adsorption work used the laser cutter to melt plastic pieces to one another with nitrocellulose sealed inside. This method, while effective to prevent leaking and channeling, showed some flow inconsistencies, **Figure C.15**. The streamlines seen as we pumped through the system suggested to us that we needed to limit the flow path further. Under lateral flow, we see more consistent flow across the width of a test strip. Because our aim is to use this system to replicate flow in lateral flow while allowing us to assay a sample after it flows across a test line, this suggested that we needed additional modifications to the system. In addition, we saw that there was flow into the nitrocellulose upstream of the inlet port and to downstream of the outlet port. We anticipated difficulties differentiating between reagent loss to these regions of the nitrocellulose and the test line itself. This was validated using COMSOL to model flow through a porous matrix, as shown in **Figure C.18**. The model used Richards Equation modeling, as described in the thesis of Dr. Joshua Buser. The regions with the lowest velocity, shown in **Figure C.18**, were consistent with the regions into which there was flow that would not follow the desired streamline.

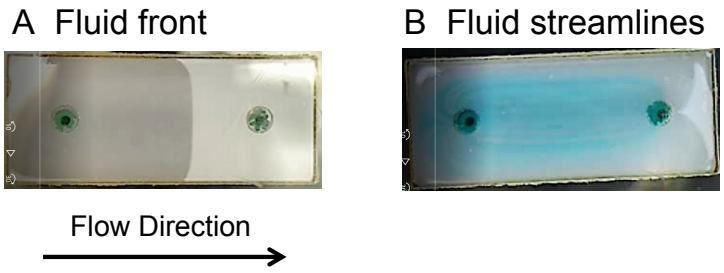

Figure C.17. Image of flow in nitrocellulose on the flow chamber.

Nitrocellulose membranes are sealed by melting mylar along the edge of the rectangle and sealing the nitrocellulose membrane between the two mylar layers. The nitrocellulose mylar sandwich is placed on the PMMA flow chamber bed and held in place with screws. Buffer is pumped through the system at 0.5 µL/second using the syringe pumps. While the fluid front appears to be consistent with flow during lateral flow (A), we see that as we continue to flow through the chamber that the majority of flow is through paths of least resistance (B).

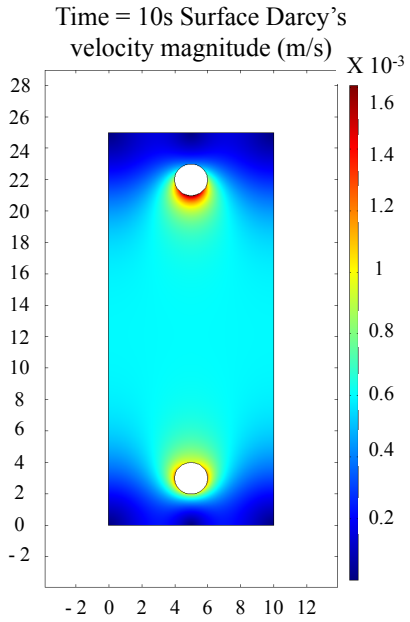

Figure C.18. COMSOL models for fluid flow in the flow chamber.

Darcy's velocity magnitude profile, with initial velocity from the inlet at 9.5 x 10^{-4} m/s. The maximum velocity across the center region is 6.0325 x 10^{-4} m/s and the variation across the center region is approximately 0.0635 x 10^{-4} m/s. Therefore, the velocity varies by 1.05% in the center region.

Therefore, we found it necessary to seal nitrocellulose in a manner that limited the fluidic path from the inlet to the outlet, and did not allow for flow outside of that. Inkjet printing of wax is commonly used in paper microfluidic development [271]–[273], therefore we first sought to use the ColorQube 8750 printer to deposit wax onto the portion of nitrocellulose where we wanted to minimize flow, **Figure C.19a**. The nitrocellulose was placed into an oven set to 150°C for 30 seconds to allow the wax to melt through the entire thickness of the nitrocellulose membrane. A layer of mylar was added on top of the nitrocellulose, and sealed to the backing of the nitrocellulose membrane using melted paraffin wax applied manually. These strips, when connected to the flow chamber, had such slow flow that the syringe pumps were unable to pump through the nitrocellulose for the size of syringe pump we were using. We hypothesized that the reason behind the slower flow had to do with the addition of a hydrophobic coating that is used on the barrel of the wax printer. The wax printer works by depositing wax in the pattern sent to the printer onto a heated barrel, which then rolls across the paper fed into the system. The hydrophobic coating on the barrel is there to prevent wax from sticking to the barrel between prints. Therefore, all locations where wax is not added onto the paper, the paper comes into contact with the hydrophobic coating instead. To test this hypothesis, we tested a series of nitrocellulose strips to determine whether the slower flow was due to the change in geometry or the process of printing itself, **Figure C.19**. By measuring the time it took for fluid to wick from one end of a strip to the other, in the geometries described in **Figure C.19**, we found that the slowest flow was seen in membranes that had come into contact with the hydrophobic coating. In this case, they flowed slower than 1 frame per second. This confirmed the hypothesis that the process of printing using our ColorQube wax printer was slowing down the flow in our nitrocellulose membrane significantly, **Figure C.20**.

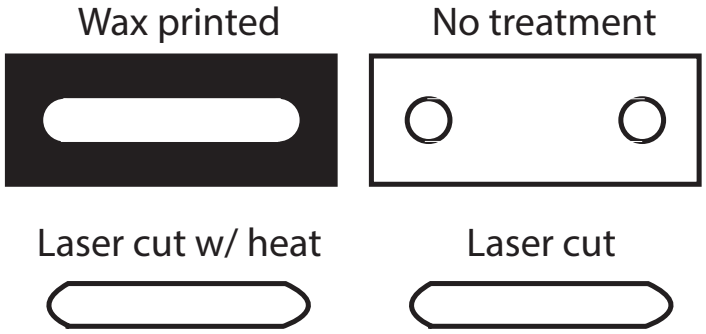

Figure C.19. Cartridge geometry for flow chamber testing.
Four geometries tested for fluid flow as compared to the wax printed cartridge.

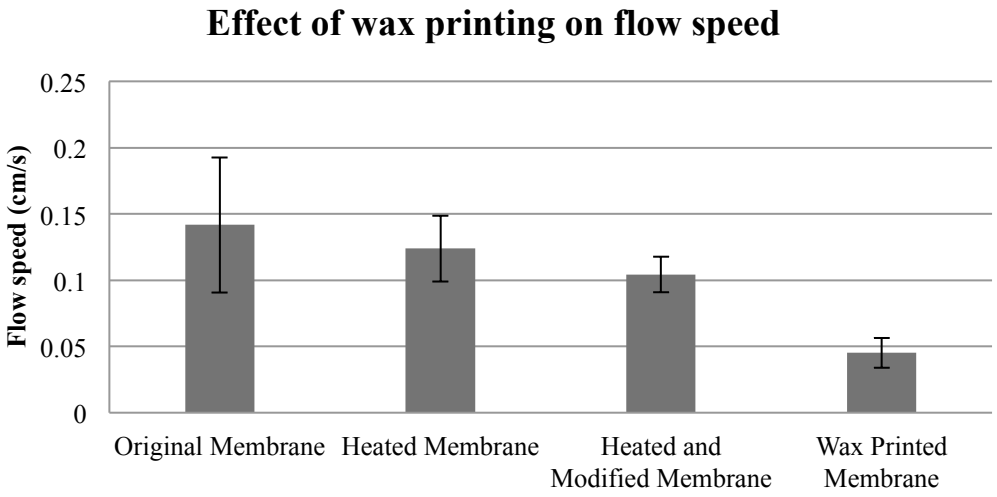

Figure C.20. Effect of wax printing on flow speed.

Flow speed measured by ImageJ to determine effect of the wax printing process on flow. Controls including the original nitrocellulose (CN95) membrane, a heated membrane, membrane heated and cut to restrict flow to area limited by wax printing, and the wax printed membrane. Four replicates were run for each condition.

There are other methods by which wax can be deposited onto nitrocellulose, and we investigated a number of such methods. Photolithography, screen-printing, stamping, and die cutting parafilm have all been demonstrated for the deposition of wax onto paper microfluidics with varying levels of complexity [271], [274]–[277]. For our purposes, and with the reagents available to us, we sought to develop a stamping method using laser cut PMMA. Using lauric acid, a long chain fatty acid that has a melting point of 43.2°C, we attempted a couple of different methods for wax deposition onto nitrocellulose. We chose lauric acid because of its low melting point, to minimize the effect of heat on the porous material during the deposition process. Due to its low melting temperature, we found that lauric acid moves readily into the nitrocellulose material during the heat step, losing a large amount of the resolution we were looking for. Other waxes will likely have more success, one such example is paraffin which we have used historically in our lab to seal porous membranes [53]. Unfortunately, due to time limitations we were not ultimately able to use any of these methods to precisely deposit wax onto our nitrocellulose membrane for use in the microfluidic flow chamber. The next steps for this work would focus on finalizing the manufacturing method for wax sealed nitrocellulose strips that can be hooked up to the microfluidic flow chamber. The potential impact of this system is

huge, as it allows us to decouple the different immunoassay steps and probe them in a more label free manner than has been previously published.

C.4 CONCLUSIONS AND FUTURE WORK

In this appendix chapter, we hoped to generate data demonstrating the utility of the flow chamber for lateral flow assay development. Specifically intended for novel molecular recognition elements, this system will allow us to separate the performance of our computationally designed proteins based on their ability to adsorb to a surface and capture an analyte of interest. By using proteins immobilized in the same manner, and in the same membrane, as the lateral flow assay format, we hope this system can be used to generate data that can be applied directly to the development of lateral flow assays.

So far, we have described progress towards the development of the microfluidic flow chamber. We first demonstrated that the flow chamber can be used to quantitatively measure protein adsorption for proteins spotted at 5 μg/test line or higher. We also developed three different injection systems, with the final injection system allowing the input of small volumes of sample without much reagent loss. Finally, we began to investigate sealing methods that would most closely resemble a lateral flow strip in terms of size and flow behavior.

This work is an attempt at a quantitative method to facilitate rational lateral flow assay development for a broader class of affinity reagents. This broader class of affinity reagents, which includes designed proteins and aptamers, have the potential for greater control over the traditionally used antibodies. With more precise numbers of conjugation sides, functional groups, and overall stability, these proteins open the door for the development of a wider range of lateral flow assays for use at the point of care. In addition, separation of the various functions of a capture agent enabled by this new class of affinity reagents enables a greater understanding of these functions in the lateral flow assay format, including immobilization and analyte capture.

The microfluidic flow chamber developed as a part of this aim has the potential to answer a number of questions that we have not previously been able to answer. One such question involves the role that flow rate plays in the amount of analyte captured, and ultimately overall assay sensitivity, under flow through porous matrices. Therefore, by the demonstration of this system with a range of materials, for a couple different applications, this will open the door for other questions important to the development of assays within porous matrices.

BIBLIOGRAPHY

[1] B. R. Lutz, P. Trinh, C. Ball, E. Fu, and P. Yager, "Two-dimensional paper networks: programmable fluidic disconnects for multi-step processes in shaped paper.," *Lab Chip*, vol. 11, no. 24, pp. 4274–8, Dec. 2011.

[2] H. Hsieh, J. Dantzler, and B. Weigl, "Analytical Tools to Improve Optimization Procedures for Lateral Flow Assays," *Diagnostics*, vol. 7, no. 2, p. 29, May 2017.

[3] M. Sajid, A. N. Kawde, and M. Daud, "Designs, formats and applications of lateral flow assay: A literature review," *J. Saudi Chem. Soc.*, vol. 19, no. 6, pp. 689–705, Nov. 2015.

[4] C. E. Anderson, K. G. Shah, and P. Yager, "Sensitive Protein Detection and Quantification in Paper-Based Microfluidics for the Point of Care," *Methods Enzymol.*, vol. 589, pp. 383–411, Jan. 2017.

[5] G. 2015 M. and C. of D. Collaborators, "Global, regional, and national life expectancy, all-cause mortality, and cause-specific mortality for 249 causes of death, 1980–2015: a systematic analysis for the Global Burden of Disease Study 2015," *Lancet*, vol. 388, no. 10053, pp. 1459–1544, Oct. 2016.

[6] S. Nayak, N. R. Blumenfeld, T. Laksanasopin, and S. K. Sia, "Point-of-Care Diagnostics: Recent Developments in a Connected Age," *Anal. Chem.*, vol. 89, no. 1, pp. 102–123, Jan. 2017.

[7] CDC, "Seasonal Influenza (Flu)," *Internet*, 2016. [Online]. Available: http://www.cdc.gov/flu/.

[8] A. C. Hurt, R. Alexander, J. Hibbert, N. Deed, and I. G. Barr, "Performance of six influenza rapid tests in detecting human influenza in clinical specimens.," *J. Clin. Virol.*, vol. 39, no. 2, pp. 132–5, Jun. 2007.

[9] NIH, "Point of Care Diagnostic Testing - Fact Sheet," *Internet*, 2010. [Online]. Available: https://report.nih.gov/nihfactsheets/Pdfs/PointofCareDiagnosticTesting(NIBIB).pdf. [Accessed: 15-Sep-2017].

[10] C. D. Chin, V. Linder, and S. K. Sia, "Commercialization of microfluidic point-of-care diagnostic devices," *Lab Chip*, vol. 12, no. 12, p. 2118, 2012.

[11] D. Mabey, R. W. Peeling, A. Ustianowski, and M. D. Perkins, "Diagnostics for the developing world," *Nat. Rev. Microbiol.*, vol. 2, no. 3, pp. 231–240, Mar. 2004.

[12] S. K. Sia, L. J. Kricka, S. Nagrath, L. Ulkus, B. Brannigan, C. V. Collura, E. Inserra, S. Diederichs, A. J. Iafrate, D. W. Bell, S. Digumarthy, A. Muzikansky, D. Irimia, J. Settleman, R. G. Tompkins, T. J. Lynch, M. Toner, and D. A. Haber, "Microfluidics and point-of-care testing," *Lab Chip*, vol. 8, no. 12, p. 1982, Dec. 2008.

[13] Markets and Markets, "Point-of-Care Diagnostics Market," *Prod. (Glucosem Cardiometabolic Monit. Infect. Dis. Test. Kits, Card. Tumor Markers), End Users (Home, Hosp. Ambul. Care), Over-the-Counter Prescr. Based - Glob. Forecast to 2021*, 2016.

[14] W. Jung, J. Han, J.-W. Choi, and C. H. Ahn, "Point-of-care testing (POCT) diagnostic systems using microfluidic lab-on-a-chip technologies," *Microelectron. Eng.*, vol. 132, pp. 46–57, Jan. 2015.

[15] D. Fitzgerald, "Making Every Nanoliter Count | The Scientist Magazine®," *The Scientist*, 2001. [Online]. Available: http://www.the-scientist.com/?articles.view/articleNo/13662/title/making-every-nanoliter-count/. [Accessed: 12-Nov-2017].

[16] E. M. Marlowe and M. J. Bankowski, "Conventional and Molecular Methods for the

Detection of Methicillin-Resistant Staphylococcus aureus," *J. Clin. Microbiol.*, vol. 49, no. 9 Supplement, pp. S53–S56, Sep. 2011.
[17] A. S. Rossney, C. M. Herra, G. I. Brennan, P. M. Morgan, and B. O'Connell, "Evaluation of the Xpert methicillin-resistant Staphylococcus aureus (MRSA) assay using the GeneXpert real-time PCR platform for rapid detection of MRSA from screening specimens.," *J. Clin. Microbiol.*, vol. 46, no. 10, pp. 3285–90, Oct. 2008.
[18] "Cepheid | Critical Infectious Diseases," 2018. [Online]. Available: http://www.cepheid.com/us/cepheid-solutions/clinical-ivd-tests/critical-infectious-diseases. [Accessed: 01-Jan-2019].
[19] "Cepheid | Healthcare Associated Infections," 2018. [Online]. Available: http://www.cepheid.com/us/cepheid-solutions/clinical-ivd-tests/healthcare-associated-infections. [Accessed: 01-Jan-2019].
[20] A. Kanabus, "Information about Tuberculosis," *GHE*, 2017.
[21] D. H. Wilson, D. M. Rissin, C. W. Kan, D. R. Fournier, T. Piech, T. G. Campbell, R. E. Meyer, M. W. Fishburn, C. Cabrera, P. P. Patel, E. Frew, Y. Chen, L. Chang, E. P. Ferrell, V. von Einem, W. McGuigan, M. Reinhardt, H. Sayer, C. Vielsack, and D. C. Duffy, "The Simoa HD-1 Analyzer: A Novel Fully Automated Digital Immunoassay Analyzer with Single-Molecule Sensitivity and Multiplexing," *J. Lab. Autom.*, vol. 21, no. 4, pp. 533–547, 2016.
[22] "Abbott Point of Care | i-STAT System & Piccolo Xpress." [Online]. Available: https://www.pointofcare.abbott/us/en/home. [Accessed: 12-Nov-2017].
[23] "Alere Triage MeterPro - Lab POC Testing Platform - Alere." [Online]. Available: http://www.alere.com/en/home/product-details/triage-meterpro.html. [Accessed: 12-Nov-2017].
[24] "i-STAT System | Abbott Point of Care." [Online]. Available: https://www.pointofcare.abbott/us/en/offerings/istat. [Accessed: 12-Nov-2017].
[25] A. W. Martinez, S. T. Phillips, G. M. Whitesides, and E. Carrilho, "Diagnostics for the Developing World: Microfluidic Paper-Based Analytical Devices," *Anal. Chem.*, vol. 82, no. 1, pp. 3–10, Jan. 2010.
[26] G. E. Fridley, C. a. Holstein, S. B. Oza, and P. Yager, "The evolution of nitrocellulose as a material for bioassays," *MRS Bull.*, vol. 38, no. 04, pp. 326–330, Apr. 2013.
[27] B. O'Farrell, "Evolution in Lateral Flow–Based Immunoassay Systems," in *Lateral Flow Immunoassay*, Totowa, NJ: Humana Press, 2009, pp. 1–33.
[28] U. K. Banik and M. L. Givner, "A simple and sensitive nonradioactive method for the detection of urinary human chorionic gonadotropin and diagnosis of early human pregnancy. I. Multiple-unit test.," *Fertil. Steril.*, vol. 32, no. 4, pp. 420–5, Oct. 1979.
[29] A. K. Yetisen, M. S. Akram, C. R. Lowe, E. Carrilho, T. M. Swager, A. Ozcan, F. Zeng, M. Prentiss, G. M. Whitesides, P. V. Baptista, K. P. Derose, M. V. Shea, C. M. Beighley, C. A. Dahl, J. Wasserman, J. Cobbing, R. Calow, C. Hunt, A. Hussain, M. C. Acreman, J. King, S. Malomo, E. L. Tate, D. O', S. Milner, and I. Steyl, "Paper-based microfluidic point-of-care diagnostic devices," *Lab Chip*, vol. 13, no. 12, p. 2210, May 2013.
[30] EMD Millipore, "Rapid lateral flow test strips: Considerations for product development.," Billerica, MA, 2013.
[31] E. Fu, B. Lutz, P. Kauffman, P. Yager, E. F. et al., A. W. M. et al., A. W. M. et al., A. W. M. et al., and E. W. Washburn, "Controlled reagent transport in disposable 2D paper networks," *Lab Chip*, vol. 10, no. 7, p. 918, 2010.

[32] A. W. Martinez, S. T. Phillips, M. J. Butte, and G. M. Whitesides, "Patterned Paper as a Platform for Inexpensive, Low-Volume, Portable Bioassays," *Angew. Chemie Int. Ed.*, vol. 46, no. 8, pp. 1318–1320, Feb. 2007.
[33] J. T. Connelly, J. P. Rolland, and G. M. Whitesides, "'Paper Machine' for Molecular Diagnostics," *Anal. Chem.*, vol. 87, no. 15, pp. 7595–7601, Aug. 2015.
[34] J. C. Jokerst, J. A. Adkins, B. Bisha, M. M. Mentele, L. D. Goodridge, and C. S. Henry, "Development of a Paper-Based Analytical Device for Colorimetric Detection of Select Foodborne Pathogens," *Anal. Chem.*, vol. 84, no. 6, pp. 2900–2907, Mar. 2012.
[35] E. Fu, T. Liang, J. Houghtaling, S. Ramachandran, S. A. Ramsey, B. Lutz, and P. Yager, "Enhanced Sensitivity of Lateral Flow Tests Using a Two-Dimensional Paper Network Format," 2011.
[36] D. M. Cate, J. A. Adkins, J. Mettakoonpitak, and C. S. Henry, "Recent Developments in Paper-Based Microfluidic Devices," *Anal. Chem.*, vol. 87, no. 1, pp. 19–41, Jan. 2015.
[37] S. Huang, K. Abe, S. Bennett, T. Liang, P. D. Ladd, L. Yokobe, C. E. Anderson, K. Shah, J. Bishop, M. Purfield, P. C. Kauffman, S. Paul, A. E. Welch, B. Strelitz, K. Follmer, K. Pullar, L. Sanchez-Erebia, E. Gerth-Guyette, G. Domingo, E. Klein, J. A. Englund, E. Fu, and P. Yager, "Disposable Autonomous Device for Swab-to-Result Diagnosis of Influenza," *Anal. Chem.*, vol. 89, no. 11, pp. 5776–5783, Jun. 2017.
[38] L. K. Lafleur, J. D. Bishop, E. K. Heiniger, R. P. Gallagher, M. D. Wheeler, P. Kauffman, X. Zhang, E. C. Kline, J. R. Buser, S. Kumar, S. A. Byrnes, N. M. J. Vermeulen, N. K. Scarr, Y. Belousov, W. Mahoney, B. J. Toley, P. D. Ladd, B. R. Lutz, and P. Yager, "A rapid, instrument-free, sample-to-result nucleic acid amplification test.," *Lab Chip*, vol. 16, no. 19, pp. 3777–87, Oct. 2016.
[39] S.-G. Jeong, J. Kim, J.-O. Nam, Y. S. Song, and C.-S. Lee, "Paper-based analytical device for quantitative urinalysis.," *Int. Neurourol. J.*, vol. 17, no. 4, pp. 155–61, Dec. 2013.
[40] G. E. Fridley, C. a. Holstein, S. B. Oza, and P. Yager, "The evolution of nitrocellulose as a material for bioassays," *MRS Bull.*, vol. 38, no. 04, pp. 326–330, 2013.
[41] J. L. Tonkinson, "Nitrocellulose: a tried and true polymer finds utility as a post-genomic substrate," *Front. Biosci.*, vol. 7, no. 1–3, p. c1, 2002.
[42] S. Ramachandran, E. Fu, B. Lutz, and P. Yager, "Long-term dry storage of an enzyme-based reagent system for ELISA in point-of-care devices.," *Analyst*, vol. 139, no. 6, pp. 1456–62, Mar. 2014.
[43] J. C. Linnes, N. M. Rodriguez, L. Liu, and C. M. Klapperich, "Polyethersulfone improves isothermal nucleic acid amplification compared to current paper-based diagnostics," *Biomed. Microdevices*, vol. 18, no. 2, p. 30, Apr. 2016.
[44] R. Wong and H. Tse, Eds., *Lateral Flow Immunoassay*. Totowa, NJ: Humana Press, 2009.
[45] A. M. López-Marzo and A. Merkoçi, "Paper-based sensors and assays: a success of the engineering design and the convergence of knowledge areas," *Lab Chip*, vol. 16, no. 17, pp. 3150–3176, Aug. 2016.
[46] B. O'Farrell, "Evolution in Lateral Flow–Based Immunoassay Systems," in *Lateral Flow Immunoassay*, Totowa, NJ: Humana Press, 2009, pp. 1–33.
[47] C. Parolo, M. Medina-Sánchez, A. de la Escosura-Muñiz, and A. Merkoçi, "Simple paper architecture modifications lead to enhanced sensitivity in nanoparticle based lateral flow immunoassays," *Lab Chip*, vol. 13, no. 3, pp. 386–390, Jan. 2013.
[48] G. A. Posthuma-Trumpie, J. Korf, and A. van Amerongen, "Lateral flow (immuno)assay: its strengths, weaknesses, opportunities and threats. A literature survey," *Anal. Bioanal.*

Chem., vol. 393, no. 2, pp. 569–582, Jan. 2009.
[49] R. Masoodi and K. M. Pillai, "Darcy's law-based model for wicking in paper-like swelling porous media," *AIChE J.*, vol. 56, no. 9, p. NA-NA, Sep. 2010.
[50] E. W. Washburn, "The Dynamics of Capillary Flow," *Phys. Rev.*, vol. 17, no. 3, pp. 273–283, Mar. 1921.
[51] S. Whitaker, "Flow in porous media I: A theoretical derivation of Darcy's law," *Transp. Porous Media*, vol. 1, no. 1, pp. 3–25, 1986.
[52] L. A. Richards, "CAPILLARY CONDUCTION OF LIQUIDS THROUGH POROUS MEDIUMS," *Physics (College. Park. Md).*, vol. 1, no. 5, pp. 318–333, Nov. 1931.
[53] J. R. Buser, "Heat, Fluid, and Sample Control in Point-of-Care Diagnostics," 2016.
[54] S. A. Byrnes, J. R. Buser, E. C. Kline, J. D. Bishop, M. D. Wheeler, and P. Yager, "An integrated sample preparation system for large volume processing at the point of care," in *MicroTAS*, 2016.
[55] R. Karlsson, A. Michaelsson, and L. Mattsson, "Kinetic analysis of monoclonal antibody-antigen interactions with a new biosensor based analytical system," *J. Immunol. Methods*, vol. 145, no. 1–2, pp. 229–240, Dec. 1991.
[56] N. S. Lipman, L. R. Jackson, L. J. Trudel, and F. Weis-Garcia, "Monoclonal versus polyclonal antibodies: distinguishing characteristics, applications, and information resources.," *ILAR J.*, vol. 46, no. 3, pp. 258–68, 2005.
[57] S. D. Jayasena, "Aptamers: an emerging class of molecules that rival antibodies in diagnostics.," *Clin. Chem.*, vol. 45, no. 9, pp. 1628–50, Sep. 1999.
[58] C. A. Holstein, "Development of a Novel Paper-Based Flu Test for Improved Diagnosis at the Point of Care," University of Washington, 2015.
[59] J. Renart, J. Reiser, and G. R. Stark, "Transfer of proteins from gels to diazobenzyloxymethyl-paper and detection with antisera: a method for studying antibody specificity and antigen structure.," *Proc. Natl. Acad. Sci.*, vol. 76, no. 7, pp. 3116–3120, Jul. 1979.
[60] T. Mairal, V. Cengiz Özalp, P. Lozano Sánchez, M. Mir, I. Katakis, and C. K. O'Sullivan, "Aptamers: molecular tools for analytical applications," *Anal. Bioanal. Chem.*, vol. 390, no. 4, pp. 989–1007, Feb. 2008.
[61] V. Marx, "Finding the right antibody for the job," *Nat. Methods*, vol. 10, no. 8, pp. 703–707, Jul. 2013.
[62] a W. Vermeer and W. Norde, "The thermal stability of immunoglobulin: unfolding and aggregation of a multi-domain protein.," *Biophys. J.*, vol. 78, no. 1, pp. 394–404, 2000.
[63] H. K. Binz, P. Amstutz, and A. Plückthun, "Engineering novel binding proteins from nonimmunoglobulin domains," *Nat. Biotechnol.*, vol. 23, no. 10, pp. 1257–1268, Oct. 2005.
[64] G. Hassanzadeh-Ghassabeh, N. Devoogdt, P. De Pauw, C. Vincke, and S. Muyldermans, "Nanobodies and their potential applications," *Nanomedicine*, vol. 8, no. 6, pp. 1013–1026, Jun. 2013.
[65] A. Chen and S. Yang, "Replacing antibodies with aptamers in lateral flow immunoassay.," *Biosens. Bioelectron.*, vol. 71, pp. 230–42, Sep. 2015.
[66] M. Famulok, G. Mayer, and M. Blind, "Nucleic Acid AptamersFrom Selection in Vitro to Applications in Vivo," *Acc. Chem. Res.*, vol. 33, no. 9, pp. 591–599, Sep. 2000.
[67] A. D. Ellington and J. W. Szostak, "In vitro selection of RNA molecules that bind specific ligands," *Nature*, vol. 346, no. 6287, pp. 818–822, Aug. 1990.

[68] C. K. O'Sullivan, "Aptasensors – the future of biosensing?," *Anal. Bioanal. Chem.*, vol. 372, no. 1, pp. 44–48, Jan. 2002.
[69] M. Lönne, S. Bolten, A. Lavrentieva, F. Stahl, T. Scheper, and J.-G. Walter, "Development of an aptamer-based affinity purification method for vascular endothelial growth factor," *Biotechnol. Reports*, vol. 8, pp. 16–23, 2015.
[70] T. A. Whitehead, A. Chevalier, Y. Song, C. Dreyfus, S. J. Fleishman, C. De Mattos, C. A. Myers, H. Kamisetty, P. Blair, I. A. Wilson, and D. Baker, "Optimization of affinity, specificity and function of designed influenza inhibitors using deep sequencing," *Nat. Biotechnol.*, vol. 30, no. 6, pp. 543–548, May 2012.
[71] J. P. Alarie, M. J. Sepaniak, and T. Vo-Dinh, "Evaluation of antibody immobilization technqiues for fiber optic-based fluoroimmunosensing," *Anal. Chim. Acta*, vol. 229, pp. 169–176, 1990.
[72] H. K. Binz and A. Plückthun, "Engineered proteins as specific binding reagents," *Curr. Opin. Biotechnol.*, vol. 16, no. 4, pp. 459–469, 2005.
[73] Y. Liu, X. Zhang, Y. L. Tan, G. Bhabha, D. C. Ekiert, Y. Kipnis, S. Bjelic, D. Baker, and J. W. Kelly, "De Novo-Designed Enzymes as Small-Molecule-Regulated Fluorescence Imaging Tags and Fluorescent Reporters," *J. Am. Chem. Soc.*, vol. 136, no. 38, pp. 13102–13105, Sep. 2014.
[74] M. Paschke, "Phage display systems and their applications," *Appl. Microbiol. Biotechnol.*, vol. 70, no. 1, pp. 2–11, Mar. 2006.
[75] S. J. Fleishman, T. A. Whitehead, D. C. Ekiert, C. Dreyfus, J. E. Corn, E.-M. Strauch, I. A. Wilson, and D. Baker, "Computational Design of Proteins Targeting the Conserved Stem Region of Influenza Hemagglutinin," *Science (80-.).*, vol. 332, no. 6031, pp. 816–821, May 2011.
[76] B. Heyd, F. Pecorari, B. Collinet, E. Adjadj, M. Desmadril, and P. Minard, "In Vitro Evolution of the Binding Specificity of Neocarzinostatin, an Enediyne-Binding Chromoprotein," *Biochemistry*, vol. 42, no. 19, pp. 5674–5683, May 2003.
[77] J. Credou, H. Volland, T. Berthelot, M. Yan, S. Ge, J. Yu, F. Zeng, and G. M. Whitesides, "Photolinker-free photoimmobilization of antibodies onto cellulose for the preparation of immunoassay membranes," *J. Mater. Chem. B*, vol. 3, no. 6, pp. 1079–1088, Jan. 2015.
[78] T. I. Přistoupil, M. Kramlová, and J. Štěrbíková, "On the mechanism of adsorption of proteins to nitrocellulose in membrane chromatography," *J. Chromatogr. A*, vol. 42, pp. 367–375, Jan. 1969.
[79] N. R. Mohamad, N. H. C. Marzuki, N. A. Buang, F. Huyop, and R. A. Wahab, "An overview of technologies for immobilization of enzymes and surface analysis techniques for immobilized enzymes.," *Biotechnol. Biotechnol. Equip.*, vol. 29, no. 2, pp. 205–220, Mar. 2015.
[80] M. A. Williams and T. Daviter, Eds., *Protein-Ligand Interactions*, vol. 1008. Totowa, NJ: Humana Press, 2013.
[81] L. Michaelis and M. L. Menten, "The kinetics of the inversion effect," *Biochem. Z.*, vol. 49, pp. 333–369, 1913.
[82] A. L. Ahmad, S. C. Low, S. R. A. Shukor, and A. Ismail, "Synthesis and characterization of polymeric nitrocellulose membranes: Influence of additives and pore formers on the membrane morphology," *J. Appl. Polym. Sci.*, vol. 108, no. 4, pp. 2550–2557, May 2008.
[83] T. Liang, R. Robinson, J. Houghtaling, G. Fridley, S. A. Ramsey, and E. Fu, "Investigation of Reagent Delivery Formats in a Multivalent Malaria Sandwich

Immunoassay and Implications for Assay Performance," *Anal. Chem.*, vol. 88, no. 4, pp. 2311–2320, Feb. 2016.
[84] K. Abe and P. Yager, "Comparing the sensitivity of pre-mixed and sequential reagent delivery for an amplified influenza A nucleoprotein immunoassay.," in *MicroTAS*, 2016.
[85] CDC, "Estimates of Death Associated with Seasonal Influenza -- United States," *Morb. Mortal. Wkly. Rep.*, vol. 59, pp. 1057–1062, 2010.
[86] IHME, "Global Burden of Disease," *Internet*, 2010. .
[87] B. N. Fields, D. M. (David M. Knipe, and P. M. Howley, *Fields virology*. Wolters Kluwer Health/Lippincott Williams & Wilkins, 2007.
[88] CDC, "CDC Reports Flu Hit Younger People Particularly Hard This Season," *Internet*, 2014. .
[89] N.-A. M. Molinari, I. R. Ortega-Sanchez, M. L. Messonnier, W. W. Thompson, P. M. Wortley, E. Weintraub, and C. B. Bridges, "The annual impact of seasonal influenza in the US: Measuring disease burden and costs," *Vaccine*, vol. 25, no. 27, pp. 5086–5096, Jun. 2007.
[90] CDC, "CDC Recommendations for Influenza Antiviral Medications Remain Unchanged," 2014. .
[91] N. C. Wu and I. A. Wilson, "A Perspective on the Structural and Functional Constraints for Immune Evasion: Insights from Influenza Virus," *J. Mol. Biol.*, vol. 429, no. 17, pp. 2694–2709, Aug. 2017.
[92] CDC, "How the Flu Virus Can Change: 'Drift' and 'Shift' | Seasonal Influenza (Flu) | CDC," 2017. [Online]. Available: https://www.cdc.gov/flu/about/viruses/change.htm. [Accessed: 15-Nov-2017].
[93] A. Cushing, A. Kamali, M. Winters, E. S. Hopmans, J. M. Bell, S. M. Grimes, L. C. Xia, N. R. Zhang, R. B. Moss, M. Holodniy, and H. P. Ji, "Emergence of Hemagglutinin Mutations During the Course of Influenza Infection," *Sci. Rep.*, vol. 5, no. 1, p. 16178, Dec. 2015.
[94] R. J. Garten, C. T. Davis, C. A. Russell, B. Shu, S. Lindstrom, A. Balish, W. M. Sessions, X. Xu, E. Skepner, V. Deyde, M. Okomo-Adhiambo, L. Gubareva, J. Barnes, C. B. Smith, S. L. Emery, M. J. Hillman, P. Rivailler, J. Smagala, M. de Graaf, D. F. Burke, R. A. M. Fouchier, C. Pappas, C. M. Alpuche-Aranda, H. López-Gatell, H. Olivera, I. López, C. A. Myers, D. Faix, P. J. Blair, C. Yu, K. M. Keene, P. D. D. Jr., D. Boxrud, A. R. Sambol, S. H. Abid, K. St. George, T. Bannerman, A. L. Moore, D. J. Stringer, P. Blevins, G. J. Demmler-Harrison, M. Ginsberg, P. Kriner, S. Waterman, S. Smole, H. F. Guevara, E. A. Belongia, P. A. Clark, S. T. Beatrice, R. Donis, J. Katz, L. Finelli, C. B. Bridges, M. Shaw, D. B. Jernigan, T. M. Uyeki, D. J. Smith, A. I. Klimov, and N. J. Cox, "Antigenic and Genetic Characteristics of Swine-Origin 2009 A(H1N1) Influenza Viruses Circulating in Humans," *Science*, vol. 325. American Association for the Advancement of Science, pp. 197–201, 2009.
[95] S. S. Shrestha, D. L. Swerdlow, R. H. Borse, V. S. Prabhu, L. Finelli, C. Y. Atkins, K. Owusu-Edusei, B. Bell, P. S. Mead, M. Biggerstaff, L. Brammer, H. Davidson, D. Jernigan, M. A. Jhung, L. A. Kamimoto, T. L. Merlin, M. Nowell, S. C. Redd, C. Reed, A. Schuchat, and M. I. Meltzer, "Estimating the Burden of 2009 Pandemic Influenza A (H1N1) in the United States (April 2009-April 2010)," *Clin. Infect. Dis.*, vol. 52, no. Supplement 1, pp. S75–S82, Jan. 2011.
[96] A. B. Bonner, K. W. Monroe, L. I. Talley, A. E. Klasner, and D. W. Kimberlin, "Impact

of the rapid diagnosis of influenza on physician decision-making and patient management in the pediatric emergency department: results of a randomized, prospective, controlled trial.," *Pediatrics*, vol. 112, no. 2, pp. 363–7, Aug. 2003.
[97] R. A. Lamb, "The Influenza Virus RNA Segments and Their Encoded Proteins," in *Genetics of Influenza Viruses*, Vienna: Springer Vienna, 1983, pp. 21–69.
[98] J. J. Skehel and D. C. Wiley, "Receptor binding and membrane fusion in virus entry: the influenza hemagglutinin.," *Annu. Rev. Biochem.*, vol. 69, pp. 531–69, Jan. 2000.
[99] W. Weis, J. H. Brown, S. Cusack, J. C. Paulson, J. J. Skehel, and D. C. Wiley, "Structure of the influenza virus haemagglutinin complexed with its receptor, sialic acid," *Nature*, vol. 333, no. 6172, pp. 426–431, Jun. 1988.
[100] R. G. Webster, W. J. Bean, O. T. Gorman, T. M. Chambers, and Y. Kawaoka, "Evolution and ecology of influenza A viruses.," *Microbiol. Rev.*, vol. 56, no. 1, pp. 152–79, Mar. 1992.
[101] V. Gubala, L. F. Harris, A. J. Ricco, M. X. Tan, and D. E. Williams, "Point of Care Diagnostics: Status and Future," *Anal. Chem.*, vol. 84, no. 2, pp. 487–515, Jan. 2012.
[102] M. A. Mansfield, "Nitrocellulose Membranes for Lateral Flow Immunoassays: A Technical Treatise," in *Lateral Flow Immunoassay*, Totowa, NJ: Humana Press, 2009, pp. 1–19.
[103] I. Shiratori, J. Akitomi, D. A. Boltz, K. Horii, M. Furuichi, and I. Waga, "Selection of DNA aptamers that bind to influenza A viruses with high affinity and broad subtype specificity," 2014.
[104] R. Wang, J. Zhao, T. Jiang, Y. M. Kwon, H. Lu, P. Jiao, M. Liao, and Y. Li, "Selection and characterization of DNA aptamers for use in detection of avian influenza virus H5N1," *J. Virol. Methods*, vol. 189, no. 2, pp. 362–369, 2013.
[105] H.-M. Woo, J.-M. Lee, S. Yim, and Y.-J. Jeong, "Isolation of single-stranded DNA aptamers that distinguish influenza virus hemagglutinin subtype H1 from H5.," *PLoS One*, vol. 10, no. 4, p. e0125060, 2015.
[106] E. M. Strauch, S. M. Bernard, D. La, A. J. Bohn, P. S. Lee, C. E. Anderson, T. Nieusma, C. A. Holstein, N. K. Garcia, K. A. Hooper, R. Ravichandran, J. W. Nelson, W. Sheffler, J. D. Bloom, K. K. Lee, A. B. Ward, P. Yager, D. H. Fuller, I. A. Wilson, and D. Baker, "Computational design of trimeric influenza-neutralizing proteins targeting the hemagglutinin receptor binding site," *Nat. Biotechnol.*, vol. 35, no. 7, pp. 667–671, 2017.
[107] L. A. Currie, "Nomenclature in evaluation of analytical methods including detection and quantification capabilities (IUPAC Recommendations 1995)," *Pure Appl. Chem.*, vol. 67, no. 10, pp. 1699–1723, Jan. 1995.
[108] C. A. Holstein, M. Griffin, J. Hong, and P. D. Sampson, "Statistical Method for Determining and Comparing Limits of Detection of Bioassays," *Anal. Chem.*, vol. 87, no. 19, pp. 9795–9801, Oct. 2015.
[109] C. A. Holstein, A. Chevalier, S. Bennett, C. E. Anderson, K. Keniston, C. Olsen, B. Li, B. Bales, D. R. Moore, E. Fu, D. Baker, and P. Yager, "Immobilizing affinity proteins to nitrocellulose: a toolbox for paper-based assay developers," *Anal. Bioanal. Chem.*, vol. 408, no. 5, pp. 1335–1346, Feb. 2016.
[110] P. M. Rodi, M. D. Bocco Gianello, M. C. Corregido, and A. M. Gennaro, "Comparative study of the interaction of CHAPS and Triton X-100 with the erythrocyte membrane," *Biochim. Biophys. Acta - Biomembr.*, vol. 1838, no. 3, pp. 859–866, Mar. 2014.
[111] M. O. Labeta, N. Fernandez, and H. Festenstein, "Solubilisation effect of Nonidet P-40,

Triton X-100 and CHAPS in the detection of MHC-like glycoproteins," *J. Immunol. Methods*, vol. 112, no. 1, pp. 133–138, Aug. 1988.
[112] M. Peach, N. Marsh, E. I. Miskiewicz, and D. J. MacPhee, "Solubilization of Proteins: The Importance of Lysis Buffer Choice," Humana Press, New York, NY, 2015, pp. 49–60.
[113] G. W. Bumgarner, J. C. Zampell, S. Nagarajan, N. J. Poloso, A. S. Dorn, M. J. D'Souza, and P. Selvaraj, "Modified cell ELISA to determine the solubilization of cell surface proteins: Applications in GPI-anchored protein purification," *J. Biochem. Biophys. Methods*, vol. 64, no. 2, pp. 99–109, Aug. 2005.
[114] CDC, "Evaluation of 11 Commercially Available Rapid Influenza Diagnostic Tests - United States," *Morb. Mortal. Wkly. Rep.*, vol. 61, pp. 873–876, 2012.
[115] K. H. Chan, K. M. Chan, Y. L. Ho, Y. P. Lam, H. L. Tong, L. L. M. Poon, B. J. Cowling, and J. S. M. Peiris, "Quantitative analysis of four rapid antigen assays for detection of pandemic H1N1 2009 compared with seasonal H1N1 and H3N2 influenza A viruses on nasopharyngeal aspirates from patients with influenza," *J. Virol. Methods*, vol. 186, no. 1, pp. 184–188, 2012.
[116] Y. Pang, Z. Rong, J. Wang, R. Xiao, and S. Wang, "A fluorescent aptasensor for H5N1 influenza virus detection based-on the core–shell nanoparticles metal-enhanced fluorescence (MEF)," *Biosens. Bioelectron.*, vol. 66, pp. 527–532, 2015.
[117] P. M. Boltovets, O. M. Polischuk, O. G. Kovalenko, and B. A. Snopok, "A simple SPR-based method for the quantification of the effect of potential virus inhibitors," *Analyst*, vol. 138, no. 2, pp. 480–486, Dec. 2013.
[118] G. Chenail, N. E. Brown, A. Shea, A. L. Feire, and G. Deng, "Real-time analysis of antibody interactions with whole enveloped human cytomegalovirus using surface plasmon resonance," *Anal. Biochem.*, vol. 411, no. 1, pp. 58–63, Apr. 2011.
[119] K. P. O'Connell, E. Kovaleva, J. H. Campbell, P. E. Anderson, S. G. Brown, D. C. Davis, J. J. Valdes, R. W. Welch, W. E. Bentley, and N. A. van Beek, "Production of a recombinant antibody fragment in whole insect larvae.," *Mol. Biotechnol.*, vol. 36, no. 1, pp. 44–51, May 2007.
[120] S. Vemula, J. Zhao, J. Liu, X. Wang, S. Biswas, and I. Hewlett, "Current Approaches for Diagnosis of Influenza Virus Infections in Humans," *Viruses*, vol. 8, no. 4, p. 96, Apr. 2016.
[121] C. E. Anderson, C. A. Holstein, E.-M. Strauch, S. Bennett, A. Chevalier, J. Nelson, E. Fu, D. Baker, and P. Yager, "Rapid Diagnostic Assay for Intact Influenza Virus Using a High Affinity Hemagglutinin Binding Protein," *Anal. Chem.*, vol. 89, no. 12, pp. 6608–6615, Jun. 2017.
[122] S. Shan, W. Lai, Y. Xiong, H. Wei, and H. Xu, "Novel Strategies To Enhance Lateral Flow Immunoassay Sensitivity for Detecting Foodborne Pathogens," *J. Agric. Food Chem.*, vol. 63, no. 3, pp. 745–753, Jan. 2015.
[123] J. Li, M. A. Baird, M. A. Davis, W. Tai, L. S. Zweifel, K. M. A. Waldorf, M. Gale Jr, L. Rajagopal, R. H. Pierce, and X. Gao, "Dramatic enhancement of the detection limits of bioassays via ultrafast deposition of polydopamine," *Nat. Biomed. Eng.*, vol. 1, no. 6, p. 0082, Jun. 2017.
[124] N. Constantine, "HIV Viral Antigen Assays," *HIV InSite Knowledge Base Chapter*, 2001. [Online]. Available: http://hivinsite.ucsf.edu/InSite?page=kb-02-02-02-02. [Accessed: 10-Oct-2017].

[125] X. Chen, M. Gan, H. Xu, F. Chen, X. Ming, H. Xu, H. Wei, F. Xu, and C. Liu, "Development of a rapid and sensitive quantum dot-based immunochromatographic strip by double labeling PCR products for detection of Staphylococcus aureus in food," *Food Control*, vol. 46, pp. 225–232, Dec. 2014.
[126] L. Chang, J. Li, and L. Wang, "Immuno-PCR: An ultrasensitive immunoassay for biomolecular detection," *Anal. Chim. Acta*, vol. 910, pp. 12–24, Mar. 2016.
[127] K. H. Chan, S. T. Lai, L. L. M. Poon, Y. Guan, K. Y. Yuen, and J. S. M. Peiris, "Analytical sensitivity of rapid influenza antigen detection tests for swine-origin influenza virus (H1N1)," *J. Clin. Virol.*, vol. 45, no. 3, pp. 205–207, Jul. 2009.
[128] X. Liu, T. Li, Y. Zheng, K.-W. Wong, S. Lu, and H. Lu, "Poor responses to oseltamivir treatment in a patient with influenza A (H7N9) virus infection," *Emerg. Microbes Infect.*, vol. 2, no. 5, p. e27, May 2013.
[129] S. Jahanshahi-Anbuhi, B. Kannan, K. Pennings, M. Monsur Ali, V. Leung, K. Giang, J. Wang, D. White, Y. Li, R. H. Pelton, J. D. Brennan, and C. D. M. Filipe, "Automating multi-step paper-based assays using integrated layering of reagents," *Lab Chip*, vol. 17, no. 5, pp. 943–950, Feb. 2017.
[130] Y. Zhang, J. Bai, and J. Y. Ying, "A stacking flow immunoassay for the detection of dengue-specific immunoglobulins in salivary fluid," *Lab Chip*, vol. 15, no. 6, pp. 1465–1471, 2015.
[131] E. Fu, T. Liang, P. Spicar-Mihalic, J. Houghtaling, S. Ramachandran, and P. Yager, "Two-dimensional paper network format that enables simple multistep assays for use in low-resource settings in the context of malaria antigen detection," *Anal. Chem.*, vol. 84, no. 10, pp. 4574–4579, 2012.
[132] B. D. Grant, C. A. Smith, K. Karvonen, and R. Richards-Kortum, "Highly Sensitive Two-Dimensional Paper Network Incorporating Biotin–Streptavidin for the Detection of Malaria," *Anal. Chem.*, vol. 88, no. 5, pp. 2553–2557, Mar. 2016.
[133] E. Fu, P. Kauffman, B. Lutz, and P. Yager, "Chemical signal amplification in two-dimensional paper networks," 2010.
[134] B. R. Lutz, P. Trinh, C. Ball, E. Fu, and P. Yager, "Two-dimensional paper networks: programmable fluidic disconnects for multi-step processes in shaped paper," *Lab Chip*, vol. 11, no. 24, p. 4274, Nov. 2011.
[135] J. R. Buser, S. A. Byrnes, C. E. Anderson, A. J. Howell, P. C. Kauffman, J. D. Bishop, M. H. Wheeler, S. Kumar, and P. Yager, "Understanding partial saturation in paper microfluidics enables alternative device architectures."
[136] A. J. Eisfeld, G. Neumann, and Y. Kawaoka, "Influenza A virus isolation, culture and identification.," *Nat. Protoc.*, vol. 9, no. 11, pp. 2663–81, Nov. 2014.
[137] Skehel, J. John, Wiley, and Don, "Receptor binding and membrane fusion in virus entry: The influenza hemagglutinin," *Annu. Rev. Biochem.*, vol. 69, 2000.
[138] J. Kuypers, N. Wright, J. Ferrenberg, M.-L. Huang, A. Cent, L. Corey, and R. Morrow, "Comparison of Real-Time PCR Assays with Fluorescent-Antibody Assays for Diagnosis of Respiratory Virus Infections in Children," *J. Clin. Microbiol.*, vol. 44, no. 7, pp. 2382–2388, Jul. 2006.
[139] B. Casado, L. K. Pannell, P. Iadarola, and J. N. Baraniuk, "Identification of human nasal mucous proteins using proteomics," *Proteomics*, vol. 5, no. 11, pp. 2949–2959, Jul. 2005.
[140] R Development Core Team, "R: A language and environment for statistical computing. R Founation for Statistical Computing, Vienna, Austria. ISBN 3-900051-07-0, URL R-

project.org.," *Foundation for Stastical Computing*, 2010. [Online]. Available: https://www.r-project.org/. [Accessed: 12-Nov-2017].
[141] E. Fu, S. A. Ramsey, P. Kauffman, B. Lutz, and P. Yager, "Transport in two-dimensional paper networks.," *Microfluid. Nanofluidics*, vol. 10, no. 1, pp. 29–35, Jan. 2011.
[142] L. K. Lafleur, J. D. Bishop, E. K. Heiniger, R. P. Gallagher, M. D. Wheeler, P. Kauffman, X. Zhang, E. C. Kline, J. R. Buser, S. Kumar, S. A. Byrnes, N. M. J. Vermeulen, N. K. Scarr, Y. Belousov, W. Mahoney, B. J. Toley, P. D. Ladd, B. R. Lutz, and P. Yager, "A rapid, instrument-free, sample-to-result nucleic acid amplification test," *Lab Chip*, vol. 16, no. 19, pp. 3777–3787, 2016.
[143] W. Wang, "Lyophilization and development of solid protein pharmaceuticals," *Int. J. Pharm.*, vol. 203, no. 1–2, pp. 1–60, Aug. 2000.
[144] S. Kadoya, K. Fujii, K. Izutsu, E. Yonemochi, K. Terada, C. Yomota, and T. Kawanishi, "Freeze-drying of proteins with glass-forming oligosaccharide-derived sugar alcohols," *Int. J. Pharm.*, vol. 389, no. 1–2, pp. 107–113, Apr. 2010.
[145] D. Kilburn, S. Townrow, V. Meunier, R. Richardson, A. Alam, and J. Ubbink, "Organization and mobility of water in amorphous and crystalline trehalose," *Nat. Mater.*, vol. 5, no. 8, pp. 632–635, Aug. 2006.
[146] W. F. Tonnis, M. A. Mensink, A. de Jager, K. van der Voort Maarschalk, H. W. Frijlink, and W. L. J. Hinrichs, "Size and Molecular Flexibility of Sugars Determine the Storage Stability of Freeze-Dried Proteins," *Mol. Pharm.*, vol. 12, no. 3, pp. 684–694, Mar. 2015.
[147] † Alexandra Simperler, *,‡ Andreas Kornherr, † Reenu Chopra, † P. Arnaud Bonnet, *,† William Jones, § and W. D. Samuel Motherwell, and G. Zifferer‡, "Glass Transition Temperature of Glucose, Sucrose, and Trehalose: An Experimental and in Silico Study," 2006.
[148] E. Kovacs, E. Kvam, B. Li, and F. Mondello, "Substrates and methods for collection, stabilization and elution of biomolecules," WO2015162093 A1, 2015.
[149] J. D. Lehe, N. E. Sitoe, O. Tobaiwa, O. Loquiha, J. I. Quevedo, T. F. Peter, and I. V. Jani, "Evaluating Operational Specifications of Point-of-Care Diagnostic Tests: A Standardized Scorecard," *PLoS One*, vol. 7, no. 10, p. e47459, Oct. 2012.
[150] B. Lutz, T. Liang, E. Fu, S. Ramachandran, P. Kauffman, and P. Yager, "Dissolvable fluidic time delays for programming multi-step assays in instrument-free paper diagnostics," *Lab Chip*, vol. 13, no. 14, p. 2840, 2013.
[151] S. Ohtake and Y. J. Wang, "Trehalose: current use and future applications.," *J. Pharm. Sci.*, vol. 100, no. 6, pp. 2020–53, Jun. 2011.
[152] M. D. Borysiak, M. J. Thompson, and J. D. Posner, "Translating diagnostic assays from the laboratory to the clinic: analytical and clinical metrics for device development and evaluation.," *Lab Chip*, vol. 16, no. 8, pp. 1293–313, Apr. 2016.
[153] B. N. Fields, D. M. (David M. Knipe, and P. M. Howley, *Fields virology*. Wolters Kluwer Health/Lippincott Williams & Wilkins, 2013.
[154] J. Wang, W. Tai, S. L. Angione, A. R. John, S. M. Opal, A. W. Artenstein, and A. Tripathi, "Subtyping clinical specimens of influenza A virus by use of a simple method to amplify RNA targets.," *J. Clin. Microbiol.*, vol. 51, no. 10, pp. 3324–30, Oct. 2013.
[155] J. L. Robinson, B. E. Lee, S. Kothapalli, W. R. Craig, and J. D. Fox, "Use of Throat Swab or Saliva Specimens for Detection of Respiratory Viruses in Children," *Clin. Infect. Dis.*, vol. 46, no. 7, pp. e61–e64, Apr. 2008.
[156] P. V. Tomazic, R. Birner-Gruenberger, A. Leitner, B. Obrist, S. Spoerk, and D. Lang-

Loidolt, “Nasal mucus proteomic changes reflect altered immune responses and epithelial permeability in patients with allergic rhinitis,” *J. Allergy Clin. Immunol.*, vol. 133, no. 3, pp. 741–750, Mar. 2014.
[157] F. Hassan, A. Nguyen, A. Formanek, J. J. Bell, and R. Selvarangan, “Comparison of the BD Veritor System for Flu A+B with the Alere BinaxNOW influenza A&B card for detection of influenza A and B viruses in respiratory specimens from pediatric patients.,” *J. Clin. Microbiol.*, vol. 52, no. 3, pp. 906–10, Mar. 2014.
[158] S. J. Prestrelski, N. Tedeschi, T. Arakawa, and J. F. Carpenter, “Dehydration-induced conformational transitions in proteins and their inhibition by stabilizers,” *Biophys. J.*, vol. 65, no. 2, pp. 661–671, Aug. 1993.
[159] E. A. Miller, S. Baniya, D. Osorio, Y. J. Al Maalouf, and H. D. Sikes, “Paper-based diagnostics in the antigen-depletion regime: High-density immobilization of rcSso7d-cellulose-binding domain fusion proteins for efficient target capture,” *Biosens. Bioelectron.*, vol. 102, pp. 456–463, Apr. 2018.
[160] G. Dai, J. Hu, X. Zhao, and P. Wang, “A colorimetric paper sensor for lactate assay using a cellulose-Binding recombinant enzyme,” *Sensors Actuators B Chem.*, vol. 238, pp. 138–144, Jan. 2017.
[161] G. Hussack, Y. Luo, L. Veldhuis, J. C. Hall, J. Tanha, R. MacKenzie, G. Hussack, Y. Luo, L. Veldhuis, J. C. Hall, J. Tanha, and R. MacKenzie, “Multivalent Anchoring and Oriented Display of Single-Domain Antibodies on Cellulose,” *Sensors*, vol. 9, no. 7, pp. 5351–5367, Jul. 2009.
[162] H.-D. Kim, S.-L. Choi, H. Kim, J. H. Sohn, and S.-G. Lee, “Enzyme-linked assay of cellulose-binding domain functions from Cellulomonas fimi on multi-well microtiter plate,” *Biotechnol. Bioprocess Eng.*, vol. 18, no. 3, pp. 575–580, Jun. 2013.
[163] M. Li, Y. Yue, Z.-J. Zhang, Z.-Y. Wang, T.-W. Tan, and L.-H. Fan, “Site-Specific and High-Loading Immobilization of Proteins by Using Cohesin–Dockerin and CBM–Cellulose Interactions,” *Bioconjug. Chem.*, vol. 27, no. 7, pp. 1579–1583, Jul. 2016.
[164] C. A. Holstein, A. Chevalier, S. Bennett, C. E. Anderson, K. Keniston, C. Olsen, B. Li, B. Bales, D. R. Moore, E. Fu, D. Baker, and P. Yager, “Immobilizing affinity proteins to nitrocellulose: a toolbox for paper-based assay developers,” *Anal. Bioanal. Chem.*, pp. 1335–1346, 2015.
[165] CDC, “Ebola Virus Disease Distribution Map: Cases of Ebola Virus Disease in Africa Since 1976 | 2014-2016 Outbreak West Africa | History | Ebola (Ebola Virus Disease) | CDC,” *2018*. [Online]. Available: https://www.cdc.gov/vhf/ebola/history/distribution-map.html. [Accessed: 20-Dec-2018].
[166] WHO, “Ebola Virus Disease External Situation Report 20,” 2018.
[167] WHO, “Ebola Situation Report - 30 March 2016 | Ebola,” 2016. [Online]. Available: http://apps.who.int/ebola/current-situation/ebola-situation-report-30-march-2016. [Accessed: 19-Dec-2018].
[168] D. M. Pigott, N. Golding, A. Mylne, Z. Huang, A. J. Henry, D. J. Weiss, O. J. Brady, M. U. Kraemer, D. L. Smith, C. L. Moyes, S. Bhatt, P. W. Gething, P. W. Horby, I. I. Bogoch, J. S. Brownstein, S. R. Mekaru, A. J. Tatem, K. Khan, and S. I. Hay, “Mapping the zoonotic niche of Ebola virus disease in Africa,” *Elife*, vol. 3, Sep. 2014.
[169] D. M. Pigott, A. I. Millear, L. Earl, C. Morozoff, B. A. Han, F. M. Shearer, D. J. Weiss, O. J. Brady, M. U. Kraemer, C. L. Moyes, S. Bhatt, P. W. Gething, N. Golding, and S. I. Hay, “Updates to the zoonotic niche map of Ebola virus disease in Africa,” *Elife*, vol. 5,

Jul. 2016.
[170] W. A. Fischer, T. M. Uyeki, and R. V. Tauxe, “Ebola virus disease: What clinicians in the United States need to know,” *Am. J. Infect. Control*, vol. 43, no. 8, pp. 788–793, Aug. 2015.
[171] J. E. Lee and E. O. Saphire, “Ebolavirus glycoprotein structure and mechanism of entry,” *Future Virol.*, vol. 4, no. 6, pp. 621–635, Nov. 2009.
[172] CDC, “Transmission | Ebola Hemorrhagic Fever | CDC,” 2018. [Online]. Available: https://www.cdc.gov/vhf/ebola/transmission/index.html. [Accessed: 19-Dec-2018].
[173] T. M. Uyeki, B. R. Erickson, S. Brown, A. K. McElroy, D. Cannon, A. Gibbons, T. Sealy, M. H. Kainulainen, A. J. Schuh, C. S. Kraft, A. K. Mehta, G. M. Lyon, J. B. Varkey, B. S. Ribner, R. T. Ellison, E. Carmody, G. J. Nau, C. Spiropoulou, S. T. Nichol, and U. Ströher, “Ebola Virus Persistence in Semen of Male Survivors,” *Clin. Infect. Dis.*, vol. 62, no. 12, pp. 1552–1555, Jun. 2016.
[174] G. F. Deen, N. Broutet, W. Xu, B. Knust, F. R. Sesay, S. L. R. McDonald, E. Ervin, J. E. Marrinan, P. Gaillard, N. Habib, H. Liu, W. Liu, A. E. Thorson, F. Yamba, T. A. Massaquoi, F. James, A. Ariyarajah, C. Ross, K. Bernstein, A. Coursier, J. Klena, M. Carino, A. H. Wurie, Y. Zhang, M. S. Dumbuya, N. Abad, B. Idriss, T. Wi, S. D. Bennett, T. Davies, F. K. Ebrahim, E. Meites, D. Naidoo, S. J. Smith, P. Ongpin, T. Malik, A. Banerjee, B. R. Erickson, Y. Liu, Y. Liu, K. Xu, A. Brault, K. N. Durski, J. Winter, T. Sealy, S. T. Nichol, M. Lamunu, J. Bangura, S. Landoulsi, A. Jambai, O. Morgan, G. Wu, M. Liang, Q. Su, Y. Lan, Y. Hao, P. Formenty, U. Ströher, and F. Sahr, “Ebola RNA Persistence in Semen of Ebola Virus Disease Survivors — Final Report,” *N. Engl. J. Med.*, vol. 377, no. 15, pp. 1428–1437, Oct. 2017.
[175] D. Sissoko, M. Keïta, B. Diallo, N. Aliabadi, D. L. Fitter, B. A. Dahl, J. Akoi Bore, F. Raymond Koundouno, K. Singethan, S. Meisel, T. Enkirch, A. Mazzarelli, V. Amburgey, O. Faye, A. Alpha Sall, N. Magassouba, M. W. Carroll, X. Anglaret, D. Malvy, P. Formenty, R. Bruce Aylward, S. Keïta, M. Harouna Djingarey, N. J. Loman, S. Günther, and S. Duraffour, “Ebola Virus Persistence in Breast Milk After No Reported Illness: A Likely Source of Virus Transmission From Mother to Child.,” *Clin. Infect. Dis.*, vol. 64, no. 4, pp. 513–516, 2017.
[176] J. B. Varkey, J. G. Shantha, I. Crozier, C. S. Kraft, G. M. Lyon, A. K. Mehta, G. Kumar, J. R. Smith, M. H. Kainulainen, S. Whitmer, U. Ströher, T. M. Uyeki, B. S. Ribner, and S. Yeh, “Persistence of Ebola Virus in Ocular Fluid during Convalescence,” *N. Engl. J. Med.*, vol. 372, no. 25, pp. 2423–2427, Jun. 2015.
[177] P. Vetter, W. A. Fischer, M. Schibler, M. Jacobs, D. G. Bausch, and L. Kaiser, “Ebola Virus Shedding and Transmission: Review of Current Evidence,” *J. Infect. Dis.*, vol. 214, no. suppl 3, pp. S177–S184, Oct. 2016.
[178] CDC, “Marburg Outbreaks 2005-2014 | Marburg Hemorrhagic Fever (Marburg HF) | CDC,” 2014. [Online]. Available: https://www.cdc.gov/vhf/marburg/outbreaks/summaries.html. [Accessed: 19-Dec-2018].
[179] D. S. Goodsell, “Ebola Virus Proteins,” *RCSB Protein Data Bank*, Oct. 2014.
[180] J. A. Wilson, M. Bray, R. Bakken, and M. K. Hart, “Vaccine Potential of Ebola Virus VP24, VP30, VP35, and VP40 Proteins,” *Virology*, vol. 286, no. 2, pp. 384–390, Aug. 2001.
[181] J. E. Lee, M. L. Fusco, A. J. Hessell, W. B. Oswald, D. R. Burton, and E. O. Saphire, “Structure of the Ebola virus glycoprotein bound to an antibody from a human survivor,”

Nature, vol. 454, no. 7201, pp. 177–182, Jul. 2008.
[182] A. Sanchez, T. G. Ksiazek, P. E. Rollin, M. E. G. Miranda, S. G. Trappier, A. S. Khan, C. J. Peters, and S. T. Nichol, "Detection and Molecular Characterization of Ebola Viruses Causing Disease in Human and Nonhuman Primates," *J. Infect. Dis.*, vol. 179, no. s1, pp. S164–S169, Feb. 1999.
[183] G. Wong, G. P. Kobinger, and X. Qiu, "Characterization of host immune responses in Ebola virus infections.," *Expert Rev. Clin. Immunol.*, vol. 10, no. 6, pp. 1–10, 2014.
[184] T. Maruyama, P. W. H. I. Parren, A. Sanchez, I. Rensink, L. L. Rodriguez, A. S. Khan, C. J. Peters, and D. R. Burton, "Recombinant Human Monoclonal Antibodies to Ebola Virus," *J. Infect. Dis.*, vol. 179, no. s1, pp. S235–S239, Feb. 1999.
[185] M.-A. de La Vega, G. Wong, G. P. Kobinger, and X. Qiu, "The multiple roles of sGP in Ebola pathogenesis.," *Viral Immunol.*, vol. 28, no. 1, pp. 3–9, Feb. 2015.
[186] J. Lee and E. Saphire, "Structure of the Ebola virus glycoprotein bound to an antibody from a human survivor," *2008*. [Online]. Available: https://www-ssrl.slac.stanford.edu/research/highlights_archive/ebolavirus.html. [Accessed: 19-Dec-2018].
[187] C. D. Murin, M. L. Fusco, Z. A. Bornholdt, X. Qiu, G. G. Olinger, L. Zeitlin, G. P. Kobinger, A. B. Ward, and E. O. Saphire, "Structures of protective antibodies reveal sites of vulnerability on Ebola virus.," *Proc. Natl. Acad. Sci. U. S. A.*, vol. 111, no. 48, pp. 17182–7, Dec. 2014.
[188] D. La, "De novo design of proteins that broadly neutralize Ebolaviruses," *prep*.
[189] D. V. Clark, P. B. Jahrling, J. V. Lawler, D. V. Clark, P. B. Jahrling, and J. V. Lawler, "Clinical Management of Filovirus-Infected Patients," *Viruses*, vol. 4, no. 9, pp. 1668–1686, Sep. 2012.
[190] S. Duraffour, D. Malvy, and D. Sissoko, "How to treat Ebola virus infections? A lesson from the field," *Curr. Opin. Virol.*, vol. 24, pp. 9–15, Jun. 2017.
[191] X. Qiu, G. Wong, J. Audet, A. Bello, L. Fernando, J. B. Alimonti, H. Fausther-Bovendo, H. Wei, J. Aviles, E. Hiatt, A. Johnson, J. Morton, K. Swope, O. Bohorov, N. Bohorova, C. Goodman, D. Kim, M. H. Pauly, J. Velasco, J. Pettitt, G. G. Olinger, K. Whaley, B. Xu, J. E. Strong, L. Zeitlin, and G. P. Kobinger, "Reversion of advanced Ebola virus disease in nonhuman primates with ZMapp," *Nature*, vol. 514, no. 7520, pp. 47–53, Oct. 2014.
[192] A. M. Henao-Restrepo, A. Camacho, I. M. Longini, C. H. Watson, W. J. Edmunds, M. Egger, M. W. Carroll, N. E. Dean, I. Diatta, M. Doumbia, B. Draguez, S. Duraffour, G. Enwere, R. Grais, S. Gunther, P.-S. Gsell, S. Hossmann, S. V. Watle, M. K. Kondé, S. Kéïta, S. Kone, E. Kuisma, M. M. Levine, S. Mandal, T. Mauget, G. Norheim, X. Riveros, A. Soumah, S. Trelle, A. S. Vicari, J.-A. Røttingen, and M.-P. Kieny, "Efficacy and effectiveness of an rVSV-vectored vaccine in preventing Ebola virus disease: final results from the Guinea ring vaccination, open-label, cluster-randomised trial (Ebola Ça Suffit!)," *Lancet*, vol. 389, no. 10068, pp. 505–518, Feb. 2017.
[193] J. A. Walldorf, K. A. Date, N. Sreenivasan, J. B. Harris, and T. B. Hyde, "Lessons Learned from Emergency Response Vaccination Efforts for Cholera, Typhoid, Yellow Fever, and Ebola," *Emerg. Infect. Dis.*, vol. 23, no. 13, Dec. 2017.
[194] M. J. Broadhurst, T. J. G. Brooks, and N. R. Pollock, "Diagnosis of Ebola Virus Disease: Past, Present, and Future.," *Clin. Microbiol. Rev.*, vol. 29, no. 4, pp. 773–93, Oct. 2016.
[195] P. Raftery, O. Condell, C. Wasunna, J. Kpaka, R. Zwizwai, M. Nuha, M. Fallah, M.

Freeman, V. Harris, M. Miller, A. Baller, M. Massaquoi, V. Katawera, J. Saindon, P. Bemah, E. Hamblion, E. Castle, D. Williams, A. Gasasira, and T. Nyenswah, "Establishing Ebola Virus Disease (EVD) diagnostics using GeneXpert technology at a mobile laboratory in Liberia: Impact on outbreak response, case management and laboratory systems strengthening," *PLoS Negl. Trop. Dis.*, vol. 12, no. 1, p. e0006135, Jan. 2018.

[196] WHO, "WHO Emergency Use Assessment and Listing for Ebola Virus Disease IVDs PUBLIC REPORT Product: ReEBOV™ Antigen Rapid Test Kit," 2014.

[197] WHO, "WHO Emergency Use Assessment and Listing for EVD IVDs PUBLIC REPORT Product: SD Q Line Ebola Zaire Ag Number: EA," 2015.

[198] WHO, "WHO Emergency Use Assessment and Listing for Ebola Virus Disease IVDs PUBLIC REPORT Product: OraQuick® Ebola Rapid Antigen Test Kit (Cadaveric Oral fluid and Whole Blood)," 2016.

[199] M. G. E. G. Bremer, J. Duval, W. Norde, and J. Lyklema, "Electrostatic interactions between immunoglobulin (IgG) molecules and a charged sorbent," *Colloids Surfaces A Physicochem. Eng. Asp.*, vol. 250, no. 1–3, pp. 29–42, Dec. 2004.

[200] S. Demanèche, J.-P. Chapel, L. J. Monrozier, and H. Quiquampoix, "Dissimilar pH-dependent adsorption features of bovine serum albumin and α-chymotrypsin on mica probed by AFM," *Colloids Surfaces B Biointerfaces*, vol. 70, no. 2, pp. 226–231, May 2009.

[201] F. Höök, M. Rodahl, B. Kasemo, and P. Brzezinski, "Structural changes in hemoglobin during adsorption to solid surfaces: effects of pH, ionic strength, and ligand binding.," *Proc. Natl. Acad. Sci. U. S. A.*, vol. 95, no. 21, pp. 12271–6, Oct. 1998.

[202] M. Rabe, D. Verdes, and S. Seeger, "Understanding protein adsorption phenomena at solid surfaces," *Adv. Colloid Interface Sci.*, vol. 162, no. 1, pp. 87–106, 2011.

[203] P. Yager, C. E. Anderson, D. Baker, Y.-R. Lin, and C. Holstein, "Porous membrane-binding peptides," US1527650, 22-Sep-2016.

[204] B. Zakeri, J. O. Fierer, E. Celik, E. C. Chittock, U. Schwarz-Linek, V. T. Moy, and M. Howarth, "Peptide tag forming a rapid covalent bond to a protein, through engineering a bacterial adhesin," *Proc. Natl. Acad. Sci.*, vol. 109, no. 12, pp. e690-7, 2012.

[205] K. D. Brune, D. B. Leneghan, I. J. Brian, A. S. Ishizuka, M. F. Bachmann, S. J. Draper, S. Biswas, and M. Howarth, "Plug-and-Display: decoration of Virus-Like Particles via isopeptide bonds for modular immunization," *Sci. Rep.*, vol. 6, no. 1, p. 19234, May 2016.

[206] W. Ma, A. Saccardo, D. Roccatano, D. Aboagye-Mensah, M. Alkaseem, M. Jewkes, F. Di Nezza, M. Baron, M. Soloviev, and E. Ferrari, "Modular assembly of proteins on nanoparticles," *Nat. Commun.*, vol. 9, no. 1, p. 1489, Dec. 2018.

[207] E. Ferrari, "A plug and play approach for the decoration of nanoparticles with recombinant proteins," *Nanomedicine*, vol. 13, no. 20, pp. 2547–2550, Oct. 2018.

[208] S. Schmidt-Dannert, G. Zhang, T. Johnston, M. B. Quin, and C. Schmidt-Dannert, "Building a toolbox of protein scaffolds for future immobilization of biocatalysts," *Appl. Microbiol. Biotechnol.*, vol. 102, no. 19, pp. 8373–8388, Oct. 2018.

[209] H. J. Park and T. H. Yoo, "Nucleic Acid Detection by a Target-Assisted Proximity Proteolysis Reaction," *ACS Sensors*, vol. 3, no. 10, pp. 2066–2070, Oct. 2018.

[210] X. Ke, Y. Zhang, F. Zheng, Y. Liu, Z. Zheng, Y. Xu, and H. Wang, "SpyCatcher–SpyTag mediated in situ labelling of progeny baculovirus with quantum dots for tracking viral infection in living cells," *Chem. Commun.*, vol. 54, no. 10, pp. 1189–1192, Jan. 2018.

[211] D. J. Gasperino, D. Leon, B. Lutz, D. M. Cate, K. P. Nichols, D. Bell, and B. H. Weigl, "Threshold-Based Quantification in a Multiline Lateral Flow Assay via Computationally Designed Capture Efficiency," *Anal. Chem.*, vol. 90, no. 11, pp. 6643–6650, Jun. 2018.
[212] B. R. Lutz, P. Trinh, C. Ball, E. Fu, P. Yager, R. Pelton, W. A. Zhao, W. Dungchai, R. F. Carvalhal, Z. H. Nie, Z. H. Nie, A. Apilux, J. L. Delaney, X. Li, X. Li, W. Dungchai, W. Wang, A. W. Martinez, A. W. Martinez, A. W. Martinez, K. Abe, H. Noh, S. T. Phillips, N. Noh, S. T. Phillips, D. R. Ballerini, M. Reches, X. Li, E. Fu, E. Fu, E. L. Fu, J. L. Osborn, P. Kauffman, E. Fu, R. Lucas, E. W. Washburn, D. A. Barry, D. A. Barry, N. Fries, M. Dreyer, E. M. Fenton, Y. Lu, and A. W. Martinez, "Two-dimensional paper networks: programmable fluidic disconnects for multi-step processes in shaped paper," *Lab Chip*, vol. 11, no. 24, p. 4274, 2011.
[213] R. Vermasvuori, "PRODUCTION OF RECOMBINANT PROTEINS AND MONOCLONAL ANTIBODIES – TECHNO-ECONOMICAL EVALUATION OF THE PRODUCTION METHODS," 2009.
[214] B. A. Clevidence, M. W. Marshall, and J. J. Canary, "Biotin levels in plasma and urine of healthy adults consuming physiological doses of biotin," *Nutr. Res.*, vol. 8, no. 10, pp. 1109–1118, Oct. 1988.
[215] E. A. Miller, Y. Jabbour Al Maalouf, and H. D. Sikes, "Design Principles for Enhancing Sensitivity in Paper-Based Diagnostics via Large-Volume Processing," *Anal. Chem.*, vol. 90, no. 15, pp. 9472–9479, Aug. 2018.
[216] L. Kaiser, J. Weisser, M. Kohl, and H.-P. Deigner, "Small molecule detection with aptamer based lateral flow assays: Applying aptamer-C-reactive protein cross-recognition for ampicillin detection," *Sci. Rep.*, vol. 8, no. 1, p. 5628, Dec. 2018.
[217] J. E. Pinto Torres, J. Goossens, J. Ding, Z. Li, S. Lu, D. Vertommen, P. Naniima, R. Chen, S. Muyldermans, Y. G.-J. Sterckx, and S. Magez, "Development of a Nanobody-based lateral flow assay to detect active Trypanosoma congolense infections," *Sci. Rep.*, vol. 8, no. 1, p. 9019, Dec. 2018.
[218] E. A. Miller, M. W. Traxlmayr, J. Shen, and H. D. Sikes, "Activity-based assessment of an engineered hyperthermophilic protein as a capture agent in paper-based diagnostic tests," *Mol. Syst. Des. Eng.*, vol. 1, no. 4, pp. 377–381, Nov. 2016.
[219] H. Kaur, J. G. Bruno, A. Kumar, and T. K. Sharma, "Aptamers in the Therapeutics and Diagnostics Pipelines.," *Theranostics*, vol. 8, no. 15, pp. 4016–4032, 2018.
[220] J. Bruno, "Predicting the Uncertain Future of Aptamer-Based Diagnostics and Therapeutics," *Molecules*, vol. 20, no. 4, pp. 6866–6887, Apr. 2015.
[221] H. Yagoda, "Applications of Confined Spot Tests in Analytical Chemistry: Preliminary Paper," *Ind. Eng. Chem. Anal. Ed.*, vol. 9, no. 2, pp. 79–82, Feb. 1937.
[222] R. Muller and D. Clegg, "SCIENTIFIC COMMUNICATIONS. Automatic Paper Chromatography," *Anal. Chem.*, vol. 21, no. 1, pp. 192–192, Jan. 1949.
[223] R. Consden, A. H. Gordon, and A. J. Martin, "Qualitative analysis of proteins: a partition chromatographic method using paper.," *Biochem. J.*, vol. 38, no. 3, pp. 224–32, 1944.
[224] J. Arora, G. Kumar, A. K. Verma, M. Bhalla, R. Sarin, and V. P. Myneedu, "Utility of MPT64 Antigen Detection for Rapid Confirmation of Mycobacterium tuberculosis Complex.," *J. Glob. Infect. Dis.*, vol. 7, no. 2, pp. 66–9, 2015.
[225] E. Fu, P. Kauffman, B. Lutz, and P. Yager, "Chemical signal amplification in two-dimensional paper networks.," *Sens. Actuators. B. Chem.*, vol. 149, no. 1, pp. 325–328, Aug. 2010.

[226] N. M. Rodriguez, J. C. Linnes, A. Fan, C. K. Ellenson, N. R. Pollock, and C. M. Klapperich, "Paper-Based RNA Extraction, *in Situ* Isothermal Amplification, and Lateral Flow Detection for Low-Cost, Rapid Diagnosis of Influenza A (H1N1) from Clinical Specimens," *Anal. Chem.*, vol. 87, no. 15, pp. 7872–7879, Aug. 2015.
[227] B. Rohrman and R. Richards-Kortum, "Inhibition of Recombinase Polymerase Amplification by Background DNA: A Lateral Flow-Based Method for Enriching Target DNA," *Anal. Chem.*, vol. 87, no. 3, pp. 1963–1967, Feb. 2015.
[228] B. A. Rohrman and R. R. Richards-Kortum, "A paper and plastic device for performing recombinase polymerase amplification of HIV DNA.," *Lab Chip*, vol. 12, no. 17, pp. 3082–8, Sep. 2012.
[229] H. Noh and S. T. Phillips, "Metering the Capillary-Driven Flow of Fluids in Paper-Based Microfluidic Devices," *Anal. Chem.*, vol. 82, no. 10, pp. 4181–4187, May 2010.
[230] H. Noh and S. T. Phillips, "Fluidic Timers for Time-Dependent, Point-of-Care Assays on Paper," *Anal. Chem.*, vol. 82, no. 19, pp. 8071–8078, Oct. 2010.
[231] H. Chen, J. Cogswell, C. Anagnostopoulos, and M. Faghri, "A fluidic diode, valves, and a sequential-loading circuit fabricated on layered paper," *Lab Chip*, vol. 12, no. 16, p. 2909, Aug. 2012.
[232] S. F. An and K. A. Fleming, "Removal of inhibitor(s) of the polymerase chain reaction from formalin fixed, paraffin wax embedded tissues.," *J. Clin. Pathol.*, vol. 44, no. 11, pp. 924–7, Nov. 1991.
[233] W. A. Al-Soud and P. Radstrom, "Purification and Characterization of PCR-Inhibitory Components in Blood Cells," *J. Clin. Microbiol.*, vol. 39, no. 2, pp. 485–493, Feb. 2001.
[234] C. Schrader, A. Schielke, L. Ellerbroek, and R. Johne, "PCR inhibitors - occurrence, properties and removal," *J. Appl. Microbiol.*, vol. 113, no. 5, pp. 1014–1026, Nov. 2012.
[235] M. Fratzl, B. Chang, S. Oyola-Reynoso, G. Blaire, and S. Delshad, "Magnetic Two-Way Valves for Paper-Based Capillary-Driven Microfluidic Devices."
[236] T. H. Kim, Y. K. Hahn, J. Lee, D. van Noort, and M. S. Kim, "Solenoid Driven Pressure Valve System: Toward Versatile Fluidic Control in Paper Microfluidics," *Anal. Chem.*, vol. 90, no. 4, pp. 2534–2541, Feb. 2018.
[237] B. J. Toley, J. A. Wang, M. Gupta, J. R. Buser, L. K. Lafleur, B. R. Lutz, E. Fu, and P. Yager, "A versatile valving toolkit for automating fluidic operations in paper microfluidic devices.," *Lab Chip*, vol. 15, no. 6, pp. 1432–44, Mar. 2015.
[238] T. Kong, S. Flanigan, M. Weinstein, U. Kalwa, C. Legner, and S. Pandey, "A fast, reconfigurable flow switch for paper microfluidics based on selective wetting of folded paper actuator strips," *Lab Chip*, vol. 17, no. 21, pp. 3621–3633, Oct. 2017.
[239] J. L. Osborn, B. Lutz, E. Fu, P. Kauffman, D. Y. Stevens, and P. Yager, "Microfluidics without pumps: reinventing the T-sensor and H-filter in paper networks," *Lab Chip*, vol. 10, no. 20, p. 2659, 2010.
[240] P. Kauffman, E. Fu, B. Lutz, and P. Yager, "Visualization and measurement of flow in two-dimensional paper networks.," *Lab Chip*, vol. 10, no. 19, pp. 2614–2617, Oct. 2010.
[241] S. Dharmaraja, L. Lafleur, S. Byrnes, P. Kauffman, J. Buser, B. Toley, E. Fu, P. Yager, and B. Lutz, "Programming paper networks for point of care diagnostics," 2013, vol. 8615, p. 86150X.
[242] B. Srinivasan and S. Tung, "Development and Applications of Portable Biosensors," *J. Lab. Autom.*, vol. 20, no. 4, pp. 365–389, Aug. 2015.
[243] S. Ahmed, M.-P. N. Bui, and A. Abbas, "Paper-based chemical and biological sensors:

Engineering aspects," *Biosens. Bioelectron.*, vol. 77, pp. 249–263, Mar. 2016.
[244] Y. He, Y. Wu, J.-Z. Fu, and W.-B. Wu, "Fabrication of paper-based microfluidic analysis devices: a review," *RSC Adv.*, vol. 5, no. 95, pp. 78109–78127, Sep. 2015.
[245] S.-G. Jeong, J. Kim, S. H. Jin, K.-S. Park, and C.-S. Lee, "Flow control in paper-based microfluidic device for automatic multistep assays: A focused minireview," *Korean J. Chem. Eng.*, vol. 33, no. 10, pp. 2761–2770, Oct. 2016.
[246] M. Chernesky, D. Jang, S. Chong, J. Sellors, and J. Mahony, "Impact of urine collection order on the ability of assays to identify Chlamydia trachomatis infections in men.," *Sex. Transm. Dis.*, vol. 30, no. 4, pp. 345–7, Apr. 2003.
[247] C. A. Wisniewski, J. A. White, C.-E. C. Michel, L. Mahilum-Tapay, J. P. V Magbanua, E. C. B. Nadala, P. J. Barber, B. T. Goh, H. H. Lee, and H. H. Lee, "Optimal method of collection of first-void urine for diagnosis of Chlamydia trachomatis infection in men.," *J. Clin. Microbiol.*, vol. 46, no. 4, pp. 1466–9, Apr. 2008.
[248] S. F. Isbey, T. M. Alcom, R. H. Davis, J. Haizlip, P. A. Leone, M. S. Cohen, S. F. Isbey, T. M. Alcom, R. H. Davis, J. Haizlip, P. A. Leone, and M. S. Cohen, "Characterisation of Neisseria gonorrhoeae in semen during urethral infection in men," *Genitourin Med*, vol. 73, pp. 378–382, 1997.
[249] A. Rogacs, L. A. Marshall, and J. G. Santiago, "Purification of nucleic acids using isotachophoresis," *J. Chromatogr. A*, vol. 1335, pp. 105–120, Mar. 2014.
[250] M. D. Borysiak, K. W. Kimura, and J. D. Posner, "NAIL: Nucleic Acid detection using Isotachophoresis and Loop-mediated isothermal amplification.," *Lab Chip*, vol. 15, no. 7, pp. 1697–707, Apr. 2015.
[251] B. Y. Moghadam, K. T. Connelly, and J. D. Posner, "Isotachophoretic Preconcenetration on Paper-Based Microfluidic Devices," *Anal. Chem.*, vol. 86, no. 12, pp. 5829–5837, Jun. 2014.
[252] M. Bercovici, G. V. Kaigala, J. C. Liao, and J. G. Santiago, "No Title," in *14th Int. Conf. Miniaturized Syst. Chem. Life Sci.*, 2010, pp. 797–799.
[253] J. C. Linnes, A. Fan, N. M. Rodriguez, B. Lemieux, H. Kong, and C. M. Klapperich, "Paper-based molecular diagnostic for Chlamydia trachomatis," *RSC Adv.*, vol. 4, no. 80, pp. 42245–42251, Sep. 2014.
[254] S. A. Byrnes, J. D. Bishop, L. Lafleur, J. R. Buser, B. Lutz, and P. Yager, "One-step purification and concentration of DNA in porous membranes for point-of-care applications," *Lab Chip*, vol. 15, no. 12, pp. 2647–2659, 2015.
[255] J. Noiphung, K. Talalak, I. Hongwarittorrn, N. Pupinyo, P. Thirabowonkitphithan, and W. Laiwattanapaisal, "A novel paper-based assay for the simultaneous determination of Rh typing and forward and reverse ABO blood groups," *Biosens. Bioelectron.*, vol. 67, pp. 485–489, May 2015.
[256] T. Songjaroen and W. Laiwattanapaisal, "Simultaneous forward and reverse ABO blood group typing using a paper-based device and barcode-like interpretation," *Anal. Chim. Acta*, vol. 921, pp. 67–76, May 2016.
[257] C. A. Schneider, W. S. Rasband, and K. W. Eliceiri, "NIH Image to ImageJ: 25 years of image analysis," *Nat. Methods*, vol. 9, no. 7, pp. 671–675, 2012.
[258] † Brian M. Paegel, ‡ William H. Grover, ‡ Alison M. Skelley, ‡ and Richard A. Mathies, and † Gerald F. Joyce*, "Microfluidic Serial Dilution Circuit," 2006.
[259] J. Nguyen, Y. Wei, Y. Zheng, C. Wang, and Y. Sun, "On-chip sample preparation for complete blood count from raw blood.," *Lab Chip*, vol. 15, no. 6, pp. 1533–44, 2015.

[260] C. Kim, K. Lee, J. H. Kim, K. S. Shin, K.-J. Lee, T. S. Kim, and J. Y. Kang, "A serial dilution microfluidic device using a ladder network generating logarithmic or linear concentrations.," *Lab Chip*, vol. 8, no. 3, pp. 473–479, 2008.
[261] D. J. J. de Gorter, M. van Dinther, and P. ten Dijke, "Measurement of Constitutive Activity of BMP Type I Receptors," *Methods Enzymol.*, vol. 484, pp. 281–293, Jan. 2010.
[262] G. L. Mosley, P. Nguyen, B. M. Wu, and D. T. Kamei, "Development of quantitative radioactive methodologies on paper to determine important lateral-flow immunoassay parameters," *Lab Chip*, vol. 16, no. 15, pp. 2871–2881, Jul. 2016.
[263] P. K. Smith, R. I. Krohn, G. T. Hermanson, A. K. Mallia, F. H. Gartner, M. D. Provenzano, E. K. Fujimoto, N. M. Goeke, B. J. Olson, and D. C. Klenk, "Measurement of protein using bicinchoninic acid," *Anal. Biochem.*, vol. 150, no. 1, pp. 76–85, Oct. 1985.
[264] B. J. S. C. Olson and J. Markwell, "Assays for Determination of Protein Concentration," in *Current Protocols in Protein Science*, vol. Chapter 3, Hoboken, NJ, USA: John Wiley & Sons, Inc., 2007, p. 3.4.1-3.4.29.
[265] ThermoFisher, "Micro BCA Protein Assay Kit - Thermo Fisher Scientific." [Online]. Available: https://www.thermofisher.com/order/catalog/product/23235. [Accessed: 26-Dec-2018].
[266] E. Fu, T. Liang, J. Houghtaling, S. Ramachandran, S. A. Ramsey, B. Lutz, and P. Yager, "Enhanced sensitivity of lateral flow tests using a two-dimensional paper network format.," *Anal. Chem.*, vol. 83, no. 20, pp. 7941–6, Oct. 2011.
[267] S. Qian and H. H. Bau, "A mathematical model of lateral flow bioreactions applied to sandwich assays," *Anal. Biochem.*, vol. 322, no. 1, pp. 89–98, Nov. 2003.
[268] S. Qian and H. H. Bau, "Analysis of lateral flow biodetectors: Competitive format," *Anal. Biochem.*, vol. 326, no. 2, pp. 211–224, Mar. 2004.
[269] D. Gasperino, B. Grant, J. Dantzler, and B. H. Weigl, "Supporting high-sensitivity lateral flow assay development through predictive modeling."
[270] J. T. Edward, "Molecular volumes and the Stokes-Einstein equation," *J. Chem. Educ.*, vol. 47, no. 4, p. 261, Apr. 1970.
[271] E. Carrilho, A. W. Martinez, and G. M. Whitesides, "Understanding Wax Printing: A Simple Micropatterning Process for Paper-Based Microfluidics," 2009.
[272] R. B. Channon, Y. Yang, K. M. Feibelman, B. J. Geiss, D. S. Dandy, and C. S. Henry, "Development of an Electrochemical Paper-Based Analytical Device for Trace Detection of Virus Particles," *Anal. Chem.*, vol. 90, no. 12, pp. 7777–7783, Jun. 2018.
[273] S. C. Fernandes, D. J. Wilson, and C. R. Mace, "Fabrication of Three-dimensional Paper-based Microfluidic Devices for Immunoassays," *J. Vis. Exp.*, no. 121, p. e55287, Mar. 2017.
[274] Y.-J. Juang, W.-S. Li, and P.-S. Chen, "Fabrication of microfluidic paper-based analytical devices by filtration-assisted screen printing," *J. Taiwan Inst. Chem. Eng.*, vol. 80, pp. 71–75, Nov. 2017.
[275] Y. He, Y. Wu, X. Xiao, J. Fu, and G. Xue, "A low-cost and rapid microfluidic paper-based analytical device fabrication method: flash foam stamp lithography," *RSC Adv.*, vol. 4, no. 109, pp. 63860–63865, Nov. 2014.
[276] P. De, T. Garcia, T. Miguel, G. Cardoso, C. D. Garcia, E. Carrilho, W. Karlos, and T. Coltro, "A handheld stamping process to fabricate microfluidic paper-based analytical devices with chemically modified surface for clinical assays †," 2014.

[277] L. Yu and Z. Z. Shi, “Microfluidic paper-based analytical devices fabricated by low-cost photolithography and embossing of Parafilm®,” *Lab Chip*, vol. 15, no. 7, pp. 1642–1645, Mar. 2015.

VITA

Caitlin E. Anderson was born in San Jose, California. She received her B.S. in Biological Engineering with a minor in Global Health from Cornell University in 2012, and a M.Eng in Biological Engineering from the same department in 2013. Before beginning her PhD at the University of Washington, she received a Whitaker Fellowship in Moshi, Tanzania. She received her PhD from the University of Washington in 2019.